The Effects of Volitional Breathing and Carbon Dioxide Inhalation on Human Local Field Potentials

Nor Faizal Ahmad Bahuri

Linacre College

University of Oxford

A thesis submitted for the degree of

Doctor of Philosophy

Trinity 2014

In the name of Allah, The Most Beneficent, The Most Merciful

Acknowledgements

I would like to thank all the patients who participate in this research, without whose generous attitude this thesis would not have existed.

I would like to thank Mr Alexander Green whose patience, intellect and friendship has been critical to help me along this programme.

I would like to thank Professor Tipu Aziz who's kind advice persuaded me to move 14000 kilometres away from my comfort zone. It has been a worthwhile journey.

I would like to thank Professor David J Paterson and Associate Professor Keith Dorrington for their invaluable advice on physiological matter.

I would like to thank Sandra Boccard Binet, Dali Wu, Alex Weiss, Holly Sistapessan, Martin Gillies, my past and present colleagues in Oxford Functional Neurosurgery for your support to make this thesis possible.

A special thanks to my good friend Emmanuel Debrah who stood by me throughout this research.

To my parents, Ahmad Bahuri Gariman and Laila Jaafar who trusted me and let go of their son for a lifetime adventure from the age of 12. Thank you and I am coming home.

A lifetime gratitude to my wife, Azriyanti Anuar Zaini who keeps me sane and to my 3 angels, Ameera Nur, Afriena Nur and Alina Nur. What an adventure did we have!

Statement of Originality

I have been the principal investigator in the work presented in this dissertation. I have been involved in the planning, experimentation and analysis of all the studies. The carbon dioxide experiment idea was first conceived by Professor David Paterson (DPAG, Oxford University). This was expanded to fit into my research questions. The respiratory experiments were supervised by Associate Professor Keith Dorrington (DPAG, Oxford University) to ensure the safety of human subjects during carbon dioxide inhalation. I am grateful for their support and advice.

Except for those parts in which it is explicitly stated to the contrary, this thesis is my own work. It has not been submitted for any degree at this or any other academic or professional institution.

Dr Nor Faizal Ahmad Bahuri

Abstract

Breathing is an automatic process that we hardly pay any attention to in our daily life. As a social species, we interact using body movement, speech and emotion and these actions require modification of the respiratory pattern.

While we understood how the respiratory rhythm is generated, we do not have clear evidence on how higher cortical signals modulate the respiratory pattern. The deep cortical structures in the human brain are inaccessible under normal circumstances, and deep brain stimulation electrode recordings offer an opportunity to understand the neurophysiological interactions ofdeeper brain structures.

In this thesis, I investigated deep brain stimulation recordings from implanted electrodes in chronic neuropathic pain subjects in the right and left anterior cingulate cortices, the ventral posterior lateral nucleus of the thalamus and periventricular gray region.

The objectives of this research were to elucidate the feed-forward mechanisms of volitional breathing, cortical autonomic regulation, and to investigate whether any of the investigated nuclei haveany carbon dioxide-sensitive neurons which may encode respiratory sensation.

The results show lateralisation of the cortical autonomic control whereby the left anterior cingulate exhibits increases in beta band activity (30 to 90 Hz) with cognition and vocalisation tasks. Meanwhile, right anterior cingulate activity increases with hyperoxia. Respiration using various carbon dioxide concentrations shows a constant rise in the alpha band (8 to 14 Hz) activity in the PVG which suggests a sensitive, nonspecific neuronal activity related to systemic carbon dioxide levels.

Contents

1 Overview **1**

2 Respiratory Physiology **3**

2.1 Respiratory Cortex 5

2.2 Volitional Breathing 7

2.3 Brain Stem Respiratory Control 8

2.4 Autonomic Influence on Respiration 10

2.5 Neuroimaging in Respiration 11

2.6 Conclusion 13

3 Neuroanatomy of the Anterior Cingulate, Periaqueductal Grey Area and the Ventroposterolateral nucleus of the Thalamus **14**

3.1 The Anterior Cingulate Cortex 17

3.1.1 The Radiological Anatomy of ACC 18

3.1.2 The Cellular Architecture of The ACC 18

3.1.3 The Functional Role of The ACC 19

3.2 The Periaqueductal Gray 22

3.2.1 The Radiological Anatomy of PAG 23

3.2.2 The Cellular Architecture of PAG 23

3.2.3 The Functional Role of PAG 24

3.3 The Ventral Posterior Lateral Nucleus of Thalamus 25

3.3.1 The Cellular Architecture of VPL 26

3.4 Conclusion 26

4 Deep Brain Stimulation **27**

4.1 The Surgical Approach 28

4.2 The Mechanics and Benefits of DBS 29

4.3 Conclusion 30

5 Aims of the Experiments **31**

5.1 The Aims 32

5.2 Conclusion 35

6 Research Methodology **36**
6.1 Demographics 37
6.2 The Experiments 40
6.2.1 Room Air 40
6.2.2 Volitional Breathing 40
6.2.3 Gases Experiment 41
6.2.4 Mental Tasks 42
6.2.5 Summary of Experimental Paradigm 42
6.3 Signal Processing and Analysis 43
6.3.1 Signal Acquisition 43
6.3.2 Post Processing 43
6.3.3 Signal Processing Script 47
6.4 Heart Rate Variability 48
6.5 DBS Electrode Localisation 52
6.6 Electrode Localisation Script 54
6.7 Statistical Analysis 56
6.7.1 Kruskal Wallis and Post Hoc Dunn Sidak Script 56
6.7.2 Kruskal Wallis and Post Hoc Dunn Sidak Result 58
6.8 Conclusion 59

7 Cardiovascular and Respiratory Changes **61**
7.1 Respiratory Changes 62
7.2 Cardiovascular Changes 66
7.3 Discussion 69
7.4 Conclusion 71

8 Volitional Breathing **72**
8.1 Room Air Result . . . 73
8.1.1 Inspiration Phase . . . 73
8.1.2 Expiration Phase . . . 75
8.2 Breath Hold Result . . . 76
8.2.1 Inspiration Phase . . . 77
8.2.2 Expiration Phase . . . 78
8.3 Deep Inspiration Result . . . 80
8.3.1 Inspiration Phase . . . 81
8.3.2 Expiration Phase . . . 82
8.4 Hyperventilation Result . . . 84
8.4.1 Inspiration Phase . . . 84
8.4.2 Expiration Phase . . . 86
8.5 Discussion . . . 88
8.6 Conclusion . . . 92

9 Various Gas Compositions **93**
9.1 100 Percent Oxygen Results . . . 94
9.1.1 Inspiration Phase . . . 94
9.1.2 Expiration Phase . . . 96
9.2 1 Percent CO2 Results . . . 98
9.2.1 Inspiration Phase . . . 98
9.2.2 Expiration Phase . . . 100
9.3 3 Percent CO2 Results . . . 102
9.3.1 Inspiration Phase . . . 103
9.3.2 Expiration Phase . . . 104
9.4 5 Percent CO2 Results . . . 106
9.4.1 Inspiration Phase . . . 106
9.4.2 Expiration Phase . . . 108
9.5 7 Percent CO2 Results . . . 110
9.5.1 Inspiration Phase . . . 110
9.5.2 Expiration Phase . . . 112
9.6 Discussion . . . 114

9.7 Conclusion 117

10 Mental Tasks **118**

10.1 Mental Arithmetic Result 119

10.1.1 Inspiration Phase 119

10.1.2 Expiration Phase 121

10.2 Word Recall Results 123

10.2.1 Inspiration Phase 123

10.2.2 Expiration Phase 125

10.3 Discussion 127

10.4 Conclusion 129

11 Conclusion **130**

11.1 Future work 133

A Post Hoc Analysis Result **134**

List of Figures

2.1 Ergometer preserved in Department of Anatomy, Physiology and Genetics, Oxford University 5

3.1 Anterior Commisure in axial view. 15
3.2 Posterior Commisure in axial view. 16
3.3 Anterior horn of the lateral ventricle in axial view. 16
3.4 Anterior horn of the lateral ventricle in sagittal view. 17

6.1 The floor plan of experiment room and equipment placement. 38
6.2 Face mask was selected for its tight seal, easy quick release and its comfort. 39
6.3 Penlon gas mixer courtesy of Dr Keith Dorrington, DPAG, Oxford University. 39
6.4 The end tidal carbon dioxide recording showing the change from room air to 100% oxygen, 3%, 1%, 7% and 5% CO2 41
6.5 The summary of experiment protocols. 42
6.6 The raw data in SPIKE2 software showing the local field potentials, the electrocardiogram and end tidal carbon dioxide recording. 43
6.7 A 6 panel overview of LFP recordings. Channel 1 to 3 were from the left anterior cingulate and channel 4 to 6 were from the right anterior cingulate. Channel 5 and 6 recording were faulty recordings. 44
6.8 A single breath tracing of end tidal carbon dioxide showing a transition from inspiration to expiration phase marked by a vertical line. 45
6.9 A 6 panel overview of time frequency analysis result. Channel 1 to 3 were from the left anterior cingulate and channel 4 to 6 were from the right anterior cingulate. Channel 5 and 6 shows the result of faulty recordings. 46
6.10 Physical comparison of Medtronic Model 3387 deep brain stimulation electrode to 1 pound coin. 53

7.1 The mean respiratory rate of all experiment conditions. 63
7.2 The mean respiratory phase of all experiment conditions. 64
7.3 The mean heart rate of all experiment conditions. 67
7.4 The heart rate variability in all experiment conditions. 68

8.1 Time frequency analysis of bilateral ACC, VPL and PVG while breathing room air.The transition of respiratory phase is marked with vertical line. 73
8.2 The summary of mean total power spectra in Delta, Theta, Alpha, Beta and Gamma band during inspiration phase using room air in ACCL, ACCR, VPL and PVG. 74
8.3 The summary of mean total power spectra in Delta, Theta, Alpha, Beta and Gamma band during expiration phase using room air in ACCL, ACCR, VPL and PVG. 75
8.4 Time frequency analysis of bilateral ACC, VPL and PVG while in inspiration phase and during the breath hold phase. The transition of respiratory phase is marked with vertical line. 76
8.5 The summary of mean percentage change in power spectra in Delta, Theta, Alpha, Beta and Gamma band during inspiration phase before breath hold ACCL, ACCR, VPL and PVG compared to quiet inspiration at room air. 77
8.6 The summary of mean percentage change in power spectra in Delta, Theta, Alpha, Beta and Gamma band during expiration breath hold phase in the ACCL, ACCR, VPL and PVG compared to quiet expiration at room air. . . 78
8.7 Time frequency analysis of bilateral ACC, VPL and PVG while performing deep inhalation. The transition of respiratory phase is marked with vertical line. 80
8.8 The summary of mean percentage change in power spectra in Delta, Theta, Alpha, Beta and Gamma band during inspiration phase of deep inspiration in ACCL, ACCR, VPL and PVG compared to quiet inspiration at room air. 81
8.9 The summary of mean percentage change in power spectra in Delta, Theta, Alpha, Beta and Gamma band during expiration phase of deep inspiration in ACCL, ACCR, VPL and PVG compared to quiet inspiration at room air. 82
8.10 Time frequency analysis of bilateral ACC, VPL and PVG while performing voluntary hyperventilation. The transition of respiratory phase is marked with vertical line. 84

8.11 The summary of mean percentage change in power spectra in Delta, Theta, Alpha, Beta and Gamma band during inspiration phase of voluntary hyperventilation in ACCL, ACCR, VPL and PVG compared to quiet inspiration at room air. 85
8.12 The summary of mean percentage change in power spectra in Delta, Theta, Alpha, Beta and Gamma band during expiration phase of voluntary hyperventilation in ACCL, ACCR, VPL and PVG compared to quiet inspiration at room air. 86

9.1 Time frequency analysis of bilateral ACC, VPL and PVG while breathing 100% oxygen. The transition of respiratory phase is marked with vertical line. 94
9.2 The summary of mean percentage change in power spectra in Delta, Theta, Alpha, Beta and Gamma band during inspiration phase using 100% oxygen in ACCL, ACCR, VPL and PVG compared to quiet inspiration at room air. 95
9.3 The summary of mean percentage change in power spectra in Delta, Theta, Alpha, Beta and Gamma band during expiration phase using 100% oxygen in ACCL, ACCR, VPL and PVG compared to quiet expiration at room air. 96
9.4 Time frequency analysis of bilateral ACC, VPL and PVG while breathing 1% carbon dioxide. The transition of respiratory phase is marked with vertical line. 98
9.5 The summary of mean percentage change in power spectra in Delta, Theta, Alpha, Beta and Gamma band during inspiration phase using 1% carbon dioxide in ACCL, ACCR, VPL and PVG compared to quiet inspiration at room air. 99
9.6 The summary of mean percentage change in power spectra in Delta, Theta, Alpha, Beta and Gamma band during expiration phase using 1% carbon dioxide in ACCL, ACCR, VPL and PVG compared to quiet expiration at room air. 100

9.7 Time frequency analysis of bilateral ACC, VPL and PVG while breathing 3% carbon dioxide. The transition of respiratory phase is marked with vertical line. 102
9.8 The summary of mean percentage change in power spectra in Delta, Theta, Alpha, Beta and Gamma band during inspiration phase using 3% carbon dioxide in ACCL, ACCR, VPL and PVG compared to quiet inspiration at room air. 103
9.9 The summary of mean percentage change in power spectra in Delta, Theta, Alpha, Beta and Gamma band during expiration phase using 3% carbon dioxide in ACCL, ACCR, VPL and PVG compared to quiet expiration at room air. 104
9.10 Time frequency analysis of bilateral ACC, VPL and PVG while breathing 5% carbon dioxide. The transition of respiratory phase is marked with vertical line. 106
9.11 The summary of mean percentage change in power spectra in Delta, Theta, Alpha, Beta and Gamma band during inspiration phase using 5% carbon dioxide in ACCL, ACCR, VPL and PVG compared to quiet inspiration at room air. 107
9.12 The summary of mean percentage change in power spectra in Delta, Theta, Alpha, Beta and Gamma band during expiration phase using 5% carbon dioxide in ACCL, ACCR, VPL and PVG compared to quiet expiration at room air. 108
9.13 Time frequency analysis of bilateral ACC, VPL and PVG while breathing 7% carbon dioxide. The transition of respiratory phase is marked with vertical line. 110
9.14 The summary of mean percentage change in power spectra in Delta, Theta, Alpha, Beta and Gamma band during inspiration phase using 7% carbon dioxide in ACCL, ACCR, VPL and PVG compared to quiet inspiration at room air. 111

9.15 The summary of mean percentage change in power spectra in Delta, Theta, Alpha, Beta and Gamma band during expiration phase using 7% carbon dioxide in ACCL, ACCR, VPL and PVG compared to quiet expiration at room air. 112

10.1 Time frequency analysis of bilateral ACC, VPL and PVG while performing mental arithmetic. The transition of respiratory phase is marked with vertical line. 119
10.2 Summary of percentage change in Delta, Theta, Alpha, Beta and Gamma band during inspiration phase of mental arithmetics in ACCL, ACCR, VPL and PVG. 120
10.3 Summary of percentage change in Delta, Theta, Alpha, Beta and Gamma band during expiration phase and vocalisaton of mental arithmetics in ACCL, ACCR, VPL and PVG. 121
10.4 Time frequency analysis of bilateral ACC, VPL and PVG while performing word recall and vocalisation. The transition of respiratory phase is marked with vertical line. 123
10.5 Summary of percentage change in Delta, Theta, Alpha, Beta and Gamma band during inspiration phase of word recall in ACCL, ACCR, VPL and PVG.124
10.6 Summary of percentage change in Delta, Theta, Alpha, Beta and Gamma band during expiration and vocalisation phase of word recall in ACCL, ACCR, VPL and PVG. 125

List of Tables

6.1 Demographic summary of research participants 37
6.2 Mean Electrode Contact In MNI Space 53

7.1 The mean respiratory rate and phases in all experimental conditions. . . 63
7.2 The mean heart rate and HRV result of all experiment conditions. 67

A.1 Kruskal Wallis Delta ACCL Inspiration 135
A.2 Kruskal Wallis Delta ACCL Expiration 136
A.3 Kruskal Wallis Theta ACCL Inspiration 137
A.4 Kruskal Wallis Theta ACCL Expiration 138
A.5 Kruskal Wallis Alpha ACCL Inspiration 139
A.6 Kruskal Wallis Alpha ACCL Expiration 140
A.7 Kruskal Wallis Beta ACCL Inspiration 141
A.8 Kruskal Wallis Beta ACCL Expiration 142
A.9 Kruskal Wallis Gamma ACCL Inspiration 143
A.10 Kruskal Wallis Gamma ACCL Expiration 144
A.11 Kruskal Wallis Delta ACCR Inspiration 145
A.12 Kruskal Wallis Delta ACCR Expiration 146
A.13 Kruskal Wallis Theta ACCR Inspiration 147
A.14 Kruskal Wallis Theta ACCR Expiration 148
A.15 Kruskal Wallis Alpha ACCR Inspiration 149
A.16 Kruskal Wallis Alpha ACCR Expiration 150
A.17 Kruskal Wallis Beta ACCR Inspiration 151
A.18 Kruskal Wallis Beta ACCR Expiration 152
A.19 Kruskal Wallis Gamma ACCR Inspiration 153
A.20 Kruskal Wallis Gamma ACCR Expiration 154
A.21 Kruskal Wallis Delta VPL Inspiration 155
A.22 Kruskal Wallis Delta VPL Expiration 156
A.23 Kruskal Wallis Theta VPL Inspiration 157
A.24 Kruskal Wallis Theta VPL Expiration 158
A.25 Kruskal Wallis Alpha VPL Inspiration 159
A.26 Kruskal Wallis Alpha VPL Expiration 160

A.27 Kruskal Wallis Beta VPL Inspiration 161
A.28 Kruskal Wallis Beta VPL Expiration 162
A.29 Kruskal Wallis Gamma VPL Inspiration 163
A.30 Kruskal Wallis Gamma VPL Expiration 164
A.31 Kruskal Wallis Delta PVG Inspiration 165
A.32 Kruskal Wallis Delta PVG Expiration 166
A.33 Kruskal Wallis Theta PVG Inspiration 167
A.34 Kruskal Wallis Theta PVG Expiration 168
A.35 Kruskal Wallis Alpha PVG Inspiration 169
A.36 Kruskal Wallis Alpha PVG Expiration 170
A.37 Kruskal Wallis Beta PVG Inspiration 171
A.38 Kruskal Wallis Beta PVG Expiration 172
A.39 Kruskal Wallis Gamma PVG Inspiration 173
A.40 Kruskal Wallis Gamma PVG Expiration 174

List of Acronyms

ECG electrocardiography

ANOVA one-way analysis of variance

ETCO2 end tidal carbon dioxide

CO2 carbon dioxide

STFT Short time Fourier transformation

HRV heart rate variability

CRW Cosman-Roberts-Wells

IPG implanted pulse generator

GPi globus pallidus interna

STN sub thalamic nuclei

vlPAG ventral lateral periaqueductal gray

lPAG lateral periaqueductal gray

dlPAG dorsal lateral periaqueductal gray

dmPAG dorsal medial periaqueductal gray

EEG Electroencephalography

MRI Magnetic Resonance Imaging

fMRI functional Magnetic Resonance Imaging

CT Computed Tomography

PET Positron Emmission Tomography

KF/PB Kolliker Fuse nucleus or parabrachial complex

pXII parahypoglossal

rVRG rostral ventral respiratory group

RTN/pFRG retrotrapezoid nucleus/parafacial respiratory group

preBotC prebotzinger complex

VPL ventral posterior lateral

ACC anterior cingulate cortex

PAG periaqueductal gray

PVG periventricular gray

DBS Deep Brain Stimulation

LFPs Local field potentials

PPN pedunculopontine nucleus

1 Overview

From birth, breathing is almost an automatic process to which we hardly pay any attention. It is a robust system whose primary objective is to supply fresh oxygen and remove carbon dioxide from the systemic circulation. The respiratory system is tightly coupled with the cardiovascular system and plays a part in a homeostatic role to maintain a balanced body pH.

Humans area social species, and we communicate with each other using speech and language, emotion and body movements. A unique human skill that sets us apart from other non-human primates is our ability to control air flow through the vocal cords and pharyngeal muscles to produce sounds for speech. Modification of air flow through the vocal cords allows production of intelligible sounds which forms words and language.

More complex modifications take place while singing or playing wind instruments. The ability to volitionally hold one's breath for a limited period gives an opportunity to swim underwater or to prevent smoke inhalation in survival situations. The seamless integration of brainstem respiratory patterns with cortical input allows humans to exhibit complex behaviour and expression as seen in excitement or grief. Exercise and postural change can be performed without any predetermined cognition to initiate hyperventilation. While we understand how the respiratory rhythm is generated in the brainstem, we do not have clear evidence on how cortical signals modulate these respiratory patterns.

Local field potential (LFP) recording is gaining ground as a neurophysiological experimental tool in Parkinson's Disease as well as in exercise physiology. Recent literature on cardiorespiratory exercise physiology has suggested a role of neurons oscillating at frequencies in the beta and gamma bands in feedforward signals recorded in human periventricular gray (PVG).

Imagined exercise requires a thought process or intention to move specific muscle groups in the limbs before the actual movement. This process includes feed forward commands to the autonomic system, cardio-respiratory centres and muscles. It also needs to integrate the feedback system to receive inputs to match the intended movements such as muscle joint position and hand-eye coordination.

Volitional breathing requires large muscle movements and the intention to move specific muscle groups is a prerequisite. The focus of this thesis is on the analysis of LFPs associated with volitional breathing patterns as a tool to investigate brain function.

I discuss the relevant human respiratory physiology in CHAPTER 2 (chapter 2), the anatomy of the anterior cingulate cortex (ACC), ventral posterior lateral (VPL) nucleus of the thalamus and PVG in CHAPTER 3 (chapter 3).

I briefly discuss deep brain stimulation in CHAPTER 4 (chapter 4), on which the main research subjects and methods were based. I present my hypothesis and the strategy I developed to answer my research hypotheses in CHAPTER 5 (chapter 5). Subsequently, I discuss the experimental methods in CHAPTER 6 (chapter 6).

The results are discussed in individual chapters starting with the cardiovascular and respiratory changes in CHAPTER 7 (chapter 7). The effects of volitional breathing on local field potentials are discussed in CHAPTER 8 (chapter 8), and the effects of respiration using various gas compositions are discussed in CHAPTER 9 (chapter 9). The impact of mental tasks on the local field potential are discussed in CHAPTER 10 (chapter 10). Finally, I conclude my thesis and the future work I intend to do in CHAPTER 11 (chapter 11).

2
Respiratory Physiology

Knowledge of the respiratory system has evolved over a few millennia. Air was initially regarded as the essence of life for animated living objects which eventually die when the air supply is cut off. This idea was recorded in Ancient Indian texts as well as by Greek scholars relating the philosophical relationship between air and life [Fitzgerald and Cherniack 2012].

Modern respiratory physiology emphasises the importance of evidence, thus experiments have been conducted to identify gas composition and the mechanics of breathing. The efforts to understand respiratory control were led by Haldane, Douglas and Campbell in the Physiological Laboratory at Oxford University during the earlier part of the twentieth century [Campbell et al. 1913, Douglas and Haldane 1909, Haldane and Priestley 1905].

Haldane and co-workers investigated the role of carbon dioxide in respiration and found that end tidal carbon dioxide remained constant in a person throughout their life. This suggests that the respiratory system works to keep a set point. The group also found that when carbon dioxide is added to an air mixture, an exaggerated respiratory response can be elicited [Douglas and Haldane 1909, Haldane and Priestley 1905].

Meanwhile, the Copenhagen group led by Lindhard, studied alveolar gas composition and its relation to respiratory control. In experiments using a cycle ergometer see Figure 2.1, Lindhard reported an increase in respiration and heart rate just before the

start of exercise and these increments did not match either the timing of exercise or alveolar gas analysis [Lindhard 1911].

Cardiorespiratory responses observed in exercise are at least partly due to increased peripheral demand of blood and oxygen associated with vasodilatation of the skeletal muscles. Peripheral vasodilatation triggers a cascading reaction that stimulates the autonomic nervous system that in turn stimulates cardiorespiratory centres.

Lindhard argued that the brain possibly has a strategy to prepare the body for the expected demand [Lindhard 1911]. The higher cortex has an influence in modifying the cardiorespiratory system prior to the physical activity and this is termed 'central command' [Krogh and Lindhard 1913].

In recent years, advanced research in exercise physiology has used Local field potentials (LFP) to detect feed-forward or central command signals. These studies were, however, unable to uncouple the respiration from the cardiovascular response [Basnayake et al. 2011; 2012, Green and Paterson 2008, Green et al. 2007b].

In this thesis, I use LFP recorded in awake humans to study the electrical activity related to volitional breathing. Inhalation of various gas composition and a mental task experiment were designed to provide an automatic respiratory response as a contrast to voluntary breathing.

Figure 2.1 Ergometer preserved in Department of Anatomy, Physiology and Genetics, Oxford University

2.1 Respiratory Cortex

Every muscle in the body has a motor representation in the cerebral cortex. This idea was championed by Hughling Jackson when he observed a characteristic 'march' of symptoms during focal motor seizures in epileptic patients. He mooted the idea of an 'electrical propagation' concept of the nervous system which suggested a laterality of the human body to the contralateral brain [York and Steinberg 2011].

Foerster demonstrated 'Jacksonian March' clinically by stimulating the motor cortex with electrical current during neurosurgical operations. He localised an area that corresponds to the respiratory muscles along the precentral gyrus in the parietal area [Foerster 1936].

A report by Penfield further enriched our understanding of cortical areas that have distinct motor, sensory and associative functions [Penfield 1947]. Bucy reported that electrical stimulation of the precentral gyrus results in contraction of respiratory muscles and it also has a role in upper airway muscle coordination [Bucy and Case 1936]. A clinical case in which electrical stimulation of the pre central gyrus of the oral region resulted in respiratory arrest in a human was also reported [Bucy and Case 1936].

In the 1930s, many animal experiments were conducted to study the effects of electrical stimulation of various parts of the brain. Experiments in anaesthetised dogs showed that electrical stimulation of the ACC produced an increase in respiratory rate and subsequent respiratory arrest [Bucy and Case 1936].

Experiments in anaesthetised monkeys showed that electrical stimulation of the medial pre motor cortex resulted in an increase in respiratory rate while electrical stimulation to the lateral part of the pre-motor cortex produced respiratory inhibition [Smith 1938]. As well as respiratory muscle contraction, locomotion was observed in the limbs of cats and dogs when electric current was passed through the thalamus [Eldridge et al. 1985].

Electrical stimulation of non-anaesthetised animal brains resulted in 'expected' cardiorespiratory changes and were often observed together with behavioural changes [Talairach et al. 1973]. Low to moderate (60 Hz square wave) electrical stimulation of the rostral cingulate cortex and the limbic system in both human and non-human primates has been shown to increase respiratory rate, produces vocalisation, dilates the pupils, cause piloerection on the neck and an elevated heart rate [Kaada 1952, Smith 1938; 1945].

A strong electrical stimulation of the rostral cingulate, on the other hand, causes bradycardia, respiratory arrest in expiration, followed by drop in blood pressure [Kaada et al. 1949]. In addition, any movement of limbs ceases immediately. Following a strong electrical current, the non-human primate's limbs were flaccid, the eyes closed, and the respiratory rate reduced [Smith 1945]. These observation are similarly seen during the induction of general anaesthesia [Fink 1961b].

Clinical observation supports the hypothesis of cortical influences to brainstem respiratory regulation during the awake state in that humans areable to perform volitional breathing without much difficulty [Fink 1961a;b, Haouzi et al. 2006, Shea 1996].

2.2 Volitional Breathing

Volitional breathing is a deliberate act to modify regular respiratory patterns. Cortical influences seamlessly integrate with the brainstem respiratory rhythm generators and this is reflected by uninterrupted transition from automatic respiratory rhythm to cortical command and back to brainstem control.

The motives behind volitional control depends on environmental circumstances. For example, one may need to increase the tidal volume and prolong the expiration phase whilst singing or playing a wind instrument. On the other hand, one takes a deep breath and holds it when trying to swim under water.

Breath holding underwater is a complex physiological process that differs from person to person, based on sex and fitness level [Castellini 2012, Cherouveim et al. 2013]. During breath hold, the sympathetic nervous system is recruited in order to maintain blood pressure through an increase in vascular tone. The changes can be measured by muscle sympathetic nerve activity of the peroneal nerve using miconeurography [Macefield et al. 2006].

Psychological factors play an important role in determining breath holding 'breaking points', with an optimistic personality being able to hold their breath longer under water as compared to a pessimist [Parkes 2006; 2012]. The mechanism of higher centre modulation is not entirely understood as compared to its brainstem counterpart.

The input from higher centres during the awake state requires an instant modification of breathing pattern while responding to the environment. This modification can be divided into 'explicit' breath control e.g. during singing or defecation and 'implicit' breath control such as during swallowing, change in posture or during exercise [Shea 1996].

The role of the primary cortex in control of inspiratory muscle contraction has been demonstrated in a clinical setting [Foerster 1936, Penfield 1947]. Recently, non-invasive trans-cranial magnetic stimulation to the motor cortex has been shown to contract the contralateral diaphragm [Corfield et al. 1998, Hopkinson et al. 2004, Maskill et al. 1991, Sharshar et al. 2003, Straus et al. 2004].

Electroencephalography during volitional breathing shows an increase in delta frequency band activity as compared to automatic respiration at rest [Macefield and Gandevia 1991].

In summary, volitional control of breathing involves a neural network composed of both primary motor and sensory cortices, basal ganglia, thalamus, limbic system, cerebellum and brainstem [Colebatch et al. 1991, Corfield et al. 1995, Evans et al. 1999, McKay et al. 2003; 2010, Murphy et al. 1997].

Cortical activation and brainstem respiratory rhythms produce similar outcomes i.e. to maintain blood gas homeostasis [Haouzi 2011, Haouzi and Bell 2009]. The structures that generate voluntary and involuntary respiratory patterns are different but integrated in the medulla and brainstem, thus producing the same output activation to respiratory motor neurones [Haouzi et al. 2006, Shea 1996].

2.3 Brain Stem Respiratory Control

Automatic breathing originates in the brain stem pontomedullary regions and passes through the bulbospinal network to the spinal cord anterior horn cells. The oscillatory rhythm of the brainstem responds only to pH and PCO2 [Guz 1997]. Recent literature on respiratory control agrees that there are two central rhythm generators in the brainstem that are distinct in anatomy and function, namely:

1. **The preBotzinger Complex** involved mainly in generating inspiratory rhythms [Feldman and Del Negro 2006, Feldman et al. 2003]. The prebotzinger complex (preBotC) drives the inspiratory activity through projections to premotor neurons in the rostral ventral respiratory group (rVRG) and parahypoglossal (pXII) nucleus that subsequently project to the main inspiratory muscle pumps:

    - The diaphragm,
    - The external intercostal muscles,
    - The laryngeal and tongue muscles.

2. **The retrotrapezoid nucleus/parafacial respiratory group** is a nucleus involved in the generation of active expiration [Janczewski and Feldman 2006]. The retrotrapezoid nucleus/parafacial respiratory group (RTN/pFRG) also has a similar network to the pre-motor neurons and is very specific to a muscular group that drives active expiration i.e.:

- The abdominal muscles,
- The internal intercostal muscles,
- The laryngeal and tongue muscles.

There are several mechanisms that can alter brainstem respiratory rhythms. These include neuro-modulatory, suprapontine and sensory input [Feldman and Del Negro 2006]. These inputs are essential to alter the normal regulation to meet increasing demand during the initial part of exercise, or during emotional output such as laughing, crying or shouting. Vocalisation, singing, and diving under water increase respiratory demand too [Boiten 1998].

During automatic respiration, brainstem nuclei send out bursts of signals to trigger inspiratory muscule contraction and re-polarisation of these neurons produces a passive recoil of the lung during expiration. However, during exercise, or fight/flight situations, there is a shift from passive expiration to active expiration. This change is mainly due to activation of RTN/pFRG [Janczewski and Feldman 2006]. These neurons are postulated to be conditionally active and quiet under resting breathing.

The activation of RTN/pFRG is possibly due to desynchronisation of preBotC and RTN/pFRG at the end of inspiration. During this phase, the RTN/pFRG signal is more prominent and promotes active expiration [Richter 1982, Richter and Smith 2014].

The Kolliker Fuse nucleus or parabrachial complex in the dorsal rostral pons is thought to be activated in breathing, as demonstrated using functional Magnetic Resonance Imaging (fMRI) in humans [Pattinson et al. 2009b]. The structure of Kolliker Fuse nucleus or parabrachial complex (KF/PB) has only recently been studied in humans [Block and Estes 1990, Lavezzi et al. 2004].

These structures however are well studied in rat models. They are the target nuclei for the nucleus tractus solitarius and they have connections to the limbic system, including the thalamus, amygdala, and insula, as well as the respiratory column in the ventral lateral medulla [Dutschmann and Herbert 2006].

KF/PB receives afferent signals from the vagus via pulmonary stretch receptors and glossopharyngeal nerves from peripheral chemoreceptors. These connections are important for integration of sensory processing to respiratory signals.

2.4 Autonomic Influence on Respiration

The lowest blood pressure is recorded at the peak of inspiration and the highest blood pressure can be recorded at peak expiration. The body achieves blood pressure homeostasis by modifying the peripheral vascular tone [Guyenet 2006, Pilowsky 2009].

This observation was correlates with muscle sympathetic nerve activity [Macefield et al. 2006] thus, it appears that the sympathetic nervous system has a role in respiratory control [Adrian 1933, Montano et al. 2001, Pilowsky 2009, Pitsikoulis et al. 2008].

The thalamus is an important autonomic regulator in animals, where electrical stimulation of the structure increases respiratory rate together with an increase in the heart rate [Kabat et al. 1935, Kabat 1936, Ranson 1933, Smith 1938].

These cardiorespiratory changes are related to animal behaviour, where electrical stimulation to the thalamus or the limbic systems produces vocalisation, pupillary dilatation and piloerection [Kaada 1952, Ranson 1933, Smith 1938]. Electrical stimulation to the anterior cingulate may also produce similar cardiorespiratory changes [Kaada et al. 1949, Kaada 1952].

Respiratory rate typically increases during wakefulness and the vigilant state, compared to sleep [McCrimmon et al. 2008]. This is due to multi sensorial inputs that modify our respiratory responses to the environment. Trigeminal nerve stimulation of the face by using a face mask or nose clip increases the respiration rate at rest [Golla et al. 1928, Golla and Antonovich 1929].

Respiration can be entrained by visual cues such as breathlessness being felt by an observer at of the sight of another person experiencing breathlessness [Kuroda et al. 2012].

An auditory signal is also capable of entraining the respiratory pattern. For example, listening to classical music may lower the respiratory rate whilst modern rock with a loud bass may do the reverse [Shea 1996, Shea et al. 1987, Thaut 2013].

At rest, the respiratory output is regulated by the brainstem whereas behavioural and voluntary breathing is regulated by the higher centres [Von Euler 2011]. Anxiety and mental stress can change the respiratory pattern through the autonomic nervous system [Homma and Masaoka 2008, Masaoka and Homma 1997; 2001, Wuyts et al. 2011].

Subtle increases in respiratory response can be observed implicitly during the start of exercise or while having an emotional breakdown and it can be explicitly expressed during singing or playing a wind instrument [Bass and Gardner 1985, Golla et al. 1928].

2.5 Neuroimaging in Respiration

Several studies using Positron Emmission Tomography (PET) report increased cerebral blood flow in the motor cortex, thalamus and cerebellum during volitional breathing [Colebatch et al. 1991, Evans et al. 1999, Fink et al. 1996, Schulz et al. 2005].

The pre-motor cortex is active in both voluntary breathing and speech as investigated using PET and fMRI [McKay et al. 2003, Murphy et al. 1997, Perry et al. 1999].

Rapid technological advancement in fMRI in recent years has largely superseded PET imaging as the former offers a superior spatial and temporal resolution [Abbott et al. 2005, Brannan et al. 2001, Evans et al. 1999, Li et al. 2006, Macey et al. 2003, Nakayama et al. 2002, Pattinson et al. 2009a, Woo et al. 2005].

Recent investigation of brainstem input during respiration using fMRI shows activation in the thalamus, periaqueductal grey and pons in CO2-stimulated breathing [Pattinson et al. 2009a]. This observation is in agreement with thalamic activity in cats and dogs [Chen et al. 1991; 1992, Eldridge and Chen 1992].

Breathlessness and pain research utilising fMRI shows that the anterior cingulate, insular and thalamus are activated when these two negative components were tested in normal healthy volunteers. This has led to the postulation that negative valences share similar networks in the higher cortex [Schön et al. 2008, von Leupoldt 2005a, von Leupoldt et al. 2007; 2009, von Leupoldt 2005b].

Neuroimaging supports MacLean's [Maclean 1955a] postulation that a role of the anterior cingulate in mammals is to decode unpleasant sensations in order to aid survival [Hsieh et al. 1999, Lenz et al. 1998, MacLean and Newman 1988, Vogt et al. 1992, Vogt 2005].

Similar areas within the anterior cingulate and the limbic system are also activated by CO2-stimulated breathing [Corfield et al. 1995, Guz 1997, Pattinson et al. 2009b].

Interestingly, respiration using 100% oxygen increases the activity of the right insula, thalamus and the anterior cingulate when investigated using fMRI in children [Macey et al. 2007, Woo et al. 2005].

These areas of activation were reduced to baseline when 5% carbon dioxide was mixed with 95% oxygen. The authors [Macey et al. 2007] argue that autonomic nervous system activation is a probable cause for the findings as these structures are related to the autonomic system.

The great American psychologist, William James defined attention as

> *'the taking of possession by the mind in clear and vivid form of one, out of hat seems several simultaneous possible objects or trains of thoughts'.*

William James suggests that when the brain is confronted with multiple inputs at one point of time, it does not process all inputs equally and the output performance is dependent on the tuning and timing of the brain at the right time. There are 3 simultaneous tasks that the brain needs to perform during an attention task:

- Increased sensitivity of a particular sensation and/or suppressing other sensations
- Prepare anticipation neurons that are related to stimulus response
- Increase the blood flow to the anticipatory neurons in the brain.

The above suggests that the when the brain is fed with multiple sensations, only one domain is dominant and the system needs more energy to sustain continuous attention. This attention theory has been tested using PET and fMRI where, during a Stroop task and learning, the left anterior cingulate activity increases compared to the resting state. As the subject become proficient with the Stroop task, the cingulate activation returns to the baseline activity [Posner 1993, Posner et al. 2007].

fMRI experiments investigating anticipation show a positive correlation with autonomic function, especially in the right anterior cingulate and the right dorsolateral prefrontal cortex [Critchley et al. 2001].

Using a similar technique, cognitive tasks and coordinated motor movement show increased activity in bilateral cingulate regions, insula, thalamus and inferior parietal somatosensory cortices associated with increased heart rate variability [Critchley et al. 2003].

Visualising emotional facial expression and anticipating error during a task increases the heart rate variability and fMRI of the brain shows similar limbic activation that

supports the role of the cingulate in the autonomic nervous system [Critchley et al. 2005a;b].

Taking the neuro-imaging results together with attention, anticipation and cognition theory, it could be argued that cerebral activation detected during fMRI is a compound of activity across many nuclei, anticipatory attention signals and cognitive processing [Critchley et al. 2001; 2003; 2005a;b, LaBerge et al. 2000, LaBerge 1990; 2001, Laberge and Brown 1989, Laberge 1990, Pardo et al. 1990; 1991, Posner 1993, Posner et al. 2007].

2.6 Conclusion

In conclusion, the cortical motor control of respiratory muscles in humans has been identified in the pre-central motor region as demonstrated in neurosurgical cases and recently using transcranial magnetic stimulation. Electrical stimulation to the anterior cingulate gyrus, the thalamus and the limbic system in general shows that limbic system activation is capable of producing cardiorespiratory response with behavioural components. fMRI investigations show that the anterior cingulate and thalamus play roles in cognition, anticipation, attention and central autonomic control.

3

Neuroanatomy of the Anterior Cingulate, Periaqueductal Grey Area and the Ventroposterolateral nucleus of the Thalamus

The neuroanatomy and functional comparison between ACC, VPL nucleus of thalamus and PVG will be reviewed in this chapter.

Anterior Commissure is a common reference in radiological imaging where a transverse anterior band crosses the midline anterior to the anterior wall of the fornices, see Figure 3.1. It consists of white matter fibres connecting the two hemisphere and the corpus callosum.

Posterior Commissure is a transverse posterior band that crosses the midline and marks the transition between the third ventricles and the aqueduct of Sylvius, see Figure 3.2. It is formed by fibres connecting the caudal wall of the pineal recesses from both sides and its constitution in man is yet to be discovered.

The anterior horns of the ventricles are the anterior most border of the lateral ventricles seen on an axial scan at the mid-pupillary line and they start approximately 4 cm from the anterior border of the frontal lobe, see Figure 3.3 and Figure 3.4.

The anterior and posterior commisure line are commonly used as indirect localisaton of intracerebral anatomy and a reference line for strereotactic surgery. These line are consistent in relation to the thalamus, brain stem and corpus callosum which can guide clinician when revewing low resolution images.

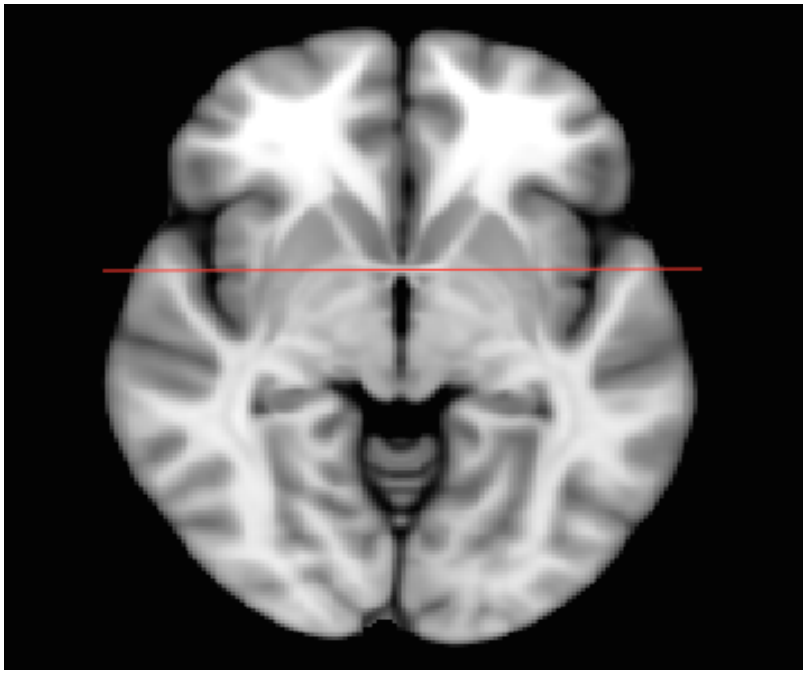

Figure 3.1 Anterior Commisure in axial view.

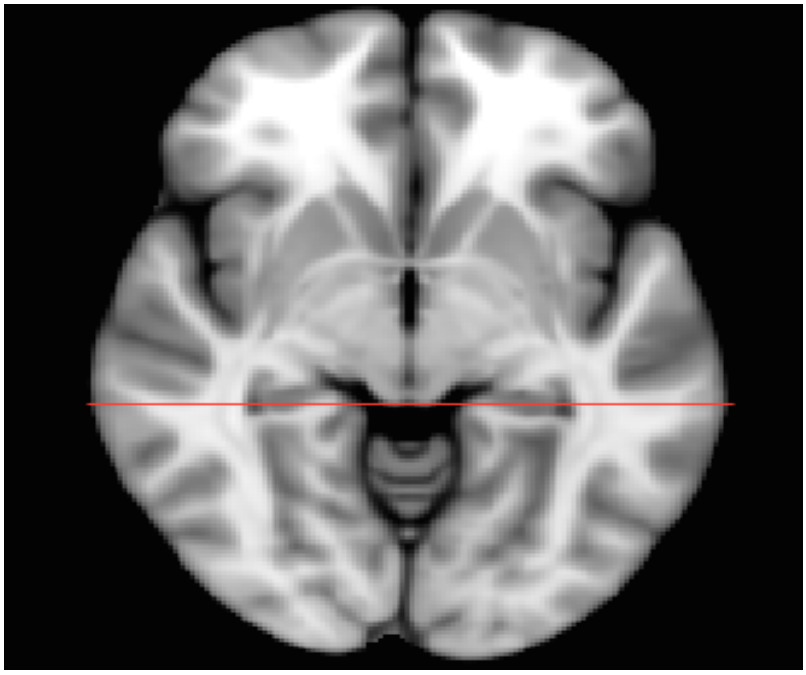

Figure 3.2 Posterior Commisure in axial view.

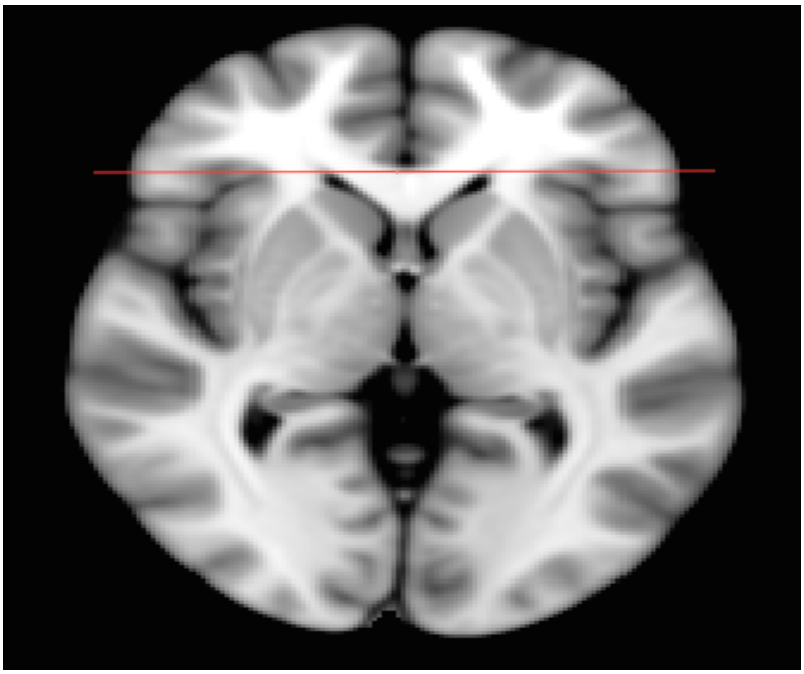

Figure 3.3 Anterior horn of the lateral ventricle in axial view.

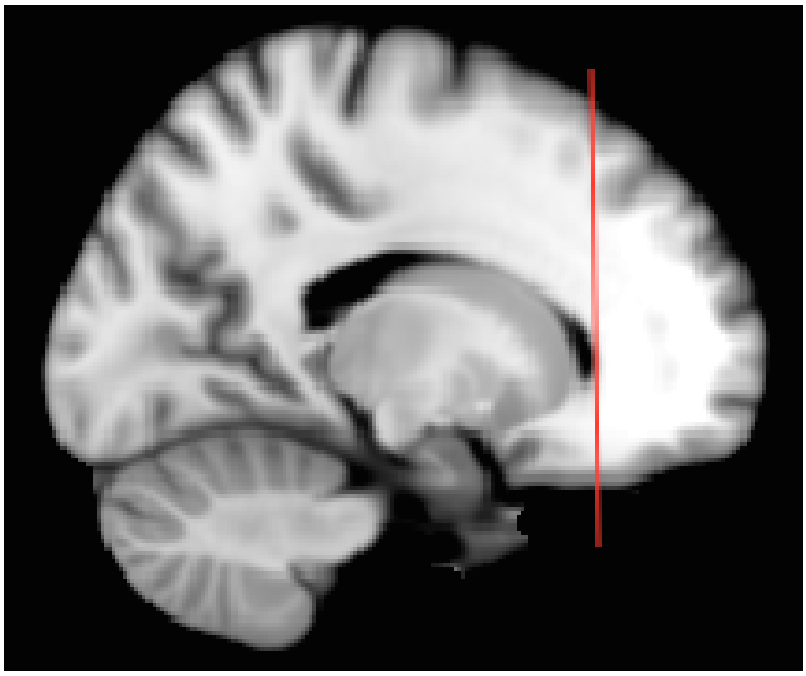

Figure 3.4 Anterior horn of the lateral ventricle in sagittal view.

3.1 The Anterior Cingulate Cortex

The anterior cingulate is a unique structure found in mammals. Its role and function was previously investigated by observing the behaviour of non-human primates.

The cingulate cortices are paired midline structures that occupy the medial wall of each cerebral hemisphere separated by the falx cerebri. They lie immediately dorsal to the corpus callosum and are separated from the frontal and parietal lobes by the cingulate sulci.

The cingulate cortex can be divided into two distinct regions; anterior and posterior, based on cytoarchitecture. The surface of the ACC starts at the genu of the cingulate cortex. Beyond and rostral to this is considered to be the cingulofrontal transition area with a mixture of cingulate, frontal and parietal lobes. The ACC continues posteriorly as the posterior cingulate where it folds to form the marginal ramus covering the corpus callosum.

The shape, size, volume and gyri of the ACC differs from one person to another based on age and gender differences [Paus 2001, Pujol et al. 2002, Vogt et al. 1995]. Pujol suggested that size difference seen in different genders probably contributes to

personality, behaviour and related associated physiological circumstances [Pujol et al. 2002].

3.1.1 The Radiological Anatomy of ACC

The gross radiological anatomy of the anterior border of the ACC can be seen upon viewing Computed Tomography (CT) or Magnetic Resonance Imaging (MRI) images in the axial view and an imaginary line is drawn on the anterior most part of the lateral ventricle. A grid system using standard anatomical landmarks was proposed by Hamani to cater for multifactorial variations of the cingulate. This has been used in particular to refer to inter-subject anatomical variation in order to localise subcategories [Hamani et al. 2009].

In the Oxford Functional Neurosurgery Unit, the neurosurgeons consistently use an area in the cingulate gyrus, 21 mm from the tip of anterior horns, mid pupillary line bilaterally as a target for deep brain stimulation in chronic pain management [Boccard et al. 2013].

3.1.2 The Cellular Architecture of The ACC

The ACC can be divided into sub-regions on the basis of function [Baleydier and Mauguiere 1980, Gasquoine 2013, Vogt et al. 1995, Vogt 2005]:

- Anterior cingulate, Brodmann area 24 and
- Posterior cingulate, Brodmann area 23.

The cells in abundance in ACC are pyramidal cells [Spruston 2008]. Brodmann described the anterior cingulate region area 24 based on cytoarchitecture of different species including humans [Brodmann 1909]. The cytoarchitecture of human cingulate cortex has also been evaluated again using post-mortem sections from 27 neurologically intact individuals [Vogt et al. 1995].

The cellular architecture of this particular region has been postulated to contribute to a higher functional role in primates [MacLean 1985b, MacLean and Newman 1988]. Horse-radish peroxidase staining in monkeys show two distinct connectivities of anterior

and posterior cingulate suggesting specialisation into different functions [Vogt et al. 1979].

The ACC is connected to the amygdala, insular, and mediodorsal and interlaminar nuclei which transmit pain and noxious stimuli via the spinothalamic tract [Sikes and Vogt 1992]. It also receives midline afferents from the medial raphe nuclei and locus coeruleus.

The ACC is an opioid-modulated network and stimulation of thalamus produced met-enkephalin consistent with pain relieve, pupillary dilatation, piloerectile response [Clark and Ward 1948, Vogt et al. 1979, Ward 1948].

The posterior cingulate, meanwhile, is connected to the medial orbito-frontal cortex, parahippocampal gyrus and posterior parietal cortex. It receives afferents from anterior thalamic nuclei (dorsal and medial divisions), as well as the lateral dorsal thalamic nucleus.

The anterior and posterior cingulate cortices are interconnected with each other despite clear differentiation between these two structures [Baleydier and Mauguiere 1980, Pandya et al. 1981]. These differences support the idea that the anterior and posterior cingulate have different roles, with the anterior cingulate concerning executive function and the posterior cingulate with evaluative functions [Vogt et al. 1992; 1995].

3.1.3 The Functional Role of The ACC

Papez first recognised the role of the cingulate in generating emotional output relevant to sensory input [Papez 1937]. This idea was elaborated further by MacLean after studying the cortex of various species, proposing that the cerebral cortex is unique to mammals and that the cingulate is involved in the socialising aspect of life [Maclean 1955b].

The limbic system consists of multiple circuits integrated into an ecosystem of sensory inputs, recent and past memory, emotions, cognition and bodily representation of emotions [Maclean 1955b]. This system does not operate as a single unit but as an integration of multiple sources of inputs and outputs [Devinsky and Luciano 1993].

The cingulate, which is part of the limbic system is thought to give mammals the ability to exhibit complex social behaviours and emotions [MacLean and Newman 1988]. Lesions in the anterior cingulate in squirrel monkeys results in disruptive antisocial

behaviours [MacLean and Newman 1988]. Tameness, loss of fear and aggression were ascribed to defective evaluative function of sensory events and behaviour [Pribram and Maclean 1953].

Clinical cases and surgical experiments have demonstrated that disruption of cingulate connectivity changes the affective domain, attention, cognition and perception of pain [Laplane et al. 1981, Posner 1993, Posner et al. 2007].

The role of the ACC in vocalisation has been demonstrated by a lesion in the cingulate that rendered the monkey unable to phonate, similar to destruction of Broca's area [Sutton et al. 1974]. Chemical stimulation of the ACC in monkeys produces vocalisation and a distal signal has been detected in the periaqueductal gray area.

The vocalisation is inhibited by a glutamate antagonist (GABA, glycine and opioids), thereby suggesting that vocalisation from the anterior cingulate requires glutamate transmission.

In another report, glutamate stimulation to periaqueductal gray (PAG) causes vocalisation and rage behaviour in cats and is always preceded by hyperventilation [Zhang et al. 1995]. There is evidence that the anterior cingulate is linked to the PAG and that the activity of these two nuclei are synchronised via glutamate networks [Davis et al. 1993].

Electrical stimulation of area 24 of the anterior cingulate in monkeys produces vocalisation together with a complex emotional behavioural expression:

- widely open eyes,
- dilated pupils and
- protrusion of the tongue.

At the same site, if the vocalisation does not occur, another set of physiological and behavioural expressions have been noted [Smith 1941]:

- bradycardia,
- arrested breathing,
- inhibition to any movement, and

- relaxation of muscular tone.

The electrical stimulation of ACC produces a complex behavioural expession characterised by motor, cardiovascular, respiratory and vocalization effects, depending on the strength of stimulation. A moderate electrical stimulation produces vocalisation, slight increase in blood pressure, pilo-erection, dilated pupils and facial muscle expression. A stronger voltage electrical stimulation on the other hand produced mutism, respiratory and cardiac arrest and loss of muscular tone.

Regional blood flow in the anterior cingulate increases with motor and cognitive tasks, however the regional blow flow reduces as the task become routine [Paus et al. 1993; 1998]. Some research groups have attributed the increased blood flow in this region to attention [LaBerge 1990; 2001; 2002, Laberge and Brown 1989, Pardo et al. 1991] while some others assert that it is due to behaviour [Allman et al. 2001; 2011, Devinsky and Luciano 1993].

Anticipation is also attributed to the increase in activity in the anterior cingulate [Murtha et al. 1996]. Anticipation, vigilance and negative emotion increase right anterior cingulate activity whilst cognitive tasks and decision making increases left anterior cingulate activity [Critchley et al. 2001; 2003; 2005b, LaBerge 2001, Macey et al. 2007, Pardo et al. 1990; 1991]

Pain, breathlessness and negative emotions increase activity in the right cingulate, insular and amygdala [Pattinson et al. 2009a, Tracey 2008, von Leupoldt et al. 2009].

Deep brain stimulation of the anterior cingulate is currently being investigated as a treatment for neuropathic pain and further understanding of this area could offer other benefits such as in autonomic control [Boccard et al. 2014a;b; 2013].

3.2 The Periaqueductal Gray

The PAG is buried deep in the midbrain and its surrounding structures are relatively small compared to other parts of the cerebral cortex. Access to the PAG in humans for clinical intervention is limited to deep brain stimulation which is used for chronic neuropathic pain.

There is good evidence that the PAG is an important structure involved in survival [Behbehani 1995, Benarroch 2012]. It has been shown that it can produce two different outputs of cardiorespiratory response to threat [Rhudy and Meagher 2000].

In experiments using rats where the chance to escape is in favour to the animal (such as in cutaneous pain stimulation or in the presence of a predator), the PAG triggers a characteristic active 'defence' mechanism [Carrive 1993, Dampney et al. 2013].

Active defensive behaviour is hallmarked by increased somatosensory motor activity and an increase in cardiorespiratory response to increased blood flow and oxygen supply to the skeletal muscles. In an extreme situation where escape is not an option such as with severe haemorrhage or deep visceral pain, passive defensive behaviour predominates.

Passive defensive behaviour is characterised by passive body posture with lack of movement either to conserve energy or to 'pretend' to be dead. The cardiorespiratory response is appropriate with reduced arterial blood pressure, heart rate ands respiratory rate [Carrive 1993, Dampney et al. 2013].

The PAG measures approximately 14 mm long and 4 to 5 mm in diameter surrounding three quarter of the cerebral aqueduct circumference. It is in continuation with the periventricular grey area that lies rostral to it.

The PAG is funnel-like in shape with its base caudal and the apex rostral. It is bordered rostrally by the posterior commissure and by part of the third nucleus. The most caudal PAG is bounded by the dorsal tegmental nucleus.

PAG microstructure can be divided into four longitudinal columns with specialised functional and neuroanatomical connectivity. It is referred to as having dorsal medial periaqueductal gray (dmPAG), dorsal lateral periaqueductal gray (dlPAG), lateral periaqueductal gray (lPAG), and ventral lateral periaqueductal gray (vlPAG) subdivisions [Bandler and Shipley 1994, Carrive 1993].

The dorsal and lateral columns are believed to be crucial components of active defence behaviour while the ventral column is critical to defensive passive behavioural responses [Bandler and Shipley 1994, Green et al. 2006a].

3.2.1 The Radiological Anatomy of PAG

The posterior commissure is identified first as a landmark and the image slices will be scrolled towards the brainstem to outline the aqueduct and the third ventricles. The target area for chronic pain relieve is halfway between these the posterior commissure line and the third ventricle, contralateral to the affected side.

The intended target for placing the deepest electrode contact was marked at the PAG at a level of less than 10 mm below the anterior commissure/posterior commissure line; between the dorsal part of the red nucleus and the superior colliculus in the anteroposterior plane; and approximately 5 mm lateral to the lateral boundary of the aqueduct and the third ventricle.

Next, the electrode trajectory was selected to avoid possible penetration of the surface vessels on the cortex and the lateral ventricle. This leads to some adjustment of the target localization for each individual patient, and likely contributes to interpatient variation in electrode placement.

In patients with post-stroke pain and severely deformed hemispheres, targeting can be very difficult. For these patients, relative anatomic landmarks, such as the third ventricle, the aqueduct, the red nucleus, and the superior colliculus, are more reliable than anterior commissure/posterior commissure measurements.

3.2.2 The Cellular Architecture of PAG

Rat PAG has been systematically analysed using a qualitative and quantitative clustering method to classify cellular morphology [Beitz 1985]. There are three major neuronal classes identified based on its morphology:

- Fusiform neurons with large ovoid nucleus,
- Trigonal shaped with an ovoid nucleus and,
- Stellate or multipolar with central nucleus.

There is a strong anatomical agreement between species where PAG can be subdivided into medial, dorsal, ventrolateral and dorsal lateral [Beitz 1985, Gioia et al. 1985, Hamilton and Skultety 1970, Laemle 1979, Mantyh 1982, Tredici et al. 1983].

There are pronounced projections from anterior cingulate cortex to periventricular grey and from the thalamus and insula [Behbehani 1995].

3.2.3 The Functional Role of PAG

PVG is involved in mediating affective defence and emotional behaviours associated with 'flight or fight' [Carrive et al. 1989, Holstege and Saper 2005, Holstege et al. 2003].

There is evidence indicating that the PAG network modulates respiration during these two situations [Dampney et al. 2013, Huang et al. 2000, Kabat 1936, Subramanian 2013, Subramanian and Holstege 2011].

Electrical stimulation of PVG in animals and humans demonstrated the role of the PVG in autonomic cardiovascular regulation [Green et al. 2006b; 2010, Kabat et al. 1935] and modulation of this area also affects micturition [Green et al. 2012]. The influence on respiratory airways also shows future potential [Hyam et al. 2012].

3.3 The Ventral Posterior Lateral Nucleus of Thalamus

The thalamus is a paired midline ovoid structure that forms the dorsal border of the third ventricle. Its anterior pole is narrow and close to the midline whilst its elongated body forms the roof the third ventricle, and its posterior lateral aspect forms parts of the floor of the lateral ventricle. Its caudal end forms an overhanging structure beyond the third ventricle and over the superior colliculus.

The superior surface of the thalamus is separated from the body of the caudate nucleus by the stria terminalis. The thalamus is separated from the reticular nucleus laterally by the external medullary lamina. Lateral to this, the posterior limb of the internal capsule lies in between the thalamus and the lentiform complex.

The thalamus is in continuation with the midbrain tegmentum, the subthalamus and the hypothalamus.

Structurally, the thalamus is divided into distinct anatomical and functional nuclear groups such as anterior, medial and lateral. These groups are separated by an inverted 'Y' shaped sheet of white matter called the internal medullary lamina.

The subdivisions of the thalamus are considered as specific nuclei that mediate specific sensory signals to and from discrete cortical sensory areas and 'nonspecific' nuclei that are part of a general arousal system.

The lateral nuclear complex is the largest division of the thalamus. It is subdivided into dorsal and ventral. The lateral dorsal, lateral posterior and pulvinar lie dorsally.

The ventral thalamus can be divided into three groups:

- Ventral anterior,
- Ventral lateral,
- Ventral posterior.

The ventral-posterior complex is comprised of two nuclei; ventral posterior medial and ventral posterior lateral. These form the principal thalamic relays to the primary somatosensory cortex, and a number of associated nuclei; the basal ventromedial nucleus and the ventral posterior inferior nuclei. All these nuclei form the visceral, taste and other ill-defined thalamic relay centres. Specific for this research, ventral lateral posterior thalamus will be discussed to elucidate its role in this thesis.

3.3.1 The Cellular Architecture of VPL

The thalamus has specific topographic reciprocal connections to the cerebral cortex. Thalamic-cortical connectivity can be grouped into:

- Specific thalamocortical fibres,
- Corticothalamic fibres and,
- Nonspecific cortico-cortical pathways.

The thalamic-cortical connection is well documented by scalp Electroencephalography (EEG) as well as microelectrode physiology which reflect the cortical state, especially comparing awake and sleep states [Contreras et al. 1996, Steriade and Deschenes 1984, Steriade et al. 1993a;c; 1996, Steriade and Timofeev 2003].

There is evidence that thalamocortical connectivity is a diffuse projection from all thalamic nuclei to superficial layers of the cortex and back to the thalamus. This is based on a immunoreactivity studies of specific calcium binding proteins, parvalbumin and calbindin in monkeys [Jones 1998, Jones and Powell 1969].

Calbindin forms a matrix throughout the thalamus whilst parvalbumin is present only in specific nuclei. Where the density of parvalbumin is low, the calbindin cells show local increases in number. Parvalbumin cells projects to middle layers (III-IV) which areordered topographically to a single cortical field while calbindin projects to superficial layer I, II, upper III and has a wide distribution that is unconstrained by architecture or functional boundaries [Jones 1998].

3.4 Conclusion

In this chapter, we have seen that each nucleus has a specialised function with connectivity that link them to each other. The anterior cingulate has a role in the cortical control of the autonomic system accompanied by specific behavioural outputs as demonstrated in animal studies. The fMRI findings show areas of activation in the anterior cingulate cortex, thalamus and other limbic structures during cognitive tasks requiring attention and anticipation.

4
Deep Brain Stimulation

Deep Brain Stimulation (DBS) is a minimal access therapeutic treatment for movement disorders in functional neurosurgery. Chronic neuropathic pain and select group of patients with chronic psychiatric illness such as severe depression or obsessive compulsive disorder are also reported to benefit from this surgery. Single or multiple intracerebral macroelectrodes are implanted into target nuclei and their function are modulated using electrical current.

The effectiveness of DBS in movement disorder as well as in neuropathic pain is well documented [Bittar et al. 2005a;b, Boccard et al. 2013, Breit et al. 2004, Franzini et al. 2010; 2011, Perlmutter and Mink 2006].

DBS is used to treat Parkinson's Disease by targeting sub thalamic nuclei (STN) or globus pallidus interna (GPi), depending on symptoms. GPi is also used for dystonia and pedunculopontine nucleus (PPN) for 'on' gait freezing in Parkinson's disease [Franzini et al. 2011, Garcia-Rill et al. 2011].

Neuro-electro-physiology using DBS electrodes paves the way to further understand pathophysiology and drug effectiveness of movement disorder and neuropathic pain [Brown 2003, Brown and Williams 2005, Green et al. 2012, Hyam et al. 2012, Sverrisdottir et al. 2014].

DBS for chronic neuropathic pain started before its use in movement disorders and started when a remarkable analgesia was observed in conscious rats after electrical

stimulation of the midbrain [Reynolds 1969]. This was later translated to humans by means of deep brain stimulation in the 1970s [Hosobuchi et al. 1973; 1977, Richardson and Akil 1977, Young and Chambi 1987, Young et al. 1985].

The lack of randomised control trial evidence for the treatment of neuropathic pain led to a downgraded use of DBS as a treatment modality to 'investigational tool' in the United States [Gardner 2013]. Despite FDA disapproval of DBS for the treatment modality in the United States, other regulatory bodies in European countries, Australia, Canada and many Asian nations except Japan continue to use deep brain stimulation to treat neuropathic pain.

4.1 The Surgical Approach

Almost all stereotactic surgery in Oxford Functional Neurosurgery is performed in two stages where the first stage is done under local anaesthesia or sedation. The first stage allows preliminary awake assessment to ascertain motor or sensory modality benefits of DBS while the second stage surgery is performed under general anaesthesia for the implantation of the pulse generator.

Accuracy in stereotactic surgery is important and this is achieved by utilising a fusion between preoperative high resolution multi-slice fine cut MRI and intra-operative CT scan with a Cosman-Roberts-Wells (CRW) head frame. On the day of surgery, stereotactic CRW frame with metal rod localiser is fixed to the patient's head under local anaesthesia.

These localiser rods or 'fiducials' are detected on CT scan as a hyperintense ring forming fixed landmarks outside the skull and provide the basis of the relationship of brain to the skull. The image fusion was done using commercial software (Neuroinspire, Renishaw, UK).

A triangulation method is used to calculate three-dimensional cartesian coordinates of the target nuclei. The coordinates of the target nuclei are transferred onto a phantom frame before it is placed on the stereotactic CRW frame. Sub thalamic nuclei and globus pallidus internus can be identified based on the distinct radiological anatomy whilst the periventricular gray and ventral posterior lateral nucleus of thalamus is based on anatomical landmarks (see above).

During the planning stage, the best position of entry and a safe electrode trajectory tract avoiding the ventricles and major cerebral vessels is selected. After routine scalp

preparation, local anaesthesia is given to the target entry point. An adequate curvilinear incision is made on the scalp and haemostasis is secured. A 2.7 mm craniostomy is performed using a twist drill.

The stereotactic frame module is then affixed to the CRW frame. A straight metal guide is introduced through a special holder fixed on the stereotactic frame within the line of the calculated trajectory into the target nuclei. This holder has a security stopper which holds the guide so it will not go any deeper than the calculated coordinate.

The dura is opened and a TM electrode (Radionics, Burlington MA) is introduced using the planned trajectory to reach the target nuclei. The DBS electrode is then passed to target. Once the final position of the electrode tip is satisfactory, the electrode is secured to the skull using a titanium bioplate.

The distal end of the electrode is connected to a temporary extension lead and tunnelled under the scalp to a safe distance from the wound as part of infection control practice. Post operative CT scan is performed after surgery to confirm final electrode location. The exposed distal end of the electrode will be connected to an external programmer to tailor the treatment according to individual clinical indication.

4.2 The Mechanics and Benefits of DBS

The exact mechanism of how deep brain stimulation works is debatable and one proposed theoretical mechanisms is based on interfering with pathological signals in the affected nuclei using pulsed energy [Dostrovsky and Lozano 2002, Kringelbach et al. 2010]. The interference of in vivo pathological signals is achieved either through oscillating cancellation principles or by obstructing the signal propagation in a network.

An implanted pulse generator (IPG) provides an electrical current to the electrode tips in the brain within a prescribed frequency, pulse width, and power. The IPG is implanted under a subcutaneous tissue commonly on a chest wall for easy access and IPG setup.

Electrical stimulation to the anterior cingulate and thalamus alters the autonomic output as discussed in CHAPTER 3 (chapter 3). This demonstrates the potential role of DBS in modifying cardiorespiratory parameters as well as the opportunity to record electrical signal surrounding the electrodes. Stimulation of the anterior cingulate cortex

in human shows an increase in skin conductance, an inferred index of autonomic arousal [Gentil et al. 2009].

Green reported central modification of blood pressure in humans where electrical stimulation to the dorsal PAG raises systolic blood pressure whilst ventral PAG stimulation lowers systolic blood pressure intra-operatively [Green et al. 2005].

The autonomic modification was tested again in patients with chronic neuropathic pain undergoing PAG stimulation and in Parkinson's disease [Green et al. 2010, Sverrisdottir et al. 2014].

Electrical stimulation of PAG has the potential to modulate the lower airway responses [Hyam et al. 2012] as well as micturition control in humans [Green et al. 2012].

4.3 Conclusion

In this chapter, I have discussed the historical background of DBS, its surgical approach and its potential benefits. The exact mechanism of how DBS works is still unknown and many potential areas of stimulation in humans is currently being explored. The ability to record Local field potentials (LFPs) in awake humans provides the opportunity to understand voluntary breathing and its relation to autonomic function. In the next two chapters, I will discuss the experimental aims and methodology used in this thesis.

5
Aims of the Experiments

As humans, we do not pay attention to every breath we take as this is automatic at brain stem level. The demand and supply of oxygen, removal of carbon dioxide and strict control of pH are the main driving forces for the respiratory system.

I discussed the physiology of cortical and brainstem respiratory control that highlighted the network from the motor cortex to the brain stem respiratory group in CHAPTER 2 (chapter 2). The cellular architecture, network and radiological evidence were presented in CHAPTER 3 (chapter 3).

Non-invasive research tools such as surface EEG are limited to a few centimetres of the cortex, and while functional MRI can show deeper structures of cortical activation involved in respiratory control, it is restricted in temporal resolution.

On the other hand, LFPs recording is a method, that can bridge these time and spatial resolution limitations and help us to understand deeper brain structures, albeit as an invasive method.

LFPs is an extra cellular electrical activity recorded from a large population of dendrosomatic cells which represent an averaged collective synaptic activity [Harris and Thiele 2011]. These intracortical recordings shows oscillating patterns due to the synchronous current change or synaptic activity in the pyramidal neurons [Kitai 2011, Steriade et al. 1993c, Wester and Contreras 2013]. Local field potential shows correlation between

neuronal activity and the associated physical or behavioural action [Llinás 2011, Poulet and Petersen 2008].

It has been realised that the LFPs also can be used to uncover many other action related activity in the targeted nuclei in controlling cardiovascular and respiratory function through the modulation of autonomic nervous system [Basnayake et al. 2011, Green et al. 2005; 2006a;c, Hyam et al. 2012, Sverrisdottir et al. 2014].

LFPs based research related to deep brain stimulation for movement disorder and neuropathic pain is gaining grounds as a tool to further understand human neurophysiology [Boccard et al. 2014a; 2013, Sverrisdottir et al. 2014].

The LFPs recording in human is invasive and not performed unless clinically indicated. In this thesis, LFPs recording was made through DBS electrode implanted in anterior cingulate cortex, ventro lateral posterior nuclei of thalamus and periventricular gray as a treatment of chronic neuropathic pain. The access to human LFPs in this thesis was provided by Oxford Functional Neurosurgery.

5.1 The Aims

'Explicit' control of respiration is used exclusively to fit behavioural rather than physiological demand, and it is likely that there is an overriding signal from the cortex that influences the brain stem respiratory system. This control, in effect, modifies the output signal to the respiratory muscles.

Behaviour and autonomic function are intimately related, and this has been highlighted in CHAPTER 2 (chapter 2). An increase in sympathetic autonomic output increases respiration and heart rate. These changes may be analysed using heart rate variability (HRV), which shows an increased ratio of sympathetic to parasympathetic influence on cardiac contraction and blood vessel diameter change.

The cardiovascular and respiratory system are coupled tightly. Attempts to understand this regulation were made from the early 20th century lead by Krogh and Lindhard [Krogh and Lindhard 1913, Lindhard 1911].

Currently our understanding shows that regulation our cardiorespiratory system in exercise involves cortical and midbrain stuctures such as periaqueductal gray [Basnayake et al. 2011; 2012, Green and Paterson 2008, Green et al. 2007b]. However, the regulation of voluntary breathing experiment that is equivalent to the voluntary

excercise experiment is limited [Basnayake et al. 2011; 2012, Green and Paterson 2008, Green et al. 2007b].

The steady state of the brain and body should be represented as a quiet event where there is no external stimulation which may increase or decrease the cardiovascular system.

This state is achieved by having the subject to sit comfortably while breathing room air, with minimum multisensory inputs.. The recording of the LFPs and physiological indices would be set as a baseline and compared to with other experimental protocols.

The volitional breathing experiments requires the subject to initiate and modulate the respiration by modifying the rate or the depth of breathing. These experiments represent a 'feed forward' command from the cortex to the respiratory centre to give 3 different respiratory patterns.

Volitional command specifically modify the brain stem respiratory output and these experiments are unique because it cannot be replicated in animal study which requires a volitional action.

Another set of experiments specifically adopted to provide events where the cortex is computing numbers or actively recalling words thus relegating the respiration control to the automation of the brain stem.

These experiments were also included to provide a simple autonomic stressor and mental tasks are recognised to provide an autonomic stimulus to the cardiovascular system [Bernardi et al. 2000, Goswami et al. 2011, Sloan et al. 1991].

There is limited literature investigating the effect of breathing pure oxygen to the brain, even though it is a safe gas prescribed in the clinical setting when there is a risk of tissue hypoxia.

A group of children with congenital central hypoventilation syndrome was studied using fMRI and shows an activated area related to autonomic function such as the cingulate, amygdala, insular and thalamus [Kumar et al. 2005, Macey et al. 2003; 2005; 2007, Woo et al. 2005].

100% oxygen silences the peripheral chemoreceptors and this reduces the firing of the carotid body to the nucleus tractus solitarius. The effect of 100% oxygen is not significant in healthy volunteers but it reduces mean arterial blood pressure, respiratory rate and increases the peripheral vascular resistance [Graff et al. 2013]. Deactivation

of chemoreceptors with hyperoxia in disease states causes significant reduction in both blood pressure and respiratory rate in hypertension [Izdebska et al. 2006] and in chronic liver cirrhosis [Moller et al. 2010].

Breathing 100% oxygen experiment is designed to investigate the effect of breathing pure oxygen to the brain using direct recording method. LFPs analysis could provide a clue on the autonomic process investigated using fMRI.

Breath hold has a complex physiology and this thesis attempted to investigate if any 'feed forward' signal can be recorded using LFPs. In this experiment, the end tidal carbon dioxide can be as high as 46 mmHg. This experiment tried to tease out feed forward from feedback signal by artifically increases and varying the partial alveolar carbon dioxide level. The feedback signal of hypercapnia should be recorded and comparable to the level of hypercapnia.

In this thesis, I proposed a hypothesis that LFPs changes recorded in ACC, VPL and PVG in humans may encode feed forward 'command' to produce explicit voluntary respiration. A cortical autonomic signal may also be encoded with the respiratory signal. We also have to consider feedback as the respiration rate may influence the autonomic output or vice versa.

The secondary aim of this thesis is to study the LFPs changes related to inhaled various gas compositions. The methods described in CHAPTER 6 (chapter 6) were designed to contrast the result of breath hold to an increase in end-tidal carbon dioxide.

The main analysis tool utilised in this thesis is digital signal analysis. The electrical signal from LFPs were analysed to show frequency and time relationshiop using short time fourier transformation (STFT).

The autonomic changes elicited by mental tasks and gas mixture was analysed using heart rate variability. The R-R interval of ECG were analysed using Fourier Transormation which reveal a low and high frequency components. The low frequency component represent sympathetic output while the high frequency component represent parasympathetic function. A ratio of LF:HF represent a balance of sympathetic:vagal balance in each experimental condition and the ratio could help in understanding the autonomic balance in each experiment. An algorithm was adapted and modified to calculate the HRV.

5.2 Conclusion

In conclusion, the primary aims of this thesis are:

1. To investigate the feed forward command of voluntary breathing using local field potentials recorded in the bilateral anterior cingulate cortices, the ventral posterior lateral nucleus of the thalamus and periaqueductal gray area.

2. To investigate the relationship of feed forward command of voluntary breathing to the central autonomic nervous system.

The methodology used to investigate the above hypotheses provide additional information on the regulation of breathing which gave a few additional aims such as:

1. To investigate the effect of carbon dioxide inhalation to local field potentials recorded in ACC, VPL, and PVG. The results may provide evidence of a carbon dioxide-sensitive population of cells that could encode breathlessness signals in the cortex.

2. To investigate the effect of 100% oxygen inhalation to local field potentials recorded in ACC, VPL, and PVG.

6
Research Methodology

The literature on volitional breathing in human using invasive local field potentials is somewhat lacking. This limitation is probably because direct electrophysiological recordings are only available in a specialist institution where deep brain stimulation or functional neurosurgery is performed.

This thesis is my work on in-vivo electro-neurophysiology analysis of local field potentials recorded from deep brain nuclei in awake non-anaesthetised humans. The local field potentials were recorded while subjects performed volitional respiration, inhaled various gas compositions and perform mental tasks.

This study was reviewed and approved by the University of Oxford Clinical and Trust Governance (UOCTrG), the Oxford B Regional Ethical Committee (Oxford B REC) with reference number 11/SC/0229 and the Oxford University Hospital Trust Management (OUHTM) with reference number 6559.

6.1 Demographics

This thesis is a prospective cohort study, and the population target was patients with chronic neuropathic pain treated with deep brain stimulation. The recruitment for the research was 15 subjects with 50% rate of participation. A total of 8 patients (n = 8) agreed to participate in this study; 5 male, 3 female. The mean age was 44.75 years (M = 44.75, SD 11.67). Five patients were treated with bilateral anterior cingulate stimulation and three patients with unilateral ventral posterior lateral of the thalamus and periventricular gray stimulation, see Table 6.1.

The purpose, protocol and risks of the study were explained, and written informed consent was obtained from each patient. None of the participating subjects has any respiratory disorder.

Table 6.1 Demographic summary of research participants

No	Age	Gender	Diagnosis	Electrodes
1	28	Female	Chronic right hip pain	Left VPL and Left PVG
2	54	Male	Chonic right arm and body pain	Left VPL and Left PVG
3	35	Male	Right ulnar nerve entrapment	Left VPL and Left PVG
4	58	Female	Right hemibody pain post head injury	Bilateral ACC
5	32	Female	Chronic neck and back pain	Bilateral ACC
6	50	Male	Chronic right hemibody pain	Bilateral ACC
7	56	Male	Left hemibody pain post stroke	Bilateral ACC
8	45	Male	Right brachial plexus injury	Bilateral ACC

The experiments were conducted in a quiet room where temperature and humidity were controlled, see Figure 6.1.

The subject was seated in a chair and was asked to breathe through a close-fitting silicone face mask which has a quick release loop, and the subject was free to pull the face mask away if necessary, see Figure 6.2. The face mask is connected to a gas mixer where oxygen, air and carbon dioxide can be regulated, see Figure 6.3. Finger blood pressure, electrocardiography, end tidal carbon dioxide concentration and oxygen saturation were recorded.

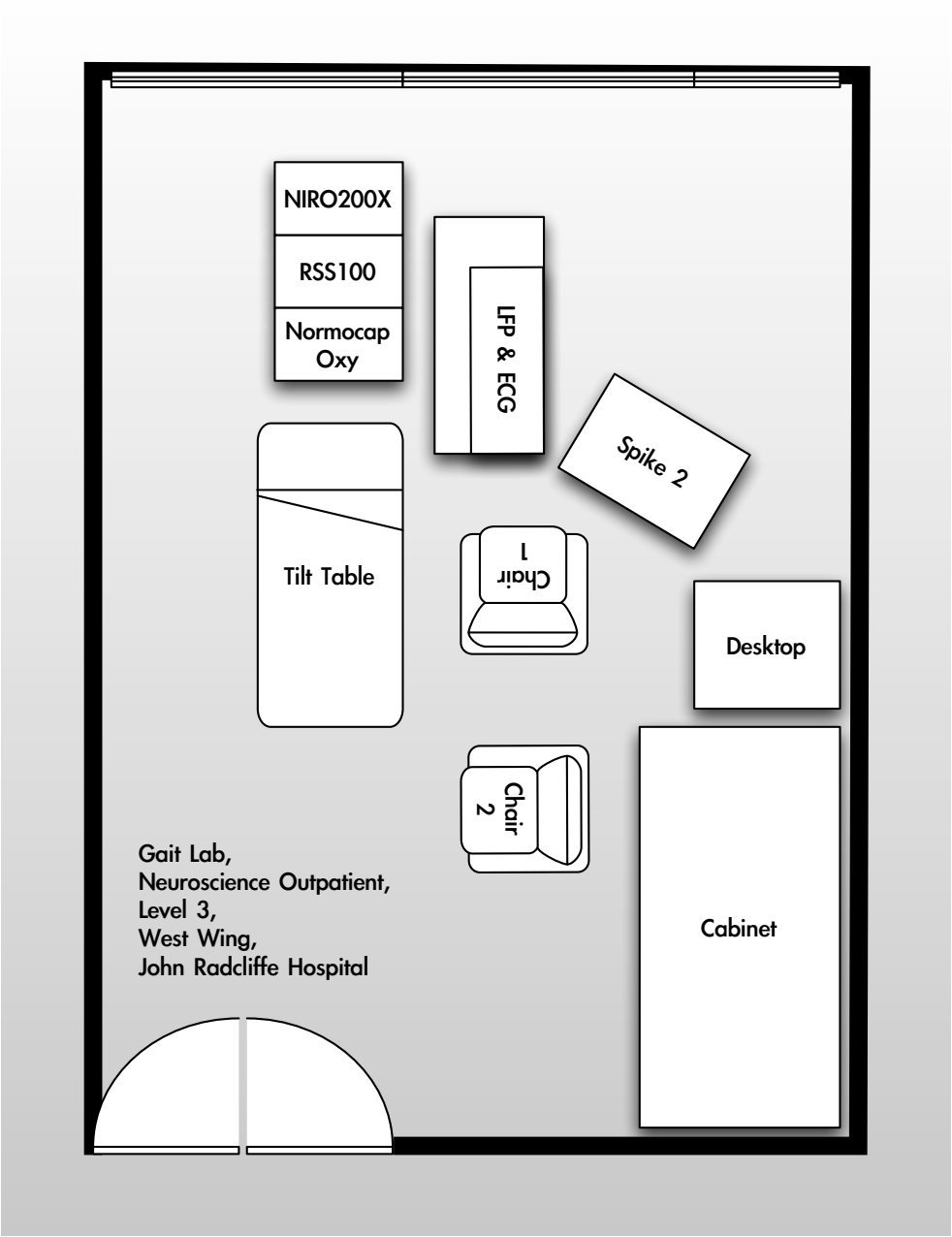

Figure 6.1 The floor plan of experiment room and equipment placement.

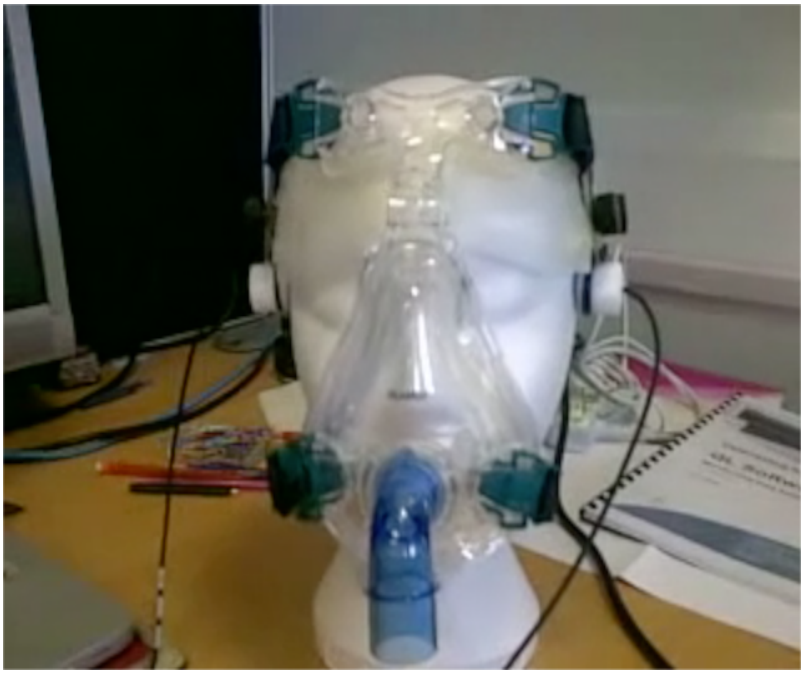

Figure 6.2 Face mask was selected for its tight seal, easy quick release and its comfort.

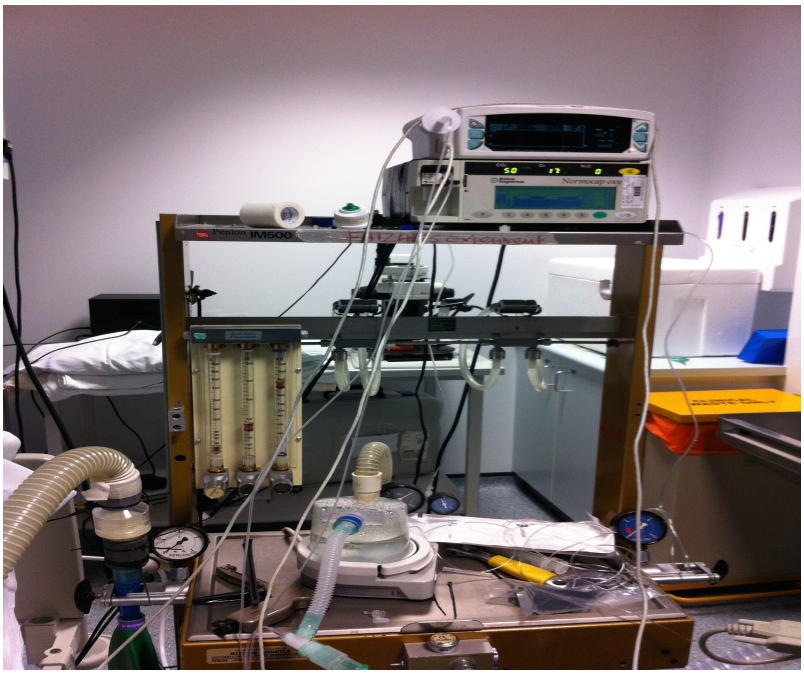

Figure 6.3 Penlon gas mixer courtesy of Dr Keith Dorrington, DPAG, Oxford University.

6.2 The Experiments

6.2.1 Room Air

Self paced respiration at rest The aim of this experiment was to record awake, resting state of local field potentials while breathing room air. The subject was asked to breathe at his or her own's pace while maintaining a sitting posture and minimization of body or head movement. The subject was encouraged not to react to any internal or external stimuli. This experiment lasted for 5 minutes.

6.2.2 Volitional Breathing

Volitional Breathing The aim of this experiment was to record local field potentials related to volitional breathing using room air. Verbal cue was given before each experiment, and three types of volitional breathing were tested:

- Hyperventilation
- Deep inspiration
- Voluntary expiratory breath hold.

In the volitional deep inspiration experiment, the subject was asked to take maximal deep inspiration several times over a period of 90 seconds.

In the volitional hyperventilation experiment, the subject was requested to take rapid short inspirations (as many as possible) in a period of 90 seconds.

In the volitional breath hold experiment, the subject was asked to exhale and hold his/her breath as long as possible in the expiration phase. The length of breath hold period was not controlled, and it is dependent on the individual's physiological capacity.

6.2.3 Gases Experiment

Respiration using 100% oxygen The aim of this experiment was to investigate the effect of breathing pure oxygen on the electrical properties of ACC, VPL, and PVG. In this experiment, the subject was asked to breathe 100% oxygen for 5 minutes at their own pace.

Carbon Dioxide Inhalation This experiment was designed to investigate any changes in local field potentials that may relate to carbon dioxide level. In this experiment, the subject was asked to breathe a random sequence of a gas mixture composed of carbon dioxide and oxygen. The subject was asked to breathe at their own pace and remove the mask if they felt uncomfortable.

Before the start of the experiment, a random sequence of 1, 3, 5, and 7 percent carbon dioxide was drawn to minimise the order effect. Four coins were marked with 1, 3, 5 and 7 and were put in a large envelope. A carbon dioxide sequence chart was prepared based on the subsequent coin picked from the envelope. The end tidal carbon dioxide (ETCO2) tracing was used to assess the change in carbon dioxide (CO2) concentration, which was immediate and stability was achieved within a few breaths, see Figure 6.4.

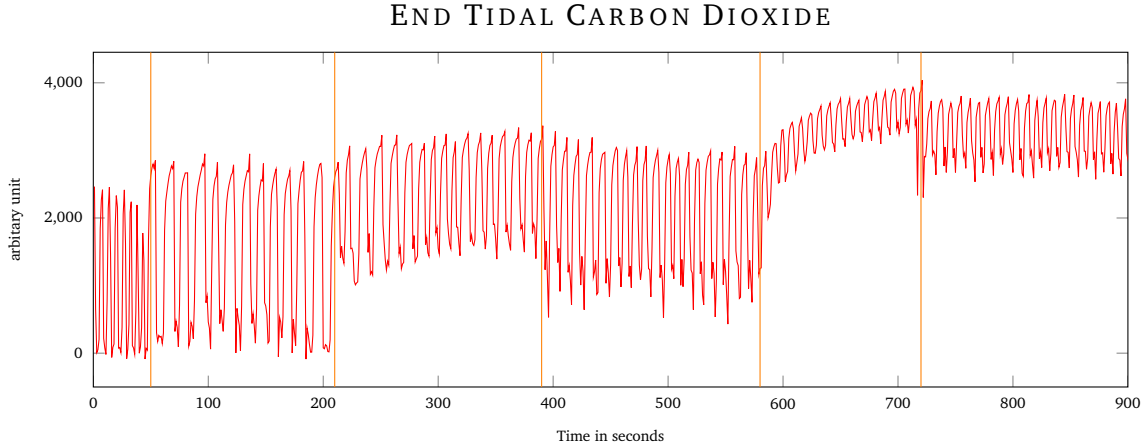

Figure 6.4 The end tidal carbon dioxide recording showing the change from room air to 100% oxygen, 3%, 1%, 7% and 5% CO2

6.2.4 Mental Tasks

Mental Tasks Experiments The aim of this experiment was to distract the subject from consciously thinking about volitional respiratory control. During the mental arithmetic task, the subject was asked to compute continuously and vocalise serial number subtractions (7 from 100). This task is a component of attention testing in the mini-mental state examination. In the word recall experiment, the subject was asked to vocalise any word that starts with the letter 'M'.

6.2.5 Summary of Experimental Paradigm

The experiments were designed to investigate the electrophysiological change in the deep brain nuclei in relation to voluntary respiration, see Figure 6.5. A baseline electrical activity was recorded in the first experiment while breathing room air quietly.

The second part of the experiment was designed to investigate the effect of voluntary respiration on electrical activity of deep brain nuclei. The electrical changes could explain a feed forward signal for voluntary respiration.

The third part of the experiment was designed to investigate the brain electrical activity when breathing 100% oxygen as well as randomised carbon dioxide gas composition of 1, 3, 5 and 7%.

The forth part of the experiment was designed as a control to the overall experiments. Mental cognition shifted the attention and forced the brain to compute and automate the respiratory cycle. These experiments is a simple tasks which triggers an autonomic reaction such as an increase in heart and respiratory rate.

Resting Room Air	Volitional Breathing			100% O2	Carbon Dioxide inhalation	Mental Tasks	
Regular tidal breathing	Deep Inspiration	Breath Hold	Hyperventilation		Randomised 1,3,5,7 %CO2 mixed with Oxygen	Math	Word
300 seconds	60 seconds	As long as the subject could hold	60 seconds	180 seconds	120 to 180 seconds each condition	60 seconds	60 seconds

Figure 6.5 The summary of experiment protocols.

6.3 Signal Processing and Analysis

6.3.1 Signal Acquisition

Two recording devices were used in this thesis:

1. Cambridge Electronic Design Limited (CED) Micro 1401, 16 channels of 16 bit waveform input with sampling rate of 2500 Hz and

2. Twente Medical Systems International B.V (TMSI) 32 channels, 16 bit with sampling rate of 2048 Hz.

6.3.2 Post Processing

The LFPs recording was performed in a unipolar mode that records electrical activity from individual metallic contacts of the DBS electrode. These are unipolar recordings that may be influenced by background noise and from the mains.

The noise can be filtered in post-recording processing using a digital filter and the signal to noise ratio can be minimised by calculating the electrical differentiation across two adjacent metallic contacts. The unipolar LFP recordings were first analysed using SPIKE2 software and bipolar differentiation were calculated before being exported as MATLAB variables, see Figure 6.6. All other signal processing and analysis were done in MATLAB.

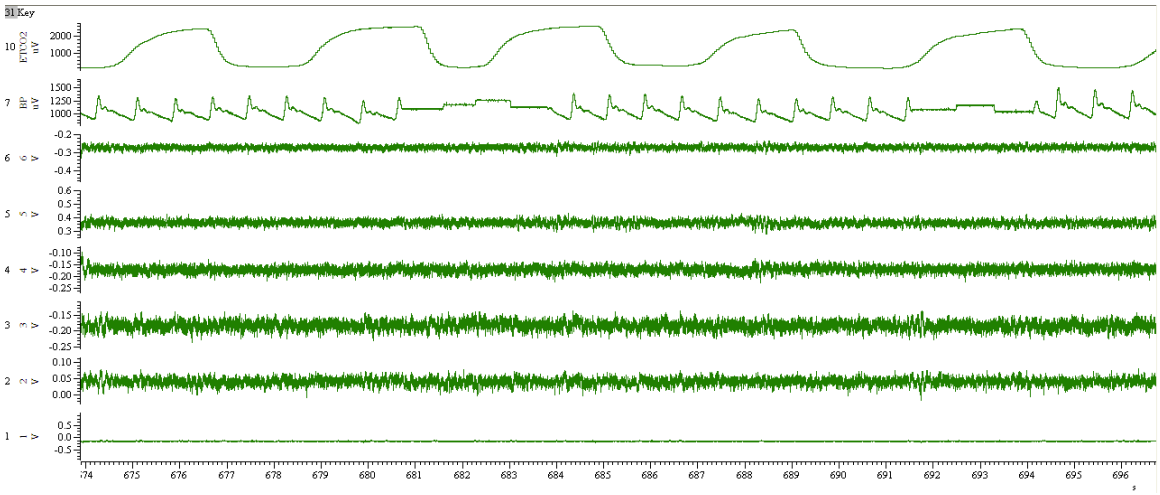

Figure 6.6 The raw data in SPIKE2 software showing the local field potentials, the electrocardiogram and end tidal carbon dioxide recording.

The local field potentials recordings were visually inspected and faulty recordings were identified and removed, see Figure 6.7. A 50 Hz infinite impulse response filter was applied to eliminate the electrical power source artefact from the signal. Data were subsequently partitioned into experimental segments based on recorded time stamps.

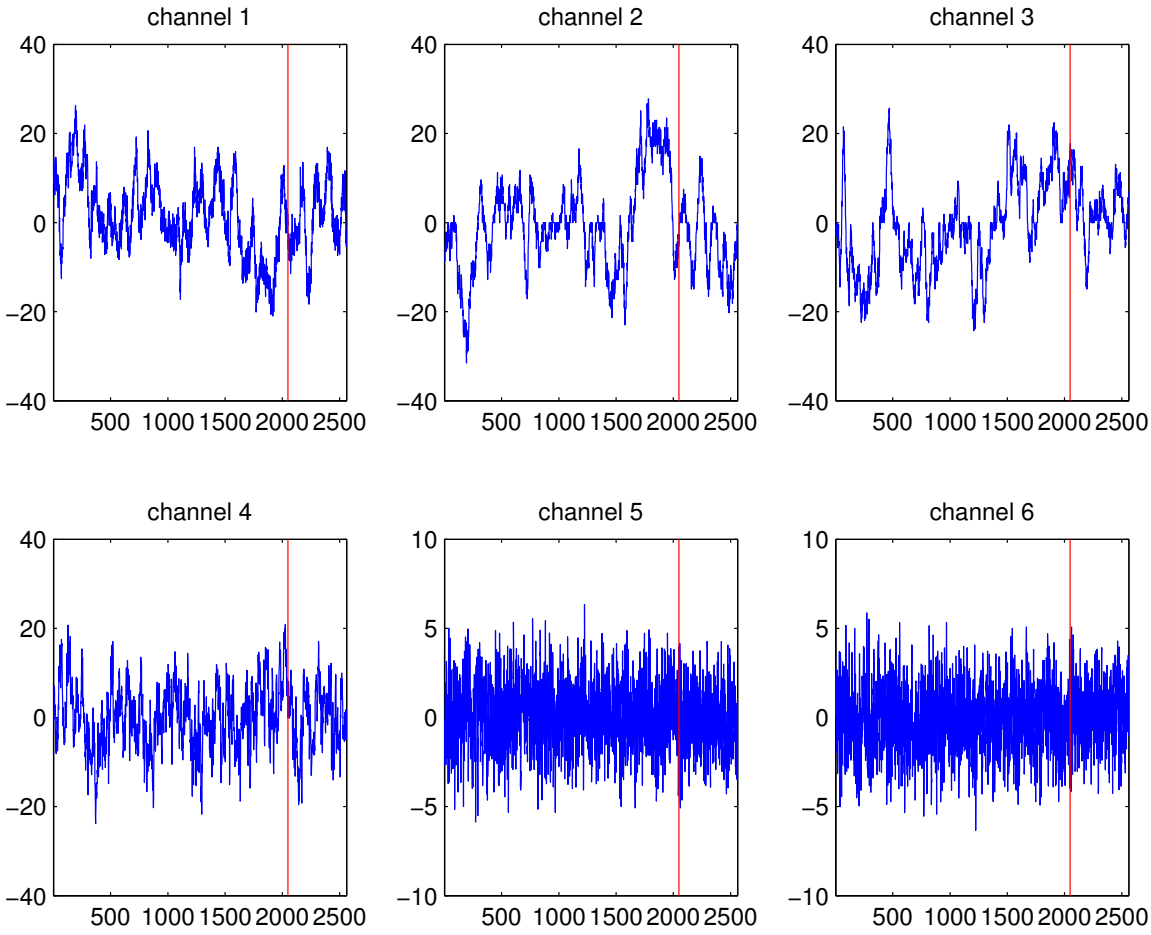

Figure 6.7 A 6 panel overview of LFP recordings. Channel 1 to 3 were from the left anterior cingulate and channel 4 to 6 were from the right anterior cingulate. Channel 5 and 6 recording were faulty recordings.

A single respiratory cycle is defined as one breath segment that consist of an inspiration and expiration phase. The start of inspiration phase is marked by a drop in end-tidal carbon dioxide (ETCO2). The beginning of expiration is characterised by the first differential increase in ETCO2 tracing, see Figure 6.8.

During the respiration experiments, the length of each inspiration and expiration phase was not controlled which resulted in a variable duration of the respiratory cycle. Each respiratory cycle was normalised into 100 segments. STFT is used to analyse the

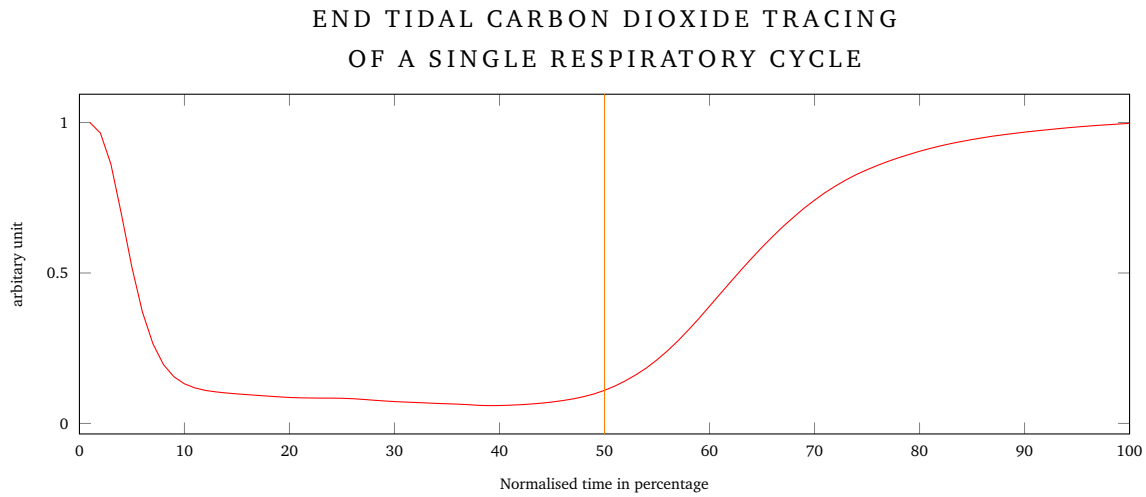

Figure 6.8 A single breath tracing of end tidal carbon dioxide showing a transition from inspiration to expiration phase marked by a vertical line.

signals' frequency distribution of power spectral density in the time domain. The signal was sub analysed using an FFT window of 256 with overlapping 128 segments resulting in 3-millisecond resolution for each power spectrum. The power spectra were then reconstructed into STFT.

1 to 100 Hz data was selected from STFT output for further analysis. Each STFT were subsequently normalised to their maximum value resulting in a ratio of 0 to 1. This normalisation is required so the spectrum visualisation will have an equal resolution, see Figure 6.9.

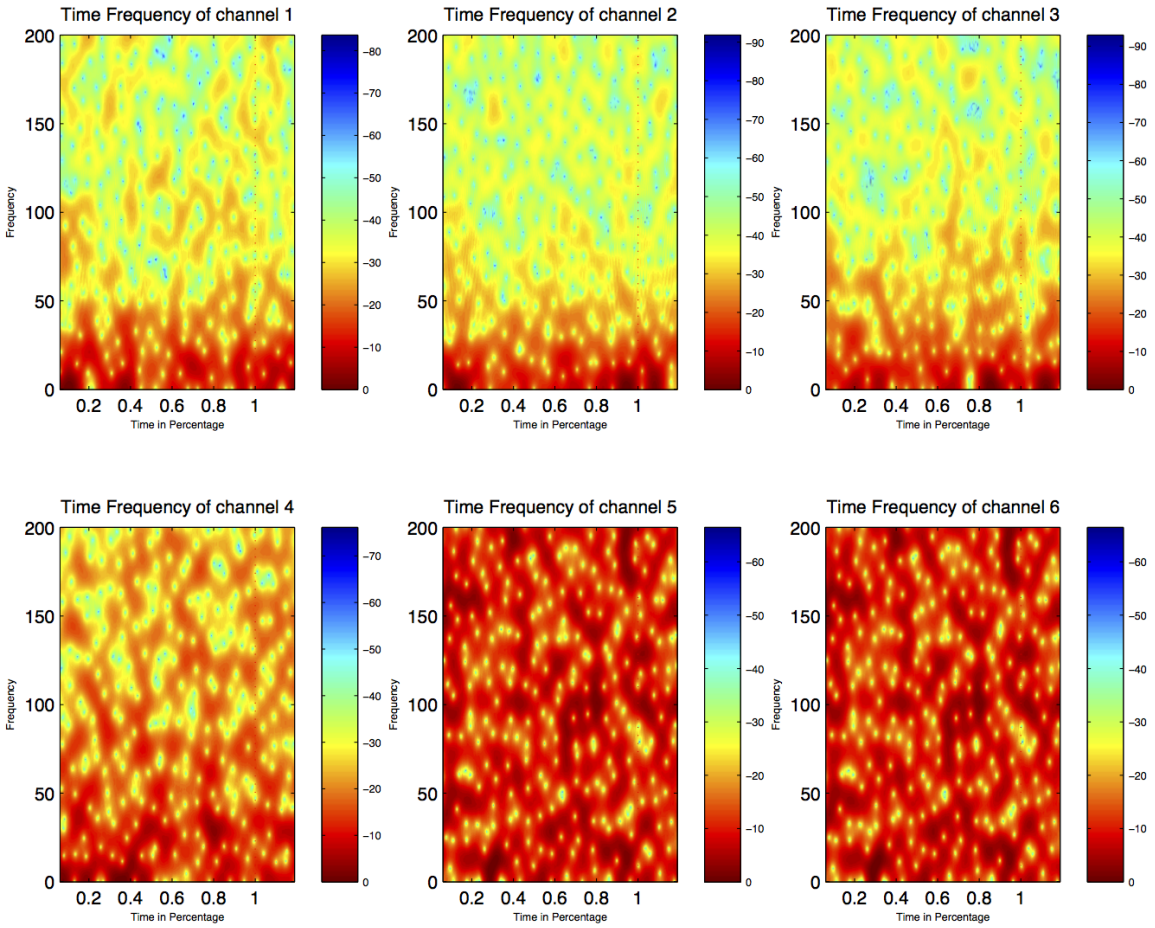

Figure 6.9 A 6 panel overview of time frequency analysis result. Channel 1 to 3 were from the left anterior cingulate and channel 4 to 6 were from the right anterior cingulate. Channel 5 and 6 shows the result of faulty recordings.

6.3.3 Signal Processing Script

The Matlab function below was written by me to incorporate the STFT and two data normalisation for this thesis.

```
% Idea concieved, developed and written by Dr Nor Faizal Ahmad Bahuri
% Supervised by Mr Alexander Green, Prof Tipu Z Aziz
% DPhil Candidate in Physiology, Oxford University
function STFTresult = FullBreathSTFT(EPsignal)
% ExpCond = {'RoomAir','O2','C1','C3','C5','C7','Math','Word',...
%     'HyperV','DeepI','HoldB'};
alldata = cellfun(@(x) STFT(x), EPsignal,'un',0);
mudata = STFTmu(alldata);
[totalAllP,muP] = totalP(alldata);

STFTresult.alldata = alldata;
STFTresult.mudata = mudata;
STFTresult.allP = totalAllP;
STFTresult.muP = muP;
end

function STFToutput = STFT(signal)
Fs = 2048;
[~,Fx,~,Px] = spectrogram(signal,256,128,Fs,Fs);
Flim = find(Fx<100,1,'last');
Px = Px(1:Flim,:);
lendata = size(Px,2);
x = linspace(0,100,lendata);

for n = 100:-1:1
target = x>=n-1 & x<= n;
n100(:,n) = nanmean(Px(:,target),2);
end
maxn100 = max(max(n100));
STFToutput = bsxfun(@rdivide,n100,maxn100);
end

function muSTFT = STFTmu(alldata)
for n = 100:-1:1
    segment1 = cellfun(@(x) x(:,n), alldata,'un',0);
    segment2 = mean(cat(2,segment1{:}),2);
    segment(:,n) = segment2;
end
muSTFT = segment;
end
```

```
41
42 function [totP,muP] = totalP(alldata)
43 tot1 = cellfun(@(x) trapz(x), alldata,'un',0);
44 totP = cat(1,tot1{:});
45 muP = mean(totP,1);
46 end
```

6.4 Heart Rate Variability

Heart rate variability is currently used as an index of autonomic nervous system response in disease state [Riganello:2012aa]. The guidelines for heart rate variability reporting was agreed upon to standardise the definition and methodology of deriving HRV [Tas 1996]. Heart rate variability is accepted as an index of sympathetic to vagal relationship using low frequency to the high-frequency ratio (LF: HF ratio).

The analysis measures the R-R interval from the electrocardiogram using an algorithm I wrote for this thesis. The Lomb-Scargle analysis method was chosen to calculate the power spectral density because this algorithm is not dependent on sampling interval, thus suitable for a short electrocardiography (ECG) recording segments [Clifford:2006aa]. The following is the MATLAB code I adapted and customised to suit the ECG recording sample rate of 2048 Hz.

```
1  function HRVout = HRVprocessing(HRVdata)
2  % This function will calculate the HRV indices of the whole group
3  % Idea concieved, and developed by Dr Nor Faizal Ahmad Bahuri
4  % Supervised by Mr Alexander Green, Prof Tipu Z Aziz
5  % DPhil Candidate in Physiology, Oxford University
6  % LombScargle algorithm was credited as the author intended below.
7  if isempty(HRVdata)==1
8      HRVout = [];
9  return
10 else
11
12 RRdata = arrayfun(@(x) x.RRt, HRVdata,'un',0);
13 HeartRate = arrayfun(@(x) 60*(length(x.RRt)/(diff([x.RRt(1),x.RRt(end)
       ])/2048)),HRVdata,'un',1);
14 [lf,hf,lfhf] = cellfun(@getHRVindex,RRdata,'un',0);
15 HRVout.HR = HeartRate;
16 HRVout.LF = cat(2,lf{:});
17 HRVout.HF = cat(2,hf{:});
18 HRVout.LFHF = cat(2,lfhf{:});
```

```
19 end
20 end
21
22 function [lf,hf,lfhf] = getHRVindex(RRdata)
23 x = RRdata;
24 lenx = length(x);
25 tempt = linspace(0,x(end)/2048,x(end));
26 t = linspace(0,tempt(end),lenx);
27 rr = tempt(x);
28 y = detrend(rr);
29 [Fx,Px] = lombScargle(t,y,4,1);
30 fx = [{Fx<0.04},{Fx>0.04 & Fx<0.15},{Fx>0.15 & Fx<0.4}];
31
32 lf = trapz(Fx(fx{2}),Px(fx{2}));
33 hf = trapz(Fx(fx{3}),Px(fx{3}));
34
35 lfnu = (lf/lf+hf);
36 hfnu = (hf/lf+hf);
37 lfhf = lfnu/hfnu;
38 end
39
40 function [f,P,prob] = lombScargle(t,h,ofac,hifac)
41 % LOMB(T,H,OFAC,HIFAC) computes the Lomb normalized periodogram (
      spectral
42 % power as a function of frequency) of a sequence of N data points H,
43 % sampled at times T, which are not necessarily evenly spaced. T and H
      must
44 % be vectors of equal size. The routine will calculate the spectral
      power
45 % for an increasing sequence of frequencies (in reciprocal units of the
46 % time array T) up to HIFAC times the average Nyquist frequency, with
      an
47 % oversampling factor of OFAC (typically >= 4).
48 %
49 % The returned values are arrays of frequencies considered (f), the
50 % associated spectral power (P) and estimated significance of the power
51 % values (prob).  Note: the significance returned is the false alarm
52 % probability of the null hypothesis, i.e. that the data is composed of
53 % independent gaussian random variables.  Low probability values
      indicate a
54 % high degree of significance in the associated periodic signal.
55 %
56 % Although this implementation is based on that described in Press,
57 % Teukolsky, et al. Numerical Recipes  In C, section 13.8, rather than
      using
```

```
58 % trigonometric rercurrences, this takes advantage of MATALB's array
59 % operators to calculate the exact spectral power as defined in
       equation
60 % 13.8.4 on page 577.  This may cause memory issues for large data sets
       and
61 % frequency ranges.
62 %
63 % Example
64 %    [f,P,prob] = lomb(t,h,4,1);
65 %    plot(f,P)
66 %    [Pmax,jmax] = max(P)
67 %    disp(['Most significant period is ',num2str(1/f(jmax)),...
68 %          ' with FAP of ',num2str(prob(jmax))])
69 %
70 % Written by Dmitry Savransky 21 May 2008
71
72 %sample length and time span
73 N = length(h);
74 T = max(t) - min(t);
75
76 %mean and variance
77 mu = mean(h);
78 s2 = var(h);
79
80 %calculate sampling frequencies
81 f = (1/(T*ofac):1/(T*ofac):hifac*N/(2*T))';
82
83 %angular frequencies and constant offsets
84 w = 2*pi*f;
85 cooff = 2*w*t;
86 tau = atan2(sum(sin(cooff),2),sum(cos(cooff),2))./(2*w);
87
88 %spectral power
89 cterm = cos(w*t - repmat(w.*tau,1,length(t)));
90 sterm = sin(w*t - repmat(w.*tau,1,length(t)));
91 P = (sum(cterm*diag(h-mu),2).^2./sum(cterm.^2,2) + ...
92      sum(sterm*diag(h-mu),2).^2./sum(sterm.^2,2))/(2*s2);
93
94 %estimate of the number of independent frequencies
95 M=2*length(f)/ofac;
96
97 %statistical significane of power
98 prob = M*exp(-P);
99 inds = prob > 0.01;
100 prob(inds) = 1-(1-exp(-P(inds))).^M;
```

```
101 end
```

6.5 DBS Electrode Localisation

The electrode used in this research is Model 3387 (Medtronic Inc., Minneapolis, MN). It has four coaxial platinum-iridium leads with circumferential contacts 1.5mm long and 1.5mm spaces in between, see Figure 6.10. In this section, I describe my electrode localisation method used on each subject and its conversion into Montreal Neurological Institute (MNI) space coordinates using FSL and MATLAB.

The workflow of deep brain stimulation surgery was described in CHAPTER 4 (chapter 4). In summary, pre-operative MRI was fused with intra-operative CT scan to increase the accuracy of targeting nuclei coordinates.

Post-operatively, another CT scan brain is acquired to document the final electrode position. The metallic contacts were marked on a mask layer using the post-operative CT brain. This scan was then converted to a normalised CT brain within MNI space.

Similarly, the pre-operative MRI was converted to a normalised MRI brain. These two scans were subsequently merged and fused together in FSL. Finally, the mask layer which contains the electrode contacts were overlaid on the fused scans and the coordinates were recorded in MNI space.

The final coordinate localisation was calculated using FSL [Jenkinson:2012aa]. All coordinates were tabulated and the mean electrode contact in all axes calculated. This method was applied to a recent publication analysing electrode contacts in Parkinson's disease and neuropathic pain [Sverrisdottir:2014aa].

The mean coordinate in Table 6.2, serves as a reference point in a normalised brain as targets for future fMRI research to investigate specific brain function.

X = medial to lateral position related to midline

Y = anterior to posterior position related to AC line

Z = superior to inf erior position related to AC line

Figure 6.10 Physical comparison of Medtronic Model 3387 deep brain stimulation electrode to 1 pound coin.

Table 6.2 Mean Electrode Contact In MNI Space

Nuclei	mean X	SD	mean Y	SD	mean Z	SD
Left ACC	–18	2	–21	2	5	4
Right ACC	–7	4	–29	3	–1	3
VPL	–11	3	14	3	32	4
PVG	12	3	14	3	32	4

6.6 Electrode Localisation Script

I adapted and modified a shell script which can be run using a command line interface, tested on a Macintosh operating system. The idea of this script is to produce an automated process to map electrode contacts.

In this method, I manually marked the metallic contact on a mask, while the script automatically converts and fuses a patient's CT and MRI scans. The data processing time was reduced from 30 minutes to just under 10 minutes per subject after utilising this automated script.

```
#!/bin/sh
# first bet the post op CT
bet postopCT ctbet1 -v
#
# bet the second time
bet ctbet1 ctbet2 -v
# threshold brain extracted CT scan
fslmaths ctbet2.nii.gz -uthr 50 -thr 0 postop_finalCT
# fslview postop_finalCT*
# #
# #  bet the MRI scan Extract brain from MRI scan
bet preopMRIT2 preopMRI_bet1 -t -v
# # check brain extraction
# fslview preopMRI_bet1.nii.gz
# # if brain extraction OK then continue, otherwise change parameter (e.g. -f 0.3)
# #
# #  Coregister the CT to MRI and get the matrix
flirt -interp trilinear -v -in postop_finalCT.nii.gz \
-ref preopMRI_bet1.nii.gz \
-out CT2MRI -omat CT2MRI.mat
fslview CT2MRI.nii.gz preopMRI_bet1.nii.gz
# # if registration OK then continue
# #
# #  Coregister the MRI to MNI space and get the matrix
flirt -in preopMRI_bet1.nii.gz \
-ref /usr/local/fsl/data/standard/MNI152_T1_1mm_brain.nii.gz \
-out MRI2MNI -omat MRI2MNI.mat -interp trilinear -v
fslview /usr/local/fsl/data/standard/MNI152_T1_1mm_brain.nii.gz MRI2MNI.nii.gz
# #
# # convert the CTMRI to CTMNI space
convert_xfm -omat CT2MNI.mat -concat MRI2MNI.mat CT2MRI.mat -v
```

```
# #
# # this is to get the CT in MNI space
flirt -interp nearestneighbour -v -in postop_finalCT.nii.gz \
-ref MRI2MNI.nii.gz \
-out CT_MNI.nii.gz \
-init CT2MNI.mat -applyxfm
# #
flirt -interp nearestneighbour -v -in electrodeMask.nii.gz \
-ref MRI2MNI.nii.gz \
-out CT_MNI_elecNN.nii.gz \
-init CT2MNI.mat -applyxfm
# #
flirt -interp trilinear -v -in electrodeMask.nii.gz \
-ref MRI2MNI.nii.gz \
-out CT_MNI_elecTL.nii.gz \
-init CT2MNI.mat -applyxfm
# #
# # use fslview on all CT_MNI image to find electrode locations
fslview /usr/local/fsl/data/standard/MNI152_T1_1mm_brain.nii.gz \
MRI2MNI.nii.gz CT_MNI.nii.gz CT_MNI_elecNN.nii.gz CT_MNI_elecTL.nii.gz
```

6.7 Statistical Analysis

The population sample in this thesis was limited to neuropathic pain patients and there were four deep brain nuclei investigated. The electrophysiological changes in both voluntary and spontaneous respiration conditions was recorded and compared to the resting state.

The initial statistical test chosen for these data was one-way analysis of variance (ANOVA). However, while the data shows normal distribution and independence, the variance in some experiments was not homogeneous. This result clearly violates the assumptions of ANOVA.

The variance was tested using Levene's Test of Variance. The data were transformed into a log dataset but the variance remained inhomogeneous. The dataset was analysed using non-parametric Kruskal-Wallis test, which is equivalent to a parametric ANOVA. Post hoc analysis using Dunn-Sidak multiple comparison was then performed.

The Kruskal-Wallis null hypothesis states that all groups' median ranks are equal, and the alternative hypothesis is that at least one of the group's median rank is statistically different from the population median rank. Post hoc analysis using Dunn-Sidak multiple comparison tests was performed to investigate which group pair differed.

The statistical analysis was done using a customised algorithm which was conceptualised and designed by me to be employed in MATLAB. This method was chosen instead of using other commercial statistical analysis software because the dataset remained in one single platform throughout the data analysis phase. This measure minimises the possibility of data transformation error.

6.7.1 Kruskal Wallis and Post Hoc Dunn Sidak Script

I wrote customised MATLAB scripts as above to incorporate Kruskal-Wallis and post hoc Dunn Sidak multiple comparison tests for automated statistical analysis.

```
1 for b = 1:5
2     [~,h,stats] = kruskalwallis(datastat(2).(Band{b}),ExpCond,'off');
3     [c,~,~,nms] = multcompare(stats,'ctype','dunn-sidak','display','off
          ');
4     cnew = c(c(:,6)<0.05,:);
5     out = [nms(cnew(:,1)), nms(cnew(:,2)), num2cell(cnew(:,3:6))];
6     report = [h{2,3},h{3,3},h{2,5},h{2,6}];
```

```
7
8       statout(b).(sprintf('Report_%s',Phase{2})) = report;
9       statout(b).(sprintf('Result_%s',Phase{2})) = out;
10  end
```

6.7.2 Kruskal Wallis and Post Hoc Dunn Sidak Result

At 0.05 level of significance, there exists enough evidence to conclude that there is a difference in the median ranks of mean normalised power of Alpha band in the left anterior cingulate during inspiration phase in all experimental conditions.

Dunn Sidak post hoc analysis for multiple comparisons was retrieved from the described function. The following result illustrates the output of pairwise comparison between conditions. The first two columns are the group being tested followed by the lower 95% confidence interval, median rank, the upper 95% confidence interval and the last column represents the p-value of the difference.

In this example, Dunn-Sidak post hoc analysis shows volitional breathing control was statistically different from the respiration controlled by the brain stem in the left anterior cingulate at Alpha band during the inspiration phase.

```
>> KSresultACCLalpha = statACCLresultKS(1).result.hIns
KSresultACCLalpha =
  Columns 1 through 5
    'Source'    'SS'            'df'     'MS'            'Chi—sq'
    'Groups'    [2.7655e+06]    [ 10]    [2.7655e+05]    [47.884]
    'Error'     [4.5229e+07]    [821]    [     55090]          []
    'Total'     [  47994128]    [831]              []          []
  Column 6
    'Prob>Chi—sq'
    [ 6.5178e—07]
                []
                []
```

6.8 Conclusion

This chapter discussed the methodology used to investigate my hypothesis of voluntary breathing feed forward signals and their relationship to the cortical control of autonomic function. LFPs were recorded, analysed and compared to resting state LFPs, which was defined as quiet respiration using room air.

Voluntary breathing is defined as a conscious act of increasing or decreasing the respiratory phase which is reflected by the respiration rate. Voluntary hyperventilation, deep inspiration and breath hold were used as categories of volitional breathing.

100% oxygen inhalation is used to investigate the effect of breathing a medically safe gas on the LFPs in the brain. Pure oxygen stabilises the peripheral chemoreceptors and the LFPs were compared to the LFPs whilst breathing room air (with 21% oxygen) at rest. Heart rate variability during these two conditions will show if there is any shift in the balance between parasympathetic and sympathetic nervous systems.

Randomised carbon dioxide concentration mixed with high oxygen content were used to investigate the effect of carbon dioxide on the central chemoreceptors while the peripheral chemoreceptors are silenced. This experiment was conducted to investigate whether the LFPs change during breath hold is influenced by feed forward signals or by a rise in end-tidal carbon dioxide level.

Within the same carbon dioxide theme, I postulate that the investigated nuclei could show LFPs changes with a change in central chemoreceptor signal. These changes hopefully will provide evidence that the cortical nuclei could encode breathlessness based on central chemoreceptor signals.

The mental tasks are used to generate an autonomic response as well as diverting the attention away from respiration awareness. The experiment will demonstrate thatwhile performing cognitive tasks, our respiration is controlled by the autonomic system. The electrode contact analysis was performed using FSL and MATLAB and I have shown that the analysis could be done using the command line instead of a graphical user interface which cuts down the processing time.

The mean electrode contact point in MNI space shows constant coordinates in all groups which suggests a standard targeting technique. The coordinate may be used as a target for future fMRI research of voluntary respiratory networks.

The signal analysis, as well as statistical tests, were performed within a MATLAB environment using a customised algorithm designed by me. These scripts are done to demonstrate my command of MATLAB programming language that I learnt and achieved in this thesis.

7

Cardiovascular and Respiratory Changes

Physiological changes in the cardio-respiratory system observed during the experiments are described in this chapter. Heart rate variability is an analysis of beat to beat variation which represents the interaction of sympathetic and parasympathetic nervous systems.

The heartrate variability guidelines suggested a minimum 5 minutes of ECG recording to accurately interpret the analysis [Tas 1996]. It is however noted that prolonged respiration using carbon dioxide is not safe, therefore the limit was set for minimum 180 seconds of gas exposure per experiment.

The LF:HF ratio shows the balance of 2 autonomic nervous components, the sympathetic and the parasympathetic nervous system [Tas 1996]. A higher ratio correlates with a shift of parasympathetic to sympathetic which is demonstrated by a higher heart rate.

7.1 Respiratory Changes

Whilst at rest, the mean respiratory rate was (M = 12, SD = 3) breaths per minute. The inspiration phase for regular inspiration was (M = 2.52 second, SD = 1.26 second) while the expiration phase was (M = 2.43, SD = 1.15) long.

Respiration using 100% oxygen reduces the mean respiratory rate (M = 10, SD = 5). The inspiration phase for this experiment was (M = 2.83, SD = 1.64) while the expiration phase was (M = 3.14, SD = 1.186) long.

This experiment validates previous knowledge that 100% oxygen stabilises the peripheral chemoreceptors [Dejours 1963, Duffin 1990]. However, to my knowledge, there is no neurophysiological report of deep cerebral nuclei activity in human whilst breathing such concentrations.

The carbon dioxide gas was mixed with a high concentration of oxygen to minimise the respiratory response to hypercapnia. This experiment was designed to study electrophysiological changes in the brain with various carbon dioxide concentrations.

The mean respiratory rate during various carbon dioxide concentration was (M = 10, SD = 3) for 1% carbon dioxide, (M = 11, SD = 4) for 3% carbon dioxide, (M = 11, SD = 3) for 5% carbon dioxide and (M = 11, SD = 2) for 7% carbon dioxide.

Vocalisation during mental arithmetic produce a mean respiratory rate of (M= 10, SD = 3), while word recall (M = 11, SD = 4). This experiment did not change the respiratory rate from the baseline as the words and numbers were vocalised in one expiration. However, the respiratory phases analysis shows that there was a longer inspiration and expiration phase per breath.

The inspiration phase for mental task was (M = 2.90, SD = 1.24) seconds whilst the expiration phase was (M = 2.90, SD = 1.12) seconds. The inspiration phase for word recall was (M = 2.69, SD = 1.44) while the expiration phase was (M = 2.78, SD = 1.55). This experiment demonstrates the role of respiration in vocalisation where longer expiration was needed to produce sounds through the vocal cord.

Volitional hyperventilation mean respiration rate was (M = 21, SD = 2) breaths per minute. The mean inspiration phase was (M = 1.55, SD = 0.70) while the expiration phase was (M = 1.25, SD = 0.70). Volitional deep inspiration was achieved with a mean respiratory rate of (M = 8, SD= 3) breaths per minute.

The respiratory changes results are tabulated in Table 7.1, Figure 7.1 and Figure 7.2.

Table 7.1 The mean respiratory rate and phases in all experimental conditions.

Conditions	Mean Respiratory rate (Breaths/Minute)	SD	Mean Inspiration Time (s)	SD	Mean Expiration Time (s)	SD
RoomAir	12	3	2.52	1.26	2.43	1.15
O2	10	5	2.83	1.65	3.14	1.86
C1	10	3	2.60	0.91	3.18	1.64
C3	11	4	2.74	1.21	2 .63	1.57
C5	11	3	2.57	1.02	2.73	1.50
C7	11	2	2.51	0.75	2.95	1.05
Math	10	3	2.90	1.24	2.90	1.12
Word	11	4	2.69	1.44	2.78	1.55
HyperV	21	2	1.55	0.70	1.25	0.70
DeepI	8	3	3.79	1.40	3.59	1.18
HoldB	5	14	5.05	3.86	7.52	6.13

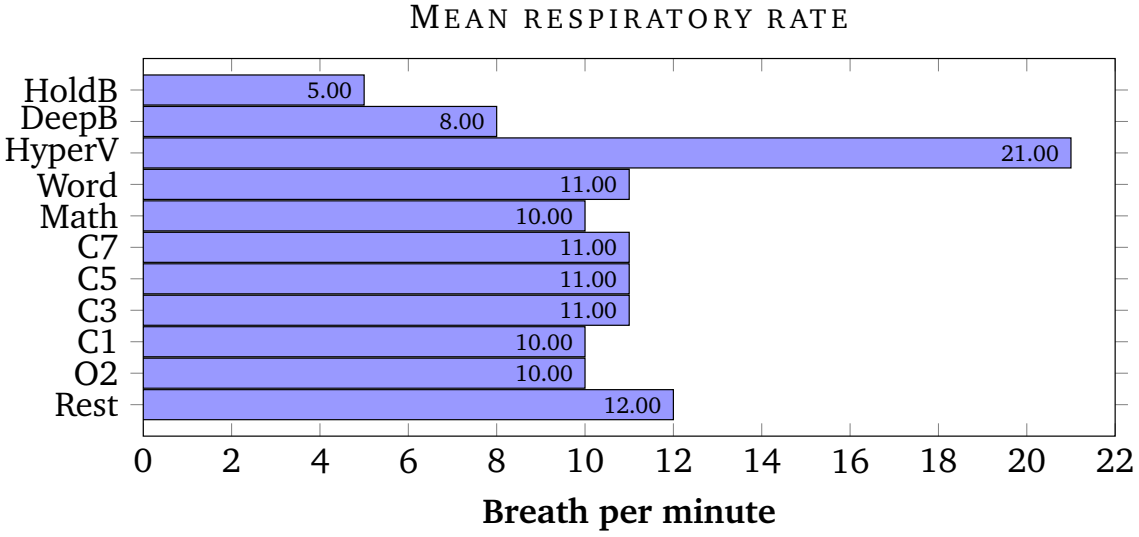

Figure 7.1 The mean respiratory rate of all experiment conditions.

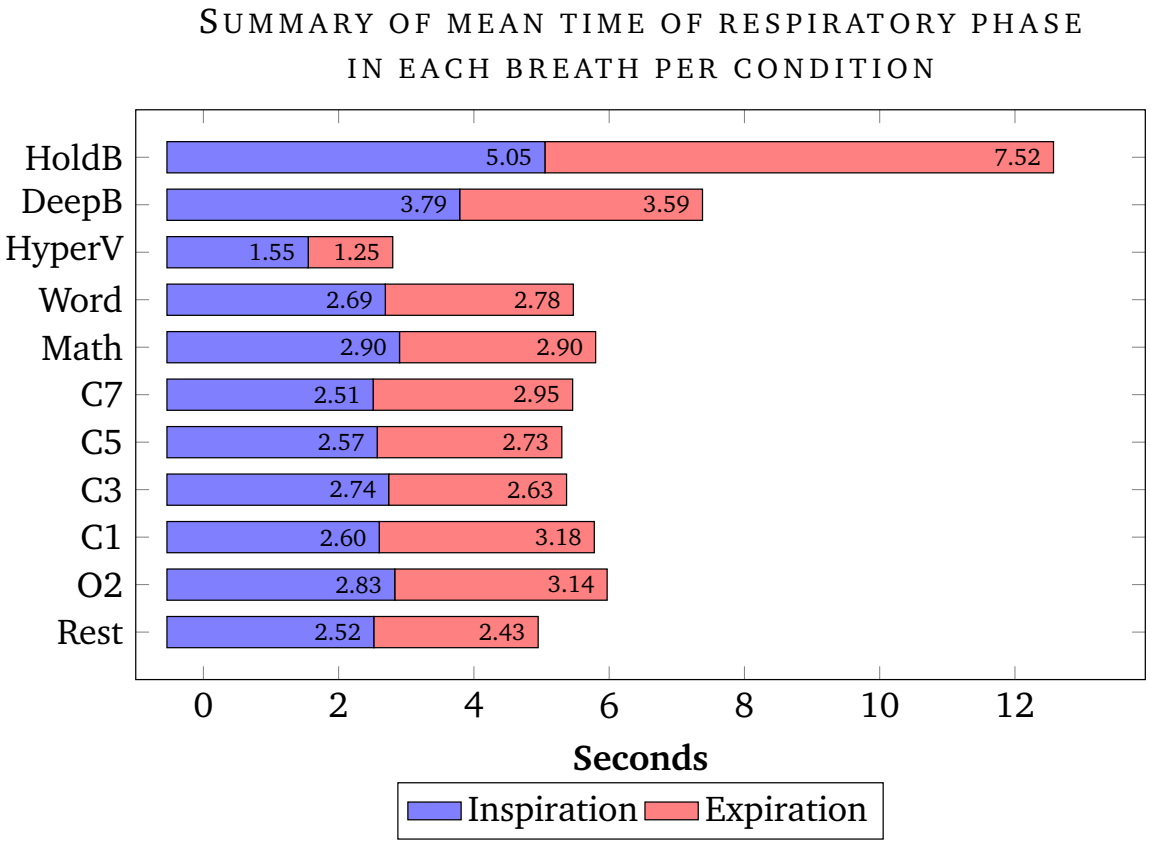

Figure 7.2 The mean respiratory phase of all experiment conditions.

The mean inspiration phase during deep inspiration experiment was (M = 3.79, SD = 1.40) while the expiration phase was (M = 3.59, SD = 1.18). The longer inspiration phase of deep inspiration was followed by a longer expiration phase and this result is similar to what happens during the Hering Breuer reflex, where increase in pulmonary stretch output inhibits central respiratory signals and prolongs the expiration phase [Giffin et al. 1996, Guz et al. 1966, Widdicombe 1982].

The mean breath hold rate was (M = 5, SD = 14) breaths per minute. The standard variation here was not valid as it is not possible to breathe with a negative rate and this shows the wide variability of subjectsâĂŹ performance in breath hold.

The mean inspiration phase for breath hold was (M = 5.05, SD = 3.86) while the expiration phase was (M = 7.52, SD = 6.13) long. The breaking point of breath hold experiment in each subjects varies and I postulate that the feedback or feedforward signal at end of breath hold should contain similar commands to hold the breath.

In summary, inspiring different gas composition with a background of high oxygen content did not change the mean respiratory rate. Volitional breathing shows how voluntary command could modulate respiratory rate and phase, while vocalisation shows a longer expiration phase to generate sound through the vocal cord.

7.2 Cardiovascular Changes

As discussed previously, the respiration system is coupled tightly to the cardiovascular system. The summary of mean heart rate in all experimetal conditions were tabulated in Table 7.2 and summarised in Figure 7.3 Heart rate analysis is one of the way to provide clues to this link and to the local field potentials.

The mean heart rate at rest was (M = 77, SD = 10) beats per minute. Respiration using 100% oxygen lowers the mean heart rate (M = 73, SD = 6) beats per minute, while respiration with 1% carbon dioxide lowers the mean heart rate to (M = 71,SD = 14) beats per minute.

The mean heart while breathing 3, 5 and 7% carbon dioxide was (M = 76, SD = 1), (M = 75, SD = 8) and (M = 76, SD = 7) beats per minute respectively.

Mental tasks increases heart rate by 10% from the baseline. In mental arithmetic, the mean heart rate was (M = 65, SD = 9) beats per minute. Word recall has a mean heart rate of (M = 83, SD = 8) beats per minute.

Volitional hyperventilation mean heart rate was (M = 77, SD = 7), while deep inspiration was (M = 76, SD = 7) beats per minute. Volitional breath hold has a mean heart rate of (M = 78, SD 6) beats per minute.

In summary, the analysis of heart rate per se did not show any major differences but a trend can be spotted, see Figure 7.4. Respiration with room air and various gas concentrations remains within the resting SD. Ventilation during mental tasks were higher because of vocalisation.

(#cardiovascularindices) and (#resultcardiovascular) shows the summary of heart rate and its variability which focus on the ratio of low to high frequency (LF:HF) power spectra of RR interval. A high LF:HF ratio suggests a high influence of sympathetic nervous system to the cardiac contraction rate. The mean LF:HF at rest was (M = 4.18, SD = 0.81). Respiring 100% oxygen at rest increases the LF:HF ratio (M = 5.4, SD = 5.4).

Breathing 1% carbon dioxide reduces the LF:HF ratio to (M = 3.90, SD = 1.85), while 3% carbon dioxide increases the ratio to (M = 4.47, SD = 0.88). 5% carbon dioxide reduces the mean LF:HF ratio to (M = 3.55, SD = 0.72) and 7% carbon dioxide mean LF:HF ratio was (M = 3.82, SD = 1.16).

Table 7.2 The mean heart rate and HRV result of all experiment conditions.

Conditions	Mean Heart Rate (Beats/Minute)	SD	Mean LF	SD	Mean HF	SD	LF:HF ratio	SD
Room Air	77	10	0.11	0.071	0.03	0.025	4.2	0.81
100% O2	74	6.4	0.076	0.053	0.018	0.014	5.4	5.4
1% CO2	72	14	0.046	0.027	0.014	0.01	3.9	1.9
3% CO2	76	7	0.063	0.044	0.014	0.0099	4.5	0.88
5% CO2	75	8.3	0.073	0.051	0.021	0.016	3.6	0.72
7% CO2	76	6.9	0.12	0.088	0.026	0.016	3.8	1.2
Math	85	8.5	0.11	0.1	0.023	0.017	4.4	1.5
Word recall	83	8.4	0.14	0.071	0.022	0.01	6.4	2.8
Hyperventi-lation	77	7.2	0.13	0.059	0.043	0.023	3.3	1.4
Deep Inspiration	77	7.1	0.18	0.099	0.11	0.093	3.5	3
Hold Breath	78	5.8	0.25	0.14	0.071	0.066	11	13

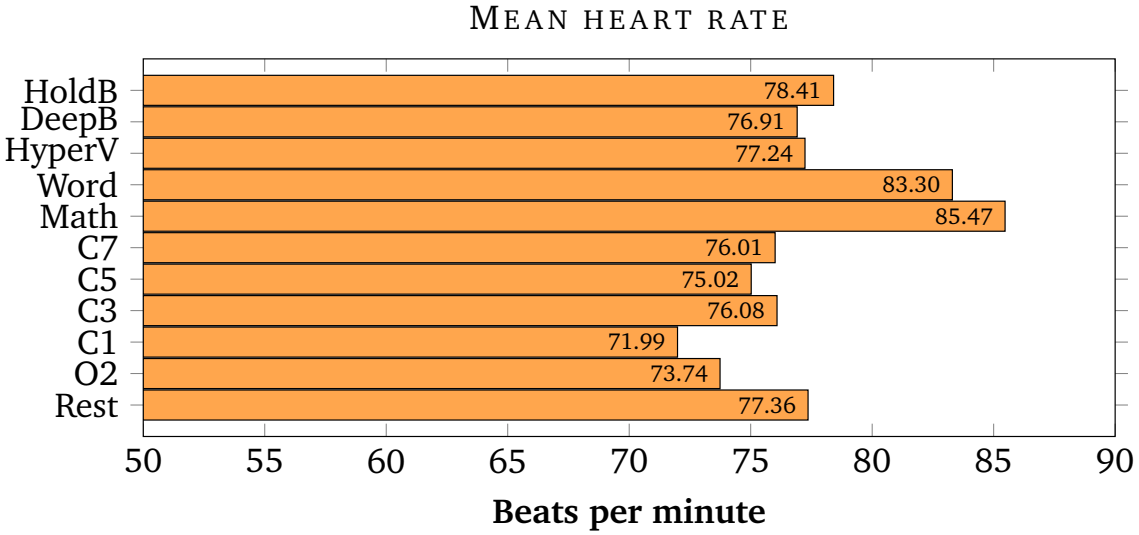

Figure 7.3 The mean heart rate of all experiment conditions.

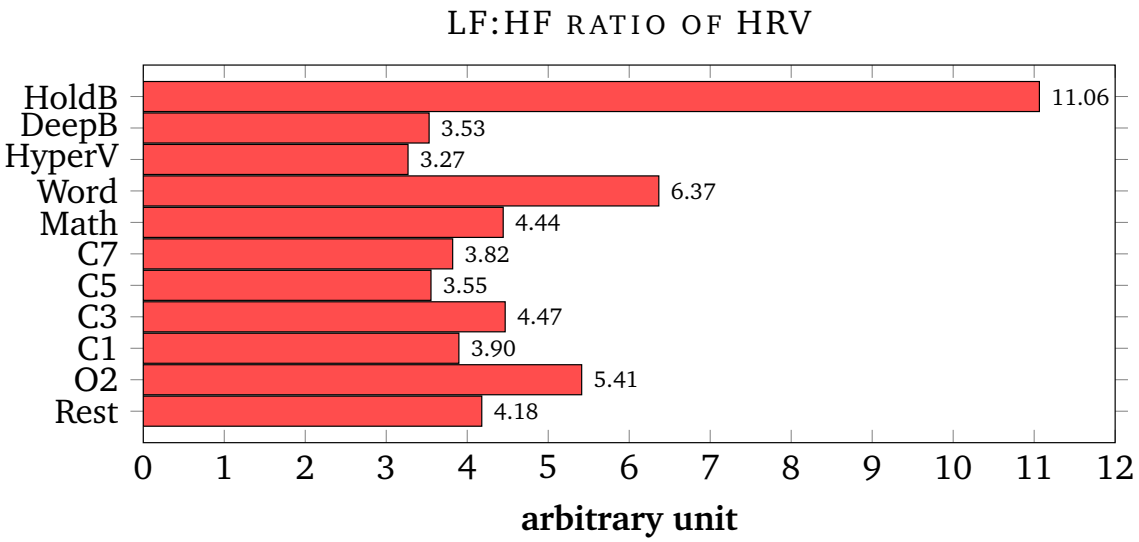

Figure 7.4 The heart rate variability in all experiment conditions.

Mental tasks increases the LF:HF ratio higher than the baseline, where mental arithmetic was ($M = 4.44$, $SD = 1.46$) and word recall was ($M = 6.37$, $SD = 2.85$). Volitional hyperventilation and deep inspiration has a lower mean LF:HF ratio than at rest, with hyperventilation mean LF:HF was ($M = 3.27$, $SD = 1.35$) and deep inspiration was ($M = 3.53$, $SD = 2.97$). Breath hold has the highest LF:HF ratio mean ($M = 11.06$, $SD = 12.79$).

7.3 Discussion

Hyperoxia silenced peripheral chemoreceptors which shows in the result of various gas compositions experiments. The respiratory rate was maintained within the standard deviation of the mean respiratory rate at rest. This is a relevant result because one of the study aims was to investigate the neuronal response to various carbon dioxide concentrations.

The mental task experiments show that cognitive processing and vocalisation increases the heart rate. This increase in low to high frequency (LF:HF) ratio suggests a shift of autonomic output from parasympathetic to sympathetic.

Schneider documented an increase on both systolic and diastolic blood pressure towards the end of breath hold and this was contributed to by sympathetic drive to sustain the peripheral vascular tone [Dempsey 2012, Macefield et al. 2006, Schneider 1930].

HRV analysis uses LF:HF ratio as an index of balance between parasympathetic and sympathetic nervous system [Sztajzel 2004]. A healthy subject has a LF:HF value between 1.5–2.0 [Tas 1996] and the experimental result show a baseline of 4.28. This is probably because of the underlying neuropathic pain with associated higher sympathetic output.

Breathing 100% oxygen increases the LF:HF ratio and this was probably due to changes in inter-beat timing which was controlled by the autonomic nervous system. It is possible that there is an increased sympathetic output when breathing 100% oxygen.

In a healthy state, delivering 100% oxygen effectively silences the peripheral chemoreceptor input [Dejours 1963]. 100% oxygen reduces mean arterial blood pressure, respiratory rate and increases the peripheral vascular resistance, but this changes were not statistically significant in healthy volunteers [Graff et al. 2013]. However, deactivation of chemoreceptors with hyperoxia in disease states causes significant reduction in both blood pressure and respiratory rate in hypertension [Izdebska et al. 2006] and in chronic liver cirrhosis [Moller et al. 2010].

The cardiovascular changes seen in hyperoxia are postulated to be a direct effect of oxygen on the vascular endothelial tissue [Graff et al. 2013, Querido et al. 2010]. Some researchers suggest that parasympathetic activity increases with hyperoxia in a dose-dependent manner [Shibata et al. 2005].

Breathing 100% oxygen caused a significant decrease in muscular sympathetic nerve activity in essential hypertensive subjects [Sinski et al. 2012; 2014]. These autonomic and vascular changes return to baseline following regular respiration of room air [Gole et al. 2011]. This experimental result supports the finding that 100% oxygen inhalation increases BOLD signals in the right anterior cingulate [Macey et al. 2007].

Breathing 1, 5, and 7% carbon dioxide mixed with oxygen reduces LF:HF ratio below the baseline while 3% carbon dioxide increases the ratio higher than resting state. These changes are postulated to be the direct effect of carbon dioxide on the autonomic nervous system or to the cerebral vasculature. The effect of carbon dioxide is prominent in awake human which suggests a cortical modulation of the autonomic nervous system contributes to the effect on HRV [Brown and Howden 2008, Poyhonen et al. 2004]. This postulation is in agreement with the reduction of BOLD signal in right anterior cingulate after 5% carbon dioxide gas inhalation [Macey et al. 2007].

Voluntary hyperventilation and deep inspiration has a lower LF:HF ratio compared to the resting state. Voluntary ventilation influences the HRV and tends to have a lower LF:HF ratio [Bernardi et al. 2000; 2001, Leung et al. 2013]. The influence is demonstrated by varied inter beat (RR interval) differences, which is the main data used in HRV computation.

Meanwhile, the breath holding experiment shows an increase in LF:HF ratio and sympathetic output is known to increase during apnea periods to maintain systolic blood pressure [Dujic et al. 2008, Kiviniemi et al. 2012, Macefield et al. 2006]. The mean heart rate did not differ much from resting heart rate because of compensatory reflex tachycardia after the breath hold period.

Mental tasks showed a higher respiratory and heart rate. The HRV result shows a higher LF:HF ratio compared to baseline which suggests an increase in sympathetic activity. This finding is consistent with psychological research in cognition and emotion [Bernardi et al. 2000, Critchley et al. 2003, Lane et al. 1998; 2009]. We can conclude that the change in heart rate in these experimental conditions was directly influenced by sympathetic output.

7.4 Conclusion

The mean LF:HF at rest in the study population was higher than healthy subjects probably because of underlying neuropathic pain. The results suggest that neuropathic pain patients have a higher sympathetic output at rest.

Mental tasks and volitional breath hold experiments demonstrated an increase in sympathetic output by having a higher LF:HF ratio. Similarly, respiration at rest using 100% oxygen increases the LF:HF ratio. Respiration using carbon dioxide mixed with oxygen lowers the LF:HF ratio which suggests that carbon dioxide may have a direct influence in reducing sympathetic nervous system output. These results support fMRI findings and provides cardiovascular changes that werelacking in the report [Macey et al. 2007].

In the next chapter, I will discuss the LFPs analysis in an attempt to investigate voluntary command of respiration. LFPs provides better time resolution data than functional magnetic resonance imaging. However, LFPs recording is invasive as compared to fMRI.

8
Volitional Breathing

Time-frequency analysis provides oscillatory nature and time information of neuronal activity. The objectives of this thesis are to investigate LFPs changes in deep brain nuclei during spontaneous, volitional breathing, inhalation of various gas compositions and mental tasks.

Human research using macro electrode reports LFPs changes in movement disorders, exercise physiology, pain perception and recently, in respiratory function [Basnayake et al. 2011, Green et al. 2007a, Green and Paterson 2008]. However, there is limited literature on LFPs and volitional breathing.

The primary premise of this thesis is that the brain stem drives awake respiration at rest that represents the physiological balance of demand and supply for individuals regardless of gender, age and fitness level.

I hypothesise that a change in brain state by means of computation, word search, and voluntary breathing requires a change in cortical output that influences the brain stem respiratory signals.

I analysed the LFPs signals during voluntary breathing tasks and compared them to awake resting state LFPs, and investigated if there is any change in the signal properties that support my hypothesis.

8.1 Room Air Result

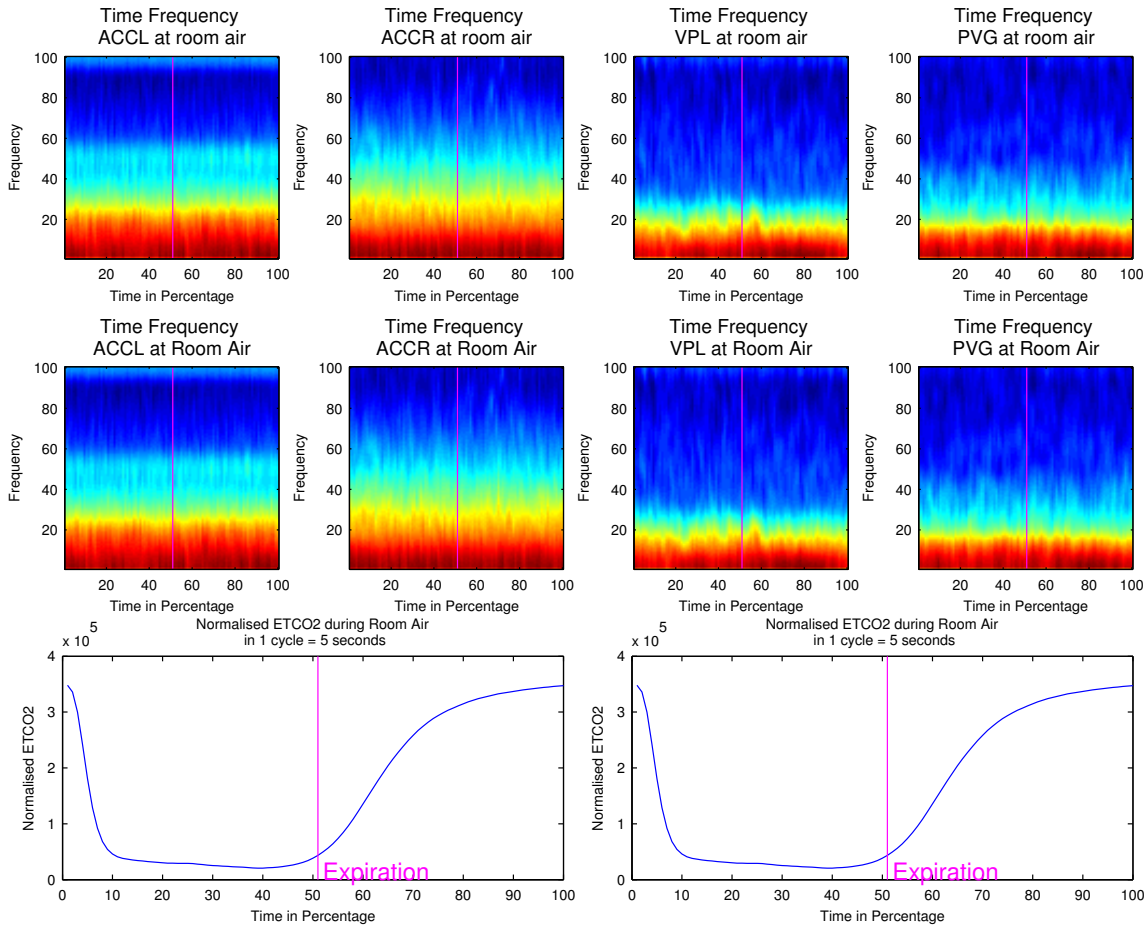

Figure 8.1 Time frequency analysis of bilateral ACC, VPL and PVG while breathing room air.The transition of respiratory phase is marked with vertical line.

Figure 8.1 shows the time-frequency analysis from 1 to 100 Hz of each investigated nuclei in one respiratory cycle. The initial general impression is that there areintensity differences in frequency power wherein the ACC nuclei exhibit higher power in beta and gamma band while the thalamus and periventricular gray shows an increased power in the lower frequency bands. The neuronal activity of beta and gamma band in the right cingulate was higher than the left cingulate throughout the respiratory cycle.

8.1.1 Inspiration Phase

The mean power of each frequency band was calculated as percentage of total power in 1 to 100 Hz, see Figure 8.2. In the delta band during inspiration phase at rest, the left

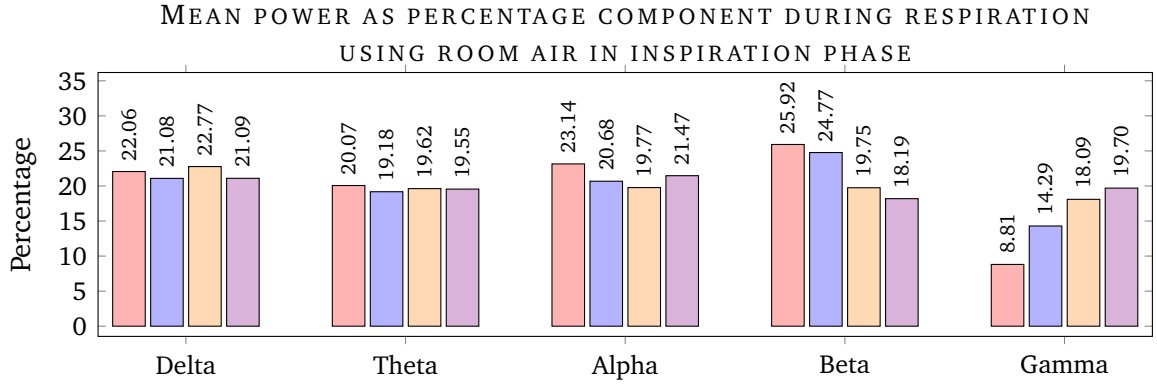

Figure 8.2 The summary of mean total power spectra in Delta, Theta, Alpha, Beta and Gamma band during inspiration phase using room air in ACCL, ACCR, VPL and PVG.

ACC had a mean power of (M = 22.07%, SD = 1.82%), the right ACC (M = 21.08%, SD = 1.05%), while the VPL (M = 22.77%, SD = 1.99%) and the PVG (M = 21.1, SD = 1.15%).

The theta band of the left ACC mean power during inspiration phase of regular inspiration using room air was (M = 20.07%, SD = 1.14%), the right ACC (M = 19.18%, SD = 0.82%), the VPL (M = 19.62%, SD = 0.95%) and the PVG (M = 19.55%, SD = 0.75%).

The alpha band of the left anterior had the highest mean during inspiration phase at rest with (M = 23.14%, SD = 1.05%). The right ACC had a mean power of (M = 20.68%, SD = 1.12%), while the VPL shows a mean of (M = 19.77%, SD = 1.3%) while the PVG had a mean of (M = 21.47%, SD = 1.22%).

The beta band of the left ACC mean power was (M = 25.92%, SD = 2.46%), the right ACC (M = 24.77%, SD = 1.66%), the VPL (M = 19.75%, SD = 1.95%) and the PVG (M = 18.19%, SD = 1.26%).

The gamma band at rest during regular inspiration phase shows left ACC mean power of (M = 8.81%, SD = 0.59%) while the right ACC was (M = 14.29%, SD = 1.07%). The VPL mean power component was (M = 18.09%, SD = 1.43%) while the PVG was (M = 19.70%, SD = 1.48%).

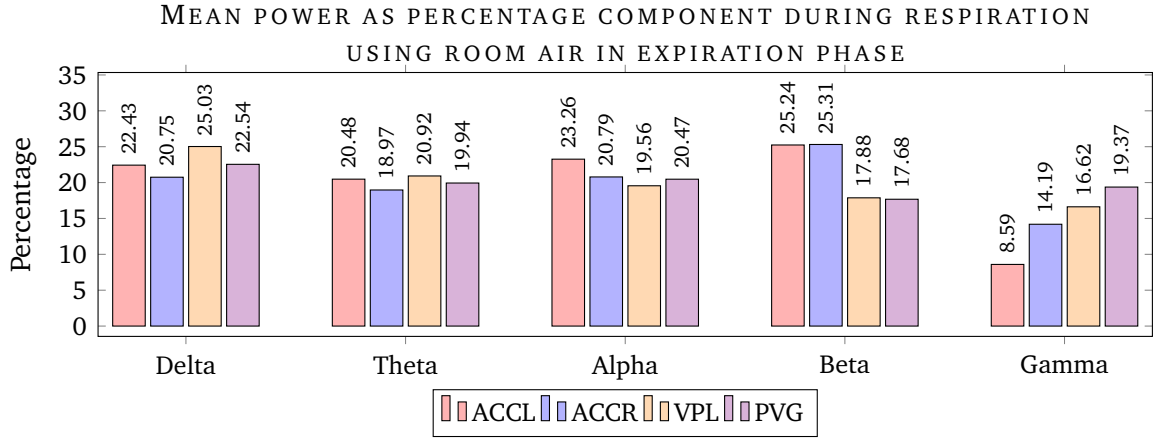

Figure 8.3 The summary of mean total power spectra in Delta, Theta, Alpha, Beta and Gamma band during expiration phase using room air in ACCL, ACCR, VPL and PVG.

8.1.2 Expiration Phase

Figure 8.3 shows the mean power spectra of each investigated frequency bands in four investigated nuclei. The delta band of the left ACC had a mean (M = 22.43%, SD = 1.91%), the right ACC (M = 20.74%, SD = 1.12%), while the VPL (M = 25.03%, SD = 2.17%) and the PVG (M = 22.54, SD = 1.88%).

The theta band of the left ACC mean power during expiration phase of regular expiration using room air was (M = 20.48%, SD = 1.05%), the right ACC (M = 18.97%, SD = 0.87%), the VPL (M = 20.92%, SD = 1.20%) and the PVG (M = 19.94%, SD = 0.88%).

The alpha band of the left anterior had the highest mean with (M = 23.26%, SD = 1.26%). The right ACC had a mean power of (M = 20.79%, SD = 0.84%), while the VPL shows a mean of (M = 19.56%, SD = 1.04%) while the PVG had a mean of (M = 20.47%, SD = 1.43%).

The mean power of beta band of the left ACC was (M = 25.24%, SD = 2.11%) and the right ACC (M = 25.31%, SD = 1.75%). The VPL and PVG had similar mean power level with (M = 17.88%, SD = 2.51%) and (M = 17.68%, SD = 1.27%) respectively.

The gamma band of the left ACC had a mean power of (M = 8.59%, SD = 0.83%) while the right ACC was (M = 14.19%, SD = 1.15%). The VPL mean power was (M = 16.62%, SD = 1.51%) while the PVG was (M = 19.37%, SD = 1.88%).

8.2 Breath Hold Result

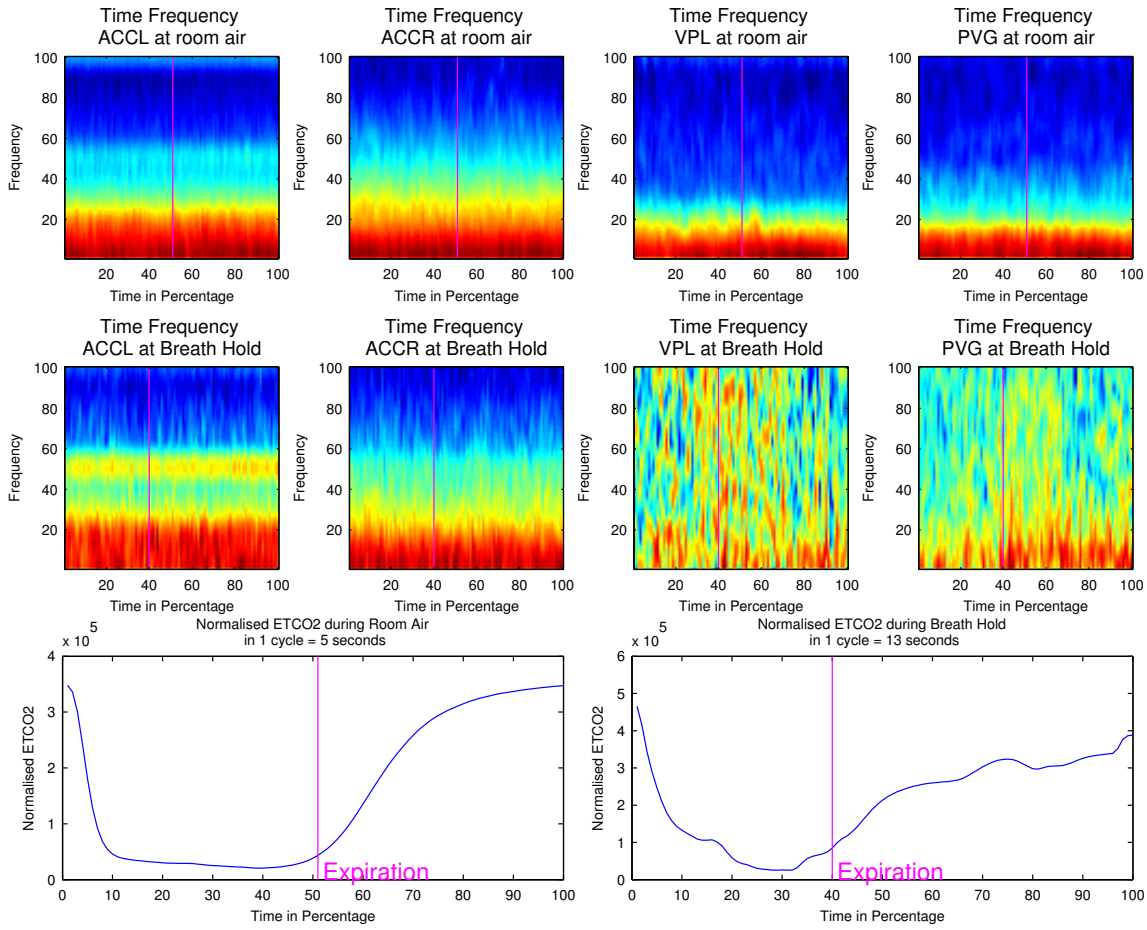

Figure 8.4 Time frequency analysis of bilateral ACC, VPL and PVG while in inspiration phase and during the breath hold phase. The transition of respiratory phase is marked with vertical line.

Time-frequency analysis in Figure 8.4 shows a global reduction in intensity in the low-frequency bands (less than 20 Hz) in all investigated nuclei. The left ACC shows an increased power in 40 to 60 Hz during the breath hold experiment with maximal power towards the end of breath hold period. The right ACC shows a lower power in the low-frequency bands during the expiration phase compared to regular expiration.

The VPL shows an increased average power in the high-frequency bands throughout the respiratory cycle. The mean power of high-frequency bands was maximal just before the transition from inspiration to expiration phase and reduced at about 80% during the actual breath hold period.

The PVG exhibited an increase in mean power in the lower frequency bands during the transition from inspiration to expiration and lasted till the end of breath hold period.

8.2.1 Inspiration Phase

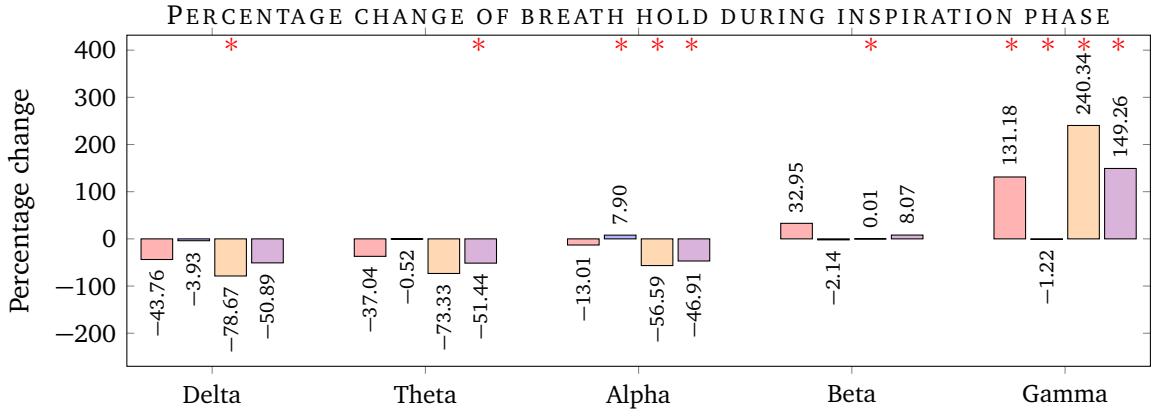

Figure 8.5 The summary of mean percentage change in power spectra in Delta, Theta, Alpha, Beta and Gamma band during inspiration phase before breath hold ACCL, ACCR, VPL and PVG compared to quiet inspiration at room air.

Figure 8.5 summarise of percentage change in Delta, Theta, Alpha, Beta and Gamma band during inspiration phase in ACCL, ACCR, VPL and PVG just before the breath hold section as compared to quiet inspiration.

Comparison between the inspiration phase of breath hold to regular inspiration shows that the delta band had an average power reduction of 78.76% ($p<0.05$) in VPL. The PVG mean power was 50.89% less ($p>0.05$). There was 43.76% less ($p>0.05$) in the left ACC and only a small reduction of the right ACC by 3.93% ($p>0.05$).

Similarly, the theta band shows a maximal reduction of mean power in VPL (73.33% ($p>0.05$) less compared to regular inspiration). The PVG had a reduction of 51.44% ($p<0.05$) and the left ACC shows a reduction of 37.04% ($p>0.05$) in mean power percentage difference. There was a small reduction of 0.51% ($p>0.05$) in the right ACC.

There was increased activity in the right ACC during the inspiratory phase in the alpha band by 7.90% ($p<0.05$). The remaining three other nuclei's activity were below the baseline. The maximal reduction was in VPL with 56.59% ($p<0.05$) less mean power. The VPL had a reduction of 46.91% ($p<0.05$) in mean power, whilst the left ACC had a reduction of 13.01% ($p>0.05$).

The beta band exhibits a higher mean power spectra in 3 nuclei. The maximum was in the left ACC with 32.95% ($p>0.05$) increment, followed by an 8.07% ($p>0.05$) increase in activity in the PVG. There was a small increase of 0.01% ($p<0.05$) activity in the VPL. The right ACC activity was reduced by 2.14% ($p>0.05$) compared to the regular inspiration phase.

The gamma band shows the highest change of mean power from baseline with 240.34% ($p<0.05$) more power in VPL during inspiration before breath hold than during the regular inspiration phase. The PVG had a higher mean power spectrum with 149.26% ($p<0.05$) more and in the left ACC with 131.18% ($p<0.05$) more than baseline. The right ACC remains lower than regular inspiration phase with a reduction of 1.22% ($p<0.05$).

8.2.2 Expiration Phase

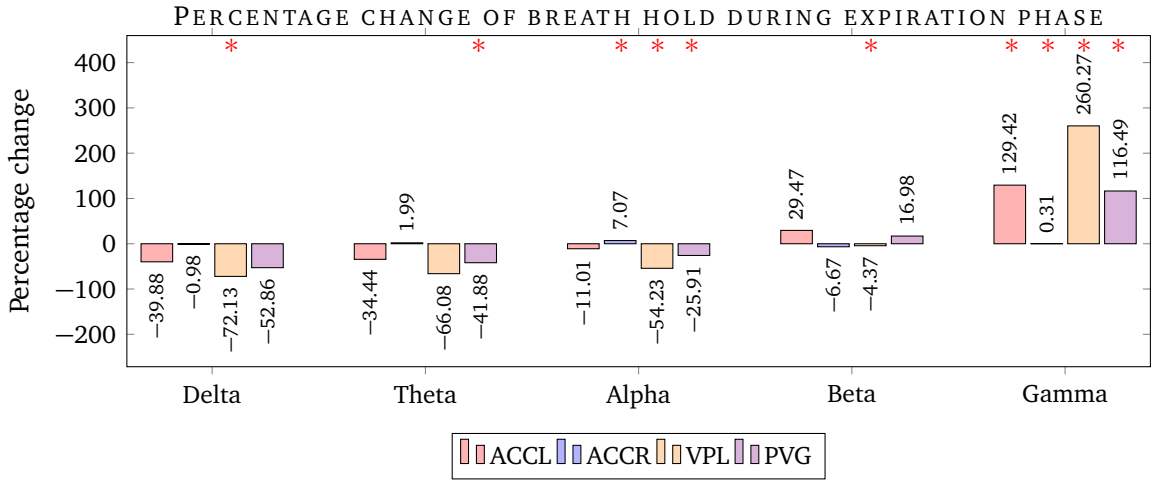

Figure 8.6 The summary of mean percentage change in power spectra in Delta, Theta, Alpha, Beta and Gamma band during expiration breath hold phase in the ACCL, ACCR, VPL and PVG compared to quiet expiration at room air.

Figure 8.6 summarise the mean power spectral percentage change in Delta, Theta, Alpha, Beta and Gamma band during expiration breath hold phase in ACCL, ACCR, VPL and PVG.

The expiration phase of the breath hold experiment exhibits a similar pattern to that seen in the inspiration phase where the nuclei activity reduced in the lower frequency and amplified in the high frequency.

There was a maximal 72.13% ($p<0.05$) reduction in mean power spectra in the delta band recorded in the VPL. The PVG had the second lowest reduction by 51.86% ($p>0.05$) during the expiration phase. The left ACC mean power spectra was reduced by 39.88% ($p>0.05$) while the right ACC shows a minimal reduction of 0.98% ($p>0.05$) less than regular expiration.

The theta band mean power spectra in the VPL, PVG and left ACC was lower than baseline in this phase with reduction of 66.08%($p>0.05$), reduction of 41.88% ($p>0.05$) and reduction of 34.44% ($p<0.05$) respectively. There was an increase of 1.99% ($p>0.05$) mean power spectra in the right ACC in the theta band during the expiration phase of breath hold.

The alpha band shows similar changes seen in the theta band where the maximal reduction in activity was in the VPL with reduction of54.23% ($p<0.05$). The PVG had reduction of 25.91% ($p<0.05$) mean power spectrum in this expiration phase. The left ACC had 11.01% ($p>0.05$) less average power than the baseline. There was an increased mean power spectral in the right ACC by 7.07% ($p<0.05$).

The beta band in expiration phase of the breath hold demonstrated a higher mean power spectra in the left ACC with 29.47% more ($p>0.05$). Meanwhile, the PVG mean power was greater with 16.98% more ($p>0.05$). The right ACC mean power spectra was lower than the baseline with a reduction of 6.67% ($p>0.05$) and the VPL was less by 4.47% ($p<0.05$).

The average power spectra in the gamma band shows positive change from the baseline. VPL had the highest change with 260.27% ($p<0.05$) more power than regular expiration. The left ACC mean power was greater by 129.24%($p<0.05$) and the PVG with 116.49% more ($p<0.05$). The right ACC mean power during expiration breath hold was 0.31% ($p<0.05$) less than the regular expiratory phase.

8.3 Deep Inspiration Result

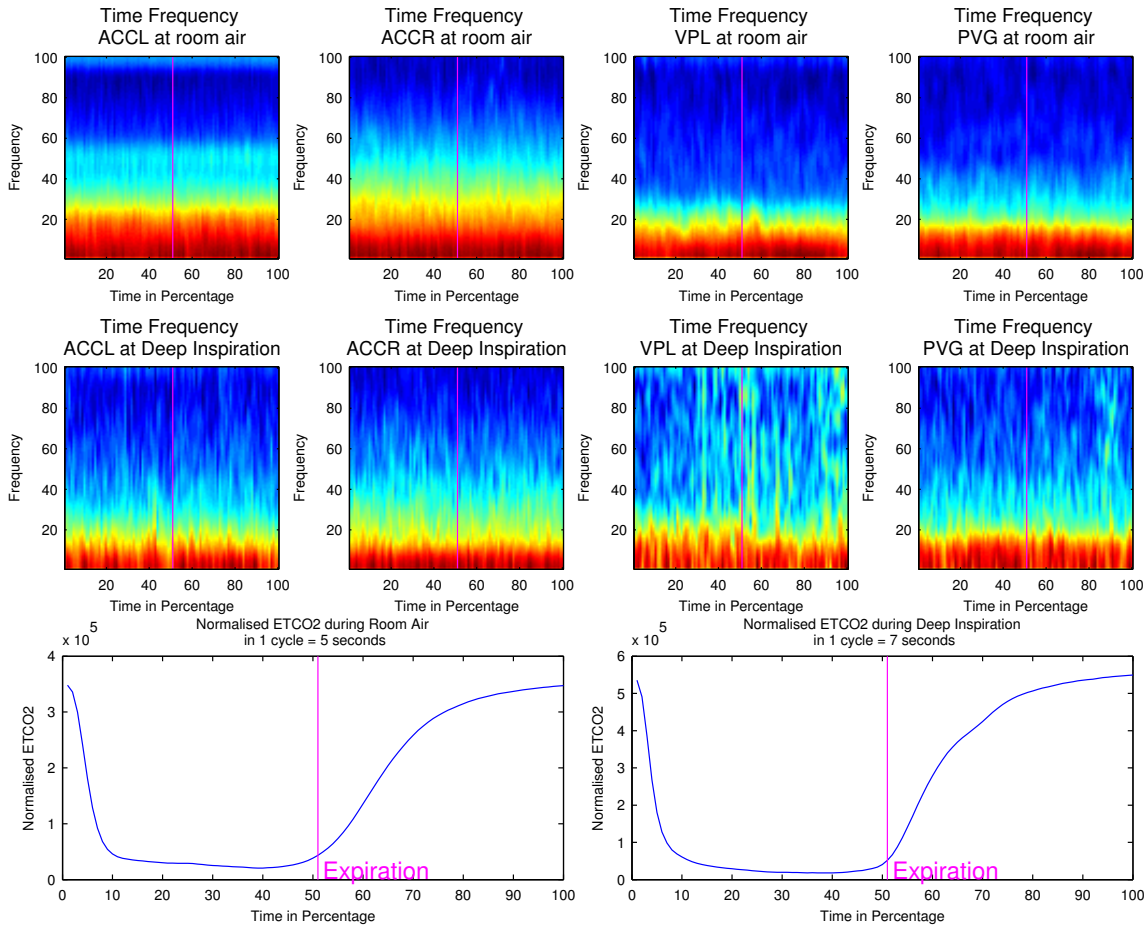

Figure 8.7 Time frequency analysis of bilateral ACC, VPL and PVG while performing deep inhalation. The transition of respiratory phase is marked with vertical line.

Time frequency analysis in Figure 8.7 shows a generalised reduction in intensity within the low frequency (less than 20 Hz) oscillations throughout the respiratory cycle in all 4 investigated nuclei. The high frequency oscillation from 30 to 100 Hz in the right ACC was reduced throughout the respiratory cycle of 1% carbon dioxide inhalation. There was a reduction in lower frequency activity in the thalamus during the inspiratory phase and a further reduction in the expiratory phase.

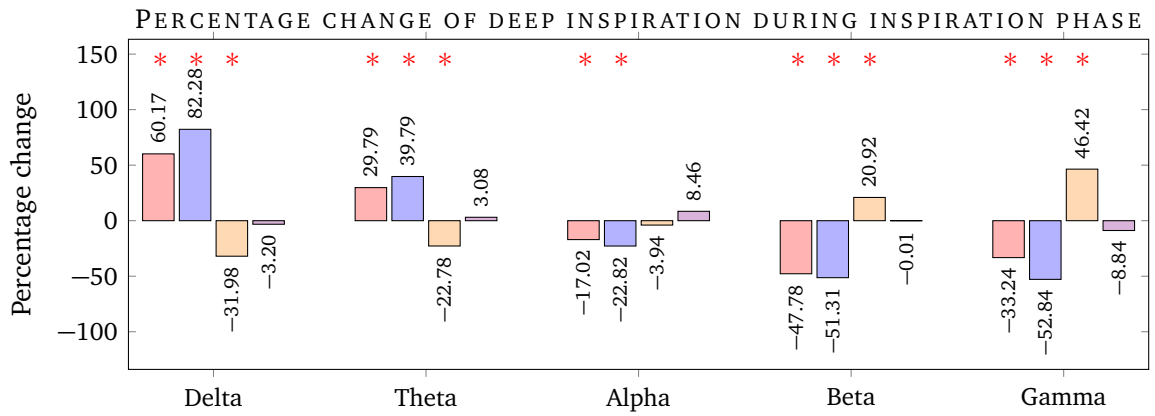

Figure 8.8 The summary of mean percentage change in power spectra in Delta, Theta, Alpha, Beta and Gamma band during inspiration phase of deep inspiration in ACCL, ACCR, VPL and PVG compared to quiet inspiration at room air.

8.3.1 Inspiration Phase

The inspiratory phase of volitional deep inspiration in Figure 8.8 shows an increased mean power in the delta band in both left and right ACC. The left ACC had a greater mean power of 60.17% ($p<0.05$) and the right ACC had 82.28% ($p<0.05$) more in this phase. There was a drop of 31.98% ($p<0.05$) in VPL mean power and a small drop of 3.2% ($p>0.05$) average power in the PVG.

The theta band in the right ACC exhibits a similar directional change as in the delta band. The increment was 39.9% more in the right ACC ($p<0.05$) and 29.79% more in the left ACC ($p<0.05$). There was 22.78% reduction in mean power in the VPL ($p<0.05$). Meanwhile, the PVG shows 3.08% more mean power in deep inspiration phase compared to spontaneous respiration ($p>0.05$). The left ACC alpha band displays a negative change of 17.02% mean power ($p<0.05$).

Similarly, the right ACC show a 22.82% reduced mean power ($p<0.05$) compared to a similar change during spontaneous inspiration. The VPL exhibits a reduction of 3.94% in average power ($p>0.05$). On the other hand, the PVG shows an increase of 8.46% ($p>0.05$) mean power compared to the quiet inspiration phase using room air.

The beta band displays a decrease in the average power in the bilateral cingulate, where the left ACC was 47.78% less ($p<0.05$). The right ACC mean power spectra was 51.31% less compared to similar spontaneous inspiration at room air ($p<0.05$). There

was an increase mean power in the VPL by 20.92% ($p>0.05$). The PVG had a lower mean power by 0.01% ($p>0.05$) during the deep inspiration phase.

The gamma band average power spectra shows a similar pattern as in beta band at this stage. There was a reduction of 33.24% in the left ACC ($p<0.05$) and a decrease of 52.84% in the right ACC ($p<0.05$). On the other hand, the VPL had an increase of 46.43% mean power ($p<0.05$). There was a reduction in mean power of 8.84% in the PVG ($p>0.05$).

8.3.2 Expiration Phase

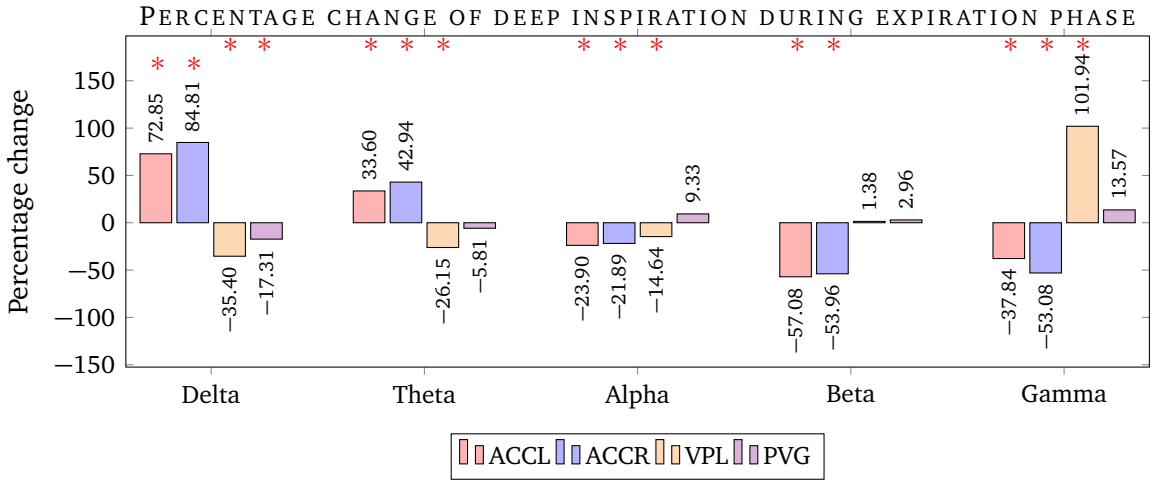

Figure 8.9 The summary of mean percentage change in power spectra in Delta, Theta, Alpha, Beta and Gamma band during expiration phase of deep inspiration in ACCL, ACCR, VPL and PVG compared to quiet inspiration at room air.

The expiration phase of the deep inspiration experiment in Figure 8.9 shows a similar directional change of mean power as in the inspiration phase. The average power spectra of delta band in the left ACC was 72.84% more ($p<0.05$) and an increase of 84.81% more in the right ACC ($p<0.05$). The VPL shows a negative change in mean power in this band by 35.40% ($p<0.05$). Similarly, the PVG mean power was lower by 17.31% ($p<0.05$).

The theta band during the expiration phase shows an increased mean power in the left ACC by 33.60% ($p<0.05$) and 42.94% more in the right ACC ($p<0.05$). The VPL and PVG mean power spectra was lesser by 26.15% ($p<0.05$) and 5.81% ($p>0.05$) respectively.

The alpha band shows a reduction of mean power in bilateral cingulate. The left ACC had a reduction of 23.9% ($p<0.05$) whilst the right ACC was less by 21.89% ($p<0.05$). The VPL mean power was lower by 14.64% ($p<0.05$) whilst the PVG shows a higher mean power by 9.33% ($p>0.05$).

There was a lower beta band mean power in bilateral cingulate with reduction of more than 50% compared to the regular expiration phase. The left ACC was 57.08% less ($p<0.05$) while the right ACC was 53.96% less ($p<0.05$) than regular LFPs activity during spontaneous exhalation. Both VPL and PVG had a minimal increase of power spectra with 1.38% ($p>0.05$) and 2.96% ($p>0.05$) respectively.

Bilateral cingulate mean power spectrum remains lower than regular mean power activity in the gamma band during the expiration phase. The left ACC had a negative change of 37.84% ($p<0.05$) and the right ACC had 53.08% less ($p<0.05$). The VPL activity in the gamma band shows an increase of 101.94% ($p<0.05$) power during this phase. Meanwhile, the PVG only showed an increase of 13.57% during the expiration phase ($p>0.05$).

8.4 Hyperventilation Result

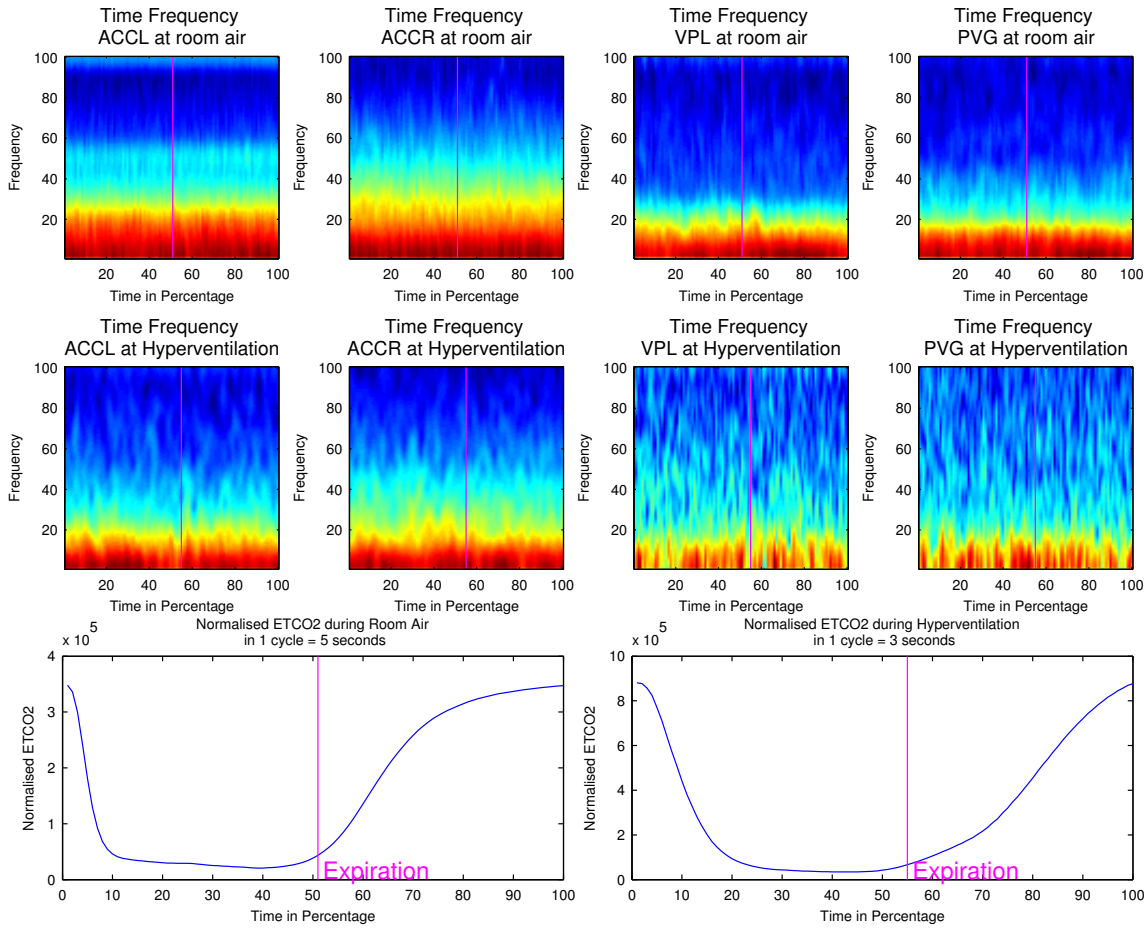

Figure 8.10 Time frequency analysis of bilateral ACC, VPL and PVG while performing voluntary hyperventilation. The transition of respiratory phase is marked with vertical line.

Time-frequency analysis in Figure 8.10 shows a generalised reduction in intensity within the low frequency (less than 20 Hz) oscillations throughout the respiratory cycle in all 4 investigated nuclei. These reductions were more prominent in the VPL, and PVG compared to the quiet expiration phase.

8.4.1 Inspiration Phase

The inspiration phase of volitional hyperventilation in Figure 8.11 shows a higher mean spectral power in the delta band in bilateral ACC. The left ACC was 47.62% higher power ($p<0.05$), and the right ACC was 44.57% higher ($p<0.05$) as compared to the

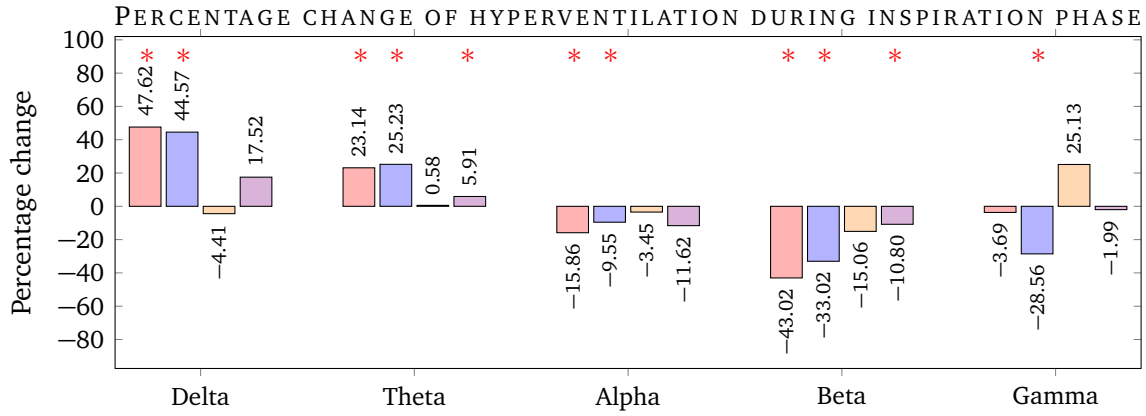

Figure 8.11 The summary of mean percentage change in power spectra in Delta, Theta, Alpha, Beta and Gamma band during inspiration phase of voluntary hyperventilation in ACCL, ACCR, VPL and PVG compared to quiet inspiration at room air.

regular inspiration phase. The VPL had a lower mean power with 4.41% less ($p>0.05$) while the PVG shows an increase in mean power by 17.52% ($p>0.05$).

The theta band average power was higher in all nuclei compared to quiet inspiration. The left ACC was 23.14% more ($p<0.05$) and the right ACC was 25.23% more ($p<0.05$). The VPL mean power spectra were higher by 0.58% more ($p>0.05$), and the PVG was 5.91% more ($p<0.05$).

On the other hand, the alpha band shows a negative percentage change of mean power in all nuclei compared to a quiet inspiration. The left ACC shows a reduction of 15.86% ($p<0.05$) and a 9.55% reduction in the right ACC ($p<0.05$). The VPL had 3.45% lower mean power ($p>0.05$) and 11.6% less in PVG ($p>0.05$) when compared to the resting state.

Similarly, the beta band in all the nuclei have a lower mean power during this phase compared to the regular inspiration phase. There was 43.02% less in the left ACC ($p<0.05$) and 33.02% less in the right ACC ($p<0.05$). The VPL demonstrated a reductionin mean power of 15.06% ($p>0.05$) and 10.8% less mean power in the PVG ($p<0.05$).

The average power in the gamma band for the left ACC was 3.69% less than quiet inspiration ($p>0.05$). Meanwhile, the right ACC had 28.56% less mean power spectra during this expiration phase ($p>0.05$). The VPL shows an increasedmean power of 25.13% ($p<0.05$) and the PVG had lower mean power by 1.99% ($p<0.05$).

8.4.2 Expiration Phase

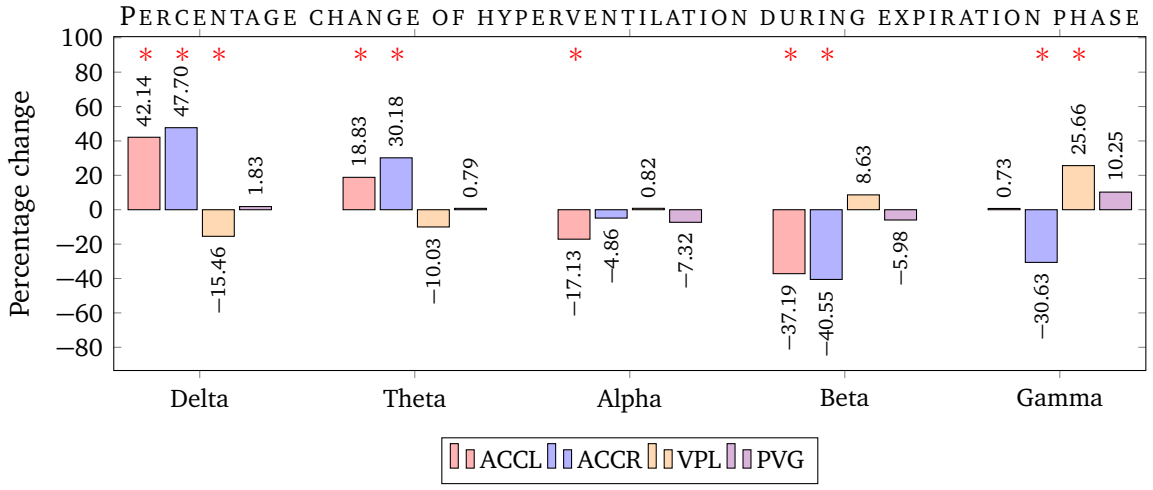

Figure 8.12 The summary of mean percentage change in power spectra in Delta, Theta, Alpha, Beta and Gamma band during expiration phase of voluntary hyperventilation in ACCL, ACCR, VPL and PVG compared to quiet inspiration at room air.

The delta band during the expiration phase in volitional hyperventilation, see Figure 8.12, demonstrates similar differences to those seen in the inspiration phase.

There was a higher mean power spectral density in the bilateral ACC. The left ACC had 42.12% more average power ($p<0.05$), and the right ACC had 47.70% more ($p<0.05$) than the regular expiration phase. The VPL shows 15.46% less mean power in the delta band ($p<0.05$) while PVG shows a minimal increase by 0.83% during the expiration phase ($p>0.05$).

The theta band shows a similar pattern of change as in delta where both ACC displays an increase in the mean power. The left ACC was higher by 18.83% ($p<0.05$), and the right ACC was 30.18% more than resting state expiration ($p<0.05$). The theta band of VPL was reduced by 10.03% ($p>0.05$) while the PVG had a minimal increase of 0.79% ($p<0.05$).

The left ACC average power of the alpha band in expiration phase was decreased by 17.17% ($p<0.05$). Even though there was a reduction in power in the right ACC by 4.86% ($p>0.05$), the change was not statistically significant. The VPL shows a minimal increase of 0.82% ($p>0.05$) mean power spectral and a decrease by 7.32% in PVG ($p>0.05$).

The beta band shows a similar direction of change as seen in the alpha band, where there was a decrease of 37.19% in mean power in the left ACC ($p<0.05$). There was a reduction of 40.55% ($p<0.05$) mean power in the right ACC. The VPL average power was higher by 8.63% ($p>0.05$) and a reduction of 5.98% was seen in the PVG ($p>0.05$).

The gamma band shows a minimal rise in the left ACC with 0.73% change ($p>0.05$) while the right ACC shows a drop by 30.63% ($p<0.05$). There was an increase of VPL mean power by 25.66% ($p<0.05$), and there was a positive 10.25% difference in the PVG ($p<0.05$) during the expiration phase of volitional hyperventilation compared to the regular expiration phase.

8.5 Discussion

Breathing at rest demonstrated similar power density patterns in all investigated nuclei. Both ACC demonstrated a predominant beta band at about 25% of total power whilst the delta, theta, and the alpha band had an average of 20% power each. The gamma band in both ACCs had the least power at rest with 8% for the left and 14% for the right inboth inspiration and expiration phases.

Both PVG and VPL had predominant delta bands with 22–25% of total power whilst the gamma band had the least power contribution at 16–19%. The power amongst theta, alpha, and the beta band were distributed almost equally.

The results of the LFPs analysis show two distinct patterns where volitional deep inspiration and hyperventilation share similar neuronal oscillatory characteristics while the volitional breath hold demonstrated a unique feature as follows.

In deep inspiration and hyperventilation, bilateral ACC shows prominent increases in the delta and theta band mean power with a reduction in activity of alpha and beta. These changes were statistically significantly different from quiet breathing at room air ($p<0.05$).

The gamma band activity during hyperventilation was preserved only in the left ACC while the right ACC activity was reduced ($p<0.05$). The gamma band during deep inspiration shows a bilateral reduction in ACC activity ($p<0.05$).

The PVG and VPL mean power in volitional hyperventilation did not differ statistically from regular respiration in both respiratory phases in all frequency bands. The PVG mean power during deep inspiration is no different to quiet breathing in all frequency bands.

VPL mean power spectra during deep inspiration show a statistically significant reduction in delta and theta band. VPL gamma band mean power was higher than resting state ($p<0.05$).

In summary, volitional deep inspiration and hyperventilation increases mean power spectra in the delta and the theta band in bilateral ACC. On the other hand, the alpha, beta, and the gamma band shows a lower mean power spectra in these two volitional breathing tasks compared to quiet breathing of room air.

The VPL shows the opposite pattern when compared to ACC in volitional hyperventilation and deep inspiration. At the low-frequency bands, an increase in cingulate power was associated with a decrease in VPL power.

On the other hand, at the high-frequency bands, a suppression of bilateral cingulate was associated with an increase in VPL mean power. The PVG mean power remains similar to the resting state in volitional hyperventilation and deep inspiration.

The theta and alpha band activity recorded from scalp EEG increases in tasks requiring attention [Jensen et al. 2002a;b, Klimesch 1999]. Multisite electroencephalograms in vertebrates has established increased theta wave oscillation during active, awake behaviour [Buzsáki 2002, Pignatelli et al. 2012].

A high cholinergic activity during cortical desynchronisation influences hippocampal theta rhythm [Buzsáki et al. 2012, Buzsáki 2002, Buzsáki et al. 2007, Pignatelli et al. 2012]. Extra-hippocampal nuclei such as the entorhinal complex drive the generation of hippocampal theta oscillations through parvalbumin positive interneurons [Pignatelli et al. 2012].

VPL, which is histologically rich in parvalbumin interneurons projecting to the higher cortex and vice versa, fits the role of thalamus as the neuronal oscillator generator in the awake state [Jones 1967; 1998, Jones and Powell 1969, Steriade 1997, Steriade and Contreras 1995, Steriade and Deschenes 1984, Steriade et al. 1993a;b;c; 1996, Steriade and Timofeev 2003].

Non-human primate experiments using LFPs in ACC show that the cingulate synchronises theta activity to serve as a temporal reference for coordinating tasks across frontal cortex and hippocampus. This synchronisation is critical to optimise the route and achieve efficient sensory-motor control [Womelsdorf et al. 2010].

Recordings of synchronisation between the thalamus and the ACC is possible based on neuroanatomical connectivity between these nuclei [I and Locke 1961, Sikes and Vogt 1992, Van Hoesen 1993, Vogt et al. 1979].

An increase in theta band across the frontal-hippocampal-temporal network is essential for coordinating tasks to optimize the processing of sensory and motor signals, and to achieve efficient control between these two signals [Fries 2009, Wang 2010].

Volitional breath holding is a complex physiology where there is an interplay between physiological limits and psychological influences. A study in naval pilots shows that the breaking point of breath hold is predominantly psychological [Schneider 1930].

Superior physiology such as fitness level and bigger lung capacity gives an added advantage to a longer breath hold time [Schneider 1930]. Modification of lung volume, the maximising oxygen carrying capacity and reducing the carbon dioxide level are some of the ways to increase the breath hold breaking point [Agostoni 1963, Flume et al. 1994, Fowler 1954, Hill 1973].

Cardiovascular physiology in breath holding is unique because, during the apneic period, the positive intrathoracic pressure acts as a tamponade, relatively reducing the cardiac output. An immediate physiological response is to maintain the systolic blood pressure through an increase in peripheral vascular resistance. This response was documented by an increase in muscle sympathetic nerve activity [Dempsey 2012, Henderson et al. 2012, Macefield et al. 2006].

The cardiovascular system is modulated not only by the brain stem but from the ACC [Burns and Michael Wyss 1985]. Experiments in human and non-human primates show that electrical stimulation to the ACC may either increase or decrease the blood pressure level depending on the strength of stimulation [Glees et al. 1950, Pool and Ransohoff 1949, Talairach et al. 1973, Ward 1948].

The cortical control of the autonomic nervous system involves multiple networks. Neuroimaging studies show that a wide variation of stimuli can provoke an increase in autonomic output, such as seen in challenging cognitive tasks and in pleasant/aversive stimuli [Cechetto 2014, Gasquoine 2013, Gianaros 2004].

Current research using invasive depth electrodes in epilepsy patients shows that electrical stimulation of the anterior mid cingulate cortex is capable of changing autonomic output [Gentil et al. 2009, Parvizi et al. 2013].

Human experiments using non-invasive transcranial magnetic stimulation to the sensorimotor cortex, the medial prefrontal cortex and the insular cortex show promising results in managing arterial hypertension [Cogiamanian et al. 2010].

Volitional breath hold shows predominantly increases in gamma band activity in the left ACC, VPL and PVG ($p<0.05$). The right ACC shows no change in mean power in all frequency bands.

Heart rate variability during volitional breath hold displays an increase in LF: HF ratio that suggests an increase in sympathetic output. In contrast, volitional deep inspiration and hyperventilation show a lower LF: HF ratio compared to the baseline. Nevertheless, these changes in HRV are not statistically significant because of small sample size and wide variability between the subjects. Therefore, we cannot confidently conclude that the increase in the gamma band activity in the left ACC, VPL and PVG is related to autonomic changes.

The thalamocortical circuit is an important network for sensory perception. It is possible that during volitional breathing, the sensory input from both nasal and auditory complexes pass through the ventral posterior thalamus as a node into a larger network of tactile motor coordination [McCormick and Bal 1994].

The persistent gamma activity in VPL in all three volitional breathing conditions suggests an increase in feedback signals from the periphery to the cortex or vice versa [Steriade 1997]. Thalamic gamma oscillations are highly dependent on alertness and tonically active during the brain âĂŸactivated state' [Steriade et al. 1996].

On a similar note, the cerebellum exerts excitatory influences on cortical activity for gamma synchrony between the sensory, and the motor cortices during tactile coordination [Popa et al. 2013] during breath hold, to coordinatelaryngeal closure, stabilisation of the diaphragn and other respiratory muscles. The high activity in the gamma band in the left ACC during volitional breath holding fits the central command hypothesis.

The suppression of low frequency activity, and emergence of gamma frequency activity, seen during tasks involving conscious prolongation of the respiratory cycle may indicate participation of the ACC in the cortical regulation of respiration to suppress and coordinate activity of afferent sensory-motor information, preventing conscious perception of visceral sensation [Fries 2009, Jensen et al. 2002a, Popa et al. 2013]

8.6 Conclusion

The volitional breathing data suggests that LFPs changes represent a feed forward signal in conscious, coordinated tasks. The left anterior cingulate is a feedforwards snchronator of the gamma band for voluntary breath hold. Low frequency desynchronisation by the cingulate in conscious coordinated tasks is more probable than just the autonomic drive of the cingulate cortex.

Conscious modification of respiratory rate as in hyperventilation and deep inspiration requires an increase in low-frequency oscillation and a suppression of higher frequency signals in the bilateral cingulate cortices.

The reduction of VPL activity in the alpha band is another feature of this modification. As compared to thebreath holding experiment, hyperventilation and deep inspiration do not require any laryngeal closure thus the VPL activity remains below the baseline. The VPL activity in the alpha band was higher than the baseline during breath hold period.

9
Various Gas Compositions

Breathing 100% oxygen is safe and necessary in clinical practice if there is a cellular hypoxia risk such as in a suspected case of myocardial infarct or poly-trauma. Respiration of 100% oxygen has beenshown to increase fMRI BOLD signal in the right anterior cingulate in children, and inhalation of 5% carbon dioxide reversed this. BOLD signal in the brain as demonstrated by fMRI has a time resolution limitation and LFPs recordings in this experiment may provide details that complement fMRI findings.

9.1 100 Percent Oxygen Results

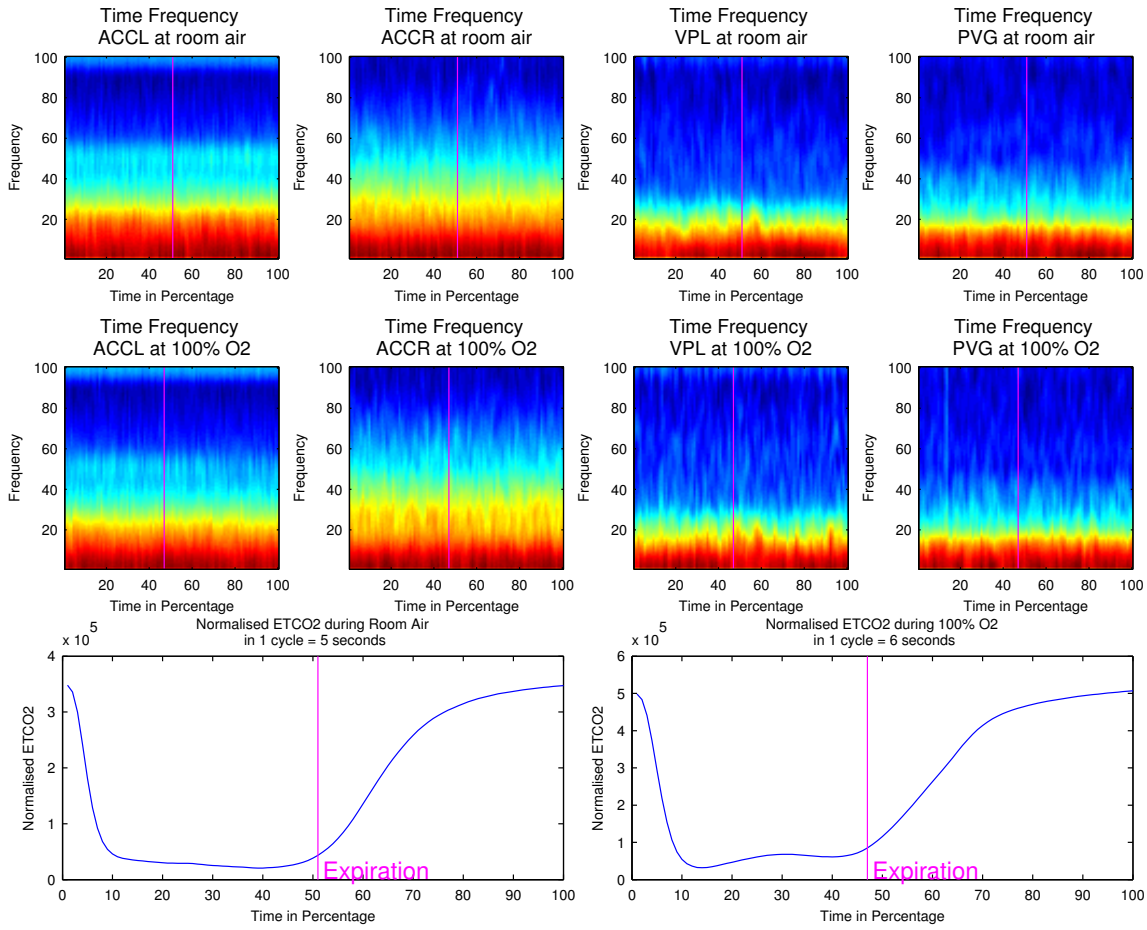

Figure 9.1 Time frequency analysis of bilateral ACC, VPL and PVG while breathing 100% oxygen. The transition of respiratory phase is marked with vertical line.

Time-frequency analysis in Figure 9.1 shows a generalised reduction in intensity within the low frequency (less than 20 Hz) oscillations throughout the respiratory cycle in all 4 investigated nuclei. The high-frequency oscillations from 30 to 100 Hz in the right ACC were low throughout the respiratory cycle of 100% oxygen inhalation.

9.1.1 Inspiration Phase

Figure 9.2 shows the summary of mean power spectral changes during inspiration phase using 100% oxygen compared to the similar phase of quiet inspiration.

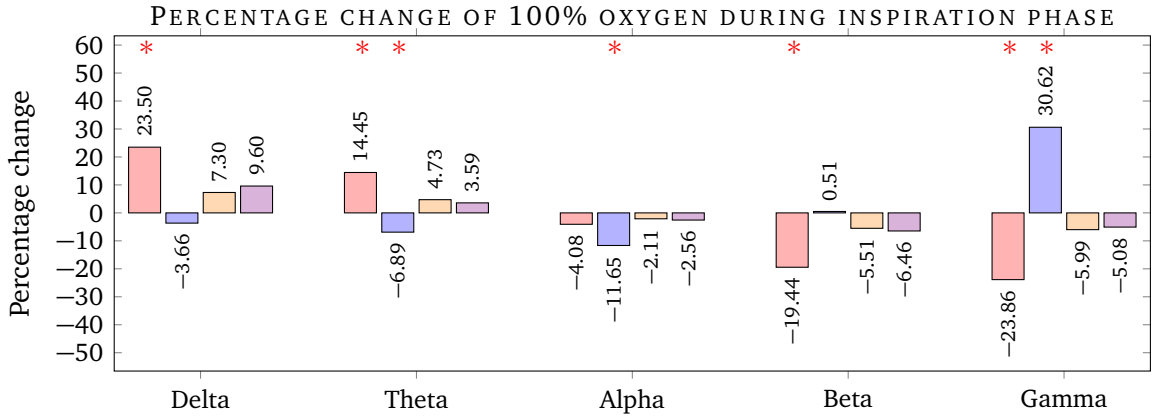

Figure 9.2 The summary of mean percentage change in power spectra in Delta, Theta, Alpha, Beta and Gamma band during inspiration phase using 100% oxygen in ACCL, ACCR, VPL and PVG compared to quiet inspiration at room air.

Inspiring 100% oxygen increases the left ACC mean power by 23.5% in the delta band ($p<0.05$). Meanwhile, the right ACC has a reduction in mean power of 3.66% ($p>0.05$). There was an increase in mean power in the VPL and PVG (7.3% more and 9.6% respectively), compared to regular inspiration using room air. Both PVG and VPL changes were not statistically significant ($p>0.05$).

Similarly, mean power difference in the left ACC was higher by 14.45% ($p<0.05$), whilst the right ACC was lower by 6.89% ($p<0.05$). The mean power in VPL and PVG remains above the baseline with 4.73% more in VPL ($p>0.05$) and 3.59% in the PVG ($p>0.05$).

The mean power in all nuclei were low in the alpha band, where the left ACC has 4.08% less mean power ($p>0.05$). The right ACC has a reduction of 11.65% ($p<0.05$). The VPL mean power spectra was lower by 2.11% ($p>0.05$) and the PVG has 2.56% less mean power ($p>0.05$).

The beta band demonstrated a lower mean power in the left ACC with of 19.44% ($p<0.05$). On the other hand, the right ACC shows a small increase in mean power by 0.51% ($p>0.05$). The VPL has a less 5.51% mean power ($p>0.05$). The PVG has a reduction of6.46% ($p>0.05$) in average power as compared to the inspiration phase of quiet breathing of room air.

The gamma band demonstrated the largestreduction of mean power in the left ACC with 23.86% less ($p>0.05$). Meanwhile, the right ACC has a maximal increase of 30.62%

more than the regular inspiration phase of room air ($p<0.05$). Both VPL and PVG mean power remains below baseline with 5.99% and 5.08% less respectively ($p>0.05$).

9.1.2 Expiration Phase

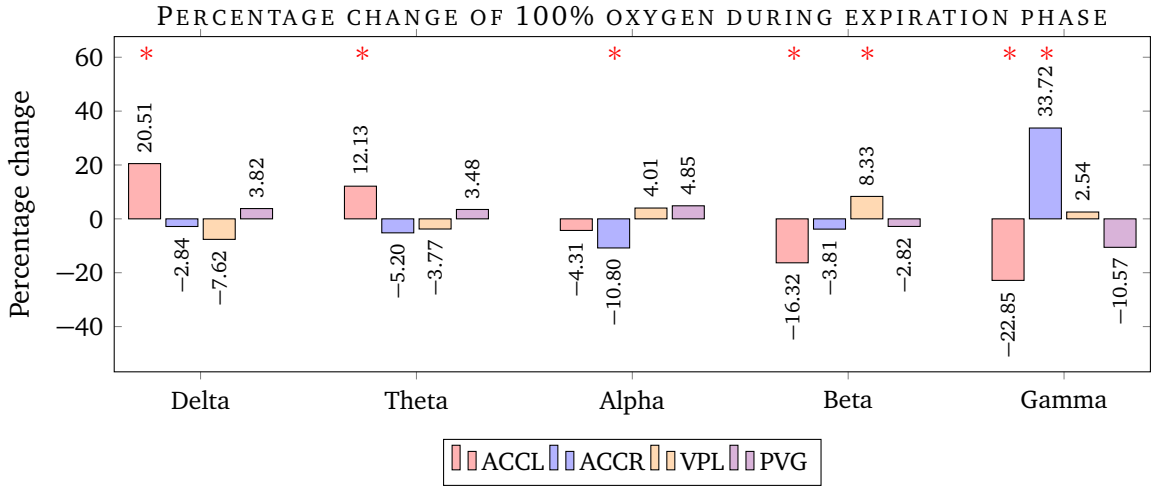

Figure 9.3 The summary of mean percentage change in power spectra in Delta, Theta, Alpha, Beta and Gamma band during expiration phase using 100% oxygen in ACCL, ACCR, VPL and PVG compared to quiet expiration at room air.

Figure 9.3 shows the summary of mean power spectral changes during inspiration phase using 100% oxygen compared to the similar phase of quiet inspiration.

The expiration phase of inspiring 100% oxygen in the delta band shows an increase of mean power in the left ACC by 20.51% ($p<0.05$). Meanwhile, the right ACC shows negative change by 2.84% ($p>0.05$). There was a reduction of VPL activity in the expiration phase by 7.62% ($p>0.05$) while the PVG activity remains higher than the baseline by 3.82% ($p>0.05$). However, these changes in VPL and PVG were not statistically significant from quiet expiration of room air.

Similarly, the theta band average power spectra in the left ACC was higher than the resting rate by 12.13% ($p<0.05$). On the other hand, the right ACC was reduced by 5.20% ($p>0.05$). The VPL activity in this theta band during expiration was lowered by 3.77% ($p>0.05$) while the PVG remained higher than regular expiration by 3.48% ($p>0.05$). Only the left ACC change in the theta band was statistical significantly different from the baseline.

The mean power of bilateral ACC remains on the negative side with 4.31% less in the left ($p>0.05$) and 10.80% less in the right ($p<0.05$). The VPL and PVG show increased activity by 4.01% and 4.85% more than the baseline, but none of these changes were statistically significant ($p>0.05$).

The beta band in the bilateral ACC shows lower mean power; the left having 16.32% less ($p<0.05$) and the right 3.81% less than baseline ($p>0.05$). The VPL mean power was higher 8.33% ($p<0.05$) in the expiration phase in this band while PVG activity was lowered by 2.82% ($p>0.05$).

The gamma band showed the highest change in both negative and positive directions, where the left ACC mean power as reduced by 22.85% ($p<0.05$). The right ACC has a higher mean power by 33.72% during the expiration phase ($p<0.05$). The VPL activity remained higher by 2.54% ($p>0.05$) and the PVG was lower than the baseline by 10.57% ($p>0.05$), but none of these changes were statistically different from quiet expiration at rest.

9.2 1 Percent CO2 Results

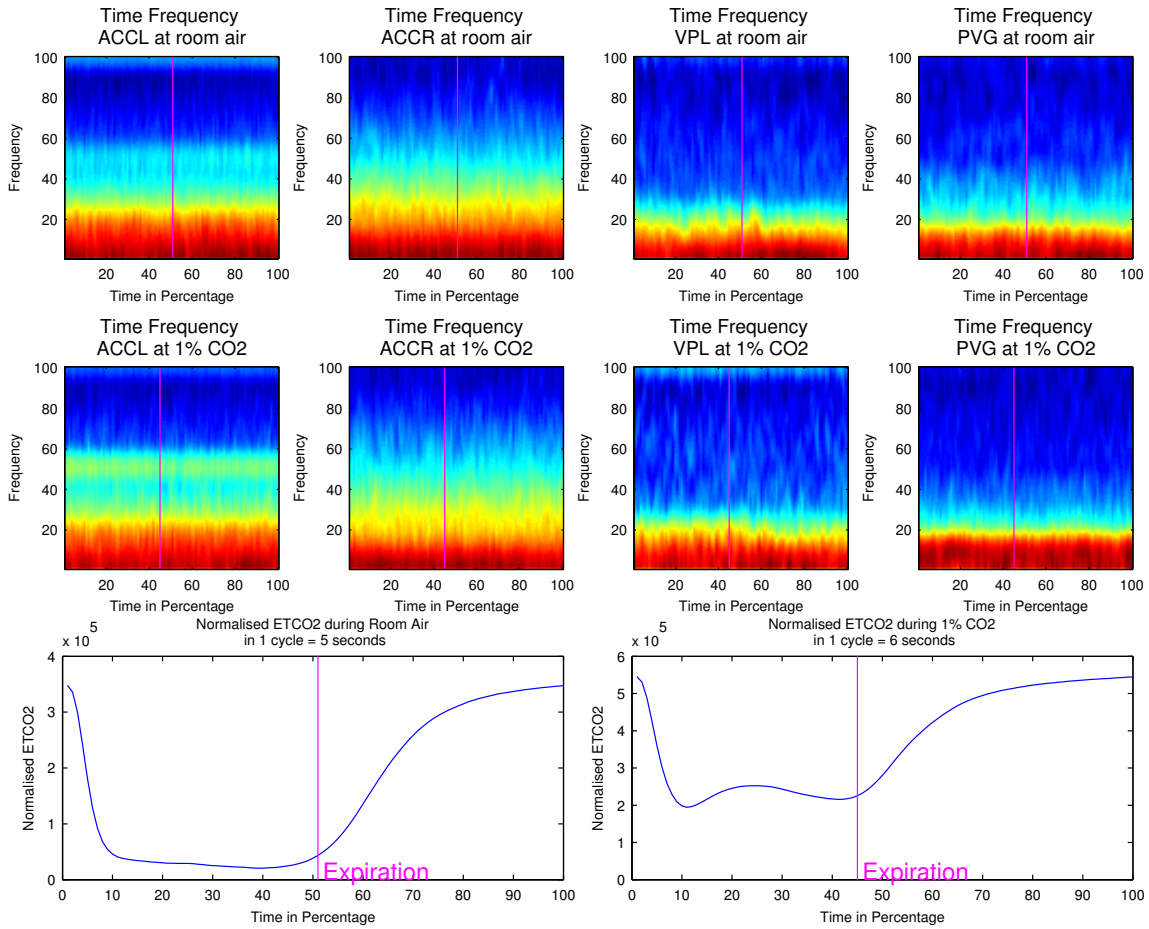

Figure 9.4 Time frequency analysis of bilateral ACC, VPL and PVG while breathing 1% carbon dioxide. The transition of respiratory phase is marked with vertical line.

Time-frequency analysis in Figure 9.4 shows a general reduction of intensity below 20 Hz in oscillations throughout the respiratory cycle in all 4 investigated nuclei whilst inhaling 1% CO2. The cingulate shows an increased intensity in the 20 to 30 Hz throughout the respiratory cycle. Both VPL and PVG power spectra were reduced compared to quiet respiration using room air.

9.2.1 Inspiration Phase

Figure 9.5 shows the summary of mean percentage changes inpower spectra during the inspiration phase of inhaling 1% CO2 compared to quiet inspiration at room air.

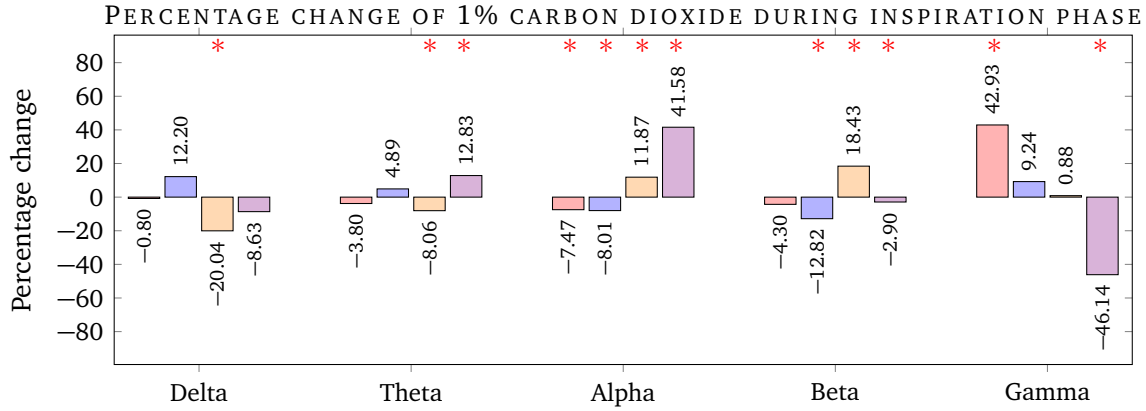

Figure 9.5 The summary of mean percentage change in power spectra in Delta, Theta, Alpha, Beta and Gamma band during inspiration phase using 1% carbon dioxide in ACCL, ACCR, VPL and PVG compared to quiet inspiration at room air.

The delta band of the left ACC shows a reduction in mean power of 0.8% ($p>0.05$), and an increase of 12.2% in the right ACC ($p>0.05$). The VPL shows a negative change from baseline with 20.04% less ($p<0.05$) whilst the PVG shows a reduction of 8.63% in mean power ($p>0.05$).

Inspiring 1% CO2 reduced the left ACC theta band mean power by 3.80% whilst the right ACC shows an increase of 4.89% compared to the quiet inspiration of room air. Both cingulate changes were not statistically significant ($p>0.05$). The VPL shows a lower mean power of 8.06% whilst the PVG displays an increase in mean power spectra by 12.83%. These changes in both VPL and PVG were statistically different from quiet inspiration of room air ($p<0.05$).

Both left and right ACC mean power spectra in the alpha band were lower than quiet inspiration with 7.74% and 8.01% less respectively. These changes were statistically different from the baseline ($p<0.05$). On the other hand, VPL and PVG demonstrated an increase by 11.87% ($p<0.05$)and 41.58% ($p<0.05$) respectively.

The beta band activity in both ACCs shows a decrease in mean power. There was 4.3% less on the left ($p>0.05$) and 12.82% in the right anterior cingulate ($p<0.05$). The VPL activity shows an increase in mean power by 18.43% ($p<0.05$). Meanwhile, the PVG demonstrated a reduction in mean power with 2.9% less than the baseline ($p<0.05$).

The Inspiration phase of 1% CO2 inhalation shows a large increase in gamma band mean power in the left ACC with a 42.93% increment ($p<0.05$). The right ACC shows a 9.24% increase in mean power compared to quiet inspiration, but it was not statistically significant ($p>0.05$). The VPL recorded a very small increase of 0.88% ($p>0.05$), while the PVG demonstrated 46.14% reduction of mean power ($p<0.05$) during the inspiration phase of 1% carbon dioxide.

9.2.2 Expiration Phase

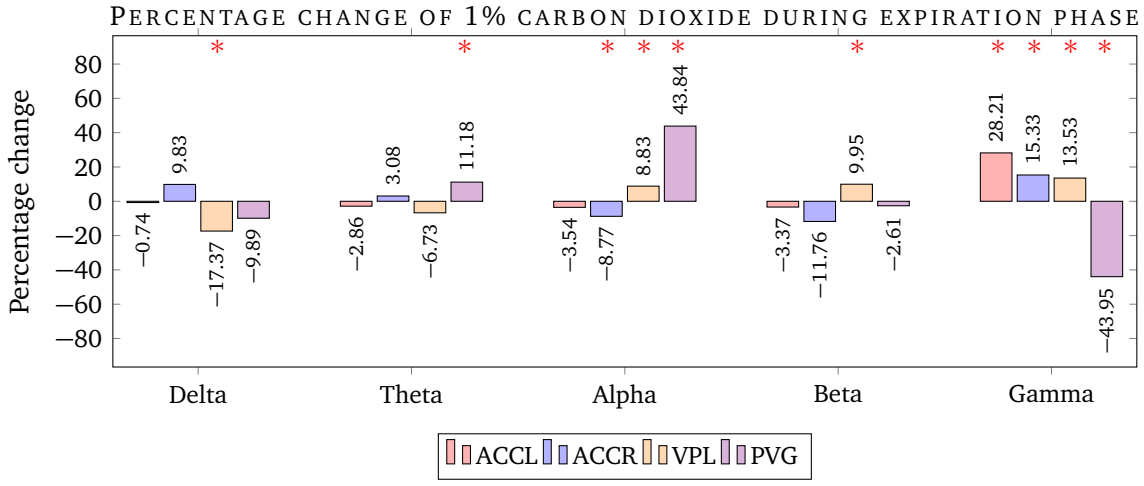

Figure 9.6 The summary of mean percentage change in power spectra in Delta, Theta, Alpha, Beta and Gamma band during expiration phase using 1% carbon dioxide in ACCL, ACCR, VPL and PVG compared to quiet expiration at room air.

Figure 9.6 shows that the delta band during expiration phase in the left ACC did not show a statistically significant mean power difference from quiet expiration of room air. The delta band of the right ACC has a 9.83% increase in mean power compared to regular expiration using room air ($p>0.05$). VPL and PVG recorded the negative difference in mean power by 17.37% ($p<0.05$) and 9.89% ($p>0.05$) respectively.

The expiration phase of 1% CO2 inhalation shows negative mean power difference in the theta band of the left ACC with 2.86% less from baseline ($p>0.05$). The right ACC theta band has 3.08% more mean power than quiet expiration at room air ($p>0.05$). VPL activity remains below the baseline with 6.73% less ($p>0.05$), while the PVG demonstrates an increase of 11.18% more ($p<0.05$).

The alpha band during an expiration phase of 1% CO2 inhalation shows a bilateral reduction of mean power in the ACC. The left ACC shows a decrease of 3.54% ($p>0.05$) and the right ACC shows 8.77% less than regular expiration power ($p<0.05$). The VPL recorded positive mean power difference by 8.83% ($p<0.05$). Meanwhile, the PVG recorded the highest percentage change with 43.84% more than regular expiration ($p<0.05$).

The beta band during the expiration phase shows a decrease in bilateral anterior cingulate mean power with a 3.37% reduction in the left ACC and 11.76% less in the right ACC. These negative changes were not statistically significant ($p>0.05$). There was 9.95% increase in VPL mean power spectra ($p<0.05$) while PVG shows a reduction of 2.61% mean power when contrasted against the regular expiration phase ($p>0.05$).

There was a positive difference of mean power in the gamma band in bilateral ACC and VPL (21.21%, 15.33% and 13.53%) respectively. The PVG recorded negative difference of 43.95% average power during the expiration phase of 1% carbon dioxide inhalation. These changes in the beta band were statistically different from quiet expiration at room air ($p<0.05$).

9.3 3 Percent CO2 Results

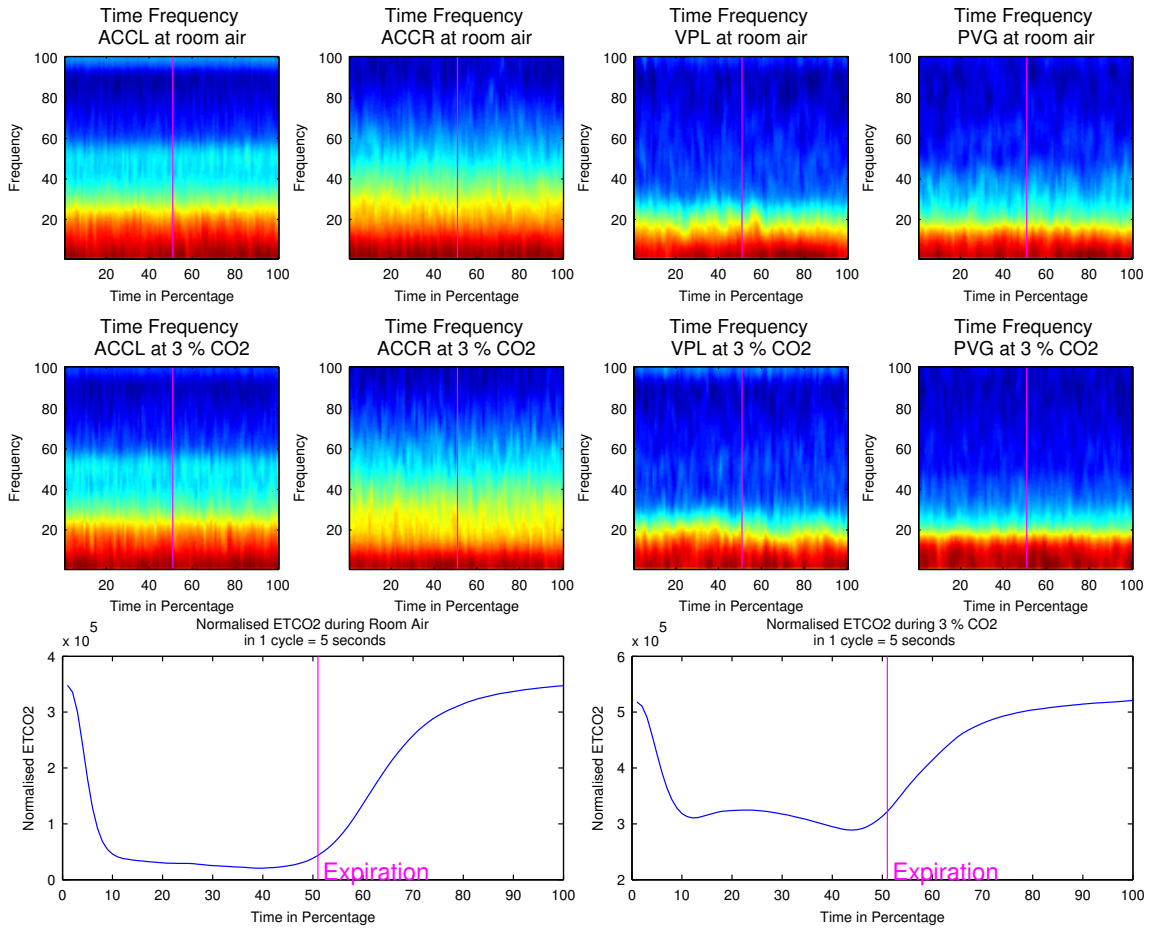

Figure 9.7 Time frequency analysis of bilateral ACC, VPL and PVG while breathing 3% carbon dioxide. The transition of respiratory phase is marked with vertical line.

Figure 9.7 show time-frequency analysis results during inspiring 3% CO2. The low-frequency power spectra were low in intensity throughout the respiratory cycle in both ACCs. The right ACC shows lower intensity power spectra below 20 Hz frequency range. The VPL displays a reduction in intensity of below 20 Hz frequency during the expiration phase while the PVG demonstrated a high intensity below 20 Hz during the inspiration phase.

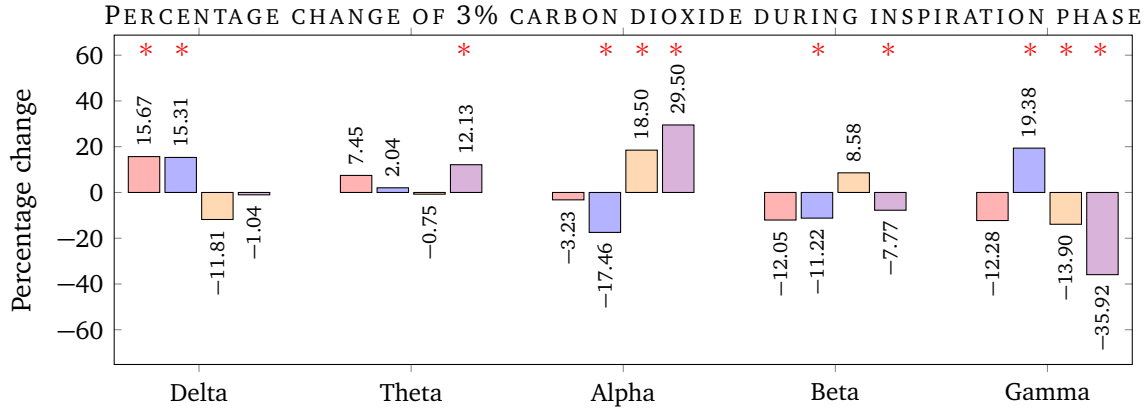

Figure 9.8 The summary of mean percentage change in power spectra in Delta, Theta, Alpha, Beta and Gamma band during inspiration phase using 3% carbon dioxide in ACCL, ACCR, VPL and PVG compared to quiet inspiration at room air.

9.3.1 Inspiration Phase

Figure 9.8 shows that the inspiratory phase of 3% carbon dioxide inhalation shows a positive change of mean power from the baseline in the delta band of bilateral ACC. There was 15.67% more in the left ACC ($p<0.05$) and 15.31% more in the right ACC ($p<0.05$).

The delta band of VPL shows a negative mean change with 11.81% less while PVG shows a negative change of 1.04%. The changes in VPL and PVG were not statistically significant ($p>0.05$).

The theta band of 3% CO2 inspiration recorded an increase of 7.45% more activity in the left ACC while the right ACC shows an increase of 2.04% in activity compared to the baseline. None of the cingulate changes differs significantly from a quiet inspiration of room air ($p>0.05$). The VPL shows a reduction of 0.75% mean power spectra ($p>0.05$). The PVG has 12.13% more mean power spectra ($p<0.05$) compared to the regular inspiration of room air.

The left ACC recorded a negative mean power difference by 3.23% in the alpha band during an inspiration phase of 3% CO2 compared to the quiet inspiration of room air. This negative change was not statistically significant ($p>0.05$). However, a reduction of 17.46% mean power spectra in the right ACC was statistically different from quiet inspiration of room air ($p<0.05$). 3% carbon dioxide inhalation increases VPL mean

power in the alpha band by 18.5%($p<0.05$). Meanwhile, PVG recorded 29.5% more mean power ($p<0.05$)than regular inspiration using room air.

Both ACCs show a reduction in mean power in the beta band with 12.05% less in the left and 11.22% less in the right ACC ($p<0.05$). The VPL beta band shows an increase in mean power by 8.58% ($p>0.05$) whilst the PVG shows 7.77% less mean power ($p<0.05$).

The gamma band average power spectra while inspiring 3% CO2 shows 12.28% less in the left ACC ($P>0.05$). Meanwhile, the right ACC shows a positive increment by 19.38% more than regular inspiration ($P<0.05$). Both VPL and PVG shows less mean power in this phase by 13.9% in VPL and 35.92% in PVG. Both changes in VPL and PVG were statistically different from quiet inspiration of room air ($p<0.05$).

9.3.2 Expiration Phase

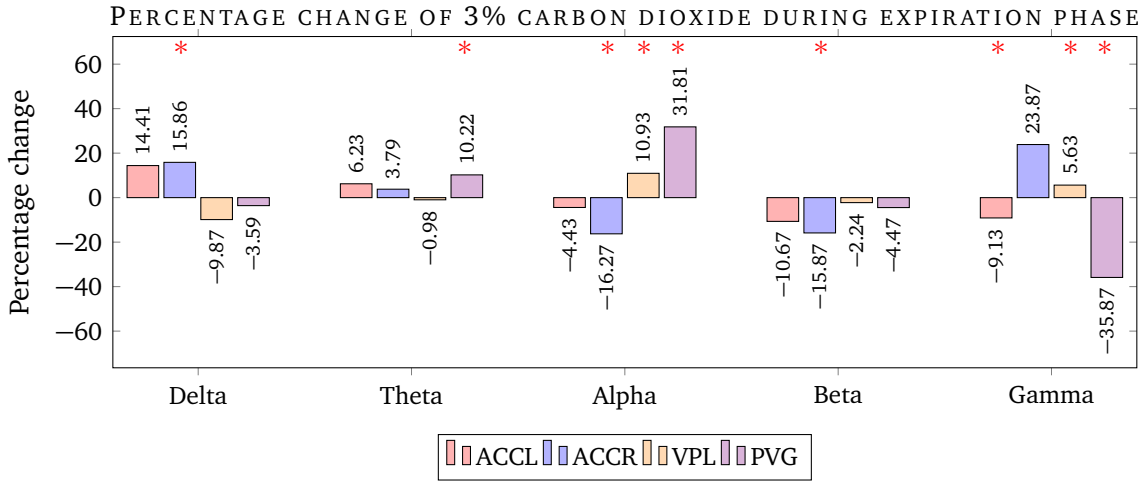

Figure 9.9 The summary of mean percentage change in power spectra in Delta, Theta, Alpha, Beta and Gamma band during expiration phase using 3% carbon dioxide in ACCL, ACCR, VPL and PVG compared to quiet expiration at room air.

The delta band in this phase demonstrated that both ACC have increases in power compared to quiet expiration as demonstrated in Figure 9.9. There was 14.41% more power in the left ACC ($p>0.05$) and 15.86% more in the right ACC ($p<0.05$). Both VPL and PVG show reductionwith 9.87% less in the VPL and 3.99% less in the PVG when

compared to quiet expiration at rest. These negative differences were not statistically significant ($p>0.05$).

The theta band of 3% CO2 expiration phase shows increased power in both ACCs with 6.23% increment in the left ACC and 3.70% more in the right ACC. However, these changes in the ACC were not statistically significant compared to quiet expiration at rest ($p>0.05$). The theta band of VPL was decreased minimally with 0.98% less ($p>0.05$). Meanwhile, the PVG demonstrated an increase of 10.22% more ($P<0.05$) compared to the quiet expiration phase.

Alpha band showed 4.43% less mean power in the left ACC ($p>0.05$) in this period. Similarly, the right ACC shows a negative difference of 16.27% ($p<0.05$). The VPL demonstrated an increased power of 10.93% ($p<0.05$). A similar positive change was observed in the PVG with an increase of 31.81% ($p<0.05$).

The beta band during theexpiration phase of 3% carbon dioxide respiration shows general negative mean power differences in all four nuclei. The right ACC has a reduction of 10.67% while the right ACC has 15.87% reduction. There was a reduction of 2.24% mean power spectra in the VPL and a decrease of 4.47% in the PVG. Only the right ACC difference was statistically different from quiet expiration phase ($p<0.05$).

The expiration phase of 3% CO2 respiration shows a negative difference in the gamma band of the left ACC with 9.13% reduction ($p<0.05$). On the other hand, the right ACC recorded positive difference of 23.87% comparedto the quiet expiration phase. However, this was not statistically significant ($p>0.05$). The gamma band in the PVG demonstrated an increase in mean power of 5.63%($p<0.05$). The PVG has the most negative change with 35.87% less mean power compared to regular expiration ($p<0.05$).

9.4 5 Percent CO2 Results

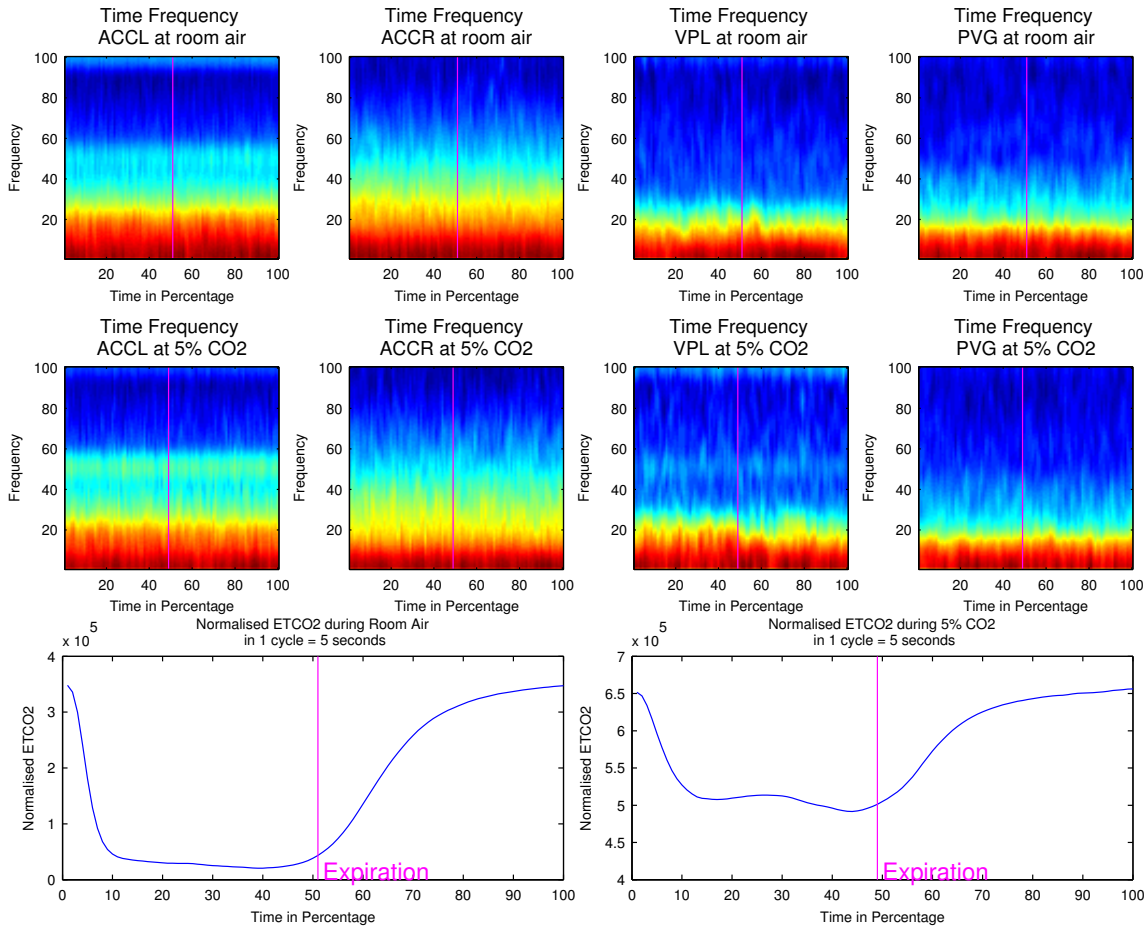

Figure 9.10 Time frequency analysis of bilateral ACC, VPL and PVG while breathing 5% carbon dioxide. The transition of respiratory phase is marked with vertical line.

The time-frequency analysis in Figure 9.10 show a general decrease in low-frequency intensity throughout the respiratory cycle in both cingulate cortices. The right ACC displays a reduction in intensity in the 20 Hz and below frequency range. The VPL shows a decrease in intensity of low-frequency oscillation during the expiration phase.

9.4.1 Inspiration Phase

The inspiratory phase of this experiment shows an increase in mean power in the delta band in bilateral ACC as demonstrated in Figure 9.11. The left ACC has 12.96% more mean power ($p>0.05$) while the right has 18.25% more mean power ($p<0.05$). The

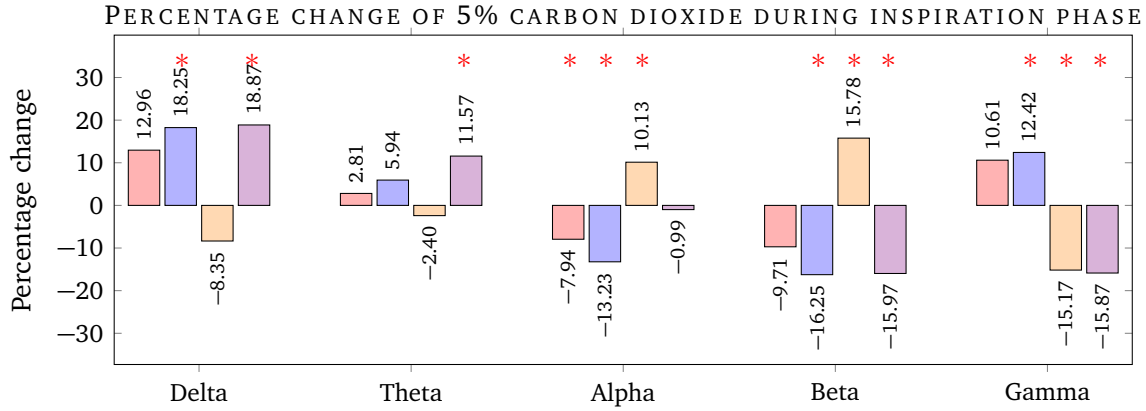

Figure 9.11 The summary of mean percentage change in power spectra in Delta, Theta, Alpha, Beta and Gamma band during inspiration phase using 5% carbon dioxide in ACCL, ACCR, VPL and PVG compared to quiet inspiration at room air.

delta band in VPL shows a negative change in by 8.35% ($p>0.05$). Meanwhile, the PVG was increased by 18.87% ($p<0.05$).

The theta band during 5% CO2 inspiration shows an increase of mean power by 2.81% in the left ACC and 5.96% in the right ACC. Nevertheless, these positive changes were not statistically different from quiet inspiration using room air ($p>0.05$). The VPL mean power reduced by 2.4% ($p>0.05$) while the PVG shows an increase of 11.57% ($p<0.05$).

Both ACCs demonstrated a reductionin mean power in the alpha band. There was 7.94% less in the left ACC ($p<0.05$), and 13.23% less in the right ACC ($p<0.05$) compared to quiet inspiration at rest. These negative changes were statistical significantly different from the baseline. The VPL shows an increase of 10.13% ($p<0.05$) while PVG has a reduction of 0.99% ($p>0.05$).

The beta band in this inspiration phase shows a reductionin mean power in both ACCs. There was 9.71% less for the left ACC ($p>0.05$), and 16.25% less in the right ACC ($p<0.05$). The VPL mean power was increased by 15.78% ($p<0.05$). On the other hand, the PVG shows 15.97% reduction ($p<0.05$).

Inspiration phase of 5% CO2 inhalation increases gamma band of bilateral ACC. There was an increase of 10.61% in the left ACC ($p>0.05$) and 12.42% more in the right ACC ($p<0.05$). Both VPL and PVG have a similar decrease in mean power, 15.17% ($p<0.05$) and 15.87% ($p<0.05$) respectively.

9.4.2 Expiration Phase

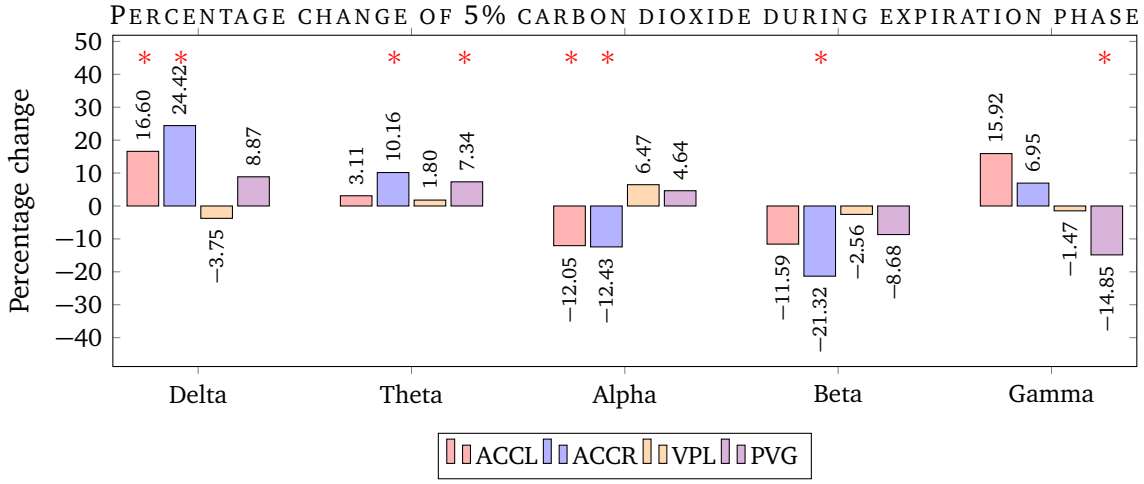

Figure 9.12 The summary of mean percentage change in power spectra in Delta, Theta, Alpha, Beta and Gamma band during expiration phase using 5% carbon dioxide in ACCL, ACCR, VPL and PVG compared to quiet expiration at room air.

The delta band in the expiration phase exhibits a positive average power spectra difference in both ACCs as demonstrated in Figure 9.12. The left ACC was 16.60% increased ($p<0.05$), and the right ACC 24.42% ($p<0.05$). Both ACC expiration phase changes were statistically different from quiet expiration using room air. The VPL has 3.7% less mean power ($p>0.05$) while the PVG shows an increase of 8.87% ($p>0.05$) compared to quiet expiration using room air. There is no statistical difference in mean power during 5% CO2 expiration phase of VPL or PVG compared to quiet expiration at room air.

The theta band average power spectra during the expiration phase of 5% CO2 inhalation shows increases from baseline in both ACCs. The left ACC has 3.11% more mean power ($p>0.05$), and the right ACC has 10.16% more ($p<0.05$). The VPL mean power was increased by 1.80% ($p>0.05$). The theta band in the PVG shows an increased mean power of 7.34% ($p<0.05$).

Both ACC mean power spectra in the alpha band were reduced; 12.05% in the left ACC ($p<0.05$), and 12.43% in the right ACC ($p<0.05$). On the other hand, both VPL and PVG exhibit an increase in mean power by 6.47% ($p<0.05$) and 4.64% ($p<0.05$) respectively. These positive changes were not statistically different from the baseline.

The beta band average power spectra during the expiration phase demonstrated a negativechange in all nuclei. There was 11.59% less in the left ACC ($p>0.05$) and 21.32% less in the right ACC ($p<0.05$). The VPL has 1.56% less ($p>0.05$) and 5.68% less in the PVG ($p>0.05$).

The gamma band average power spectra during the expiration phase demonstrated an increase of 11.92% in the left ACC ($p>0.05$). This change was accompanied by a rise of 6.95% in the right ($p>0.05$). The VPL shows less mean power in this phase with 1.47% less ($p>0.05$). The PVG has the most deficit by 14.85% ($p<0.05$).

9.5 7 Percent CO2 Results

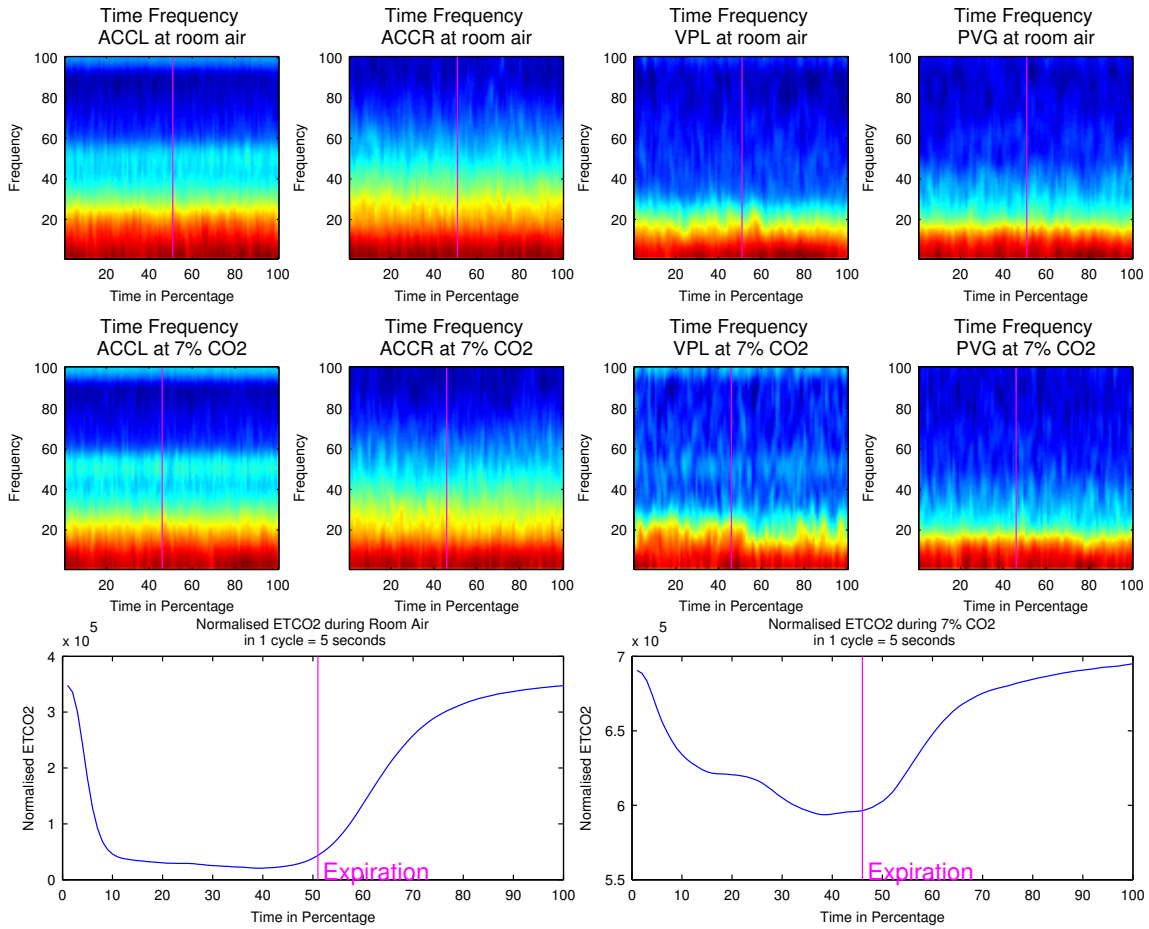

Figure 9.13 Time frequency analysis of bilateral ACC, VPL and PVG while breathing 7% carbon dioxide. The transition of respiratory phase is marked with vertical line.

Figure 9.13 demonstrated a general reduction in intensity in all nuclei throughout the respiratory cycle. There is a prominent decrease in the VPL mean power spectra at low frequency during the expiration phase. The average percentage difference in 5 frequency bands is calculated and statistically compared to the average power spectra during quiet respiration using room air.

9.5.1 Inspiration Phase

The delta band of inspiration phase during 7% CO2 inhalation shows an increased mean power in the left ACC with 12.96% more ($p>0.05$), see Figure 9.14. On the other hand,

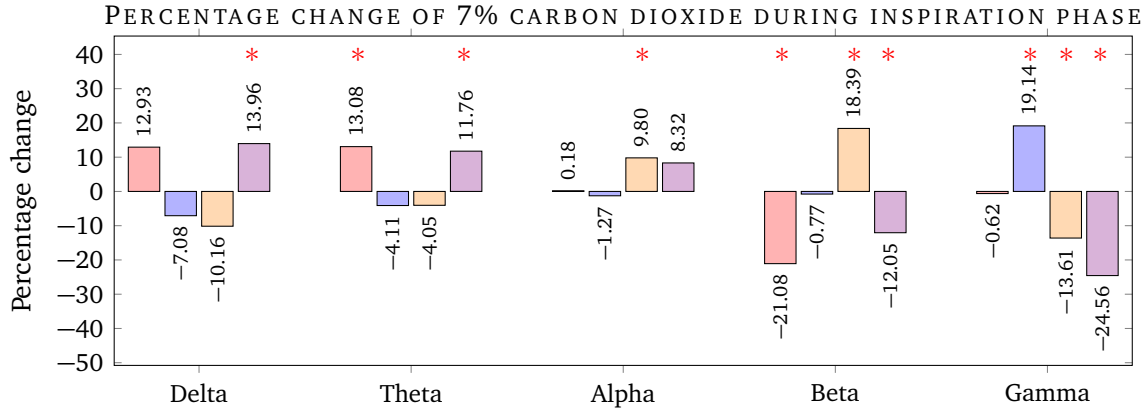

Figure 9.14 The summary of mean percentage change in power spectra in Delta, Theta, Alpha, Beta and Gamma band during inspiration phase using 7% carbon dioxide in ACCL, ACCR, VPL and PVG compared to quiet inspiration at room air.

the right ACC demonstrated a decrease in mean power of 7.08% ($p>0.05$). The VPL shows a negative change in mean power by 10.16% ($p>0.05$). The PVG demonstrated an increment of 18.87% ($p<0.05$) more.

The left ACC shows an increase in mean power by 13.08% ($p<0.05$) in the theta band while inspiring 7% carbon dioxide. The right ACC show a reduction in mean power by 4.11%. Nonetheless, this change was not statistically significantly different from the baseline. The VPL shows 4.05% ($p>0.05$) reduction in mean power spectra during this period. The PVG demonstrated a significant increase of mean power spectra by 11.76% ($p<0.05$) in the theta band.

Inspiration phase of 7% CO2 did not show any statistical differences in either ACC compared to quiet inspiration using room air. The right ACC shows an increment of 0.18% ($p>0.05$) more mean power spectra while the right ACC show a reduction by 1.27% ($p>0.05$). The VPL and PVG show a positive change in mean power with 9.80% ($p<0.05$), and 8.32% ($p<0.05$) respectively.

The beta band during the inspiration phase of 7% carbon dioxide shows a reduced mean power in the left ACC by 21.08% ($p<0.05$). The right ACC did not show any statistical difference from the baseline with a small decrement of 0.77% ($p>0.05$). The VPL shows an increased in mean power by 18.39% ($p<0.05$) while PVG demonstrated an reduction of 12.05% ($p<0.05$).

The left ACC gamma band shows a minimal drop in mean power during the inspiration phase with 0.62% more ($p>0.05$). On the other hand, the right ACC exhibit an increase of 19.14% ($p<0.05$) in mean power change during this phase. Both VPL and PVG mean power were reduced in this band with 13.61% ($p<0.05$) and 24.56% ($p<0.05$) respectively.

9.5.2 Expiration Phase

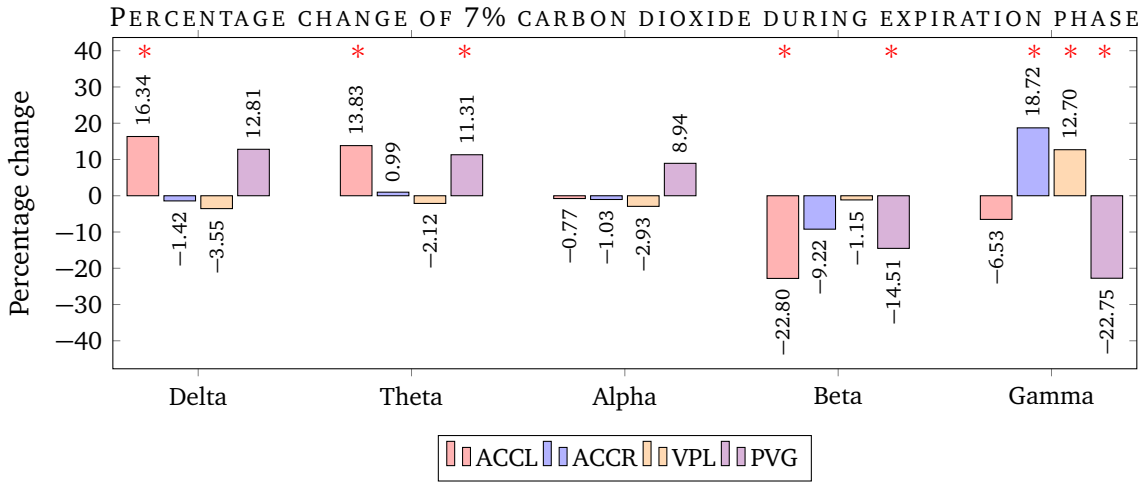

Figure 9.15 The summary of mean percentage change in power spectra in Delta, Theta, Alpha, Beta and Gamma band during expiration phase using 7% carbon dioxide in ACCL, ACCR, VPL and PVG compared to quiet expiration at room air.

The expiration phase in the theta band shows a higher mean power compared to quiet expiration in the left ACC by 16.34% ($p<0.05$), see Figure 9.15. The right ACC, meanwhile, shows a reduced mean power spectrum by 1.42% ($p>0.05$). The VPL also demonstrated a drop in mean power by 3.55% ($p>0.05$) when compared to the baseline expiration phase. The PVG has an increase of 12.81% ($p>0.05$).

The theta band of the expiration phase shows an increase in mean power that was statistically significant in the left ACC by 13.83% ($p<0.05$). The right ACC mean power remained similar to baseline; increase of 0.09% ($p>0.05$). The VPL mean power was reduced by 2.12% ($p>0.05$) while the PVG showed an increase of 11.31% ($p<0.05$).

Both ACCs showed minimal reduction in mean power in the alpha band during the expiration phase. The left ACC had 0.77% less ($p>0.05$) and 1.03% less in the right

($p>0.05$). The VPL has a reduction by 2.93% ($p>0.05$). The PVG has an increase of 8.94% ($p>0.05$) when compared to regular expiration.

There was a reduction in the beta band during 7% CO2 expiration phase compared to baseline. The left ACC reduced 22.80% ($p<0.05$), and the right ACC 9.22% ($p>0.05$). The VPL reduced by 1.15% ($p>0.05$). The PVG has 14.51% less ($p<0.05$).

The left ACC gamma band shows 4.53% reduction ($p>0.05$) and theright 18.72% ($p<0.05$) more mean power during this expiration phase. The VPL also registered an increase of 12.70% ($p<0.05$ whilst the PVG mean power was reduced by 22.75% ($p<0.05$).

9.6 Discussion

Breathing 100% oxygen is not physiological, though it is a safe gas in a clinical practice for resuscitation and hypoxia prevention. In a healthy state, delivering 100% oxygen effectively silences the peripheral chemoreceptor input [Dejours 1963].

100% oxygen reduces mean arterial blood pressure, respiratory rate and increases the peripheral vascular resistance, but this changes were not statistically significant in healthy volunteers [Graff et al. 2013].

However, deactivation of chemoreceptors with hyperoxia in disease states causes significant reduction in both blood pressure and respiratory rate in hypertension [Izdebska et al. 2006] and in chronic liver cirrhosis [Moller et al. 2010].

The cardiovascular changes seen in hyperoxia are postulated to be a direct effect of oxygen on the vascular endothelial tissue [Graff et al. 2013, Querido et al. 2010]. Some researchers suggest that parasympathetic activity increases with hyperoxia in a dose-dependent manner [Shibata et al. 2005].

Breathing 100% oxygen caused a significant decrease in muscular sympathetic nerve activity in essential hypertensive subjects [Sinski et al. 2012; 2014]. These autonomic and vascular changes return to baseline following regular respiration of room air [Gole et al. 2011].

The study of hyperoxia in children shows an increase in BOLD activity in the right more than the left insula, hypothalamus and hippocampus, with a pronounced autonomic response. These changes are subsequently diminished after delivery of supplementary 5% carbon dioxide with 95% oxygen [Macey:2007wu].

Hyperoxia ventilation in children with the congenital central hypoventilation syndrome increases BOLD signals in the limbic structures, especially the amygdala, basal ganglia, pons and medulla [Woo et al. 2005].

In this thesis, breathing 100% oxygen at normal atmospheric pressure did not show any statistically significant changes in the VPL and PVG in any of the frequency bands compared to regular respiration using room air. The results suggests that hyperoxia, and its cardiovascular effects did not influence these nuclei, and autonomic changes may not involve these nuclei.

On the other hand, the anterior cingulate shows an interesting pattern during hyperoxia. The left anterior cingulate activity was statistically increased in the lower frequency

(delta and theta) bands whilst the activity of higher oscillations was significantly lower. The gamma band in the right anterior cingulate during hyperoxia exhibits a statistically significant change in mean power from quiet respiration using room air.

The results of the hyperoxia experiments in this thesis support the findings of Macey and Woo where there was a right sided preferential increase of BOLD signal in the insular and other parts of the limbic system [Macey et al. 2007, Woo et al. 2005].

This result demonstrates laterality in which the lower frequency oscillations are dominant in the left anterior cingulate is whilst the higher frequencies dominate the right anterior cingulate. It is possible that there is a reciprocal change in the anterior cingulate cortices in the gamma band i.e. when the activity in the right increases, the left decreases.

The laterality control of the cerebral hemisphere in autonomic regulation is unique and it is possible that there are associations with the right hemisphere's involvement in emotional and more automatic behaviour compared with the left's involvement in cognitive control.

An experiment in rabbits supports the hemispheric role of autonomic function where ligated right common carotid artery rabbits shows hyperventilation postoperatively compared to hypoventilation in animal with left common carotid artery ligation [Shoja et al. 2008].

Literature shows that insular cortex has a role in autonomic regulation [Meyer et al. 2004, Nagai et al. 2010, Oppenheimer et al. 1996]. Lateralisation of autonomic control is also evident in patients with insular stroke. These patients with right insular stroke are most susceptible to develop cardio-autonomic dysfunction [Meyer et al. 2004]. The experiment result shows that autonomic function be regulated by the anterior cingulate cortex and feed forward signal is send to a lower nuclei and cortices.

Carbon dioxide is a major metabolite of aerobic metabolism. It increases respiratory rate by acting on peripheral and central chemoceptors that allow for anhydrase buffering. A mixture of carbon dioxide and high oxygen concentration was given to investigate the direct effect of carbon dioxide on central chemoreceptors utilising local field potential change [Duffin 1990].

Respiring a mixture of carbon dioxide and oxygen in my experiments gave mixed results. The presence of a high oxygen content together with 1, 3, 5 and 7% carbon

dioxide showed increased activity of the right anterior cingulate in the gamma band. These changes were statistically significant and thus provide robust evidence to support the effects of hyperoxia in the right anterior cingulate.

Respiring 3, 5 and 7% carbon dioxide demonstrated an increased activity in the left anterior cingulate in the delta and theta band. The hyperoxia experiment reveals similar findings. These changes were statistically significant except in the expiratory phase of 3% carbon dioxide, and inspiration phases of 5 and 7% carbon dioxide concentration.

The reduced activity in the left anterior cingulate during hyperoxia in the beta band was seen in all four carbon dioxide concentrations. However, these changes were only statistically significant at the highest carbon dioxide concentrations in both respiratory phases.

The periventricular gray region show a consistent increase in activity at a mean of 11% more than the resting state in the theta band in all four carbon dioxide concentrations. The hyperoxia experiment did not show these changes. This observation was statistically significant which suggest that the changes in PVG activity were not dose-dependent and not related to the oxygen concentration.

The consistent response of PVG neurons in theta band demonstrated a sensitive but not specific response to carbon dioxide levels. Evidence in animal studies suggests a role of the periaqueductal gray in modulating respiration through a projection to the nucleus tracts solitarius which is prominent during survival behaviour [Behbehani 1995, Benarroch 2012, Farkas et al. 1997, Holstege et al. 1997, Huang et al. 2000, Lopes et al. 2012, Subramanian 2013, Subramanian et al. 2008, Zhang 2005].

A 'false suffocation alarm' theory has been posited by Klein, and suggests the presence of a carbon dioxide sensor which triggers a panic attack [Klein 1993]. The carbon dioxide provocation test is one of the diagnostic tools to subdivide panic attack patients into a 'carbon dioxide hypersensitive' group or non-hypersensitive group [Klein 1993, Mongeluzi et al. 2003, Rassovsky et al. 2006].

Current literature did not reveal any active research in uncovering the 'faulty sensor' in the brain. It is possible that the pathology of panic attack is not thoroughly understood and pharmaco and phychotherapy did manage to control the symptoms.

A preliminary animal study in rats suggests the possible role of PAG as the locus of this disabling condition [Schimitel et al. 2012]. The finding of the carbon dioxide

inhalation experiments is the first to report human electrophysiological recordings that provide same evidence as in rats i.e. that the PVG may contain a carbon dioxide sensor.

However, the result of carbon dioxide experiments does not preclude the ACC receiving chemoreceptor information from the medullary central chemoreceptors as a 'feedback mechanism'. This certainly requires an extensive study with a lot of samples and a mechanism to unpick the 'feedback' signal using chemical block. Such study definitely suitable for a smaller animal model similar to Schimitel [Schimitel et al. 2012].

9.7 Conclusion

In this thesis, respiration using 100% oxygen produced an increase in sympathetic output whilst respiration using carbon dioxide reduces the heart rate variability. This result was consistent with Macey [Macey et al. 2007]. The right anterior cingulate shows a consistent increase in gamma band oscillations with high oxygen concentration.

Meanwhile, the left anterior cingulate demonstrated an increase in activity in the delta and theta bands. It is possible that both hemispheres modulate the autonomic and cardiovascular changes seen with hyperoxia in different frequency bands and circumstances. The data suggest that the right cingulate modulates autonomic responses during the 'background', or autonomous state.

Laterality of the anterior cingulate cortex in regulating the autonomic nervous system is exciting as this could explain various autonomic dysfunction in patients with insular cortex stroke or in a more generalised hemispheric stroke.

The carbon dioxide inhalation data suggests a nonspecific carbon dioxide sensitive role of the periventricular grey area. This data strongly supports a plateau point with a consistent 11% increase in activity in the theta band with various carbon dioxide concentrations.

10
Mental Tasks

Mental cognition, attention, pain, dyspnea and other sensory-related tasks increase the activity in common brain areas as demonstrated by fMRI. These activations are postulated to be associated with the autonomic response. The mental task experiments were designed to increase sympathetic output using simple tasks.

Respiration and cardiovascular changes in mental tasks were discussed in CHAPTER 7 (chapter 7). The results show an increase in LF: HF ratio that suggests an increase in sympathetic output.

10.1 Mental Arithmetic Result

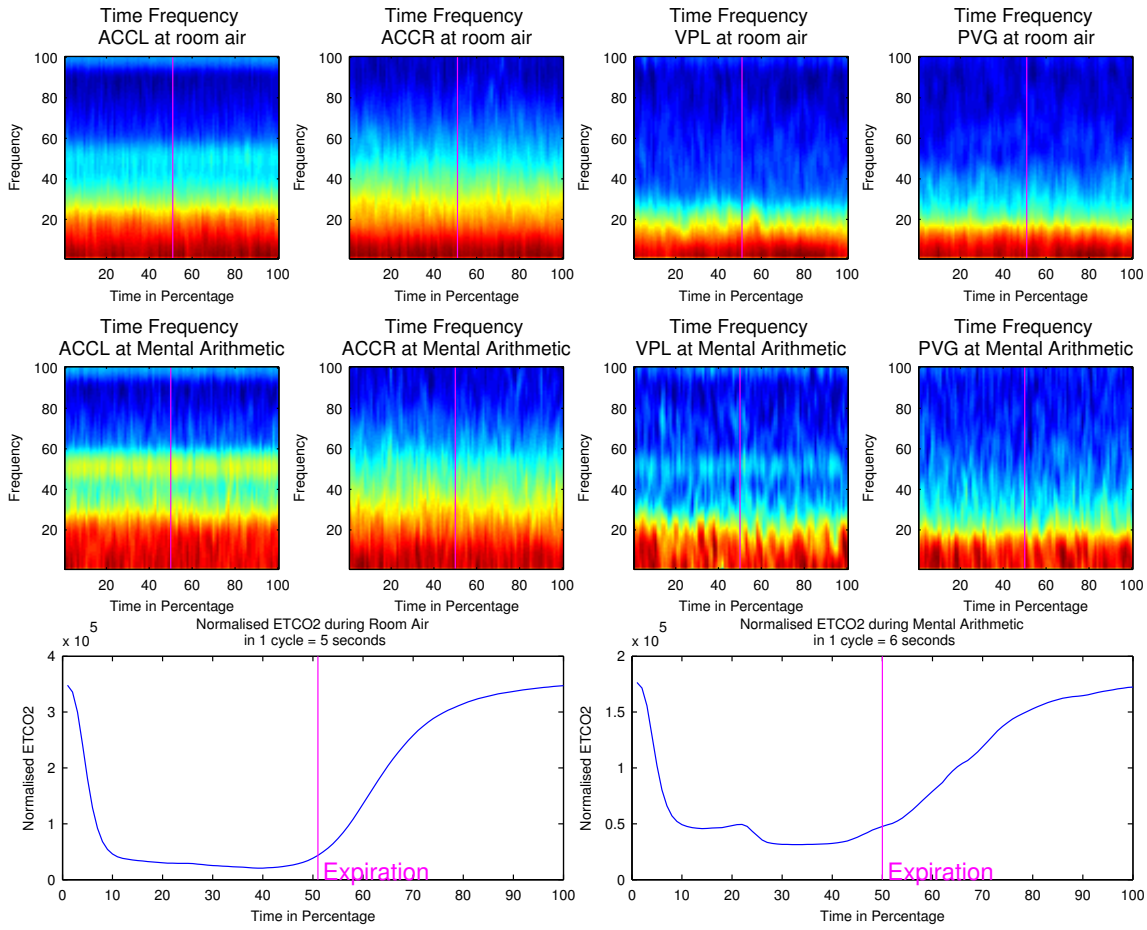

Figure 10.1 Time frequency analysis of bilateral ACC, VPL and PVG while performing mental arithmetic. The transition of respiratory phase is marked with vertical line.

Time-frequency analysis in Figure 10.1 shows a general reduction in intensity below 20 Hz oscillations in the left ACC during the expiratory phase. The right ACC demonstrated 20 to 40 Hz intensity as compared to the rest of the nuclei throughout the respiratory cycle. The cingulate shows a wide range of oscillation intensities while the VPL and PVG activity were predominantly in the low frequency.

10.1.1 Inspiration Phase

Figure 10.2 shows the summary of mean power spectral changes during inspiration phase of mental arithmetic compared to the similar phase of quiet inspiration.

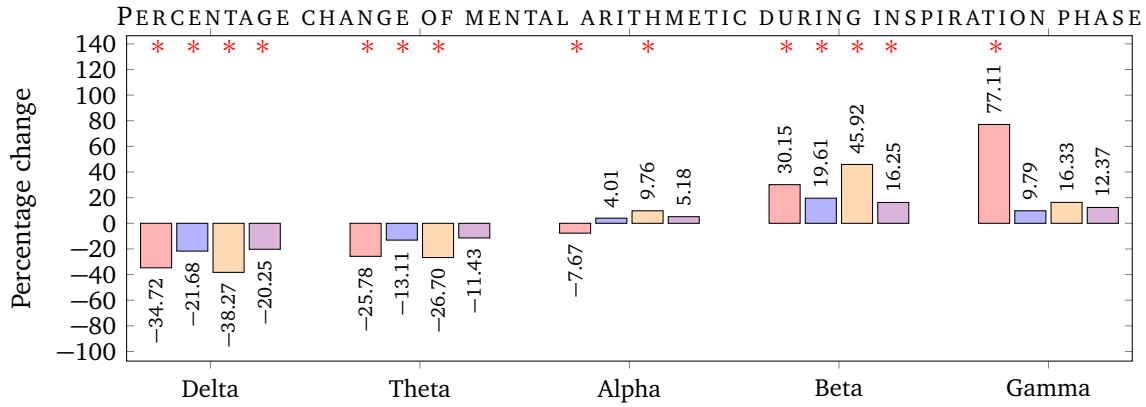

Figure 10.2 Summary of percentage change in Delta, Theta, Alpha, Beta and Gamma band during inspiration phase of mental arithmetics in ACCL, ACCR, VPL and PVG.

The average power in the delta band in all four nuclei was lower during the mental arithmetic inspiration phase than spontaneous, quiet inspiration ($p<0.05$). The VPL mean power was reduced by 38.27%, followed by the left ACC by 34.71%, the VPL mean power reduced by 21.68% and the PVG by 20.25%.

Likewise, the average power in the theta band in all nuclei in this phase was lower than spontaneous inspiration. The VPL demonstrated maximal reduction by 26.7% ($p<0.05$). The left ACC had a reduction inmean power of 25.78% ($p<0.05$) and the right ACC by 13.11% ($p<0.05$). The least reduction was in PVG with 11.43% reduction ($p>0.05$).

The left ACC average power was reducedin the alpha band by7.67% ($p<0.05$) while the right ACC shows an increase of 4.01% ($p>0.05$). The VPL shows an increment by 9.76% ($p<0.05$) and 5.18% increase in the PVG ($p>0.05$). All investigated nuclei demonstrated higher mean power in the beta band. The maximal change seen in the VPL was 45.92% ($p<0.05$), followed by the left ACC by 30.15% ($p<0.05$). The right ACC shows a higher mean power of 19.61% ($p<0.05$), and the PVG showed an increase of 16.25% ($p<0.05$).

All nuclei show a higher mean power in the gamma band during the inspiration phase. The left ACC was statistical significantly different from the quiet, spontaneous inspiration with 77.11% more mean power ($p<0.05$). This was followed by VPL with 16.33% more($p>0.05$). The PVG mean power was lower by 12.37% ($p>0.05$) and the right ACC by 9.79% ($p>0.05$).

10.1.2 Expiration Phase

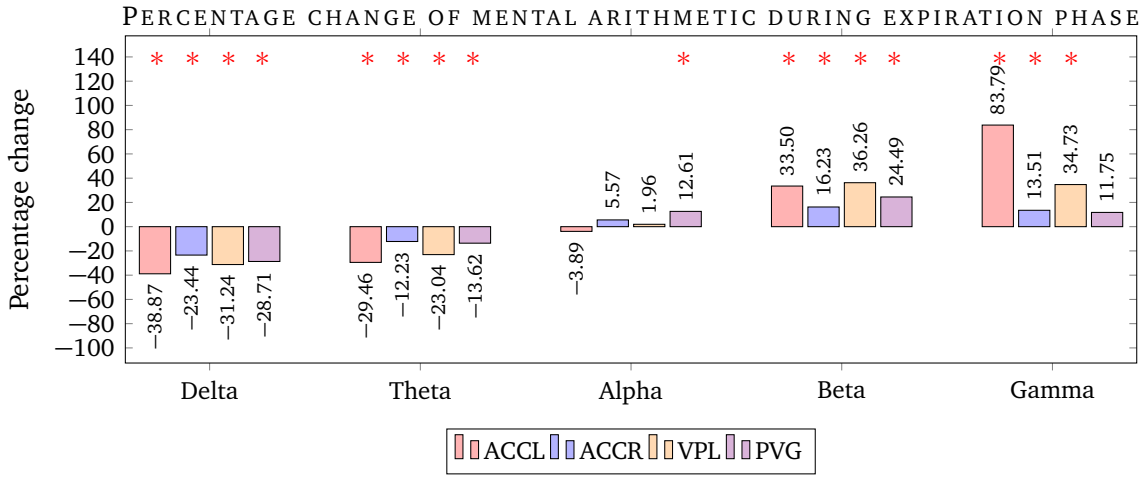

Figure 10.3 Summary of percentage change in Delta, Theta, Alpha, Beta and Gamma band during expiration phase and vocalisaton of mental arithmetics in ACCL, ACCR, VPL and PVG.

Figure 10.3 shows the summary of mean power spectral changes during expiration and vocalisation during mental arithmetic compared to the similar phase of quiet expiration.

The delta band in this period demonstrated a negative mean power change. The maximal reduction was in the left ACC with 38.87% less than regular expiration ($p<0.05$), followed by VPL with 31.24% less mean power ($p<0.05$). The PVG mean power was 28.71% less than regular expiration ($p<0.05$) while the right ACC shows a reduction of 23.44% ($p<0.05$).

The theta band shows a general reduction in mean power in this expiration phase compared to regular expiration. The maximal reduction of power was in the left ACC with 29.46% less($p<0.05$). The VPL mean power was lower by 23.04% ($p<0.05$) and the PVG with 13.62% less ($p<0.05$). The right ACC has the least reduction of 12.23% ($p<0.05$).

There was 3.89% reduction of mean power in the left ACC in the alpha band during the expiration phase of mental arithmetic. The right ACC shows an increased mean power of 5.57%. The VPL mean power was least affected with a rise of 1.96% more than regular expiration. The PVG shows an increase of 12.61% compared to regular

expiration. Only PVG changes were statistically significant compared to quiet expiration ($p<0.05$).

The beta band shows a general increase in mean power spectra during the expiration phase of mental arithmetic. The maximal increase was in the VPL where there was 36.26% more power ($p<0.05$) followed by the left ACC with 33.50% more than baseline ($p<0.05$). The PVG demonstrated a higher mean power spectra with 24.49% more ($p<0.05$) while the right ACC showed 16.23% more power compared to the baseline ($p<0.05$).

There was a maximal 83.79% more power in the gamma band in the left ACC ($p<0.05$) during the expiration and vocalisation phase. The VPL mean power spectra was higher by 34.73% ($p<0.05$). The right ACC average power was higher by 13.51% ($p<0.05$), and the PVG with 1.75% more compared to regular expiration ($p>0.05$).

10.2 Word Recall Results

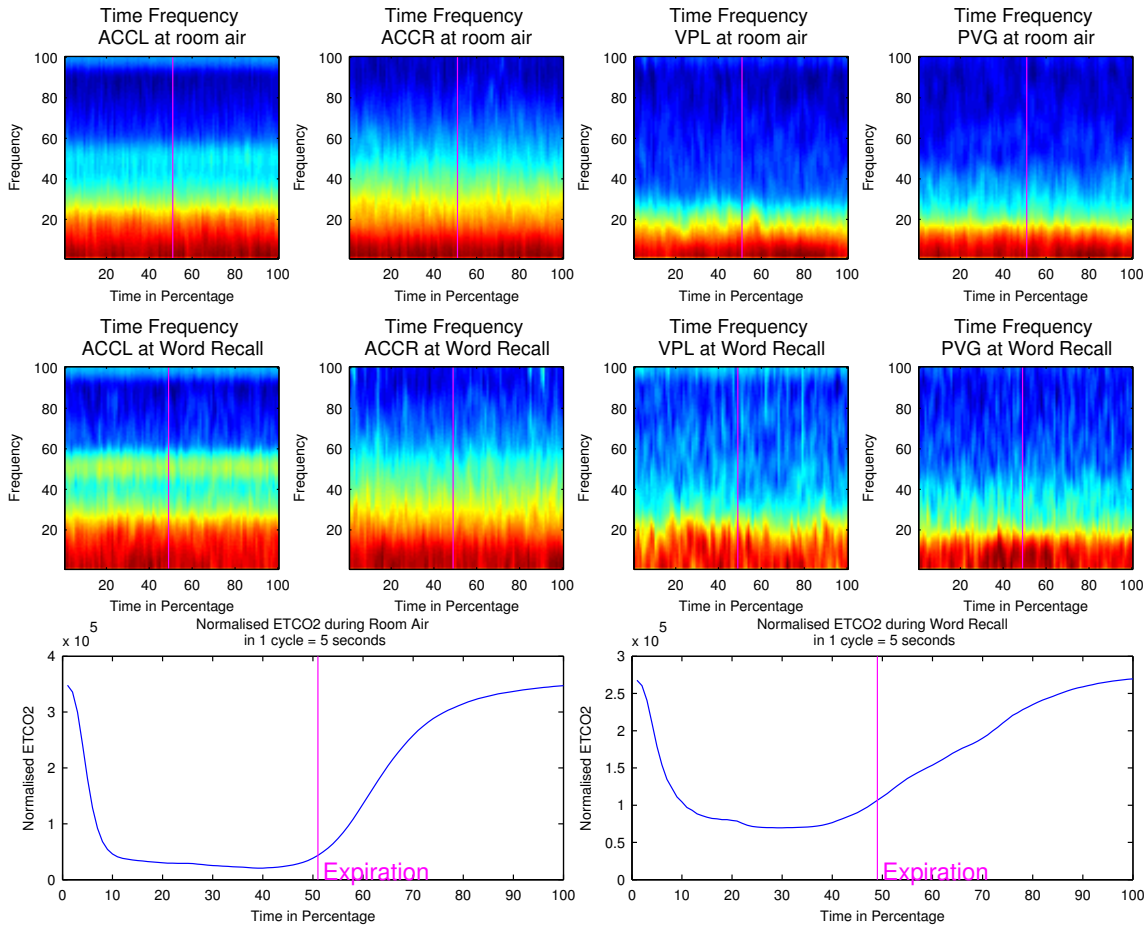

Figure 10.4 Time frequency analysis of bilateral ACC, VPL and PVG while performing word recall and vocalisation. The transition of respiratory phase is marked with vertical line.

Time-frequency analysis in Figure 10.4 shows a general low average power in oscillations under 20 Hz in the left ACC during the expiratory phase. The cingulate shows a broad range of oscillation activity. Meanwhile, the thalamus and periventricular gray area were predominantly active at lower frequency.

10.2.1 Inspiration Phase

Figure 10.5] shows the summary of mean power spectra percentage change during the inspiration phase of the word recall experiment compared to quiet inspiration phase in all investigated nuclei.

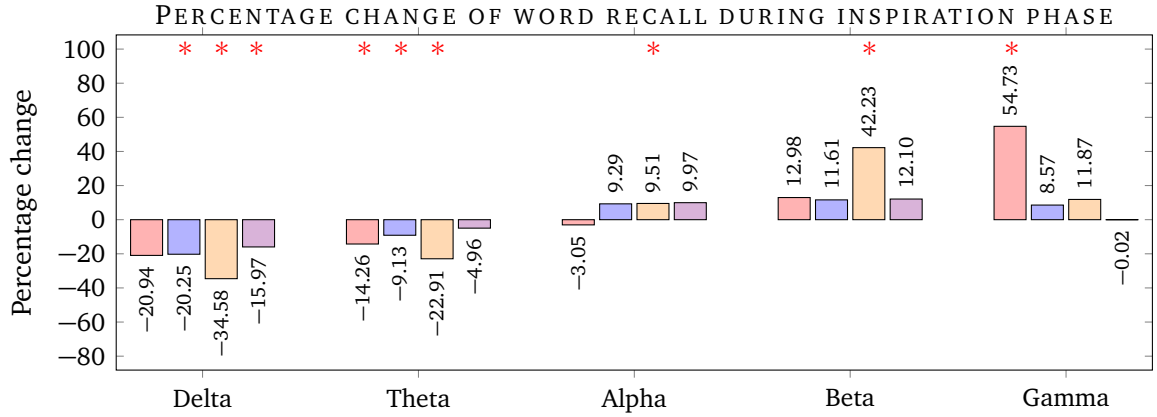

Figure 10.5 Summary of percentage change in Delta, Theta, Alpha, Beta and Gamma band during inspiration phase of word recall in ACCL, ACCR, VPL and PVG.

The delta band of the inspiration phase during word recall shows a general reduction of mean power in all 4 investigated nuclei. There was a 20.94% lower average power in the left ACC ($p>0.05$) and 20.25% less in the right ACC ($p<0.05$). The VPL shows a maximal reduction of 34.58% mean power ($p<0.05$). The PVG exhibits a 15.97% reduction ($p<0.05$) compared to the inspiration phase of quiet breathing at rest.

The theta band demonstrated a lower mean power compared to quiet inspiration at rest. The left ACC has 14.26% less mean power ($p<0.05$) and 9.13% less in the right ACC ($p<0.05$). The VPL had a maximal drop of 22.91% ($p<0.05$) while the PVG shows 4.96% reduction ($p>0.05$).

The alpha band of the left ACC shows a reduction of 3.05% mean power ($p>0.05$). On the other hand, the right ACC shows 9.29% increase in mean power ($p>0.05$). There was 9.51% increase in the VPL ($p<0.05$) and a rise of 9.97% in the PVG ($p>0.05$).

The beta band of word recall during the inspiration phase shows a higher mean power in all four nuclei. The left ACC shows an increased mean power of 12.98% ($p>0.05$) and the right ACC has an increase of 11.61% ($p>0.05$). The VPL showed maximal power changes in this band with an increase of 42.23% ($p<0.05$) while the PVG showeda 12.10% increase ($p>0.05$).

The left ACC demonstrated a maximal increase in power during the inspiration phase of word recall in the gamma band with 54.73% more than baseline ($p<0.05$). The right ACC showed an increase of 8.57% ($p>0.05$) while VPL has 11.87% more power

(p>0.05) than the quiet inspiratory phase using room air. There was a minimal change in the PVG where it showed a decrease of 0.02% change from the baseline (p>0.05).

10.2.2 Expiration Phase

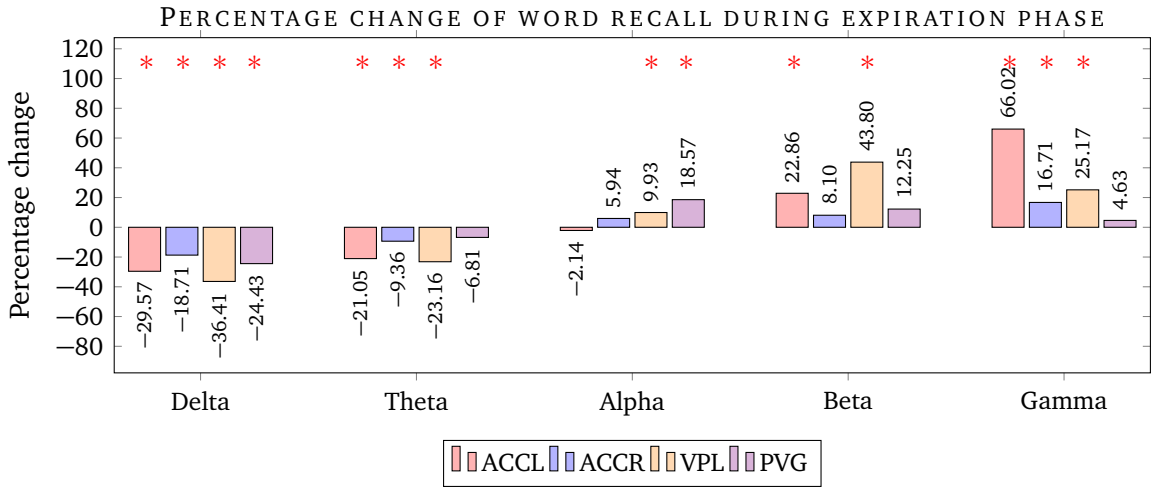

Figure 10.6 Summary of percentage change in Delta, Theta, Alpha, Beta and Gamma band during expiration and vocalisation phase of word recall in ACCL, ACCR, VPL and PVG.

Figure 10.6] shows the summary of mean power spectra percentage change during the expiration phase of the word recall and vocalisation experiment compared to quiet expiration phase in all investigated nuclei.

There was a reduction in the delta band in all four nuclei during the expiratory period of word recall compared to quiet expiration at room air. The left ACC shows 29.57% mean power reduction (p<0.05) while the right ACC shows 18.71% reduction (p<0.05). The VPL shows a maximal reduction of mean power 36.41% less (<0.05). Meanwhile, the PVG has 24.43% less mean power from the baseline (p<0.05).

Similarly, the delta band shows a negative change of mean power in all investigated nuclei during the expiration phase. The left ACC showed a reduction of 21.05% (p<0.05) while the right ACC shows 9.36% less power from the baseline (p<0.05). The VPL demonstrated maximal reduction of mean power by 23.16% (p<0.05) while the PVG showed 6.18% less than quiet expiration (p>0.05).

The left ACC alpha band has a reduction of 2.14% mean power compared to quiet expiration (p>0.05). Meanwhile, the right ACC has 5.94% more mean power (p>0.05).

The VPL has 9.93% more power ($p<0.05$) in the alpha band compared to the quiet expiration phase. The PVG has the highest increase in power by 18.57% ($p<0.05$).

The beta band shows 22.86% more activity in the left anterior cingulate ($p<0.05$) whilst the the anterior cingulate has 8.10% more activity in the expiration phase ($p>0.05$). There was a maximal increase of activity by 43.80% in the VPL while there was 12.25% more activity in the PVG.

The left anterior cingulate activity in the gamma band has the highest percentage change from baseline in the expiration phase with 66.02% more mean power ($p<0.05$). The right ACC has a positive change in mean power by 16.71% more ($p<0.05$). The VPL has 25.17% more mean power ($p>0.05$), and PVG has a small increase of 4.63% more average power in this expiration phase.

10.3 Discussion

Complex human behaviour necessitates speech as a form of communication. During speech, spontaneous respiration is intermingled with voluntary sound generation, memory, and emotion [Boiten 1998, Maclean 1955a, MacLean 1985a;b]

Interaction between Broca's and Wernicke's areas generate speech while medullary pacemaker systems mediate spontaneous breathing. In the experiments in this thesis, the effect of cognitive computation and verbalisation were recorded in the bilateral anterior cingulate, VPL and PVG.

Non-human primate studies of the cingulate gyrus show a relationship between the cingulate gyrus and vocalisation. Electrical stimulation to the cingulate produces excitatory behaviours such as piloerection, pupil dilatation, vocalisation, an increase in blood pressure and respiratory rate. Meanwhile, lesioning these nuclei produces a tamed animal with a lower blood pressure, respiratory rate as well as mutism [Glees et al. 1950, Pribram and Maclean 1953, Smith 1945; 1941, Ward 1948].

The periaqueductal gray is postulated to have a role in respiratory modification, especially in a survival situation, and chemical stimulation to the midbrain can produce vocalisation and rage behaviour [Bandler 1982, Subramanian 2013, Subramanian and Holstege 2011, Subramanian et al. 2008, Zhang et al. 1995].

The thalamus is also implicated in the vocalisation circuit [Schmidt et al. 2012].

The precise network of volitional breathing and vocalisation is unknown but the availability of neuroimaging has increases our understanding in this field [Fink et al. 1996, Haouzi and Bell 2009, Haouzi et al. 2006, Huckabee et al. 2003, Loucks et al. 2007, Šmejkal et al. 2000].

Multiple structures in the brain can be activated from the cortex, thalamus, amygdala and the periventricular gray [Colebatch et al. 1991, Corfield et al. 1995, Macefield and Gandevia 1991, Murphy et al. 1990, Pattinson et al. 2009a].

The most prominent finding in my mental tasks experiments was the statistically significant increase in beta and gamma band power in the left anterior cingulate during both inspiration and expiration. There was also a concomitant reduction of low frequency activity in the delta and theta bands ($p>0.05$). These observations were similar to the LFPs changes in the left anterior cingulate during the breath holding manoeuvre.

Right anterior cingulate activity was lower in delta and theta bands during mental cognition, and these results were statistically significant, ($p<0.05$). VPL and PVG activity was lower in the delta, and theta bands in both respiratory phases and these finding were similarly observed in the breath hold experiments, ($p<0.05$).

On the other hand, VPL and PVG activity during the mental task experiments were higher in the alpha and beta bands as compared to a reduction in activity during breath holding. These reciprocal difference were statistically significant compared to the resting state ($p<0.05$).

The reproducibility of similar results of the left anterior cingulate, VPL and PVG in low frequency (delta and theta) and in the high frequency (beta and gamma) in three different experiments strongly suggests a common network in these behaviours.

The findings suggest that VPL and PVG have intrinsic roles in tasks requiring complex motor sensory coordination of the laryngeal muscles as these three conditions have a common muscle group to modulate. This supports the role of the PVG in producing sounds during rage or survival behaviour [Bandler 1982, Zhang et al. 1995].

An increase of VPL and PVG activity in the alpha band is associated with vocalisation whilst breath holding demonstrated a significant reduction in activity. These changes in the VPL, as well as PVG, were not observed in volitional hyperventilation, volitional deep inspiration, hyperoxia and inconsistent in 4 carbon dioxide concentrations.

Gamma band activity in the left anterior cingulate was consistently higher than the resting state during mental tasks. On the other hand, the delta and theta band were suppressed in both respiratory phases in volitional breath hold and mental tasks with vocalisation.

Smith demonstrated that anterior cingulate area 24 stimulation in lightly anaesthetised monkeys produced similar low guttering sounds as in the awake state [Smith 1941].

The vocalisation was coupled with a complex emotional, behavioural expression of wide open eyes, dilatation of pupils, open mouth and retraction or protrusion of the tongue. On the other hand, high electrical voltage current stimulation resulted in pronounced inhibitory effects such as the absence of vocalisation, minimal movement, and muscle flaccidity [Smith 1941].

Our reproducible results with statistically significant differences in three different experiments strongly supports the role of the left ACC as a higher functional region coordinating the laryngeal muscles through the VPL and PVG.

10.4 Conclusion

The results of mental tasks and vocalisation demonstrate the role of the left anterior cingulate as the primer for voice generation with the VPL and PVG acting simultaneously to possibly coordinate the laryngeal muscles and vocal cords. The left anterior cingulate operates at both high frequency in gamma and lower frequencies bands to modulate cognition and vocalisation.

The VPL and PVG influence on the laryngeal muscles can be inferred by the direction of the mean power spectra in the alpha band. A suppression of this frequency activity is related to constant glottic closure whilst vocalisation increases the alpha band activity. In conclusion, the results of the mental tasks support my hypothesis of a feed-forward signal for voluntary breathing.

11 Conclusion

This thesis studies the feed-forward signals involved in volitional breathing in humans by comparing local field potentials in various brain areas during several respiratory experiments including quiet respiration at rest.

The voluntary breathing experiments include voluntary expiratory apnea, deep inspiration and volitional hyperventilation. Several other controlled experiments were conducted to identify the direct effect of 100% oxygen and carbon dioxide to the local field potentials.

Direct recordings of LFPs whilst breathing 100% oxygen is not documented in the literature. The results of respiration using 100% oxygen supports fMRI findings of an increased BOLD signal in the limbic system which includes the cingulate cortex [Macey et al. 2003; 2005; 2007, Woo et al. 2005].

Breathing 100% oxygen increases the activity of the right anterior cingulate especially in the gamma band which was statistically significantly different from quiet respiration using room air.

The hyperoxia experiment also confirms classic respiratory experiments which silence the peripheral chemoreceptors causing a slightly lower respiratory rate. The heart rate variability analysis during this experiment shows a higher LF: HF ratio which suggests an increase in the sympathetic output.

Taking all the results together, an inference can be made that the right anterior cingulate modulates the sympathetic output autonomously in the background without requiring any cognitive function and this function operates in the gamma band.

The breath holding experiment result show a statistically significant increase of the left anterior cingulate signal in the gamma band with a reduction in the lower frequencies. The gamma band activity was replicated in two mental tasks which require cognition and vocalisation.

The heart rate variability analysis of breath hold and mental tasks shows an increase in sympathetic output. Several inferences can be made, firstly that the left anterior cingulate is involved in voluntary feed-forward signals in tasks such as voluntary breath hold and mental cognition.

Secondly, the left anterior cingulate has a role in driving cortical sympathetic output parallel with feed-forward signals. These functionsof the left anterior cingulate appear to operate at a high-frequency gamma band.

The VPL has a role in coordinating the laryngeal muscles and coordinates tasks by modulating its activity in the alpha band. A positive change from the baseline is related to vocalisation and closure of the glottis whilesta reduction in activity is related to opening up the airway as in voluntary deep inspiration and hyperventilation.

During the carbon dioxide experiment, the PVG registered a plateau of 11% in increased activity in the theta band at all four carbon dioxide concentrations. This suggests a possible role of the PVG as a sensitive but non-specific central carbon dioxide sensor and this result supports preliminary report of carbon dioxide sensitive cells in rats' PVG [Lopes et al. 2012, Schimitel et al. 2012].

The conclusions can be summarised in 3 sections:

1. **The Feed-Forward Signal** The volitional breathing and mental tasks data suggests the role of the left anterior cingulate as a feed forward mechanism, synchronised through gamma band with low frequency desynchronisation in conscious coordinated tasks involving laryngeal control. The alpha band activity in the VPL seems to be the involved with the finer control of laryngeal muscles. A suppression of VPL activity in the alpha band is related to modulation of the vocal cords or the laryngeal muscles such as during the breath hold manoeuvre. The left ACC synchronises the feed forward signal via the gamma band and a suppression of all

other lower frequencies activity. On the other hand, a suppression of gamma activity in the left ACC, with an increase synchronisation of bilateral cingulate in the delta and theta bands are related to voluntary breathing such as deep inspiration and hyperventilation.

2. **The Cortical Control of Autonomic Function** The heart rate variability analysis shows a possible role of the cingulate in controlling the sympathetic output with differences between left and right. The common denominator in a higher LF: HF ratio is an increase in the gamma band activity in the cingulate. The right ACC shows an increase in gamma activity with 100% oxygen inhalation which stabilises the peripheral chemo and possibly baroreceptors. This suggest that the right anterior cingulate constantly monitors the autonomic function in the background. On the other hand, the left ACC shows a higher gamma band activity which is related to mental tasks and breath holding. These tasks require cognition and a feed-forward signal. This suggests that the left anterior cingulate modulates the autonomic function in a parallel network.

3. **The carbon dioxide sensitive role of periaqueductal gray** The carbon dioxide inhalation results suggest a nonspecific carbon dioxide sensitive role of the periaqueductal grey area with a plateau point in the theta band. This finding is the first in human to link the possible role of PAG to the 'pathological suffocation alarm' in a panic attack. The higher cortical carbon dioxide sensitive nucleus hypothesis suggests that the cortex has a center to interpret suffocation sensation based on the central carbon dioxide level. This hypothesis is similar to the idea that the anterior cingulate cortex has a role in interpreting positive and negative valance systems.

11.1 Future work

The immediate work that I have to undertake is to publish and disseminate new idea and knowledge I gained from this learning process to a wider audience. The role of hemispheric cortex in regulating autonomic function at rest and during cognition is an initial step to understand the cortical function in cardiorespiratory regulation in human.

A combination of voluntary respiration and imagined exercise experiment in human could possibly allow us to uncouple the cardiovascular from the respiratory system. An imporved experiment designed by Green and Basnayake could help in taking this research further [Basnayake et al. 2011; 2012, Green and Paterson 2008, Green et al. 2007b].

The carbon dioxide sensitive role of periaqueductal gray could be further investigated as the nucleus is already accessible as part of chronic neuropathic pain treatment. The next step is to ensure that the PAG signal is not because of direct signal from the ventral. The saturating point of 11% more than baseline with an identified operating frequency band is a starting point to secure deep brain stimulation as a possible mode of treatment in panic attack.

The carbon dioxide sensitivity should be studied further to validate the higher cortical carbon dioxide sensitive nucleus hypothesis. Clinical work in human may not have the adequate volume to investigate the association between carbon dioxide level and autonomic function, which necessitate the need to go back to the bench work using smaller animal.

The respiratory experiment involving gas mixture can be implement in small animal model as these experiments did not require any volitional effort or cognitive functions. Microelectrode electrical recordings has been used before in cats and dogs model to understand respiratory physiology which was then translated in clinical practice. Feedback chemoreceptor information from the medullary central chemoreceptors can be bloked by chemical agent and this could help to test the cortical carbon dioxide sensitive hypothesis.

A

Post Hoc Analysis Result

Table A.1 Kruskal Wallis Delta ACCL Inspiration

Source	**SS**	**df**	**MS**	**Chi-Square**	***p* value**
Groups	10981333.994	10	1098133.399	461.255	0.000
Error	1708063.506	523	3265.896		
Total	12689397.500	533			
Nuclei 1	**Nuclei 2**	**Lower CI 95%**	**Mean difference**	**Upper CI 95%**	**P value <0.05**
Room Air	100% Oxygen	-279.283	-176.008	-72.733	0.0000
Room Air	3% Carbon Dioxide	-216.204	-115.059	-13.913	0.0091
Room Air	Mental Arithmetic	39.253	140.903	242.553	0.0002
Room Air	Hyperventilation	-353.101	-253.811	-154.522	0.0000
Room Air	Deep Inspiration	-376.518	-275.373	-174.227	0.0000
Room Air	Breath Hold	57.243	165.118	272.993	0.0000
Room Air	1% Carbon Dioxide	-100.242	4.221	108.683	1.0000 [1]
Room Air	5% Carbon Dioxide	-200.105	-97.932	4.240	0.0797 [1]
Room Air	7% Carbon Dioxide	-203.297	-99.439	4.418	0.0806 [1]
Room Air	Word Recall	-5.186	96.986	199.158	0.0882 [1]

[1] No statistical significant difference between nuclei.

Table A.2 Kruskal Wallis Delta ACCL Expiration

Source	**SS**	**df**	**MS**	**Chi-Square**	***p* value**
Groups	13196461.911	10	1319646.191	493.446	0.000
Error	1913615.589	555	3447.956		
Total	15110077.500	565			
Nuclei 1	**Nuclei 2**	**Lower CI 95%**	**Mean difference**	**Upper CI 95%**	**P value <0.05**
Room Air	100% Oxygen	-261.221	-153.937	-46.654	0.0001
Room Air	5% Carbon Dioxide	-229.541	-121.252	-12.963	0.0115
Room Air	7% Carbon Dioxide	-226.427	-119.622	-12.817	0.0114
Room Air	Mental Arithmetic	55.563	164.382	273.200	0.0000
Room Air	Word Recall	16.479	124.768	233.057	0.0075
Room Air	Hyperventilation	-370.133	-258.363	-146.592	0.0000
Room Air	Deep Inspiration	-411.714	-302.347	-192.980	0.0000
Room Air	Breath Hold	60.781	165.015	269.249	0.0000
Room Air	1% Carbon Dioxide	-107.697	-1.355	104.987	1.0000 [1]
Room Air	3% Carbon Dioxide	-214.183	-104.816	4.550	0.0798 [1]

[1] No statistical significant difference between nuclei.

Table A.3 Kruskal Wallis Theta ACCL Inspiration

Source	**SS**	**df**	**MS**	**Chi-Square**	***p* value**
Groups	11062745.592	10	1106274.559	464.675	0.000
Error	1626651.908	523	3110.233		
Total	12689397.500	533			
Nuclei 1	**Nuclei 2**	**Lower CI 95%**	**Mean difference**	**Upper CI 95%**	**P value <0.05**
Room Air	100% Oxygen	-268.173	-164.898	-61.623	0.0000
Room Air	7% Carbon Dioxide	-253.069	-149.212	-45.354	0.0001
Room Air	Mental Arithmetic	52.999	154.649	256.299	0.0000
Room Air	Word Recall	2.744	104.916	207.089	0.0365
Room Air	Hyperventilation	-326.740	-227.451	-128.162	0.0000
Room Air	Deep Inspiration	-358.400	-257.255	-156.110	0.0000
Room Air	Breath Hold	79.899	187.774	295.649	0.0000
Room Air	1% Carbon Dioxide	-67.491	36.971	141.434	1.0000 [1]
Room Air	3% Carbon Dioxide	-186.008	-84.863	16.283	0.2608 [1]
Room Air	5% Carbon Dioxide	-132.378	-30.206	71.966	1.0000 [1]

[1] No statistical significant difference between nuclei.

Table A.4 Kruskal Wallis Theta ACCL Expiration

Source	**SS**	**df**	**MS**	**Chi-Square**	***p* value**
Groups	13481448.409	10	1348144.841	504.102	0.000
Error	1628629.091	555	2934.467		
Total	15110077.500	565			
Nuclei 1	**Nuclei 2**	**Lower CI 95%**	**Mean difference**	**Upper CI 95%**	**P value <0.05**
Room Air	100% Oxygen	-255.435	-148.152	-40.868	0.0003
Room Air	7% Carbon Dioxide	-274.482	-167.677	-60.872	0.0000
Room Air	Mental Arithmetic	69.711	178.530	287.348	0.0000
Room Air	Word Recall	25.965	134.255	242.544	0.0022
Room Air	Hyperventilation	-329.948	-218.177	-106.406	0.0000
Room Air	Deep Inspiration	-391.938	-282.571	-173.205	0.0000
Room Air	Breath Hold	93.956	198.190	302.423	0.0000
Room Air	1% Carbon Dioxide	-78.907	27.435	133.777	1.0000 [1]
Room Air	3% Carbon Dioxide	-183.428	-74.061	35.305	0.7513 [1]
Room Air	5% Carbon Dioxide	-146.721	-38.432	69.857	1.0000 [1]

[1] No statistical significant difference between nuclei.

Table A.5 Kruskal Wallis Alpha ACCL Inspiration

Source	**SS**	**df**	**MS**	**Chi-Square**	***p* value**
Groups	4033298.168	10	403329.817	169.413	0.000
Error	8656099.332	523	16550.859		
Total	12689397.500	533			
Nuclei 1	**Nuclei 2**	**Lower CI 95%**	**Mean difference**	**Upper CI 95%**	**P value <0.05**
Room Air	1% Carbon Dioxide	46.794	151.256	255.719	0.0001
Room Air	5% Carbon Dioxide	59.396	161.568	263.740	0.0000
Room Air	Mental Arithmetic	36.529	138.178	239.828	0.0004
Room Air	Hyperventilation	159.135	258.424	357.713	0.0000
Room Air	Deep Inspiration	139.482	240.627	341.773	0.0000
Room Air	Breath Hold	112.278	220.153	328.029	0.0000
Room Air	100% Oxygen	-22.111	81.164	184.438	0.4012 [1]
Room Air	3% Carbon Dioxide	-28.910	72.235	173.381	0.6333 [1]
Room Air	7% Carbon Dioxide	-100.344	3.513	107.371	1.0000 [1]
Room Air	Word Recall	-40.767	61.405	163.577	0.9278 [1]

[1] No statistical significant difference between nuclei.

Table A.6 Kruskal Wallis Alpha ACCL Expiration

Source	**SS**	**df**	**MS**	**Chi-Square**	***p* value**
Groups	5926716.635	10	592671.663	221.613	0.000
Error	9183360.865	555	16546.596		
Total	15110077.500	565			

Nuclei 1	**Nuclei 2**	**Lower CI 95%**	**Mean difference**	**Upper CI 95%**	**P value <0.05**
Room Air	5% Carbon Dioxide	122.242	230.531	338.820	0.0000
Room Air	Hyperventilation	171.715	283.485	395.256	0.0000
Room Air	Deep Inspiration	206.613	315.980	425.346	0.0000
Room Air	Breath Hold	81.774	186.007	290.241	0.0000
Room Air	100% Oxygen	-22.809	84.475	191.758	0.3968 [1]
Room Air	1% Carbon Dioxide	-38.010	68.332	174.674	0.8458 [1]
Room Air	3% Carbon Dioxide	-26.816	82.551	191.918	0.4985 [1]
Room Air	7% Carbon Dioxide	-92.931	13.874	120.679	1.0000 [1]
Room Air	Mental Arithmetic	-26.838	81.981	190.799	0.5031 [1]
Room Air	Word Recall	-65.072	43.217	151.506	1.0000 [1]

[1] No statistical significant difference between nuclei.

Table A.7 Kruskal Wallis Beta ACCL Inspiration

Source	**SS**	**df**	**MS**	**Chi-Square**	***p* value**
Groups	10551714.950	10	1055171.495	443.210	0.000
Error	2137682.550	523	4087.347		
Total	12689397.500	533			
Nuclei 1	**Nuclei 2**	**Lower CI 95%**	**Mean difference**	**Upper CI 95%**	**P value <0.05**
Room Air	100% Oxygen	59.997	163.272	266.547	0.0000
Room Air	7% Carbon Dioxide	69.832	173.689	277.547	0.0000
Room Air	Mental Arithmetic	-229.831	-128.181	-26.531	0.0016
Room Air	Hyperventilation	179.570	278.859	378.148	0.0000
Room Air	Deep Inspiration	187.443	288.588	389.734	0.0000
Room Air	Breath Hold	-237.916	-130.041	-22.166	0.0036
Room Air	1% Carbon Dioxide	-70.737	33.725	138.188	1.0000 [1]
Room Air	3% Carbon Dioxide	-5.832	95.314	196.459	0.0950 [1]
Room Air	5% Carbon Dioxide	-26.522	75.651	177.823	0.5458 [1]
Room Air	Word Recall	-169.746	-67.574	34.598	0.7970 [1]

[1] No statistical significant difference between nuclei.

Table A.8 Kruskal Wallis Beta ACCL Expiration

Source	**SS**	**df**	**MS**	**Chi-Square**	***p* value**
Groups	12825269.494	10	1282526.949	479.566	0.000
Error	2284808.006	555	4116.771		
Total	15110077.500	565			
Nuclei 1	**Nuclei 2**	**Lower CI 95%**	**Mean difference**	**Upper CI 95%**	**P value <0.05**
Room Air	100% Oxygen	28.652	135.936	243.219	0.0015
Room Air	7% Carbon Dioxide	78.630	185.435	292.240	0.0000
Room Air	Mental Arithmetic	-265.781	-156.962	-48.144	0.0001
Room Air	Word Recall	-228.489	-120.200	-11.911	0.0130
Room Air	Hyperventilation	153.483	265.254	377.024	0.0000
Room Air	Deep Inspiration	202.674	312.041	421.408	0.0000
Room Air	Breath Hold	-240.602	-136.369	-32.135	0.0008
Room Air	1% Carbon Dioxide	-78.590	27.753	134.095	1.0000 [1]
Room Air	3% Carbon Dioxide	-19.959	89.408	198.775	0.3132 [1]
Room Air	5% Carbon Dioxide	-12.960	95.329	203.619	0.1784 [1]

[1] No statistical significant difference between nuclei.

Table A.9 Kruskal Wallis Gamma ACCL Inspiration

Source	**SS**	**df**	**MS**	**Chi-Square**	***p* value**
Groups	10699584.643	10	1069958.464	449.421	0.000
Error	1989812.857	523	3804.613		
Total	12689397.500	533			
Nuclei 1	**Nuclei 2**	**Lower CI 95%**	**Mean difference**	**Upper CI 95%**	**P value <0.05**
Room Air	100% Oxygen	52.016	155.291	258.566	0.0000
Room Air	1% Carbon Dioxide	-257.873	-153.410	-48.948	0.0001
Room Air	Mental Arithmetic	-326.951	-225.302	-123.652	0.0000
Room Air	Word Recall	-283.502	-181.330	-79.158	0.0000
Room Air	Deep Inspiration	70.972	172.118	273.263	0.0000
Room Air	Breath Hold	-375.422	-267.547	-159.671	0.0000
Room Air	3% Carbon Dioxide	-18.616	82.529	183.675	0.3172 [1]
Room Air	5% Carbon Dioxide	-150.380	-48.207	53.965	0.9990 [1]
Room Air	7% Carbon Dioxide	-94.714	9.144	113.001	1.0000 [1]
Room Air	Hyperventilation	-61.138	38.151	137.440	1.0000 [1]

[1] No statistical significant difference between nuclei.

Table A.10 Kruskal Wallis Gamma ACCL Expiration

Source	**SS**	**df**	**MS**	**Chi-Square**	***p* value**
Groups	13353630.736	10	1335363.074	499.322	0.000
Error	1756446.764	555	3164.769		
Total	15110077.500	565			
Nuclei 1	**Nuclei 2**	**Lower CI 95%**	**Mean difference**	**Upper CI 95%**	**P value <0.05**
Room Air	100% Oxygen	37.654	144.937	252.221	0.0004
Room Air	1% Carbon Dioxide	-240.660	-134.318	-27.976	0.0016
Room Air	Mental Arithmetic	-358.900	-250.082	-141.263	0.0000
Room Air	Word Recall	-331.586	-223.297	-115.008	0.0000
Room Air	Deep Inspiration	66.899	176.265	285.632	0.0000
Room Air	Breath Hold	-399.215	-294.982	-190.748	0.0000
Room Air	3% Carbon Dioxide	-50.081	59.286	168.652	0.9843 [1]
Room Air	5% Carbon Dioxide	-194.155	-85.866	22.423	0.3806 [1]
Room Air	7% Carbon Dioxide	-64.257	42.548	149.353	1.0000 [1]
Room Air	Hyperventilation	-115.963	-4.193	107.578	1.0000[1]

[1] No statistical significant difference between nuclei.

Table A.11 Kruskal Wallis Delta ACCR Inspiration

Source	**SS**	**df**	**MS**	**Chi-Square**	***p* value**
Groups	10750571.468	10	1075057.147	451.562	0.000
Error	1938826.032	523	3707.124		
Total	12689397.500	533			
Nuclei 1	**Nuclei 2**	**Lower CI 95%**	**Mean difference**	**Upper CI 95%**	**P value <0.05**
Room Air	3% Carbon Dioxide	-220.459	-119.314	-18.168	0.0052
Room Air	5% Carbon Dioxide	-245.691	-143.519	-41.346	0.0002
Room Air	Mental Arithmetic	51.716	153.366	255.016	0.0000
Room Air	Word Recall	52.309	154.481	256.654	0.0000
Room Air	Hyperventilation	-327.511	-228.221	-128.932	0.0000
Room Air	Deep Inspiration	-383.616	-282.471	-181.325	0.0000
Room Air	100% Oxygen	-67.931	35.344	138.619	1.0000[1]
Room Air	1% Carbon Dioxide	-205.157	-100.694	3.768	0.0751 [1]
Room Air	7% Carbon Dioxide	-36.804	67.054	170.911	0.8383[1]
Room Air	Breath Hold	-76.944	30.931	138.806	1.0000 [1]

[1] No statistical significant difference between nuclei.

Table A.12 Kruskal Wallis Delta ACCR Expiration

Source	**SS**	**df**	**MS**	**Chi-Square**	***p* value**
Groups	11984351.080	10	1198435.108	448.122	0.000
Error	3125726.420	555	5631.939		
Total	15110077.500	565			
Nuclei 1	**Nuclei 2**	**Lower CI 95%**	**Mean difference**	**Upper CI 95%**	**P value <0.05**
Room Air	3% Carbon Dioxide	-255.999	-146.633	-37.266	0.0005
Room Air	5% Carbon Dioxide	-305.425	-197.136	-88.846	0.0000
Room Air	Mental Arithmetic	64.962	173.781	282.599	0.0000
Room Air	Word Recall	38.399	146.688	254.977	0.0004
Room Air	Hyperventilation	-358.952	-247.181	-135.411	0.0000
Room Air	Deep Inspiration	-416.959	-307.592	-198.225	0.0000
Room Air	100% Oxygen	-78.035	29.248	136.532	1.0000 [1]
Room Air	1% Carbon Dioxide	-203.283	-96.941	9.401	0.1309 [1]
Room Air	7% Carbon Dioxide	-92.320	14.485	121.290	1.0000 [1]
Room Air	Breath Hold	-104.143	0.091	104.324	1.0000 [1]

[1] No statistical significant difference between nuclei.

Table A.13 Kruskal Wallis Theta ACCR Inspiration

Source	**SS**	**df**	**MS**	**Chi-Square**	***p* value**
Groups	9703548.068	10	970354.807	407.584	0.000
Error	2985849.432	523	5709.081		
Total	12689397.500	533			
Nuclei 1	**Nuclei 2**	**Lower CI 95%**	**Mean difference**	**Upper CI 95%**	**P value <0.05**
Room Air	100% Oxygen	17.640	120.914	224.189	0.0058
Room Air	Mental Arithmetic	76.525	178.175	279.825	0.0000
Room Air	Word Recall	36.103	138.275	240.448	0.0004
Room Air	Hyperventilation	-304.998	-205.709	-106.419	0.0000
Room Air	Deep Inspiration	-353.067	-251.922	-150.776	0.0000
Room Air	1% Carbon Dioxide	-185.719	-81.256	23.206	0.4255 [1]
Room Air	3% Carbon Dioxide	-133.753	-32.608	68.537	1.0000 [1]
Room Air	5% Carbon Dioxide	-201.366	-99.194	2.978	0.0696 [1]
Room Air	7% Carbon Dioxide	-30.146	73.711	177.569	0.6480 [1]
Room Air	Breath Hold	-98.495	9.380	117.255	1.0000 [1]

[1] No statistical significant difference between nuclei.

Table A.14 Kruskal Wallis Theta ACCR Expiration

Source	**SS**	**df**	**MS**	**Chi-Square**	***p* value**
Groups	10576186.840	10	1057618.684	395.468	0.000
Error	4533890.660	555	8169.172		
Total	15110077.500	565			
Nuclei 1	**Nuclei 2**	**Lower CI 95%**	**Mean difference**	**Upper CI 95%**	**P value <0.05**
Room Air	5% Carbon Dioxide	-263.566	-155.277	-46.988	0.0001
Room Air	Mental Arithmetic	61.960	170.779	279.597	0.0000
Room Air	Word Recall	26.061	134.351	242.640	0.0022
Room Air	Hyperventilation	-362.832	-251.061	-139.291	0.0000
Room Air	Deep Inspiration	-400.244	-290.878	-181.511	0.0000
Room Air	100% Oxygen	-20.458	86.826	194.109	0.3348 [1]
Room Air	1% Carbon Dioxide	-159.767	-53.425	52.917	0.9962 [1]
Room Air	3% Carbon Dioxide	-178.571	-69.204	40.163	0.8684[1]
Room Air	7% Carbon Dioxide	-123.718	-16.913	89.892	1.0000[1]
Room Air	Breath Hold	-122.661	-18.428	85.806	1.0000[1]

[1] No statistical significant difference between nuclei.

Table A.15 Kruskal Wallis Alpha ACCR Inspiration

Source	**SS**	**df**	**MS**	**Chi-Square**	***p* value**
Groups	8103670.384	10	810367.038	340.383	0.000
Error	4585727.116	523	8768.121		
Total	12689397.500	533			
Nuclei 1	**Nuclei 2**	**Lower CI 95%**	**Mean difference**	**Upper CI 95%**	**P value <0.05**
Room Air	100% Oxygen	67.428	170.703	273.977	0.0000
Room Air	1% Carbon Dioxide	11.616	116.078	220.541	0.0128
Room Air	3% Carbon Dioxide	154.129	255.275	356.420	0.0000
Room Air	5% Carbon Dioxide	89.573	191.745	293.917	0.0000
Room Air	Hyperventilation	37.438	136.727	236.016	0.0003
Room Air	Deep Inspiration	174.227	275.373	376.518	0.0000
Room Air	7% Carbon Dioxide	-87.873	15.984	119.842	1.0000 [1]
Room Air	Mental Arithmetic	-131.665	-30.015	71.635	1.0000 [1]
Room Air	Word Recall	-193.488	-91.316	10.856	0.1566 [1]
Room Air	Breath Hold	-176.030	-68.155	39.720	0.8706 [1]

[1] No statistical significant difference between nuclei.

Table A.16 Kruskal Wallis Alpha ACCR Expiration

Source	**SS**	**df**	**MS**	**Chi-Square**	***p* value**
Groups	9233748.761	10	923374.876	345.271	0.000
Error	5876328.739	555	10587.980		
Total	15110077.500	565			
Nuclei 1	**Nuclei 2**	**Lower CI 95%**	**Mean difference**	**Upper CI 95%**	**P value <0.05**
Room Air	100% Oxygen	75.431	182.714	289.997	0.0000
Room Air	1% Carbon Dioxide	46.908	153.250	259.592	0.0001
Room Air	3% Carbon Dioxide	155.817	265.184	374.550	0.0000
Room Air	5% Carbon Dioxide	100.964	209.253	317.542	0.0000
Room Air	Deep Inspiration	175.409	284.776	394.142	0.0000
Room Air	7% Carbon Dioxide	-89.124	17.681	124.486	1.0000[1]
Room Air	Mental Arithmetic	-162.399	-53.581	55.238	0.9975 [1]
Room Air	Word Recall	-179.487	-71.198	37.091	0.8076 [1]
Room Air	Hyperventilation	-19.878	91.893	203.663	0.3013 [1]
Room Air	Breath Hold	-168.874	-64.641	39.593	0.8946[1]

[1] No statistical significant difference between nuclei.

Table A.17 Kruskal Wallis Beta ACCR Inspiration

Source	**SS**	**df**	**MS**	**Chi-Square**	***p* value**
Groups	9594973.027	10	959497.303	403.023	0.000
Error	3094424.473	523	5916.682		
Total	12689397.500	533			
Nuclei 1	**Nuclei 2**	**Lower CI 95%**	**Mean difference**	**Upper CI 95%**	**P value <0.05**
Room Air	1% Carbon Dioxide	34.564	139.026	243.489	0.0006
Room Air	3% Carbon Dioxide	21.208	122.353	223.498	0.0034
Room Air	5% Carbon Dioxide	71.169	173.341	275.514	0.0000
Room Air	Mental Arithmetic	-233.953	-132.303	-30.653	0.0009
Room Air	Hyperventilation	145.939	245.228	344.517	0.0000
Room Air	Deep Inspiration	204.659	305.804	406.949	0.0000
Room Air	100% Oxygen	-111.989	-8.714	94.561	1.0000 [1]
Room Air	7% Carbon Dioxide	-97.372	6.485	110.343	1.0000 [1]
Room Air	Word Recall	-199.627	-97.455	4.718	0.0839 [1]
Room Air	Breath Hold	-75.763	32.112	139.987	1.0000 [1]

[1] No statistical significant difference between nuclei.

Table A.18 Kruskal Wallis Beta ACCR Expiration

Source	**SS**	**df**	**MS**	**Chi-Square**	***p* value**
Groups	10946499.965	10	1094649.996	409.314	0.000
Error	4163577.535	555	7501.942		
Total	15110077.500	565			
Nuclei 1	**Nuclei 2**	**Lower CI 95%**	**Mean difference**	**Upper CI 95%**	**P value <0.05**
Room Air	1% Carbon Dioxide	27.171	133.513	239.855	0.0018
Room Air	3% Carbon Dioxide	71.572	180.939	290.305	0.0000
Room Air	5% Carbon Dioxide	127.895	236.184	344.474	0.0000
Room Air	Mental Arithmetic	-220.714	-111.896	-3.077	0.0359
Room Air	Hyperventilation	206.922	318.693	430.464	0.0000
Room Air	Deep Inspiration	252.450	361.816	471.183	0.0000
Room Air	100% Oxygen	-63.532	43.751	151.035	1.0000 [1]
Room Air	7% Carbon Dioxide	-3.342	103.463	210.268	0.0712 [1]
Room Air	Word Recall	-166.830	-58.541	49.748	0.9850 [1]
Room Air	Breath Hold	-25.796	78.437	182.671	0.5059[1]

[1] No statistical significant difference between nuclei.

Table A.19 Kruskal Wallis Gamma ACCR Inspiration

Source	**SS**	**df**	**MS**	**Chi-Square**	***p* value**
Groups	8410367.478	10	841036.748	353.265	0.000
Error	4279030.022	523	8181.702		
Total	12689397.500	533			
Nuclei 1	**Nuclei 2**	**Lower CI 95%**	**Mean difference**	**Upper CI 95%**	**P value <0.05**
Room Air	100% Oxygen	-362.955	-259.680	-156.405	0.0000
Room Air	3% Carbon Dioxide	-284.636	-183.490	-82.345	0.0000
Room Air	5% Carbon Dioxide	-219.305	-117.132	-14.960	0.0081
Room Air	7% Carbon Dioxide	-292.721	-188.864	-85.006	0.0000
Room Air	Hyperventilation	13.601	112.891	212.180	0.0092
Room Air	Deep Inspiration	72.776	173.922	275.067	0.0000
Room Air	1% Carbon Dioxide	-193.695	-89.233	15.230	0.2278 [1]
Room Air	Mental Arithmetic	-197.205	-95.555	6.095	0.0973 [1]
Room Air	Word Recall	-182.876	-80.704	21.468	0.3895 [1]
Room Air	Breath Hold	-117.530	-9.655	98.220	1.0000 [1]

[1] No statistical significant difference between nuclei.

Table A.20 Kruskal Wallis Gamma ACCR Expiration

Source	**SS**	**df**	**MS**	**Chi-Square**	***p* value**
Groups	9636837.991	10	963683.799	360.343	0.000
Error	5473239.509	555	9861.693		
Total	15110077.500	565			

Nuclei 1	**Nuclei 2**	**Lower CI 95%**	**Mean difference**	**Upper CI 95%**	**P value <0.05**
Room Air	100% Oxygen	-396.948	-289.665	-182.381	0.0000
Room Air	1% Carbon Dioxide	-249.612	-143.270	-36.928	0.0005
Room Air	3% Carbon Dioxide	-325.632	-216.265	-106.899	0.0000
Room Air	7% Carbon Dioxide	-284.982	-178.176	-71.371	0.0000
Room Air	Mental Arithmetic	-230.285	-121.466	-12.648	0.0120
Room Air	Word Recall	-255.654	-147.365	-39.076	0.0004
Room Air	Hyperventilation	10.390	122.161	233.931	0.0162
Room Air	Deep Inspiration	60.756	170.122	279.489	0.0000
Room Air	5% Carbon Dioxide	-173.909	-65.620	42.669	0.9199 [1]
Room Air	Breath Hold	-137.790	-33.556	70.677	1.0000 [1]

[1] No statistical significant difference between nuclei.

Table A.21 Kruskal Wallis Delta VPL Inspiration

Source	**SS**	**df**	**MS**	**Chi-Square**	***p* value**
Groups	7747667.502	10	774766.750	325.430	0.000
Error	4941729.998	523	9448.815		
Total	12689397.500	533			
Nuclei 1	**Nuclei 2**	**Lower CI 95%**	**Mean difference**	**Upper CI 95%**	**P value <0.05**
Room Air	1% Carbon Dioxide	65.225	169.688	274.150	0.0000
Room Air	Mental Arithmetic	173.820	275.470	377.120	0.0000
Room Air	Word Recall	149.766	251.938	354.111	0.0000
Room Air	Deep Inspiration	137.776	238.922	340.067	0.0000
Room Air	Breath Hold	279.260	387.135	495.010	0.0000
Room Air	100% Oxygen	-148.191	-44.916	58.359	0.9999[1]
Room Air	3% Carbon Dioxide	-3.341	97.804	198.949	0.0726 [1]
Room Air	5% Carbon Dioxide	-33.050	69.122	171.294	0.7533 [1]
Room Air	7% Carbon Dioxide	-16.500	87.358	191.215	0.2561 [1]
Room Air	Hyperventilation	-14.561	84.728	184.017	0.2296 [1]

[1] No statistical significant difference between nuclei.

Table A.22 Kruskal Wallis Delta VPL Expiration

Source	**SS**	**df**	**MS**	**Chi-Square**	***p* value**
Groups	9312667.036	10	931266.704	348.222	0.000
Error	5797410.464	555	10445.785		
Total	15110077.500	565			

Nuclei 1	**Nuclei 2**	**Lower CI 95%**	**Mean difference**	**Upper CI 95%**	**P value <0.05**
Room Air	1% Carbon Dioxide	69.922	176.265	282.607	0.0000
Room Air	Mental Arithmetic	156.513	265.332	374.150	0.0000
Room Air	Word Recall	186.734	295.023	403.312	0.0000
Room Air	Hyperventilation	35.443	147.214	258.985	0.0007
Room Air	Deep Inspiration	174.633	284.000	393.367	0.0000
Room Air	Breath Hold	306.242	410.475	514.709	0.0000
Room Air	100% Oxygen	-29.786	77.497	184.781	0.6060 [1]
Room Air	3% Carbon Dioxide	-6.836	102.531	211.897	0.1000 [1]
Room Air	5% Carbon Dioxide	-71.286	37.004	145.293	1.0000 [1]
Room Air	7% Carbon Dioxide	-68.343	38.462	145.267	1.0000 [1]

[1] No statistical significant difference between nuclei.

Table A.23 Kruskal Wallis Theta VPL Inspiration

Source	**SS**	**df**	**MS**	**Chi-Square**	***p* value**
Groups	7622513.627	10	762251.363	320.173	0.000
Error	5066883.873	523	9688.114		
Total	12689397.500	533			
Nuclei 1	**Nuclei 2**	**Lower CI 95%**	**Mean difference**	**Upper CI 95%**	**P value <0.05**
Room Air	1% Carbon Dioxide	9.856	114.319	218.781	0.0159
Room Air	Mental Arithmetic	147.758	249.408	351.058	0.0000
Room Air	Word Recall	118.374	220.547	322.719	0.0000
Room Air	Deep Inspiration	110.364	211.510	312.655	0.0000
Room Air	Breath Hold	244.108	351.983	459.858	0.0000
Room Air	100% Oxygen	-162.625	-59.350	43.925	0.9607 [1]
Room Air	3% Carbon Dioxide	-88.675	12.471	113.616	1.0000 [1]
Room Air	5% Carbon Dioxide	-67.258	34.914	137.086	1.0000 [1]
Room Air	7% Carbon Dioxide	-50.424	53.434	157.291	0.9939 [1]
Room Air	Hyperventilation	-64.881	34.408	133.697	1.0000[1]

[1] No statistical significant difference between nuclei.

Table A.24 Kruskal Wallis Theta VPL Expiration

Source	**SS**	**df**	**MS**	**Chi-Square**	***p* value**
Groups	9678521.337	10	967852.134	361.902	0.000
Error	5431556.163	555	9786.588		
Total	15110077.500	565			
Nuclei 1	**Nuclei 2**	**Lower CI 95%**	**Mean difference**	**Upper CI 95%**	**P value <0.05**
Room Air	Mental Arithmetic	141.929	250.748	359.566	0.0000
Room Air	Word Recall	143.804	252.094	360.383	0.0000
Room Air	Deep Inspiration	150.756	260.122	369.489	0.0000
Room Air	Breath Hold	278.187	382.421	486.655	0.0000
Room Air	100% Oxygen	-52.009	55.275	162.558	0.9937 [1]
Room Air	1% Carbon Dioxide	-7.300	99.042	205.384	0.1067 [1]
Room Air	3% Carbon Dioxide	-93.612	15.755	125.122	1.0000 [1]
Room Air	5% Carbon Dioxide	-132.568	-24.279	84.010	1.0000 [1]
Room Air	7% Carbon Dioxide	-72.714	34.091	140.897	1.0000 [1]
Room Air	Hyperventilation	-1.916	109.854	221.625	0.0608 [1]

[1] No statistical significant difference between nuclei.

Table A.25 Kruskal Wallis Alpha VPL Inspiration

Source	**SS**	**df**	**MS**	**Chi-Square**	***p* value**
Groups	5054813.589	10	505481.359	212.320	0.000
Error	7634583.911	523	14597.675		
Total	12689397.500	533			
Nuclei 1	**Nuclei 2**	**Lower CI 95%**	**Mean difference**	**Upper CI 95%**	**P value <0.05**
Room Air	1% Carbon Dioxide	-246.593	-142.131	-37.668	0.0004
Room Air	3% Carbon Dioxide	-312.734	-211.588	-110.443	0.0000
Room Air	5% Carbon Dioxide	-220.471	-118.299	-16.126	0.0069
Room Air	7% Carbon Dioxide	-224.174	-120.317	-16.459	0.0069
Room Air	Mental Arithmetic	-211.476	-109.826	-8.176	0.0190
Room Air	Word Recall	-211.777	-109.605	-7.432	0.0209
Room Air	Breath Hold	58.364	166.239	274.114	0.0000
Room Air	100% Oxygen	-85.493	17.782	121.057	1.0000 [1]
Room Air	Hyperventilation	-89.630	9.659	108.948	1.0000 [1]
Room Air	Deep Inspiration	-95.420	5.725	106.871	1.0000 [1]

[1] No statistical significant difference between nuclei.

Table A.26 Kruskal Wallis Alpha VPL Expiration

Source	**SS**	**df**	**MS**	**Chi-Square**	***p* value**
Groups	6755815.655	10	675581.566	252.615	0.000
Error	8354261.845	555	15052.724		
Total	15110077.500	565			
Nuclei 1	**Nuclei 2**	**Lower CI 95%**	**Mean difference**	**Upper CI 95%**	**P value <0.05**
Room Air	1% Carbon Dioxide	-223.355	-117.013	-10.670	0.0147
Room Air	3% Carbon Dioxide	-249.999	-140.633	-31.266	0.0011
Room Air	Word Recall	-222.758	-114.469	-6.179	0.0254
Room Air	Deep Inspiration	7.429	116.796	226.163	0.0222
Room Air	Breath Hold	125.851	230.084	334.318	0.0000
Room Air	100% Oxygen	-161.996	-54.713	52.570	0.9949 [1]
Room Air	5% Carbon Dioxide	-190.836	-82.547	25.742	0.4743 [1]
Room Air	7% Carbon Dioxide	-75.161	31.644	138.449	1.0000 [1]
Room Air	Mental Arithmetic	-132.387	-23.569	85.250	1.0000 [1]
Room Air	Hyperventilation	-136.509	-24.738	87.033	1.0000 [1]

[1] No statistical significant difference between nuclei.

Table A.27 Kruskal Wallis Beta VPL Inspiration

Source	**SS**	**df**	**MS**	**Chi-Square**	***p* value**
Groups	5144580.169	10	514458.017	216.091	0.000
Error	7544817.331	523	14426.037		
Total	12689397.500	533			

Nuclei 1	**Nuclei 2**	**Lower CI 95%**	**Mean difference**	**Upper CI 95%**	**P value <0.05**
Room Air	1% Carbon Dioxide	-251.707	-147.244	-42.782	0.0002
Room Air	5% Carbon Dioxide	-226.029	-123.857	-21.685	0.0033
Room Air	7% Carbon Dioxide	-237.314	-133.457	-29.599	0.0012
Room Air	Mental Arithmetic	-364.950	-263.300	-161.650	0.0000
Room Air	Word Recall	-334.601	-232.429	-130.256	0.0000
Room Air	Deep Inspiration	-242.773	-141.627	-40.482	0.0002
Room Air	100% Oxygen	-64.147	39.128	142.403	1.0000 [1]
Room Air	3% Carbon Dioxide	-170.204	-69.059	32.087	0.7344 [1]
Room Air	Hyperventilation	-61.853	37.436	136.726	1.0000 [1]
Room Air	Breath Hold	-140.275	-32.400	75.475	1.0000 [1]

[1] No statistical significant difference between nuclei.

Table A.28 Kruskal Wallis Beta VPL Expiration

Source	**SS**	**df**	**MS**	**Chi-Square**	***p* value**
Groups	3942466.391	10	394246.639	147.418	0.000
Error	11167611.109	555	20121.822		
Total	15110077.500	565			

Nuclei 1	**Nuclei 2**	**Lower CI 95%**	**Mean difference**	**Upper CI 95%**	**P value <0.05**
Room Air	Mental Arithmetic	-306.510	-197.692	-88.873	0.0000
Room Air	Word Recall	-332.744	-224.455	-116.165	0.0000
Room Air	100% Oxygen	-168.592	-61.309	45.975	0.9638 [1]
Room Air	1% Carbon Dioxide	-186.370	-80.028	26.314	0.5058 [1]
Room Air	3% Carbon Dioxide	-98.305	11.061	120.428	1.0000 [1]
Room Air	5% Carbon Dioxide	-93.842	14.447	122.737	1.0000 [1]
Room Air	7% Carbon Dioxide	-94.064	12.741	119.547	1.0000 [1]
Room Air	Hyperventilation	-156.474	-44.703	67.068	1.0000 [1]
Room Air	Deep Inspiration	-111.530	-2.163	107.203	1.0000 [1]
Room Air	Breath Hold	-72.342	31.891	136.125	1.0000 [1]

[1] No statistical significant difference between nuclei.

Table A.29 Kruskal Wallis Gamma VPL Inspiration

Source	**SS**	**df**	**MS**	**Chi-Square**	***p* value**
Groups	6913626.661	10	691362.666	290.397	0.000
Error	5775770.839	523	11043.539		
Total	12689397.500	533			
Nuclei 1	**Nuclei 2**	**Lower CI 95%**	**Mean difference**	**Upper CI 95%**	**P value <0.05**
Room Air	3% Carbon Dioxide	40.306	141.451	242.596	0.0002
Room Air	5% Carbon Dioxide	45.326	147.499	249.671	0.0001
Room Air	7% Carbon Dioxide	27.992	131.850	235.707	0.0015
Room Air	Deep Inspiration	-247.459	-146.314	-45.168	0.0001
Room Air	Breath Hold	-355.316	-247.441	-139.565	0.0000
Room Air	100% Oxygen	-40.789	62.486	165.761	0.9214 [1]
Room Air	1% Carbon Dioxide	-110.145	-5.682	98.780	1.0000 [1]
Room Air	Mental Arithmetic	-149.425	-47.776	53.874	0.9991 [1]
Room Air	Word Recall	-152.551	-50.379	51.793	0.9974 [1]
Room Air	Hyperventilation	-133.596	-34.307	64.983	1.0000 [1]

[1] No statistical significant difference between nuclei.

Table A.30 Kruskal Wallis Gamma VPL Expiration

Source	**SS**	**df**	**MS**	**Chi-Square**	***p* value**
Groups	9501311.512	10	950131.151	355.276	0.000
Error	5608765.988	555	10105.885		
Total	15110077.500	565			

Nuclei 1	**Nuclei 2**	**Lower CI 95%**	**Mean difference**	**Upper CI 95%**	**P value <0.05**
Room Air	1% Carbon Dioxide	-226.420	-120.078	-13.735	0.0102
Room Air	7% Carbon Dioxide	-224.275	-117.470	-10.665	0.0148
Room Air	Mental Arithmetic	-320.976	-212.158	-103.339	0.0000
Room Air	Word Recall	-300.382	-192.093	-83.804	0.0000
Room Air	Hyperventilation	-234.515	-122.744	-10.974	0.0152
Room Air	Deep Inspiration	-446.244	-336.878	-227.511	0.0000
Room Air	Breath Hold	-502.694	-398.461	-294.227	0.0000
Room Air	100% Oxygen	-134.784	-27.500	79.783	1.0000[1]
Room Air	3% Carbon Dioxide	-164.020	-54.653	54.714	0.9966 [1]
Room Air	5% Carbon Dioxide	-96.990	11.299	119.588	1.0000 [1]

[1] No statistical significant difference between nuclei.

Table A.31 Kruskal Wallis Delta PVG Inspiration

Source	**SS**	**df**	**MS**	**Chi-Square**	***p* value**
Groups	6571098.399	10	657109.840	276.010	0.000
Error	6118299.101	523	11698.469		
Total	12689397.500	533			
Nuclei 1	**Nuclei 2**	**Lower CI 95%**	**Mean difference**	**Upper CI 95%**	**P value <0.05**
Room Air	5% Carbon Dioxide	-253.584	-151.412	-49.240	0.0001
Room Air	7% Carbon Dioxide	-234.368	-130.511	-26.653	0.0018
Room Air	Mental Arithmetic	55.888	157.538	259.188	0.0000
Room Air	Word Recall	20.579	122.751	224.923	0.0038
Room Air	Breath Hold	113.223	221.098	328.973	0.0000
Room Air	100% Oxygen	-193.879	-90.604	12.671	0.1837 [1]
Room Air	1% Carbon Dioxide	-34.009	70.454	174.916	0.7595 [1]
Room Air	3% Carbon Dioxide	-92.224	8.922	110.067	1.0000 [1]
Room Air	Hyperventilation	-155.719	-56.429	42.860	0.9666 [1]
Room Air	Deep Inspiration	-78.577	22.569	123.714	1.0000[1]

[1] No statistical significant difference between nuclei.

Table A.32 Kruskal Wallis Delta PVG Expiration

Source	**SS**	**df**	**MS**	**Chi-Square**	***p* value**
Groups	9436430.867	10	943643.087	352.850	0.000
Error	5673646.633	555	10222.787		
Total	15110077.500	565			

Nuclei 1	**Nuclei 2**	**Lower CI 95%**	**Mean difference**	**Upper CI 95%**	**P value <0.05**
Room Air	Mental Arithmetic	120.855	229.673	338.492	0.0000
Room Air	Word Recall	101.325	209.614	317.903	0.0000
Room Air	Deep Inspiration	31.143	140.510	249.877	0.0012
Room Air	Breath Hold	190.136	294.370	398.603	0.0000
Room Air	100% Oxygen	-148.423	-41.139	66.144	1.0000
Room Air	1% Carbon Dioxide	-3.762	102.580	208.922	0.0745 [1]
Room Air	3% Carbon Dioxide	-71.979	37.388	146.754	1.0000 [1]
Room Air	5% Carbon Dioxide	-200.734	-92.445	15.844	0.2289 [1]
Room Air	7% Carbon Dioxide	-201.356	-94.551	12.254	0.1701 [1]
Room Air	Hyperventilation	-91.584	20.186	131.957	1.0000 [1]

[1] No statistical significant difference between nuclei.

Table A.33 Kruskal Wallis Theta PVG Inspiration

Source	**SS**	**df**	**MS**	**Chi-Square**	***p* value**
Groups	7294632.313	10	729463.231	306.401	0.000
Error	5394765.187	523	10315.039		
Total	12689397.500	533			

Nuclei 1	**Nuclei 2**	**Lower CI 95%**	**Mean difference**	**Upper CI 95%**	**P value <0.05**
Room Air	1% Carbon Dioxide	-311.051	-206.588	-102.126	0.0000
Room Air	3% Carbon Dioxide	-297.479	-196.333	-95.188	0.0000
Room Air	5% Carbon Dioxide	-284.774	-182.602	-80.430	0.0000
Room Air	7% Carbon Dioxide	-291.634	-187.777	-83.919	0.0000
Room Air	Hyperventilation	-216.271	-116.982	-17.693	0.0053
Room Air	Breath Hold	62.270	170.145	278.020	0.0000
Room Air	100% Oxygen	-159.445	-56.170	47.105	0.9834 [1]
Room Air	Mental Arithmetic	-16.525	85.125	186.775	0.2645 [1]
Room Air	Word Recall	-72.101	30.072	132.244	1.0000 [1]
Room Air	Deep Inspiration	-165.498	-64.353	36.792	0.8606 [1]

[1] No statistical significant difference between nuclei.

Table A.34 Kruskal Wallis Theta PVG Expiration

Source	**SS**	**df**	**MS**	**Chi-Square**	***p* value**
Groups	9730832.838	10	973083.284	363.858	0.000
Error	5379244.662	555	9692.333		
Total	15110077.500	565			
Nuclei 1	**Nuclei 2**	**Lower CI 95%**	**Mean difference**	**Upper CI 95%**	**P value <0.05**
Room Air	1% Carbon Dioxide	-307.794	-201.452	-95.109	0.0000
Room Air	3% Carbon Dioxide	-289.428	-180.061	-70.695	0.0000
Room Air	5% Carbon Dioxide	-236.438	-128.149	-19.860	0.0049
Room Air	7% Carbon Dioxide	-300.630	-193.825	-87.020	0.0000
Room Air	Mental Arithmetic	9.735	118.554	227.372	0.0169
Room Air	Breath Hold	94.060	198.294	302.527	0.0000
Room Air	100% Oxygen	-164.023	-56.740	50.543	0.9898 [1]
Room Air	Word Recall	-41.850	66.439	174.728	0.9070 [1]
Room Air	Hyperventilation	-177.432	-65.662	46.109	0.9464 [1]
Room Air	Deep Inspiration	-69.510	39.857	149.224	1.0000 [1]

[1] No statistical significant difference between nuclei.

Table A.35 Kruskal Wallis Alpha PVG Inspiration

Source	**SS**	**df**	**MS**	**Chi-Square**	***p* value**
Groups	7922495.362	10	792249.536	332.773	0.000
Error	4766902.138	523	9114.536		
Total	12689397.500	533			

Nuclei 1	**Nuclei 2**	**Lower CI 95%**	**Mean difference**	**Upper CI 95%**	**P value <0.05**
Room Air	1% Carbon Dioxide	-396.308	-291.846	-187.383	0.0000
Room Air	3% Carbon Dioxide	-350.459	-249.314	-148.168	0.0000
Room Air	Breath Hold	69.118	176.993	284.868	0.0000
Room Air	100% Oxygen	-83.538	19.737	123.012	1.0000[1]
Room Air	5% Carbon Dioxide	-94.492	7.680	109.852	1.0000 [1]
Room Air	7% Carbon Dioxide	-200.558	-96.700	7.157	0.1070 [1]
Room Air	Mental Arithmetic	-160.767	-59.117	42.533	0.9534 [1]
Room Air	Word Recall	-203.533	-101.361	0.811	0.0548 [1]
Room Air	Hyperventilation	-59.283	40.007	139.296	1.0000 [1]
Room Air	Deep Inspiration	-183.930	-82.784	18.361	0.3107 [1]

[1] No statistical significant difference between nuclei.

Table A.36 Kruskal Wallis Alpha PVG Expiration

Source	**SS**	**df**	**MS**	**Chi-Square**	***p* value**
Groups	8809993.541	10	880999.354	329.426	0.000
Error	6300083.959	555	11351.503		
Total	15110077.500	565			
Nuclei 1	**Nuclei 2**	**Lower CI 95%**	**Mean difference**	**Upper CI 95%**	**P value <0.05**
Room Air	1% Carbon Dioxide	-451.529	-345.187	-238.845	0.0000
Room Air	3% Carbon Dioxide	-394.550	-285.184	-175.817	0.0000
Room Air	Mental Arithmetic	-234.833	-126.014	-17.196	0.0069
Room Air	Word Recall	-288.945	-180.655	-72.366	0.0000
Room Air	100% Oxygen	-163.752	-56.469	50.814	0.9907 [1]
Room Air	5% Carbon Dioxide	-163.474	-55.185	53.104	0.9949 [1]
Room Air	7% Carbon Dioxide	-211.427	-104.622	2.183	0.0631 [1]
Room Air	Hyperventilation	-108.663	3.108	114.879	1.0000 [1]
Room Air	Deep Inspiration	-209.979	-100.612	8.754	0.1202 [1]
Room Air	Breath Hold	-8.648	95.586	199.819	0.1238 [1]

[1] No statistical significant difference between nuclei.

Table A.37 Kruskal Wallis Beta PVG Inspiration

Source	**SS**	**df**	**MS**	**Chi-Square**	***p* value**
Groups	4448737.505	10	444873.750	186.863	0.000
Error	8240659.995	523	15756.520		
Total	12689397.500	533			
Nuclei 1	**Nuclei 2**	**Lower CI 95%**	**Mean difference**	**Upper CI 95%**	**P value <0.05**
Room Air	3% Carbon Dioxide	1.266	102.412	203.557	0.0432
Room Air	5% Carbon Dioxide	99.467	201.639	303.812	0.0000
Room Air	7% Carbon Dioxide	54.737	158.594	262.452	0.0000
Room Air	Mental Arithmetic	-212.736	-111.087	-9.437	0.0162
Room Air	Hyperventilation	16.135	115.424	214.714	0.0065
Room Air	100% Oxygen	-16.346	86.929	190.204	0.2547 [1]
Room Air	1% Carbon Dioxide	-62.174	42.289	146.751	1.0000[1]
Room Air	Word Recall	-177.594	-75.422	26.750	0.5532[1]
Room Air	Deep Inspiration	-78.341	22.804	123.949	1.0000 [1]
Room Air	Breath Hold	-108.817	-0.942	106.934	1.0000 [1]

[1] No statistical significant difference between nuclei.

Table A.38 Kruskal Wallis Beta PVG Expiration

Source	**SS**	**df**	**MS**	**Chi-Square**	***p* value**
Groups	4373297.356	10	437329.736	163.527	0.000
Error	10736780.144	555	19345.550		
Total	15110077.500	565			

Nuclei 1	**Nuclei 2**	**Lower CI 95%**	**Mean difference**	**Upper CI 95%**	**P value <0.05**
Room Air	7% Carbon Dioxide	51.666	158.471	265.276	0.0000
Room Air	Mental Arithmetic	-268.593	-159.774	-50.956	0.0001
Room Air	100% Oxygen	-64.752	42.531	149.814	1.0000 [1]
Room Air	1% Carbon Dioxide	-69.711	36.631	142.973	1.0000 [1]
Room Air	3% Carbon Dioxide	-50.285	59.082	168.448	0.9852 [1]
Room Air	5% Carbon Dioxide	-0.141	108.148	216.438	0.0508 [1]
Room Air	Word Recall	-206.847	-98.557	9.732	0.1329 [1]
Room Air	Hyperventilation	-32.863	78.908	190.679	0.6603 [1]
Room Air	Deep Inspiration	-117.999	-8.633	100.734	1.0000 [1]
Room Air	Breath Hold	-153.915	-49.681	54.553	0.9988 [1]

[1] No statistical significant difference between nuclei.

Table A.39 Kruskal Wallis Gamma PVG Inspiration

Source	**SS**	**df**	**MS**	**Chi-Square**	***p* value**
Groups	8303859.047	10	830385.905	348.792	0.000
Error	4385538.453	523	8385.351		
Total	12689397.500	533			
Nuclei 1	**Nuclei 2**	**Lower CI 95%**	**Mean difference**	**Upper CI 95%**	**P value <0.05**
Room Air	1% Carbon Dioxide	210.009	314.472	418.934	0.0000
Room Air	3% Carbon Dioxide	154.972	256.118	357.263	0.0000
Room Air	5% Carbon Dioxide	22.020	124.192	226.364	0.0031
Room Air	7% Carbon Dioxide	80.784	184.642	288.499	0.0000
Room Air	Breath Hold	-268.706	-160.831	-52.956	0.0000
Room Air	100% Oxygen	-61.747	41.528	144.803	1.0000 [1]
Room Air	Mental Arithmetic	-145.656	-44.006	57.644	0.9999 [1]
Room Air	Word Recall	-81.327	20.845	123.017	1.0000 [1]
Room Air	Hyperventilation	-14.832	84.458	183.747	0.2353 [1]
Room Air	Deep Inspiration	-12.851	88.294	189.439	0.1915 [1]

[1] No statistical significant difference between nuclei.

Table A.40 Kruskal Wallis Gamma PVG Expiration

Source	**SS**	**df**	**MS**	**Chi-Square**	***p* value**
Groups	11456004.951	10	1145600.495	428.366	0.000
Error	3654072.549	555	6583.915		
Total	15110077.500	565			
Nuclei 1	**Nuclei 2**	**Lower CI 95%**	**Mean difference**	**Upper CI 95%**	**P value <0.05**
Room Air	1% Carbon Dioxide	193.874	300.216	406.558	0.0000
Room Air	3% Carbon Dioxide	147.041	256.408	365.775	0.0000
Room Air	5% Carbon Dioxide	5.906	114.195	222.484	0.0261
Room Air	7% Carbon Dioxide	68.637	175.443	282.248	0.0000
Room Air	Breath Hold	-294.104	-189.870	-85.637	0.0000
Room Air	100% Oxygen	-27.549	79.734	187.018	0.5366 [1]
Room Air	Mental Arithmetic	-168.479	-59.660	49.158	0.9810 [1]
Room Air	Word Recall	-127.466	-19.177	89.112	1.0000 [1]
Room Air	Hyperventilation	-103.436	8.335	120.106	1.0000 [1]
Room Air	Deep Inspiration	-143.122	-33.755	75.612	1.0000 [1]

[1] No statistical significant difference between nuclei.

Bibliography

Heart rate variability: standards of measurement, physiological interpretation and clinical use. task force of the european society of cardiology and the north american society of pacing and electrophysiology. *Circulation*, 93(5):1043–1065, Mar 1996. ISSN 0009-7322 (Print); 0009-7322 (Linking).

D F Abbott, H I Opdam, R S Briellmann, and G D Jackson. Brief breath holding may confound functional magnetic resonance imaging studies. *Hum. Brain Mapp.*, 24(4):284–290, 2005. ISSN 1065-9471. URL papers://2869f907-86c9-45b4-b3a1-9fd72ada1eca/Paper/p45670.

E D Adrian. Afferent impulses in the vagus and their effect on respiration. *J. Physiol.*, 1933.

E Agostoni. Diaphragm activity during breath holding: factors related to its onset. *J. Appl. Physiol.*, 1963.

J M Allman, a Hakeem, J M Erwin, E Nimchinsky, and P Hof. The anterior cingulate cortex. The evolution of an interface between emotion and cognition. *Ann. N. Y. Acad. Sci.*, 935:107–117, 2001. ISSN 0077-8923. doi: 10.1111/j.1749-6632.2001.tb03476.x.

John M. Allman, Nicole a. Tetreault, Atiya Y. Hakeem, Kebreten F. Manaye, Katerina Semendeferi, Joseph M. Erwin, Soyoung Park, Virginie Goubert, and Patrick R. Hof. The von Economo neurons in the frontoinsular and anterior cingulate cortex. *Ann N Y Acad Sci*, 1225(1):59–71, April 2011. ISSN 00778923. doi: 10.1111/j.1749-6632.2011.06011.x.

C Baleydier and F Mauguiere. The duality of the cingulate gyrus in monkey. Neuroanatomical study and functional hypothesis. *Brain a J. Neurol.*, 1980.

R Bandler. Induction of 'rage' following microinjections of glutamate into midbrain but not hypothalamus of cats. *Neurosci Lett*, 30(2):183–188, May 1982. ISSN 0304-3940 (Print); 0304-3940 (Linking).

Richard Bandler and Michael T. Shipley. Columnar organization in the midbrain periaqueductal gray: modules for emotional expression? *Trends Neurosci.*, 17(9): 379–389, January 1994. ISSN 01662236. doi: 10.1016/0166-2236(94)90047-7. URL http://linkinghub.elsevier.com/retrieve/pii/0166223694900477.

Shanika D Basnayake, Jonathan a Hyam, Erlick a Pereira, Patrick M Schweder, J.-S. Brittain, Tipu Z Aziz, Alexander L Green, and David J Paterson. Identifying cardiovascular neurocircuitry involved in the exercise pressor reflex in humans using functional neurosurgery. *J. Appl. Physiol.*, 110(4):881–891, April 2011. ISSN 8750-7587. doi: 10.1152/japplphysiol.00639.2010. URL http://jap.physiology.org/cgi/doi/10.1152/japplphysiol.00639.2010.

Shanika D Basnayake, Alexander L Green, and David J Paterson. Mapping the central neurocircuitry that integrates the cardiovascular response to exercise in humans. *Exp. Physiol.*, 97(1):29–38, 2012. ISSN 1469-445X. doi: 10.1113/expphysiol.2011.060848. URL http://www.ncbi.nlm.nih.gov/pubmed/21984730.

C Bass and W Gardner. Emotional influences on breathing and breathlessness. *J. Psychosom. Res.*, 29(6):599–609, 1985. ISSN 00223999. doi: 10.1016/0022-3999(85)90069-8.

M M Behbehani. Functional characteristics of the midbrain periaqueductal gray. *Prog. Neurobiol.*, 46(6):575–605, 1995. ISSN 03010082. doi: 10.1016/0301-0082(95)00009-K.

Alvin J Beitz. The midbrain periaqueductal gray in the rat. I. Nuclear volume, cell number, density, orientation, and regional subdivisions. *J. Comp. Neurol.*, 237(4): 445–459, July 1985. ISSN 0021-9967. doi: 10.1002/cne.902370403. URL http://doi.wiley.com/10.1002/cne.902370403.

Eduardo E. Benarroch. Periaqueductal gray: An interface for behavioral control. *Neurology*, 78(3):210–217, 2012. ISSN 00283878. doi: 10.1212/WNL.0b013e31823fcdee.

Luciano Bernardi, Joanna Wdowczyk-Szulc, Cinzia Valenti, Stefano Castoldi, Claudio Passino, Giammario Spadacini, and Peter Sleight. Effects of controlled breathing, mental activity and mental stress with or without verbalization on heart rate variability. *J. Am. Coll. Cardiol.*, 35(6):1462–1469, May 2000. ISSN 07351097. doi: 10.1016/S0735-1097(00)00595-7. URL http://linkinghub.elsevier.com/retrieve/pii/S0735109700005957.

Luciano Bernardi, Cesare Porta, Alessandra Gabutti, Lucia Spicuzza, and Peter Sleight. Modulatory effects of respiration. *Auton. Neurosci.*, 90(1-2):47–56, July 2001. ISSN 15660702. doi: 10.1016/S1566-0702(01)00267-3. URL http://linkinghub.elsevier.com/retrieve/pii/S1566070201002673.

Richard G. Bittar, Ishani Kar-Purkayastha, Sarah L. Owen, Renee E. Bear, Alex Green, ShouYan Wang, and Tipu Z. Aziz. Deep brain stimulation for pain relief: A meta-analysis. *J. Clin. Neurosci.*, 12(5):515–519, June 2005a. ISSN 09675868. doi: 10.1016/j.jocn.2004.10.005. URL http://linkinghub.elsevier.com/retrieve/pii/S0967586805001086.

Richard G. Bittar, Sofia Otero, Helen Carter, and Tipu Z. Aziz. Deep brain stimulation for phantom limb pain. *J. Clin. Neurosci.*, 12(4):399–404, May 2005b. ISSN 09675868. doi: 10.1016/j.jocn.2004.07.013. URL http://linkinghub.elsevier.com/retrieve/pii/S0967586804003819.

Christine H Block and Melinda L Estes. The cytoarchitectural organization of the human parabrachial nuclear complex. *Brain Res. Bull.*, 24(4):617–626, 1990. ISSN 0361-9230. doi: 10.1016/0361-9230(90)90168-Y. URL http://www.sciencedirect.com/science/article/pii/036192309090168Y.

Sandra G J Boccard, James J. Fitzgerald, Erlick a C Pereira, Liz Moir, Tim J. Van Hartevelt, Morten L. Kringelbach, Alexander L. Green, and Tipu Z. Aziz. Targeting the affective component of chronic pain: A case series of deep brain stimulation of the anterior cingulate cortex. *Neurosurgery*, 74(6):628–635, 2014a. ISSN 15244040. doi: 10.1227/NEU.0000000000000321.

Sandra G J Boccard, Erlick A C Pereira, Liz Moir, Tim J Van Hartevelt, Morten L Kringelbach, James J FitzGerald, Ian W Baker, Alexander L Green, and Tipu Z Aziz. Deep brain stimulation of the anterior cingulate cortex: targeting the affective component of chronic pain. *Neuroreport*, 25(2):83–88, January 2014b. ISSN 1473-558X (Electronic); 0959-4965 (Linking). doi: 10.1097/WNR.0000000000000039.

Sandra G.J. Boccard, Erlick A.C. Pereira, Liz Moir, Tipu Z Aziz, and Alexander L. Green. Long-term Outcomes of Deep Brain Stimulation for Neuropathic Pain. *Neurosurgery*, 72(2):221–231, February 2013. ISSN 0148-396X. doi: 10.1227/NEU.0b013e31827b97d6. URL http://content.wkhealth.com/linkback/openurl?sid=WKPTLP:landingpage&an=00006123-201302000-00021.

Frans A Boiten. The effects of emotional behaviour on components of the respiratory cycle. *Biol. Psychol.*, 49(1–2):29–51, 1998. ISSN 0301-0511. doi: http://dx.doi.org/10.1016/S0301-0511(98)00025-8. URL http://www.sciencedirect.com/science/article/pii/S0301051198000258.

S Brannan, M Liotti, G Egan, R Shade, L Madden, R Robillard, B Abplanalp, K Stofer, D Denton, and P T Fox. Neuroimaging of cerebral activations and deactivations associated with hypercapnia and hunger for air. *Proc. Natl. Acad. Sci.*, 98(4):2029–2034, February 2001. ISSN 0027-8424. doi: 10.1073/pnas.98.4.2029. URL http://www.pnas.org/cgi/doi/10.1073/pnas.98.4.2029.

Sorin Breit, Jï£ırg B Schulz, and Alim-Louis Benabid. Deep brain stimulation. *Cell Tissue Res.*, 318(1):275–288, October 2004. ISSN 0302-766X. doi: 10.1007/s00441-004-0936-0. URL http://link.springer.com/10.1007/s00441-004-0936-0.

K. Brodmann. *Localisation in the Cerebral Cortex*. 1909. ISBN 9780387269177.

Peter Brown. Oscillatory nature of human basal ganglia activity: Relationship to the pathophysiology of Parkinson's disease. *Mov. Disord.*, 18(4):357–363, 2003.

Peter Brown and David Williams. Basal ganglia local field potential activity: Character and functional significance in the human. *Clin. Neurophysiol.*, 116(11):2510–2519, November 2005. ISSN 13882457. doi: 10.1016/j.clinph.2005.05.009. URL http://linkinghub.elsevier.com/retrieve/pii/S1388245705002142.

S J Brown and R Howden. The effects of a respiratory acidosis on human heart rate variability. *Adv Exp Med Biol*, 605:361–365, 2008. ISSN 0065-2598 (Print); 0065-2598 (Linking). doi: 10.1007/978-0-387-73693-8{_}63.

Paul C. Bucy and Theodore J. Case. Cortical Innervation of Respiratory Movements I. Slowing of Respiratory Movements By Cerebral Stimulation. *J. Nerv. Ment. Dis.*, 84(2):156–168, August 1936. ISSN 0022-3018. doi: 10.1097/00005053-193608000-00004. URL http://content.wkhealth.com/linkback/openurl?sid=WKPTLP:landingpage&an=00005053-193608000-00004.

Scott M. Burns and J. Michael Wyss. The involvement of the anterior cingulate cortex in blood pressure control. *Brain Res.*, 340(1):71–77, August 1985. ISSN 00068993. doi: 10.1016/0006-8993(85)90774-7. URL http://linkinghub.elsevier.com/retrieve/pii/0006899385907747.

G Buzsáki, C A Anastassiou, and C Koch. The origin of extracellular fields and currents{\textemdash}EEG, ECoG, LFP and spikes. *Nat. Rev. Neurosci.*, 2012.

György Buzsáki. Theta oscillations in the hippocampus. *Neuron*, 33(3):325–340, 2002. ISSN 08966273. doi: 10.1016/S0896-6273(02)00586-X.

György Buzsáki, Kai Kaila, and Marcus Raichle. Inhibition and brain work. *Neuron*, 56 (5):771–783, 2007.

J M Campbell, C G Douglas, J S Haldane, and F G Hobson. The response of the respiratory centre to carbonic acid, oxygen, and hydrogen ion concentration. *J. Physiol.*, 46(4-5): 301–318, 1913. ISSN 00223751. doi: 10.1113/jphysiol.1913.sp001593.

Pascal Carrive. The periaqueductal gray and defensive behavior: Functional representation and neuronal organization. *Behav. Brain Res.*, 58(1-2):27–47, December 1993. ISSN 01664328. doi: 10.1016/0166-4328(93)90088-8. URL http://linkinghub.elsevier.com/retrieve/pii/0166432893900888.

Pascal Carrive, Richard Bandler, and Roger A.L. Dampney. Somatic and autonomic integration in the midbrain of the unanesthetized decerebrate cat: a distinctive pattern evoked by excitation of neurones in the subtentorial portion of the midbrain periaqueductal grey. *Brain Res.*, 483(2):251–258, April 1989. ISSN 00068993. doi: 10.1016/0006-8993(89)90169-8. URL http://linkinghub.elsevier.com/retrieve/pii/0006899389901698.

Michael Castellini. *Life Under Water: Physiological Adaptations to Diving and Living at Sea*. John Wiley & Sons, Inc., Hoboken, NJ, USA, July 2012. ISBN 9780470650714. doi: 10.1002/cphy.c110013. URL http://doi.wiley.com/10.1002/cphy.c110013.

David F Cechetto. Cortical control of the autonomic nervous system. *Exp Physiol*, 99(2): 326–331, February 2014. doi: 10.1113/expphysiol.2013.075192.

Z Chen, F L Eldridge, and P G Wagner. Respiratory-associated rhythmic firing of midbrain neurones in cats: relation to level of respiratory drive. *J. Physiol.*, 1991.

Z Chen, F L Eldridge, and P G Wagner. Respiratory-associated thalamic activity is related to level of respiratory drive. *Respir. Physiol.*, 90(1):99–113, 1992.

EvgeniaD. Cherouveim, PetrosG. Botonis, MariaD. Koskolou, and NickosD. Geladas. Effect of gender on maximal breath-hold time. *Eur. J. Appl. Physiol.*, 113(5):1321–1330, 2013. doi: 10.1007/s00421-012-2552-0. URL http://dx.doi.org/10.1007/s00421-012-2552-0.

George Clark and James W. Ward. Responses elicited from the cortex of monkeys by electrical stimulation through fixed electrodes. *Brain*, 71(3):332–342, 1948. ISSN 00068950. doi: 10.1093/brain/71.3.332.

F. Cogiamanian, a. R. Brunoni, P. S. Boggio, F. Fregni, M. Ciocca, and a. Priori. Non-invasive brain stimulation for the management of arterial hypertension. *Med. Hypotheses*, 74(2):332–336, February 2010. ISSN 03069877. doi: 10.1016/j.mehy.2009.08.037.

J G Colebatch, L Adams, K Murphy, a J Martin, a a Lammertsma, H J Tochon-Danguy, J C Clark, K J Friston, and A Guz. Regional cerebral blood flow during volitional breathing in man. *J. Physiol.*, 443(1):91–103, November 1991. ISSN 00223751. doi: 10.1113/jphysiol.1991.sp018824. URL http://doi.wiley.com/10.1113/jphysiol.1991.sp018824.

D Contreras, A Destexhe, T J Sejnowski, and M Steriade. Control of spatiotemporal coherence of a thalamic oscillation by corticothalamic feedback. *Science (80-.).*, 274 (5288):771–774, November 1996.

D R Corfield, G R Fink, S C Ramsay, K Murphy, H R Harty, J D Watson, L Adams, R S Frackowiak, and A Guz. Evidence for limbic system activation during CO2-stimulated breathing in man. *J. Physiol.*, 488 (Pt 1:77–84, October 1995.

D.R. Corfield, K. Murphy, and A. Guz. Does the motor cortical control of the diaphragm 'bypass' the brain stem respiratory centres in man? *Respir. Physiol.*, 114(2):109–117, November 1998. ISSN 00345687. doi: 10.1016/S0034-5687(98)00083-8. URL http://linkinghub.elsevier.com/retrieve/pii/S0034568798000838.

Hugo D Critchley, Christopher J Mathias, and Raymond J Dolan. Neural Activity in the Human Brain Relating to Uncertainty and Arousal during Anticipation. *Neuron*, 29(2):537–545, 2001. ISSN 0896-6273. doi: http://dx.doi.org/10.1016/S0896-6273(01)00225-2. URL http://www.sciencedirect.com/science/article/pii/S0896627301002252.

Hugo D. Critchley, Christopher J. Mathias, Oliver Josephs, John O'Doherty, Sergio Zanini, Bonnie Kate Dewar, Lisa Cipolotti, Tim Shallice, and Raymond J. Dolan. Human cingulate cortex and autonomic control: Converging neuroimaging and clinical evidence. *Brain*, 126(10):2139–2152, October 2003. ISSN 00068950. doi: 10.1093/brain/awg216.

Hugo D. Critchley, Pia Rotshtein, Yoko Nagai, John O'Doherty, Christopher J. Mathias, and Raymond J. Dolan. Activity in the human brain predicting differential heart rate responses to emotional facial expressions. *Neuroimage*, 24(3):751–762, 2005a. ISSN 10538119. doi: 10.1016/j.neuroimage.2004.10.013. URL http://www.sciencedirect.com/science/article/pii/S1053811904006159.

Hugo D Critchley, Joey Tang, Daniel Glaser, Brian Butterworth, and Raymond J Dolan. Anterior cingulate activity during error and autonomic response. *Neuroimage*, 27(4): 885–895, October 2005b. doi: 10.1016/j.neuroimage.2005.05.047.

Roger a L Dampney, Teri M. Furlong, Jouji Horiuchi, and Kamon Iigaya. Role of dorsolateral periaqueductal grey in the coordinated regulation of cardiovascular and respiratory function. *Auton. Neurosci. Basic Clin.*, 175(1-2):17–25, 2013. ISSN 15660702. doi: 10.1016/j.autneu.2012.12.008. URL http://dx.doi.org/10.1016/j.autneu.2012.12.008.

P J Davis, S P Zhang, and R Bandler. Pulmonary and upper airway afferent influences on the motor pattern of vocalization evoked by excitation of the midbrain periaqueductal gray of the cat. *Brain Res.*, 607(1-2):61–80, 1993. ISSN 00068993. doi: 10.1016/0006-8993(93)91490-J.

P Dejours. Control of respiration by arterial chemoreceptors. *Ann. N. Y. Acad. Sci.*, 1963.

Jerome a Dempsey. New perspectives concerning feedback influences on cardiorespiratory control during rhythmic exercise and on exercise performance. *J. Physiol.*, 590(Pt 17):4129–44, 2012. ISSN 1469-7793. doi: 10.1113/jphysiol.2012.233908. URL http://www.pubmedcentral.nih.gov/articlerender.fcgi?artid=3473272&tool=pmcentrez&rendertype=abstract.

Orrin Devinsky and Daniel Luciano. The Contributions of Cingulate Cortex to Human Behavior. *Neurobiol. Cingulate Cortex Limbic Thalamus*, pages 527–556, 1993. doi: 10.1007/978-1-4899-6704-6_19. URL http://link.springer.com/10.1007/978-1-4899-6704-6_19.

Jonathan O Dostrovsky and Andres M Lozano. Mechanisms of deep brain stimulation. *Mov Disord*, 17 Suppl 3:S63–8, 2002. ISSN 0885-3185 (Print); 0885-3185 (Linking).

C Gordon Douglas and J S Haldane. The regulation of normal breathing. *J. Physiol.*, 38(5):420–440, June 1909. ISSN 00223751. doi: 10.1113/jphysiol.1909.sp001315. URL http://doi.wiley.com/10.1113/jphysiol.1909.sp001315.

J Duffin. The chemoreflex control of breathing and its measurement. *Can J Anaesth*, 37 (8):933–942, November 1990. ISSN 0832-610X (Print); 0832-610X (Linking). doi: 10.1007/BF03006641.

Zeljko Dujic, Vladimir Ivancev, Karsten Heusser, Gordan Dzamonja, Ivan Palada, Zoran Valic, Jens Tank, Ante Obad, Darija Bakovic, Andre Diedrich, Michael J Joyner, and Jens Jordan. Central chemoreflex sensitivity and sympathetic neural outflow in elite breath-hold divers. *J. Appl. Physiol.*, 104(1):205–211, January 2008. ISSN 8750-7587. doi: 10.1152/japplphysiol.00844.2007.

Mathias Dutschmann and Horst Herbert. The Kolliker-Fuse nucleus gates the postinspiratory phase of the respiratory cycle to control inspiratory off-switch and upper airway resistance in rat. *Eur. J. Neurosci.*, 24(4):1071–1084, 2006. ISSN 0953816X. doi: 10.1111/j.1460-9568.2006.04981.x.

F. L. Eldridge and Z. Chen. Respiratory-associated rhythmic firing of midbrain neurons is modulated by vagal input. *Respir. Physiol.*, 90(1):31–46, 1992. ISSN 00345687. doi: 10.1016/0034-5687(92)90132-G.

F L Eldridge, J P Kiley, and D E Millhorn. Respiratory responses to medullary hydrogen ion changes in cats: different effects of respiratory and metabolic acidoses. *J. Physiol.*, 358:285–297, 1985. ISSN 00223751.

Karleyton C. Evans, Steven a. Shea, and Andrew J. Saykin. Functional MRI localisation of central nervous system regions associated with volitional inspiration in humans. *J. Physiol.*, 520(2):383–392, 1999. ISSN 00223751. doi: 10.1111/j.1469-7793.1999.00383.x.

Eszter Farkas, Arthur S P Jansen, and Arthur D Loewy. Periaqueductal gray matter projection to vagal preganglionic neurons and the nucleus tractus solitarius. *Brain Res.*, 764(1-2):257–261, 1997. ISSN 0006-8993. doi: S0006-8993(97)00592-1[pii]. URL `http://www.ncbi.nlm.nih.gov/pubmed/9295220`.

Jack L Feldman and Christopher A. Del Negro. Looking for inspiration: new perspectives on respiratory rhythm. *Nat. Rev. Neurosci.*, 7(3):232–241, March 2006. ISSN 1471-003X. doi: 10.1038/nrn1871. URL http://www.nature.com/doifinder/10.1038/nrn1871.

Jack L Feldman, Gordon S Mitchell, and Eugene E Nattie. Breathing: rhythmicity, plasticity, chemosensitivity. *Annu. Rev. Neurosci.*, 26:239–266, 2003. ISSN 0147-006X. doi: 10.1146/annurev.neuro.26.041002.131103.

B R Fink. Influence of cerebral activity in wakefulness on regulation of breathing. *J. Appl. Physiol.*, 16(1):15–20, January 1961a. ISSN 0039-6206. doi: 10.1097/00132586-196204010-00002.

B R Fink. The stimulant effect of wakefulness on respiration: clinical aspects. *Br. J. Anaesth.*, 1961b.

G R Fink, D R Corfield, K Murphy, I Kobayashi, C Dettmers, L Adams, R S Frackowiak, and a Guz. Human cerebral activity with increasing inspiratory force: a study using positron emission tomography. *J. Appl. Physiol.*, 81(3):1295–1305, September 1996. ISSN 8750-7587.

Robert S. Fitzgerald and Neil S. Cherniack. Historical Perspectives on the Control of Breathing. In *Compr. Physiol.*, volume 2, pages 915–932. John Wiley & Sons, Inc., Hoboken, NJ, USA, April 2012. ISBN 2040-4603. doi: 10.1002/cphy.c100007. URL http://doi.wiley.com/10.1002/cphy.c100007.

Patrick a Flume, Frederic L Eldridge, Lloyd J Edwards, and Lynn M Houser. The Fowler breathholding study revisited: continuous rating of respiratory sensation. *Respir. Physiol.*, 95(1):53–66, January 1994. ISSN 00345687. doi: 10.1016/0034-5687(94)90047-7. URL http://linkinghub.elsevier.com/retrieve/pii/0034568794900477.

O. Foerster. The motor cortex in man in the light of hughlings jackson's doctrines. *Brain*, 59(2):135–159, 1936. ISSN 00068950. doi: 10.1093/brain/59.2.135. URL http://brain.oxfordjournals.org/cgi/doi/10.1093/brain/59.2.135.

W S Fowler. Breaking point of breath-holding. *J Appl Physiol*, 6(9):539–545, March 1954.

Angelo Franzini, Giuseppe Messina, Roberto Cordella, Carlo Marras, and Giovanni Broggi. Deep brain stimulation of the posteromedial hypothalamus: indications, long-term results, and neurophysiological considerations. *Neurosurg. Focus*, 29(2):E13, 2010. ISSN 1092-0684. doi: 10.3171/2010.5.FOCUS1094.

Angelo Franzini, Roberto Cordella, Giuseppe Messina, Carlo Efisio Marras, Luigi Michele Romito, Francesco Carella, Alberto Albanese, Michele Rizzi, Nardo Nardocci, Giovanna Zorzi, Edvin Zekay, and Giovanni Broggi. Deep brain stimulation for movement disorders. Considerations on 276 consecutive patients. *J. Neural Transm.*, 118(10): 1497–1510, October 2011. ISSN 03009564. doi: 10.1007/s00702-011-0656-z.

Pascal Fries. Neuronal Gamma-Band Synchronization as a Fundamental Process in Cortical Computation. *Annu. Rev. Neurosci.*, 32(1):209–224, June 2009. ISSN 0147-006X. doi: 10.1146/annurev.neuro.051508.135603. URL `http://www.annualreviews.org/doi/abs/10.1146/annurev.neuro.051508.135603`.

Edgar Garcia-Rill, Christen Simon, Kristen Smith, Nebosja Kezunovic, and James Hyde. The pedunculopontine tegmental nucleus: From basic neuroscience to neurosurgical applications arousal from slices to humans: Implications for DBS. *J. Neural Transm.*, 118(10):1397–1407, 2011. ISSN 03009564. doi: 10.1007/s00702-010-0500-x.

John Gardner. A history of deep brain stimulation: Technological innovation and the role of clinical assessment tools. *Social Studies of Science*, 43(5):707–728, 10 2013. doi: 10.1177/0306312713483678. URL `http://www.ncbi.nlm.nih.gov/pmc/articles/PMC3785222/`.

Philip Gerard Gasquoine. Localization of function in anterior cingulate cortex: from psychosurgery to functional neuroimaging. *Neurosci. Biobehav. Rev.*, 37(3):340–348, March 2013.

André Felix Gentil, Emad N. Eskandar, Carl David Marci, Karleyton Conroy Evans, and Darin Dean Dougherty. Physiological Responses to Brain Stimulation During Limbic Surgery: Further Evidence of Anterior Cingulate Modulation of Autonomic Arousal. *Biol. Psychiatry*, 66(7):695–701, October 2009. ISSN 00063223. doi: 10.1016/j.biopsych.2009.05.009. URL http://dx.doi.org/10.1016/j.biopsych.2009.05.009.

Pj Gianaros. Regional cerebral blood flow correlates with heart period and high-frequency heart period variability during working-memory task. *Psychophysiology*, 41:521–530, 2004. doi: 10.1111/j.1469-8986.2004.00179.x. URL http://onlinelibrary.wiley.com/doi/10.1111/1469-8986.2004.00179.x/full.

F. Giffin, A. Greenough, and S. Naik. The Hering-Breuer reflex in ventilated children. *Respir. Med.*, 90(8):463–466, 1996. ISSN 09546111. doi: 10.1016/S0954-6111(96)90172-9.

M Gioia, G Tredici, and R Bianchi. A Golgi study of the periaqueductal gray matter in the cat. Neuronal types and their distribution. *Exp. brain Res.*, 1985.

P Glees, J Cole, C W M Whitty, and H Cairns. The effects of lesions in the cingular gyrus and adjacent areas in monkeys. *J. Neurol. Neurosurg. Psychiatry*, 13(3):178, 1950.

Yoann Gole, Ombeline Gargne, Mathieu Coulange, Jean-Guillaume Steinberg, Malika Bouhaddi, Yves Jammes, Jacques Regnard, and Alain Boussuges. Hyperoxia-induced alterations in cardiovascular function and autonomic control during return to normoxic breathing. *Eur J Appl Physiol*, 111(6):937–946, Jun 2011. ISSN 1439-6327 (Electronic); 1439-6319 (Linking). doi: 10.1007/s00421-010-1711-4.

F. Golla, S. a. Mann, and R. G. B. Marsh. Part III. The Respiratory Regulation in Psychotic Subjects. *Br. J. Psychiatry*, 74(306):443–453, 1928. ISSN 0007-1250. doi: 10.1192/bjp.74.306.443.

F. L. Golla and S. Antonovich. The respiratory rhythm in its relation to the mechanism of thought. *Brain*, 52(4):491–509, December 1929. ISSN 0006-8950. doi: 10.1093/brain/52.4.491. URL http://brain.oxfordjournals.org/cgi/doi/10.1093/brain/52.4.491.

Nandu Goswami, Helmut Karl Lackner, Ilona Papousek, Jean-Pierre Montani, Daniela Jezova, and Helmut G Hinghofer-Szalkay. Does mental arithmetic before head up tilt have an effect on the orthostatic cardiovascular and hormonal responses? *Acta Astronautica*, 68(9):1589–1594, 2011.

Beata Graff, Anna Szyndler, Krzysztof Czechowicz, Wies\lawa Wiesława Kucharska, Grzegorz Graff, Pierre Boutouyrie, Stephane Laurent, and Krzysztof Narkiewicz. Relationship between heart rate variability, blood pressure and arterial wall properties during air and oxygen breathing in healthy subjects. *Auton. Neurosci. Basic Clin.*, 178 (1–2):60–66, 2013. ISSN 15660702. doi: 10.1016/j.autneu.2013.04.009. URL http://www.sciencedirect.com/science/article/pii/S1566070213000957.

A.L. Green, S. Wang, R.G. Bittar, S.L.F. Owen, D.J. Paterson, J.F. Stein, P.G. Bain, D. Shlugman, and T.Z. Aziz. Deep brain stimulation: A new treatment for hypertension? *J. Clin. Neurosci.*, 14(6):592–595, June 2007a. ISSN 09675868. doi: 10.1016/j.jocn.2006.04.015. URL http://linkinghub.elsevier.com/retrieve/pii/S0967586806002876http://linkinghub.elsevier.com/retrieve/pii/S0967586806002864.

Alexander L Green and David J Paterson. Identification of neurocircuitry controlling cardiovascular function in humans using functional neurosurgery: implications for exercise control. *Exp. Physiol.*, 93(9):1022–1028, 2008. ISSN 0958-0670. doi: 10.1113/expphysiol.2007.039461.

Alexander L Green, Shouyan Wang, Sarah L F Owen, Kangning Xie, Xuguang Liu, David J Paterson, John F Stein, Peter G Bain, and Tipu Z Aziz. Deep brain stimulation can regulate arterial blood pressure in awake humans. *Neuroreport*, 16(16):1741–1745, 2005. ISSN 0959-4965. doi: 10.1097/01.wnr.0000183904.15773.47.

Alexander L. Green, Shouyan Wang, Sarah L F Owen, David J. Paterson, John F. Stein, and Tipu Z. Aziz. Controlling the heart via the brain: A potential new therapy for orthostatic hypotension. *Neurosurgery*, 58(6):1176–1182, 2006a. ISSN 0148396X. doi: 10.1227/01.NEU.0000215943.78685.01. URL http://eprints.soton.ac.uk/49595/.

Alexander L. Green, Shouyan Wang, Sarah L F Owen, David J. Paterson, Kangning Xie, Xuguang Liu, Peter G. Bain, John F. Stein, and Tipu Z. Aziz. Functional Neurosurgery Resident Award: controlling the cardiovascular system with deep brain stimulation. *Clin. Neurosurg.*, 53:316–323, 2006b. ISSN 00694827.

Alexander L. Green, Shouyan Wang, Sarah L F Owen, Kangning Xie, Richard G. Bittar, John F. Stein, David J. Paterson, and Tipu Z. Aziz. Stimulating the human midbrain to reveal the link between pain and blood pressure. *Pain*, 124(3):349–359, 2006c. ISSN 03043959. doi: 10.1016/j.pain.2006.05.005.

Alexander L Green, Shouyan Wang, Sarah Purvis, Sarah L F Owen, Peter G Bain, John F Stein, Abe Guz, Tipu Z Aziz, and David J Paterson. Identifying cardiorespiratory neurocircuitry involved in central command during exercise in humans. *J. Physiol.*, 578(Pt 2):605–612, 2007b. ISSN 0022-3751. doi: 10.1113/jphysiol.2006.122549.

Alexander L Green, Jonathan a Hyam, Charles Williams, Shouyan Wang, David Shlugman, John F Stein, David J Paterson, and Tipu Z Aziz. Intra-operative deep brain stimulation of the periaqueductal grey matter modulates blood pressure and heart rate variability in humans. *Neuromodulation*, 13(3):174–81, 2010. ISSN 1525-1403. doi: 10.1111/j.1525-1403.2010.00274.x. URL `http://www.ncbi.nlm.nih.gov/pubmed/21992829`.

Alexander L. Green, Ella Stone, Holly Sitsapesan, Benjamin W. Turney, John H. Coote, Tipu Z. Aziz, Jonny a. Hyam, and Thelma a. Lovick. Switching off micturition using deep brain stimulation at midbrain sites. *Ann. Neurol.*, 72(1):144–147, July 2012. ISSN 03645134. doi: 10.1002/ana.23571. URL `http://doi.wiley.com/10.1002/ana.23571`.

P G Guyenet. The sympathetic control of blood pressure. *Nat. Rev. Neurosci.*, 2006.

a. Guz. Brain, breathing and breathlessness. *Respir. Physiol.*, 109(3):197–204, September 1997. ISSN 00345687. doi: 10.1016/S0034-5687(97)00050-9. URL `http://linkinghub.elsevier.com/retrieve/pii/S0034568797000509`.

A Guz, M I M Noble, D Trenchard, and A J Smith. The Hering-Breuer inflation reflex in man: studies of unilateral lung inflation and vagus nerve block. *Respir. Physiol.*, 1966.

J S Haldane and J G Priestley. The regulation of the lung-ventilation. *J. Physiol.*, 32 (3-4):225–266, 1905. ISSN 0022-3751. doi: 10.1113/jphysiol.1905.sp001081.

Clement Hamani, Helen Mayberg, Brian Snyder, Peter Giacobbe, Sidney Kennedy, and Andres M Lozano. Deep brain stimulation of the subcallosal cingulate gyrus for depression: anatomical location of active contacts in clinical responders and a suggested guideline for targeting. *J. Neurosurg.*, 111(6):1209–1215, December 2009. ISSN 0022-3085. doi: 10.3171/2008.10.JNS08763. URL http://thejns.org/doi/abs/10.3171/2008.10.JNS08763.

B L Hamilton and F M Skultety. Efferent connections of the periaqueductal gray matter in the cat. *J. Comp. Neurol.*, 1970.

P Haouzi. Initiating inspiration outside the medulla does produce eupneic breathing. *J. Appl. Physiol.*, 2011.

Philippe Haouzi and Harold J Bell. Control of breathing and volitional respiratory rhythm in humans. *J. Appl. Physiol.*, 106(3):904–910, March 2009. ISSN 8750-7587. doi: 10.1152/japplphysiol.90675.2008. URL http://jap.physiology.org/cgi/doi/10.1152/japplphysiol.90675.2008.

Philippe Haouzi, Bruno Chenuel, and Gerard Barroche. Interactions between volitional and automatic breathing during respiratory apraxia. *Respir. Physiol. Neurobiol.*, 152 (2):169–175, 2006. ISSN 15699048. doi: 10.1016/j.resp.2005.08.004.

Kenneth D Harris and Alexander Thiele. Cortical state and attention. *Nat. Rev. Neurosci.*, 12(9):509–523, 2011. ISSN 1471-003X. doi: 10.1038/nrn3084. URL http://dx.doi.org/10.1038/nrn3084.

Luke A Henderson, Cheree James, and Vaughan G Macefield. Identification of sites of sympathetic outflow during concurrent recordings of sympathetic nerve activity and fMRI. *Anat Rec*, 295(9):1396–1403, September 2012. ISSN 1932-8494 (Electronic); 1932-8486 (Linking). doi: 10.1002/ar.22513.

P.McN. Hill. Hyperventilation, breath holding and alveolar oxygen tensions at the breaking point1. *Respir. Physiol.*, 19(2):201–209, November 1973. ISSN 00345687. doi: 10.1016/0034-5687(73)90078-9. URL http://linkinghub.elsevier.com/retrieve/pii/0034568773900789.

G Holstege and C B Saper. Special issue: The anatomy of the soul. *J. Comp. Neurol.*, 2005.

G. Holstege, L. Kerstens, M. C. Moes, and V. G J M Vanderhorst. Evidence for a periaqueductal gray-nucleus retroambiguus-spinal cord pathway in the rat. *Neuroscience*, 80 (2):587–598, 1997. ISSN 03064522. doi: 10.1016/S0306-4522(97)00061-4.

Gert G. Holstege, Leonora J. Mouton, and Nicolaas M. Gerrits. Emotional Motor System. *Hum. Nerv. Syst. Second Ed.*, pages 1306–1324, 2003. doi: 10.1016/B978-012547626-3/50037-5.

Ikuo Homma and Yuri Masaoka. Breathing rhythms and emotions. *Exp. Physiol.*, 93(9): 1011–1021, 2008. ISSN 0958-0670. doi: 10.1113/expphysiol.2008.042424.

Nicholas S Hopkinson, Tarek Sharshar, Ewen T Ross, Annabel H Nickol, Mark J Dayer, Raphaël Porcher, Sophie Jonville, John Moxham, and Michael I Polkey. Corticospinal control of respiratory muscles in chronic obstructive pulmonary disease. *Respir. Physiol. Neurobiol.*, 141(1):1–12, July 2004. ISSN 15699048. doi: 10.1016/j.resp.2004.04.003. URL http://linkinghub.elsevier.com/retrieve/pii/S1569904804000801.

Y Hosobuchi, J E Adams, and B Rutkin. Chronic thalamic stimulation for the control of facial anesthesia dolorosa. *Arch. Neurol.*, 29(3):158–161, 1973. ISSN 0003-9942. doi: 10.1001/archneur.1973.00490270040005.

Yoshio Hosobuchi, John E Adams, and Rita Linchitz. Pain Relief by Electrical Stimulation of the Central Gray Matter in Humans and Its Reversal by Naloxone. *Science (80-.).*, 197(4299):183–186, July 1977.

J C Hsieh, S Stone-Elander, and M Ingvar. Anticipatory coping of pain expressed in the human anterior cingulate cortex: a positron emission tomography study. *Neurosci. Lett.*, 262(1):61–64, 1999. ISSN 0304-3940.

Z G Huang, S H Subramanian, and R J Balnave. Roles of periaqueductal gray and nucleus tractus solitarius in cardiorespiratory function in the rat brainstem. *Respiration*, 2000.

Maggie Lee Huckabee, Lueder Deecke, Michael P. Cannito, Herbert J. Gould, and Wilfred Mayr. Cortical control mechanisms in volitional swallowing: The Bereitschaftspotential. *Brain Topogr.*, 16(1):3–17, 2003. ISSN 08960267. doi: 10.1023/A:1025671914949. URL `http://link.springer.com/10.1023/A:1025671914949`.

Jonathan A Hyam, Morten L Kringelbach, Peter A Silburn, Tipu Z Aziz, and Alexander L Green. The autonomic effects of deep brain stimulation–a therapeutic opportunity. *Nat Rev Neurol*, 8(7):391–400, July 2012. ISSN 1759-4766 (Electronic); 1759-4758 (Linking). doi: 10.1038/nrneurol.2012.100.

Yakolev P I and S Locke. Limbic nuclei of thalamus and connections of limbic cortex. III. Corticocortical connections of the anterior cingulate gyrus, the cingulum, and the subcallosal bundle in monkey. *Arch. Neurol.*, 5:364–400, 1961. ISSN 0003-9942. doi: 10.1001/archneur.1961.00450160014002.

E Izdebska, J Izdebski, I Cybulska, M Makowiecka-Ciesla, and A Trzebski. Moderate exercise training reduces arterial chemoreceptor reflex drive in mild hypertension. *J Physiol Pharmacol*, 57 Suppl 11:93–102, Nov 2006. ISSN 1899-1505 (Electronic); 0867-5910 (Linking).

W A Janczewski and J L Feldman. Distinct rhythm generators for inspiration and expiration in the juvenile rat. *J. Physiol.*, 2006.

O Jensen, R Hari, and K Kaila. Visually evoked gamma responses in the human brain are enhanced during voluntary hyperventilation. *Neuroimage*, 2002a.

Ole Jensen, Jack Gelfand, John Kounios, and John E Lisman. Oscillations in the Alpha Band (9–12 Hz) Increase with Memory Load during Retention in a Short-term Memory Task. *Cereb. Cortex*, 12(8):877–882, 2002b. doi: 10.1093/cercor/12.8.877. URL `http://cercor.oxfordjournals.org/content/12/8/877.abstract`.

E G Jones. Pattern of cortical and thalamic connexions of the somatic sensory cortex. *Nature*, 216(5116):704–705, 1967. ISSN 0028-0836. doi: 10.1038/216704a0.

E G Jones. Viewpoint: the core and matrix of thalamic organization. *Neuroscience*, 1998.

E.G. Jones and T.P.S. Powell. The cortical projection of the ventroposterior nucleus of the thalamus in the cat. *Brain Res.*, 13(2):298–318, April 1969. ISSN 00068993. doi: 10.1016/0006-8993(69)90289-3. URL http://linkinghub.elsevier.com/retrieve/pii/0006899369902893.

B R Kaada, K H Pribram, and J a Epstein. Respiratory and vascular responses in monkeys from temporal pole, insula, orbital surface and cingulate gyrus; a preliminary report. *J. Neurophysiol.*, 12(5):347–356, 1949. ISSN 0022-3077.

Birger R. Kaada. Respiratory Responses To Stimulation of Temporal Pole, Insula, and Hippocampal and Limbic Gyri in Man. *Arch. Neurol. Psychiatry*, 68(5):609, 1952. ISSN 0096-6754. doi: 10.1001/archneurpsyc.1952.02320230035004. URL http://archneurpsyc.jamanetwork.com/article.aspx?doi=10.1001/archneurpsyc.1952.02320230035004.

H. Kabat, Magoun H. W., and S. W. Ranson. Electrical Stimulation of Points in the Forebrain and Midbrain. *J. Nerv. Ment. Dis.*, 85(3):345, August 1935. ISSN 0022-3018. doi: 10.1001/archneurpsyc.1935.02250230003001. URL qap2.onlinelibrary.wiley.com/doi/10.1002/cne.900640202/references.

Herman Kabat. Electrical stimulation of points in the forebrain and mid-brain: The resultant alterations in respiration. *J. Comp. Neurol.*, 64(2):187–208, August 1936. ISSN 0021-9967. doi: 10.1002/cne.900640202. URL http://doi.wiley.com/10.1002/cne.900640202.

S T Kitai. *Electrophysiology of the Corpus Striatum and Brain Stem Integrating Systems*. John Wiley & Sons, Inc., 2011. ISBN 9780470650714. doi: 10.1002/cphy.cp010220. URL http://dx.doi.org/10.1002/cphy.cp010220.

Antti M. Kiviniemi, Toni Breskovic, Lovro Uglesic, Benjamin Kuch, Petra Zubin Maslov, Arne Sieber, Tapio Seppänen, Mikko P. Tulppo, and Zeljko Dujic. Heart rate variability during static and dynamic breath-hold dives in elite divers. *Auton. Neurosci. Basic Clin.*, 169(2):95–101, 2012. ISSN 15660702. doi: 10.1016/j.autneu.2012.05.004. URL http://dx.doi.org/10.1016/j.autneu.2012.05.004.

D F Klein. False suffocation alarms, spontaneous panics, and related conditions: an integrative hypothesis. *Arch. Gen. Psychiatry*, 1993.

W Klimesch. EEG alpha and theta oscillations reflect cognitive and memory performance: a review and analysis. *Brain Res. Brain Res. Rev.*, 29(2-3):169–195, 1999. ISSN 01650173. doi: 10.1016/S0165-0173(98)00056-3.

Morten L. Kringelbach, Alexander L. Green, Sarah L F Owen, Patrick M. Schweder, and Tipu Z. Aziz. Sing the mind electric - principles of deep brain stimulation. *Eur. J. Neurosci.*, 32(7):1070–1079, 2010. ISSN 0953816X. doi: 10.1111/j.1460-9568.2010.07419.x.

A Krogh and J Lindhard. The regulation of respiration and circulation during the initial stages of muscular work. *J. Physiol.*, 47(1-2):112–136, October 1913. ISSN 00223751. doi: 10.1113/jphysiol.1913.sp001616. URL `http://doi.wiley.com/10.1113/jphysiol.1913.sp001616`.

Rajesh Kumar, Paul M. Macey, Mary a. Woo, Jeffry R. Alger, Thomas G. Keens, and Ronald M. Harper. Neuroanatomic deficits in congenital central hypoventilation syndrome. *J. Comp. Neurol.*, 487(4):361–371, 2005. ISSN 00219967. doi: 10.1002/cne.20565.

Takeshi Kuroda, Yuri Masaoka, Hideyo Kasai, Kengo Noguchi, Mitsuru Kawamura, and Ikuo Homma. Sharing breathlessness: Investigating respiratory change during observation of breath-holding in another. *Respir. Physiol. Neurobiol.*, 180(2-3):218–222, 2012. ISSN 15699048. doi: 10.1016/j.resp.2011.11.010. URL `http://dx.doi.org/10.1016/j.resp.2011.11.010`.

D LaBerge, L Auclair, and E Sieroff. Preparatory attention: experiment and theory. *Conscious. Cogn.*, 9(3):396–434, 2000. ISSN 1053-8100. doi: 10.1006/ccog.1999.0429.

David LaBerge. Thalamic and Cortical Mechanisms of Attention Suggested by Recent Positron Emission Tomographic Experiments. *J. Cogn. Neurosci.*, 2(4):358–372, 1990. ISSN 0898-929X. doi: 10.1162/jocn.1990.2.4.358.

David LaBerge. Attention, consciousness, and electrical wave activity within the cortical column. *Int. J. Psychophysiol.*, 43(1):5–24, 2001. ISSN 01678760. doi: 10.1016/S0167-8760(01)00176-3.

David LaBerge. Attentional control: Brief and prolonged. *Psychol. Res.*, 66(4):220–233, 2002. ISSN 03400727. doi: 10.1007/s00426-002-0097-2.

David Laberge and Vincent Brown. Theory of attentional operations in shape identification. *Psychol. Rev.*, page 124, 1989.

David L Laberge. Attention. *Psychol. Sci.*, 1(3):156–162, May 1990.

L K Laemle. Neuronal populations of the human periaqueductal gray, nucleus lateralis. *J Comp Neurol*, 186(1):93–107, July 1979. doi: 10.1002/cne.901860107.

Richard D Lane, Eric M Reiman, Beatrice Axelrod, Lang-Sheng Yun, Andrew Holmes, and Gary E Schwartz. Neural Correlates of Levels of Emotional Awareness: Evidence of an Interaction between Emotion and Attention in the Anterior Cingulate Cortex. *J. Cogn. Neurosci.*, 10(4):525–535, July 1998. ISSN 0898-929X. doi: 10.1162/089892998562924. URL http://www.mitpressjournals.org/doi/abs/10.1162/089892998562924.

Richard D. Lane, Kateri McRae, Eric M. Reiman, Kewei Chen, Geoffrey L. Ahern, and Julian F. Thayer. Neural correlates of heart rate variability during emotion. *Neuroimage*, 44(1):213–222, 2009. ISSN 10538119. doi: http://dx.doi.org/10.1016/j.neuroimage.2008.07.056. URL http://www.sciencedirect.com/science/article/pii/S1053811908008926http://dx.doi.org/10.1016/j.neuroimage.2008.07.056.

D Laplane, J.D. Degos, M Baulac, and F Gray. Bilateral infarction of the anterior cingulate gyri and of the fornices. *J. Neurol. Sci.*, 51(2):289–300, August 1981. ISSN 0022510X. doi: 10.1016/0022-510X(81)90107-6. URL http://linkinghub.elsevier.com/retrieve/pii/0022510X81901076.

Anna Maria Lavezzi, Giulia Ottaviani, Lino Rossi, and Luigi Matturri. Cytoarchitectural organization of the parabrachial/Kölliker-Fuse complex in man. *Brain Dev.*, 26(5):316–320, 2004. ISSN 03877604. doi: 10.1016/j.braindev.2003.09.002.

F a Lenz, M Rios, a Zirh, D Chau, G Krauss, and R P Lesser. Painful stimuli evoke potentials recorded over the human anterior cingulate gyrus. *J. Neurophysiol.*, 79(4): 2231–2234, 1998. ISSN 0022-3077.

Mei-Kei Kei Leung, Chetwyn C H Chan, Jing Yin, Chack-Fan Fan Lee, Kwok-Fai Fai So, and Tatia M C Lee. Increased gray matter volume in the right angular and posterior parahippocampal gyri in loving-kindness meditators. *Soc. Cogn. Affect. Neurosci.*, 8 (1):34–39, January 2013. ISSN 1749-5024 (Electronic); 1749-5016 (Linking). doi: 10.1093/scan/nss076.

Wan Li, Els Daems, Karel P. Van de Woestijne, Ilse Van Diest, Jorge Gallego, Steven De Peuter, Katleen Bogaerts, and Omer Van den Bergh. Air hunger and ventilation in response to hypercapnia: Effects of repetition and anxiety. *Physiol. Behav.*, 88(1-2): 47–54, 2006. ISSN 00319384. doi: 10.1016/j.physbeh.2006.03.001.

J Lindhard. On the excitability of the respiratory centre. *J. Physiol.*, 42(4):337–358, May 1911. ISSN 00223751. doi: 10.1113/jphysiol.1911.sp001439. URL `http://doi.wiley.com/10.1113/jphysiol.1911.sp001439`.

Rodolfo R. Llinás. Electrophysiology of the Cerebellar Networks. In *Compr. Physiol.*, number 17, pages 376–831. John Wiley & Sons, Inc., Hoboken, NJ, USA, January 2011. ISBN 9780470650714. doi: 10.1002/cphy.cp010217. URL `http://doi.wiley.com/10.1002/cphy.cp010217`.

Luana T. Lopes, Luis G a Patrone, Kênia C. Bícego, Norberto C. Coimbra, and Luciane H. Gargaglioni. Periaqueductal gray matter modulates the hypercapnic ventilatory response. *Pflugers Arch. Eur. J. Physiol.*, 464(2):155–166, 2012. ISSN 00316768. doi: 10.1007/s00424-012-1119-6.

T. M J Loucks, Christopher J. Poletto, Kristina Simonyan, Catherine L. Reynolds, and Christy L. Ludlow. Human brain activation during phonation and exhalation: Common volitional control for two upper airway functions. *Neuroimage*, 36(1):131–143, 2007. ISSN 10538119. doi: 10.1016/j.neuroimage.2007.01.049.

G Macefield and S C Gandevia. The cortical drive to human respiratory muscles in the awake state assessed by premotor cerebral potentials. *J. Physiol.*, 439(1):545–558, July 1991. ISSN 00223751. doi: 10.1113/jphysiol.1991.sp018681. URL http://doi.wiley.com/10.1113/jphysiol.1991.sp018681.

V G Macefield, S C Gandevia, and L a Henderson. Neural sites involved in the sustained increase in muscle sympathetic nerve activity induced by inspiratory capacity apnea: a fMRI study. *J. Appl. Physiol.*, 100(1):266–273, January 2006. ISSN 8750-7587. doi: 10.1152/japplphysiol.00588.2005.

P. M. Macey, K. E. Macey, L. a. Henderson, J. R. Alger, R. C. Frysinger, M. a. Woo, F. Yan-Go, and R. M. Harper. Functional magnetic resonance imaging responses to expiratory loading in obstructive sleep apnea. *Respir. Physiol. Neurobiol.*, 138(2-3):275–290, 2003. ISSN 15699048. doi: 10.1016/j.resp.2003.09.002.

P M Macey, M a Woo, K E Macey, T G Keens, M M Saeed, J R Alger, and R M Harper. Hypoxia reveals posterior thalamic, cerebellar, midbrain, and limbic deficits in congenital central hypoventilation syndrome. *J. Appl. Physiol.*, 98(3):958–969, 2005. ISSN 8750-7587. doi: 10.1152/japplphysiol.00969.2004.

Paul M. Macey, Mary a. Woo, and Ronald M. Harper. Hyperoxic brain effects are normalized by addition of CO2. *PLoS Med.*, 4(5):0828–0835, 2007. ISSN 15491277. doi: 10.1371/journal.pmed.0040173.

P D Maclean. The limbic system (visceral brain) in relation to central gray and reticulum of the brain stem; evidence of interdependence in emotional processes. *Psychosom. Med.*, 17(5):355–366, 1955a. ISSN 0033-3174.

P D Maclean. The limbic system ("visceral brain") and emotional behavior. *A. M. A. Arch. Neurol. psychiatry*, 73(2):130–134, 1955b. ISSN 0096-6886.

P D MacLean. Brain evolution relating to family, play, and the separation call. *Arch. Gen. Psychiatry*, 42(4):405–417, 1985a. ISSN 0003-990X. doi: 10.1001/archpsyc.1985.01790270095011.

P D MacLean. Evolutionary psychiatry and the triune brain. *Psychol. Med.*, 15(2):219–221, 1985b. ISSN 0033-2917. doi: 10.1017/S0033291700023485.

P D MacLean and J D Newman. Role of midline frontolimbic cortex in production of the isolation call of squirrel monkeys. *Brain Res.*, 450(1-2):111–123, 1988. ISSN 00068993. doi: 10.1016/0006-8993(88)91550-8.

Patrick W Mantyh. The ascending input to the midbrain periaqueductal gray of the primate. *J. Comp. Neurol.*, 211(1):50–64, October 1982. ISSN 0021-9967. doi: 10.1002/cne.902110106. URL `http://doi.wiley.com/10.1002/cne.902110106`.

Y Masaoka and I Homma. Anxiety and respiratory patterns: their relationship during mental stress and physical load. *Int. J. Psychophysiol.*, 1997.

Yuri Masaoka and Ikuo Homma. The effect of anticipatory anxiety on breathing and metabolism in humans. *Respir. Physiol.*, 128(2):171–177, 2001. ISSN 00345687. doi: 10.1016/S0034-5687(01)00278-X.

D Maskill, K Murphy, A Mier, M Owen, and A Guz. Motor cortical representation of the diaphragm in man. *J. Physiol.*, 443(1991):105–121, 1991. ISSN 0022-3751.

D A McCormick and T Bal. Sensory gating mechanisms of the thalamus. *Curr. Opin. Neurobiol.*, 1994.

Donald R. McCrimmon, Gordon S. Mitchell, and George F. Alheid. Overview: The neurochemistry of respiratory control. *Respir. Physiol. Neurobiol.*, 164(1-2):1–2, December 2008. ISSN 15699048. doi: 10.1016/j.resp.2008.07.021. URL `http://linkinghub.elsevier.com/retrieve/pii/S1569904808002115`.

L C McKay, K C Evans, R S J Frackowiak, and D R Corfield. Neural correlates of voluntary breathing in humans. *J. Appl. Physiol.*, 95(3):1170–1178, 2003. ISSN 8750-7587. doi: 10.1152/japplphysiol.00641.2002.

L C McKay, H D Critchley, K Murphy, and R S J Frackowiak. Sub-cortical and brainstem sites associated with chemo-stimulated increases in ventilation in humans. *Neuroimage*, 2010.

S Meyer, M Strittmatter, C Fischer, T Georg, and B Schmitz. Lateralization in autonomic dysfunction in ischemic stroke involving the insular cortex. *Neuroreport*, 15(2):357–361, Feb 2004. ISSN 0959-4965 (Print); 0959-4965 (Linking).

Soren Moller, Jens S Iversen, Aleksander Krag, Peter Bie, Andreas Kjaer, and Flemming Bendtsen. Reduced baroreflex sensitivity and pulmonary dysfunction in alcoholic cirrhosis: effect of hyperoxia. *Am J Physiol Gastrointest Liver Physiol*, 299(3):G784–90, Sep 2010. ISSN 1522-1547 (Electronic); 0193-1857 (Linking). doi: 10.1152/ajpgi.00078.2010.

Donna L Mongeluzi, Robert a Rosellini, Ronald Ley, Barbara J Caldarone, and Howard S Stock. The conditioning of dyspneic suffocation fear. Effects of carbon dioxide concentration on behavioral freezing and analgesia. *Behav. Modif.*, 27(5):620–636, 2003. ISSN 01454455. doi: 10.1177/0145445503256316.

Nicola Montano, Chiara Cogliati, V. J. Dias Da Silva, Tomaso Gnecchi-Ruscone, and Alberto Malliani. Sympathetic rhythms and cardiovascular oscillations. In *Auton. Neurosci. Basic Clin.*, volume 90, pages 29–34, 2001. ISBN 1-2. doi: 10.1016/S1566-0702(01)00264-8. URL `http://www.sciencedirect.com/science/article/pii/S1566070201002648`.

K Murphy, Anne Mier, L Adams, and A Guz. Putative cerebral cortical involvement in the ventilatory response to inhaled CO2 in conscious man. *J. Physiol.*, 420(1):1–18, January 1990. ISSN 00223751. doi: 10.1113/jphysiol.1990.sp017898. URL `http://doi.wiley.com/10.1113/jphysiol.1990.sp017898`.

K Murphy, D R Corfield, a Guz, G R Fink, R J Wise, J Harrison, and L Adams. Cerebral areas associated with motor control of speech in humans. *J. Appl. Physiol.*, 83(5):1438–1447, 1997. ISSN 8750-7587.

S Murtha, H Chertkow, M Beauregard, R Dixon, and a Evans. Anticipation causes increased blood flow to the anterior cingulate cortex. *Hum. Brain Mapp.*, 4(2):103–112, 1996. ISSN 1065-9471. doi: 10.1002/(SICI)1097-0193(1996)4:2<103::AID-HBM2>3.0.CO;2-7.

Michiaki Nagai, Satoshi Hoshide, and Kazuomi Kario. The insular cortex and cardiovascular system: a new insight into the brain-heart axis. *J Am Soc Hypertens*, 4(4):174–182, Jul-Aug 2010. ISSN 1933-1711 (Print); 1878-7436 (Linking). doi: 10.1016/j.jash.2010.05.001.

Hideaki Nakayama, Curtis a. Smith, Joshua R. Rodman, James B. Skatrud, and Jerome a. Dempsey. Effect of ventilatory drive on carbon dioxide sensitivity below eupnea during sleep. *Am. J. Respir. Crit. Care Med.*, 165(9):1251–1259, 2002. ISSN 1073449X. doi: 10.1164/rccm.2110041.

S M Oppenheimer, G Kedem, and W M Martin. Left-insular cortex lesions perturb cardiac autonomic tone in humans. *Clin Auton Res*, 6(3):131–140, Jun 1996. ISSN 0959-9851 (Print); 0959-9851 (Linking).

D. N. Pandya, G. W. Van Hoesen, and M. M. Mesulam. Efferent connections of the cingulate gyrus in the rhesus monkey. *Exp. Brain Res.*, 42(3-4):319–330, 1981. ISSN 00144819. doi: 10.1007/BF00237497.

J W Papez. The brain considered as an organ: Neural systems and central levels of organization. *J. Nerv. Ment. Dis.*, 1937.

José V Pardo, Patricia J Pardo, Kevin W Janer, and Marcus E Raichle. The anterior cingulate cortex mediates processing selection in the Stroop attentional conflict paradigm. *Proc. Natl. Acad. Sci.*, 87(1):256–259, 1990.

J.V. V Pardo, P.T. T Fox, and M.E. E Raichle. Localization of a human system for sustained attention by positron emission tomography. *Nature*, 349 (6304):61–64, 1991. ISSN 0028-0836. doi: 10.1038/349061a0. URL `http://www.ncbi.nlm.nih.gov/pubmed/1985266$\delimiter"026E30F$nhttp://www.nature.com/nature/journal/v349/n6304/abs/349061a0.html`.

M J Parkes. Breath-holding and its breakpoint. *Exp. Physiol.*, 2006.

M J Parkes. The limits of breath holding. *Sci. Am.*, 2012.

Josef Parvizi, Vinitha Rangarajan, William R. Shirer, Nikita Desai, and Michael D. Greicius. The will to persevere induced by electrical stimulation of the human cingulate gyrus. *Neuron*, 80(6):1359–1367, 2013. ISSN 10974199. doi: 10.1016/j.neuron.2013.10.057. URL `http://dx.doi.org/10.1016/j.neuron.2013.10.057`.

K T S Pattinson, G D Mitsis, A K Harvey, and S Jbabdi. Determination of the human brainstem respiratory control network and its cortical connections in vivo using functional and structural imaging. *Neuroimage*, 2009a.

Kyle T S Pattinson, Ricardo J Governo, Bradley J MacIntosh, Elizabeth C Russell, Douglas R Corfield, Irene Tracey, and Richard G Wise. Opioids depress cortical centers responsible for the volitional control of respiration. *J. Neurosci.*, 29(25):8177–8186, 2009b. ISSN 0270-6474. doi: 10.1523/JNEUROSCI.1375-09.2009.

T Paus. Primate anterior cingulate cortex: where motor control, drive and cognition interface. *Nat. Rev. Neurosci.*, 2(6):417–424, 2001. ISSN 14710048. doi: 10.1038/35077500.

T Paus, M Petrides, a C Evans, and E Meyer. Role of the human anterior cingulate cortex in the control of oculomotor, manual, and speech responses: a positron emission tomography study. *J. Neurophysiol.*, 70(2):453–469, 1993. ISSN 0022-3077.

Tomáš Paus, Lisa Koski, Zografos Caramanos, and Chris Westbury. Regional differences in the effects of task difficulty and motor output on blood flow response in the human anterior cingulate cortex: A review of 107 PET activation., 1998. ISSN 0959-4965. URL `http://journals.lww.com/neuroreport/Abstract/1998/06220/Regional_differences_in_the_effects_of_task.1.aspx`.

W Penfield. Ferrier Lecture : Some Observations on the Cerebral Cortex of Man Author. *Proc. R. Soc. London. Ser. B, Biol. Sci.*, 134(876):329–347, 1947.

J S Perlmutter and J W Mink. Deep brain stimulation. *Annu. Rev. Neurosci.*, 2006.

D W Perry, R J Zatorre, M Petrides, and B Alivisatos. Localization of cerebral activity during simple singing. *Cephalalgia*, 1999.

Michele Pignatelli, Anna Beyeler, and Xavier Leinekugel. Neural circuits underlying the generation of theta oscillations. *J. Physiol.*, 106(3):81–92, 2012. ISSN 09284257. doi: 10.1016/j.jphysparis.2011.09.007. URL `http://dx.doi.org/10.1016/j.jphysparis.2011.09.007`.

Paul M Pilowsky. Every breath you take: why sympathetic nerve activity comes in bursts. *J. Physiol.*, 587(Pt 2):297, 2009. ISSN 1469-7793. doi: 10.1113/jphysiol.2008.167205.

Chris Pitsikoulis, Matthew N. Bartels, Gregory Gates, Rebecca a. Rebmann, Aimee M. Layton, and Ronald E. De Meersman. Sympathetic drive is modulated by central chemoreceptor activation. *Respir. Physiol. Neurobiol.*, 164(3):373–379, 2008. ISSN 15699048. doi: 10.1016/j.resp.2008.08.010.

J L Pool and J Ransohoff. Autonomic effects on stimulating rostral portion of cingulate gyri in man. *J. Neurophysiol.*, 12(6):385–392, 1949. ISSN 0022-3077.

Daniela Popa, Maria Spolidoro, Rémi D Proville, Nicolas Guyon, Lucile Belliveau, and Clément Léna. Functional role of the cerebellum in gamma-band synchronization of the sensory and motor cortices. *J. Neurosci.*, 33(15):6552–6, April 2013. ISSN 1529-2401. doi: 10.1523/JNEUROSCI.5521-12.2013. URL `http://www.ncbi.nlm.nih.gov/pubmed/23575852`.

M I Posner. Seeing the mind. *Science*, 262(5134):673–674, October 1993. ISSN 0036-8075. doi: 10.1126/science.8235585.

M I Posner, M K Rothbart, B E Sheese, and Y Tang. The anterior cingulate gyrus and the mechanism of self-regulation. *Cognitive*, 2007.

J F A Poulet and C C H Petersen. Internal brain state regulates membrane potential synchrony in barrel cortex of behaving mice. *Nature*, 454(7206):881–885, 2008.

M Poyhonen, S Syvaoja, J Hartikainen, E Ruokonen, and J Takala. The effect of carbon dioxide, respiratory rate and tidal volume on human heart rate variability. *Acta Anaesthesiol Scand*, 48(1):93–101, Jan 2004. ISSN 0001-5172 (Print); 0001-5172 (Linking).

K H Pribram and P D Maclean. Neuronographic analysis of medial and basal cerebral cortex. II. Monkey. *J. Neurophysiol.*, 16(3):324–340, 1953. ISSN 0022-3077.

J Pujol, A López, J Deus, N Cardoner, and J Vallejo. Anatomical variability of the anterior cingulate gyrus and basic dimensions of human personality. *Neuroimage*, 2002.

Jordan S Querido, Paul M Kennedy, and A William Sheel. Hyperoxia attenuates muscle sympathetic nerve activity following isocapnic hypoxia in humans. *J Appl Physiol (1985)*, 108(4):906–912, Apr 2010. ISSN 1522-1601 (Electronic); 0161-7567 (Linking). doi: 10.1152/japplphysiol.01228.2009.

S. W. Ranson. Respiratory and Pupillary Reactions. *Arch. Neurol. Psychiatry*, 29(6):1179, June 1933. ISSN 0096-6754. doi: 10.1001/archneurpsyc.1933.02240120002001. URL http://archneurpsyc.jamanetwork.com/article.aspx?doi=10.1001/archneurpsyc.1933.02240120002001.

Y Rassovsky, K Abrams, and M G Kushner. Suffocation and respiratory responses to carbon dioxide and breath holding challenges in individuals with panic disorder. *J. Psychosom. Res.*, 2006.

D V Reynolds. Surgery in the rat during electrical analgesia induced by focal brain stimulation. *Science (80-.).*, 1969.

J L Rhudy and M W Meagher. Fear and anxiety: divergent effects on human pain thresholds. *Pain*, 2000.

D E Richardson and H Akil. Pain reduction by electrical brain stimulation in man. Part 2: Chronic self-administration in the periventricular gray matter. *J. Neurosurg.*, 47(2): 184–194, 1977. ISSN 0022-3085. doi: 10.3171/jns.1977.47.2.0184.

D W Richter. Generation and maintenance of the respiratory rhythm. *J. Exp. Biol.*, 100 (1):93–107, 1982. ISSN 0022-0949. URL http://jeb.biologists.org/content/100/1/93.abstract.

Diethelm W Richter and Jeffrey C Smith. Respiratory rhythm generation in vivo. *Physiol.*, 29(1):58–71, January 2014. ISSN 1548-9221 (Electronic); 1548-9221 (Linking). doi: 10.1152/physiol.00035.2013.

F G Schimitel, G M de Almeida, D N Pitol, and R S Armini. Evidence of a suffocation alarm system within the periaqueductal gray matter of the rat. *Neuroscience*, 2012.

Marc F Schmidt, Judith McLean, and Franz Goller. Breathing and vocal control: the respiratory system as both a driver and a target of telencephalic vocal motor circuits in songbirds. *Exp. Physiol.*, 97(4):455–461, April 2012. ISSN 09580670. doi: 10.1113/expphysiol.2011.058669. URL `http://www.pubmedcentral.nih.gov/articlerender.fcgi?artid=3332150&tool=pmcentrez&rendertype=abstracthttp://doi.wiley.com/10.1113/expphysiol.2011.058669`.

E C Schneider. Observations on holding the breath. *Am. J. Physiol. {...}*, 1930.

Daniela Schön, Michael Rosenkranz, Jan Regelsberger, Bernhard Dahme, Christian Büchel, and Andreas Von Leupoldt. Reduced perception of dyspnea and pain after right insular cortex lesions. *Am. J. Respir. Crit. Care Med.*, 178(11):1173–1179, 2008. ISSN 1073449X. doi: 10.1164/rccm.200805-731OC.

G M Schulz, M Varga, K Jeffires, C L Ludlow, and a R Braun. Functional neuroanatomy of human vocalization: an H215O PET study. *Cereb. Cortex*, 15(12):1835–1847, 2005. ISSN 1047-3211. doi: 10.1093/cercor/bhi061.

Tarek Sharshar, Ewen Ross, Nicholas S Hopkinson, Mark Dayer, Annabel Nickol, Frederic Lofaso, John Moxham, Thomas Similowski, and Michael I Polkey. Effect of voluntary facilitation on the diaphragmatic response to transcranial magnetic stimulation. *J. Appl. Physiol.*, 95(1):26–34, 2003. ISSN 8750-7587. doi: 10.1152/japplphysiol.00918.2002.

S a Shea. Behavioural and arousal-related influences on breathing in humans. *Exp. Physiol.*, 81(1):1–26, 1996. ISSN 0958-0670. doi: VL-81.

S A Shea, J Walter, C Pelley, K Murphy, and A Guz. The effect of visual and auditory stimuli upon resting ventilation in man. *Respir. Physiol.*, 1987.

Shigeki Shibata, Ken-Ichi Iwasaki, Yojiro Ogawa, Jitsu Kato, and Setsuro Ogawa. Cardiovascular neuroregulation during acute exposure to 40, 70, and 100% oxygen at sea level. *Aviat Space Environ Med*, 76(12):1105–1110, Dec 2005. ISSN 0095-6562 (Print); 0095-6562 (Linking).

M M Shoja, R S Tubbs, M Jamshidi, G Shokouhi, and K Ansarin. Lateralization of the respiratory control following unilateral cerebral ischemia-reperfusion injury. *Respir Physiol Neurobiol*, 160(2):204–207, 2008. ISSN 1569-9048. doi: 10.1016/j.resp.2007.09.014. URL http://www.ncbi.nlm.nih.gov/pubmed/17981519.

R W Sikes and B a Vogt. Nociceptive neurons in area 24 of rabbit cingulate cortex. *J. Neurophysiol.*, 68(5):1720–1732, November 1992. ISSN 0022-3077.

Maciej Sinski, Jacek Lewandowski, Jacek Przybylski, Joanna Bidiuk, Piotr Abramczyk, Agnieszka Ciarka, and Zbigniew Gaciong. Tonic activity of carotid body chemoreceptors contributes to the increased sympathetic drive in essential hypertension. *Hypertens Res*, 35(5):487–491, May 2012. ISSN 1348-4214 (Electronic); 0916-9636 (Linking). doi: 10.1038/hr.2011.209.

Maciej Sinski, Jacek Lewandowski, Jacek Przybylski, Pawel Zalewski, Bartosz Symonides, Piotr Abramczyk, and Zbigniew Gaciong. Deactivation of carotid body chemoreceptors by hyperoxia decreases blood pressure in hypertensive patients. *Hypertens Res*, 37 (9):858–862, Sep 2014. ISSN 1348-4214 (Electronic); 0916-9636 (Linking). doi: 10.1038/hr.2014.91.

R.P. Sloan, J.B. Korten, and M.M. Myers. Components of heart rate reactivity during mental arithmetic with and without speaking. *Physiology Behavior*, 50(5):1039 – 1045, 1991. ISSN 0031-9384. doi: http://dx.doi.org/10.1016/0031-9384(91)90434-P. URL http://www.sciencedirect.com/science/article/pii/003193849190434P.

Wilbur K Smith. the Representation of Respiratory Movements in the Cerebral Cortex. *J Neurophysiol*, 1(1):55–68, 1938. URL http://jn.physiology.org.

Wilbur K. Smith. The functional significance of the rostral cingular cortex as revealed by its responses to electrical excitation. *J. Neurophysiol.*, 8(4):241, 1945. URL http://jn.physiology.org/cgi/reprint/8/4/241.pdf.

W.K. Smith. Vocalization and other responses elicited by excitation of the regio cingularis in the monkey. *Amer. J. Physiol*, 133:451–452, 1941.

Nelson Spruston. Pyramidal neurons: dendritic structure and synaptic integration. *Nat. Rev. Neurosci.*, 9(3):206–221, March 2008. ISSN 1471-003X. doi: 10.1038/nrn2286. URL `http://www.nature.com/doifinder/10.1038/nrn2286`.

M Steriade. Synchronized activities of coupled oscillators in the cerebral cortex and thalamus at different levels of vigilance. *Cereb. Cortex*, 7(6):583–604, September 1997.

M Steriade and D Contreras. Relations between cortical and thalamic cellular events during transition from sleep patterns to paroxysmal activity. *J. Neurosci.*, 1995.

M. Steriade and M. Deschenes. The thalamus as a neuronal oscillator. *Brain Res. Rev.*, 8 (1):1–63, 1984. ISSN 01650173. doi: 10.1016/0165-0173(84)90017-1.

M Steriade, D Contreras, R Curró Dossi, and a Nuñez. The slow (< 1 Hz) oscillation in reticular thalamic and thalamocortical neurons: scenario of sleep rhythm generation in interacting thalamic and neocortical networks. *J. Neurosci.*, 13(8):3284–3299, August 1993a. ISSN 0270-6474.

M Steriade, D A McCormick, and T J Sejnowski. Thalamocortical oscillations in the sleeping and aroused brain. *Science (80-.).*, 262(5134):679–685, October 1993b.

M Steriade, A Nuñez, and F Amzica. Intracellular analysis of relations between the slow (< 1 Hz) neocortical oscillation and other sleep rhythms of the electroencephalogram. *J Neurosci*, 13(8):3266–3283, August 1993c.

M Steriade, D Contreras, F Amzica, and I Timofeev. Synchronization of fast (30-40 Hz) spontaneous oscillations in intrathalamic and thalamocortical networks. *J. Neurosci.*, 16(8):2788–2808, 1996. ISSN 0270-6474.

Mircea Steriade and Igor Timofeev. Neuronal plasticity in thalamocortical networks during sleep and waking oscillations. *Neuron*, 37(4):563–576, 2003. ISSN 08966273. doi: 10.1016/S0896-6273(03)00065-5.

C Straus, C Locher, M Zelter, J P Derenne, and T Similowski. Facilitation of the diaphragm response to transcranial magnetic stimulation by increases in human respiratory drive. *J Appl Physiol*, 97(3):902–912, September 2004.

Hari H Subramanian. Descending control of the respiratory neuronal network by the midbrain periaqueductal grey in the rat in vivo. *J. Physiol.*, 591(1):109–122, January 2013. ISSN 00223751. doi: 10.1113/jphysiol.2012.245217. URL http://doi.wiley.com/10.1113/jphysiol.2012.245217.

Hari H Subramanian and Gert Holstege. Midbrain and medullary control of postinspiratory activity of the crural and costal diaphragm in vivo. *J. Neurophysiol.*, 105 (6):2852–2862, June 2011. ISSN 0022-3077. doi: 10.1152/jn.00168.2011. URL http://jn.physiology.org/cgi/doi/10.1152/jn.00168.2011.

Hari H Subramanian, Ron J Balnave, and Gert Holstege. The midbrain periaqueductal gray control of respiration. *J. Neurosci.*, 28(47):12274–12283, 2008. ISSN 0270-6474. doi: 10.1523/JNEUROSCI.4168-08.2008.

D Sutton, C Larson, and R C Lindeman. Neocortical and limbic lesion effects on primate phonation. *Brain Res.*, 71(1):61–75, May 1974. ISSN 00068993. doi: 10.1016/0006-8993(74)90191-7.

Yrsa B Sverrisdottir, Alexander L Green, Tipu Z Aziz, Nor Faizal A Bahuri, Jonathan Hyam, Shanika D Basnayake, and David J Paterson. Differentiated baroreflex modulation of sympathetic nerve activity during deep brain stimulation in humans. *Hypertension*, 63 (5):1000–1010, May 2014. ISSN 1524-4563 (Electronic); 0194-911X (Linking). doi: 10.1161/HYPERTENSIONAHA.113.02970.

Juan Sztajzel. Heart rate variability: A noninvasive electrocardiographic method to measure the autonomic nervous system. *Swiss Med. Wkly.*, 134(35-36):514–522, 2004. ISSN 14247860. doi: 2004/35/smw-10321.

J Talairach, J Bancaud, S Geier, M Bordas-Ferrer, a Bonis, G Szikla, and M Rusu. The cingulate gyrus and human behaviour. *Electroencephalogr. Clin. Neurophysiol.*, 34(1): 45–52, 1973. ISSN 00134694. doi: 10.1016/0013-4694(73)90149-1.

Michael H Thaut. Entrainment and the Motor System. *Music Ther. Perspect.*, 31(1): 31–34, 2013. doi: 10.1093/mtp/31.1.31. URL http://mtp.oxfordjournals.org/content/31/1/31.abstract.

I. Tracey. Imaging pain. *Br. J. Anaesth.*, 101(1):32–39, 2008. ISSN 00070912. doi: 10.1093/bja/aen102.

G. Tredici, R. Bianchi, and M. Gioia. Short intrinsic circuit in the periaqueductal gray matter of the cat. *Neurosci. Lett.*, 39(2):131–136, 1983. ISSN 03043940. doi: 10.1016/0304-3940(83)90065-4.

G. W. Van Hoesen. The modern concept of association cortex. *Curr. Opin. Neurobiol.*, 3 (2):150–154, 1993. ISSN 09594388. doi: 10.1016/0959-4388(93)90202-A.

B. Vogt, D. Rosene, and D. Pandya. Thalamic and cortical afferents differentiate anterior from posterior cingulate cortex in the monkey. *Science (80-.).*, 204(4389):205–207, April 1979. ISSN 0036-8075. doi: 10.1126/science.107587. URL `http://www.sciencemag.org/cgi/doi/10.1126/science.107587`.

B A Vogt, D M Finch, and C R Olson. Functional heterogeneity in cingulate cortex: the anterior executive and posterior evaluative regions. *Cereb. Cortex*, 1992.

B. a. Vogt, E. a. Nimchinsky, L. J. Vogt, and P. R. Hof. Human cingulate cortex: Surface features, flat maps, and cytoarchitecture. *J. Comp. Neurol.*, 359(3):490–506, 1995. ISSN 00219967. doi: 10.1002/cne.903590310.

Brent a Vogt. Pain and emotion interactions in subregions of the cingulate gyrus. *Nat. Rev. Neurosci.*, 6(7):533–544, 2005. ISSN 1471-003X. doi: 10.1038/nrn1704.

Curt Von Euler. Brain Stem Mechanisms for Generation and Control of Breathing Pattern. In *Compr. Physiol.*, volume 2, pages 1–68. John Wiley & Sons, Inc., Hoboken, NJ, USA, January 2011. doi: 10.1002/cphy.cp030201. URL `http://onlinelibrary.wiley.com/doi/10.1002/cphy.cp030201/fullhttp://doi.wiley.com/10.1002/cphy.cp030201`.

A. von Leupoldt. Differentiation Between the Sensory and Affective Dimension of Dyspnea During Resistive Load Breathing in Normal Subjects. *Chest*, 128(5): 3345–3349, November 2005a. ISSN 0012-3692. doi: 10.1378/chest.128.5.3345. URL `http://journal.publications.chestnet.org/article.aspx?doi=10.1378/chest.128.5.3345`.

A von Leupoldt, N Seemann, T Gugleva, and B Dahme. Attentional distraction reduces the affective but not the sensory dimension of perceived dyspnea. *Respir. Med.*, 2007.

A von Leupoldt, T Sommer, S Kegat, and H J Baumann. Dyspnea and pain share emotion-related brain network. *Neuroimage*, 2009.

Andreas von Leupoldt. Cortical Substrates for the Perception of Dyspnea<xref rid="AFF1">[*]</xref>. *CHEST J.*, 128(1):345, July 2005b. ISSN 0012-3692. doi: 10.1378/chest.128.1.345. URL `http://journal.publications.chestnet.org/article.aspx?doi=10.1378/chest.128.1.345`.

V. Šmejkal, R. Druga, and J. Tintěra. Brain activation during volitional control of breathing. *Physiol. Res.*, 49(6):659–663, 2000. ISSN 08628408.

Xiao-Jing Wang. Neurophysiological and computational principles of cortical rhythms in cognition. *Physiol. Rev.*, 90(3):1195–1268, 2010. ISSN 0031-9333. doi: 10.1152/physrev.00035.2008.

a a Ward. The cingular gyrus, area 24. *J. Neurophysiol.*, 11(1):13–23, 1948. ISSN 0022-3077.

Jason C Wester and Diego Contreras. Generating waves in corticothalamocortical networks. *Neuron*, 77(6):995–997, March 2013. doi: 10.1016/j.neuron.2013.03.002.

J G Widdicombe. Pulmonary and respiratory tract receptors. *J. Exp. Biol.*, 100:41–57, 1982. ISSN 0022-0949.

Thilo Womelsdorf, Kevin Johnston, Martin Vinck, and Stefan Everling. Theta-activity in anterior cingulate cortex predicts task rules and their adjustments following errors. In *Proc. Natl. Acad. Sci. U. S. A.*, volume 107, pages 5248–5253, 2010. ISBN 1091-6490 (Electronic)\n0027-8424 (Linking). doi: 10.1073/pnas.0906194107.

Mary a. Woo, Paul M. Macey, Katherine E. Macey, Thomas G. Keens, Marlyn S. Woo, Rebecca K. Harper, and Ronald M. Harper. FMRI responses to hyperoxia in congenital central hypoventilation syndrome. *Pediatr. Res.*, 57(4):510–518, 2005. ISSN 00313998. doi: 10.1203/01.PDR.0000155763.93819.46.

Ruth Wuyts, Elke Vlemincx, Katleen Bogaerts, Ilse van Diest, and Omer van den Bergh. Sigh rate and respiratory variability during normal breathing and the role of negative affectivity. *Int. J. Psychophysiol.*, 82(2):175–179, 2011. ISSN 01678760. doi: 10.1016/j.ijpsycho.2011.07.021.

George K. York and David A. Steinberg. Hughlings jackson's neurological ideas. *Brain*, 134 (10):3106–3113, 10 2011. URL `http://brain.oxfordjournals.org/content/134/10/3106.abstract`.

R F Young and V I Chambi. Pain relief by electrical stimulation of the periaqueductal and periventricular gray matter: evidence for a non-opioid mechanism. *J. Neurosurg.*, 1987.

R.F. Young, Richard Kroening, Wayne Fulton, R.a. Feldman, and Israel Chambi. Electrical stimulation of the brain in treatment of chronic pain. *J. Neurosurg.*, 62(3):389–396, 1985. URL `http://thejns.org/doi/pdf/10.3171/jns.1985.62.3.0389`.

S P Zhang, R Bandler, and P J Davis. Brain stem integration of vocalization: role of the nucleus retroambigualis. *J. Neurophysiol.*, 74(6):2500–2512, 1995. ISSN 0022-3077.

Weirong Zhang. Respiratory muscle responses elicited by dorsal periaqueductal gray stimulation in rats. *AJP Regul. Integr. Comp. Physiol.*, 289(5):R1338–R1347, November 2005. ISSN 0363-6119. doi: 10.1152/ajpregu.00828.2004. URL `http://ajpregu.physiology.org/cgi/doi/10.1152/ajpregu.00828.2004`.